SEDIMENT RESUSPENSION IN A SHALLOW LAKE

Vol 1

by

Richard A. Luettich, Jr.

Submitted to the Department of

Civil Engineering

in partial fulfillment of the

Requirement of the Degree of

DOCTOR OF SCIENCE

at the

MASSACHUSETTS INSTITUTE OF TECHNOLOGY

January 1987

Massachusetts Institute of Technology

Signature of Author__

Department of Civil Engineering
January 22, 1987

Certified by ____

Professor Donald R. F. Harleman
Thesis Supervisor

Accepted by_____

Professor Ole S. Madsen
Chairman, Department Committee

SEDIMENT RESUSPENSION IN A SHALLOW LAKE

by
Richard Albert Luettich, Jr.

Submitted to the Department of Civil Engineering
on January 22, 1987, in partial fulfillment of the requirements
for the degree of Doctor of Science in Civil Engineering

Abstract

Episodic resuspension and deposition of bottom sediment can have a large influence on water quality thereby making it important to be able to predict the amount of sediment which is resuspended in shallow water bodies during storm events. In response to this need an instrument system was assembled having the capability of measuing wind speed and direction, wave characteristics, water velocities and suspended sediment concentration. Field experiments were planned and executed in Lake Balaton, a large (700 km^2 surface area) but shallow (mean depth 3.1 m) lake in Hungary, as part of a co-operative study with the Hungarian government into the causes and effects of various processes on the eutrophication of the lake.

The data collected in the field study was used to show that the bottom stress associated with surface waves was typically much greater than that due to the mean current in Lake Balaton and therefore wave stress dominates the resuspension process.

A wave hindcasting model, based on shallow water modifications made to the SMB relationships as presented in CERC (1977), was found to match measured time histories of significant wave height extremely well at the two field sites. Variations in the observed wave periods were not as well reproduced in a dynamic sense.

A review of previous research on cohesive sediment transport led to the recommendation of a boundary condition appropriate for use with field data. A simple model of the depth-averaged suspended sediment concentration using this boundary condition was calibrated to 11 hours of hydrodynamic and concentration data measured during a storm. A verification of the model using wind data from a nearby meteorological station, the wave hindcasting model and 15 days of concentration measurements yielded excellent results.

Thesis Supervisor: Dr. Donald R. F. Harleman
Title: Professor of Civil Engineering and Ford Professor of Engineering

Table of Contents

List of Figures

List of Tables

Acknowledgements

This work was jointly sponsored by the National Science Foundation and the Hungarian Academy of Science under the U.S.-Hungary Cooperative Science Program grant nos. INT-8112452 and INT-8411545 and by the National Science Foundation Environmental Engineering Program, administered by NSF program director Dr. Edward H. Bryan, under grant no. ECE-8211525.

I would like to thank of Dr. Ference Mate, who oversaw this project for the Hungarian Academy of Sciences and who allowed me the use of his laboratory in Keszthely. I am also grateful to Dr. Laszlo Somlyody, who directly supervised the major part of the cooperative research through his position as the Director of the Institute of Water Pollution Control, Research Center for Water Resources Development, Budapest, Hungary. In particular, I appreciate his having a tripod constructed on sort notice and then being patient through a year of postponements and delays caused by equipment failures both here and in Hungary before the actual field study was conducted. He was also most generous in sharing the concentration and wind data for the 15 day study period at Keszthely as well as any other pertinant information that I asked for.

I feel particularly fortunate to have had the opportunity to travel to Hungary during the course of this thesis research. I genuinely fell in love with this country and its people. I can only hope that I treat visitors to the United States with the same kindness which was shown to me during my stays there. I would like to thank everyone who personally went out of his way to make my work in Hungary successful. However, to list all the names here would be almost impossible and would certainly result in several unintended omissions. Worse than that, I fear my spelling of many of these names would probably lead more to confusion than to recognition. Let me simply say that if my children and grandchildren never have the opportunity to know your faces, they will at least know your names.

I feel very privileged to have had Professor Donald R. F. Harleman as my thesis supervisor. His confidence in my ability was an inspiration for me in times of disappointment, and his practical experience and technical expertise provided the focus I was often looking for but unable to find on my own. I am particularly grateful for the many things which he and Martha have done for Dana and me. As a couple, they are a role model which we will always hold dear.

I would also like to thank the members of my thesis committee, Professor Ole Madsen, Dr. Eric Adams and Dr. Sandy Williams, as well as Professor Keith Stolzenbach and Dr. Laszlo Samlyody, for their friendship and helpful discussions during the course of this work. I'd like to express special thanks to Sandy Williams and Dick Koehler for rescuing me from Sea Data's messes and getting BASS to work with my equipment system. Had it not been for their efforts, Chapter 2 would have been much shorter.

During the course of this study, Pat Dixon and Elizabeth Williamson helped me with countless odds and ends like sending replacement parts to Hungary when my equipment broke, performing data analysis and many other meanial chores. Without this help, I might still be working on this thesis as you read this.

I would like to thank Read Schusky and Ingrid Christiansen for their help in typing this thesis. It has been a particular pleasure to work with Ingrid whose cheerie attitude and genuine concern over my progress has been greatly appreciated.

It is impossible to fully aknowledge the role which my parents have had in this accomplishment. They encouraged my curiosities and brought me up to believe all things are possible with perseverence and hard work. However, the thing I appreciate the most was their providing me with a Christian foundation which I could draw upon in happy as well as difficult times. This, more than anything else, has seen me through these past few years.

I have also been very lucky to have friends at MIT and outside with whom I could share the good times and bad. In particular I would like to thank Pat and Brian Dixon for the love they have given to me over the past five plus years. They, together with the FBC family, have helped to show me how to draw upon the foundations that my parents provided.

Finally, I am in debted to my wife, Dana, for sticking with me through these years at MIT. Without her I am afraid my work would be my life. Fortunately, she has refused to allow this to happen. Together we have shared the happiest moments of my life. I can ask for nothing more.

Chapter 1

Introduction

The progression of our understanding of aquatic environmental pollution problems has revealed the fact that many aspects of water quality depend critically on physical processes in addition to more readily recognized chemical and biological processes. Examples of this include (i) horizontal transport and its influence on lateral inhomogeneity within a water body, (ii) vertical transport of nutrients and organisms through the thermocline in a stratified water body, (iii) micro-scale transport of nutrients into a cell's immediate environment and (iv) effects on light penetration, heat absorption and internal loading due to the resuspension of bottom sediments.

The purpose of this study is to examine the processes responsible for the resuspension and transport of fine sediments in a shallow water body and to include them in a model capable of predicting the sediment concentration in the water column. Ultimately, this could be used as a component of a water quality model. This work concentrates on the behavior of fine sediments, (i.e., silts and clays), for several reasons:

(i) fine sediments have the largest surface area to volume ratio and therefore provide the largest available space for the bonding of chemical substances per unit volume,

(ii) fine sediments (particularly clays) typically have excess negative surface charge which facilitates bonding with positively charged ions,

(iii) fine sediments have smaller fall velocities than coarser fractions and therefore remain in suspension the longest. As a consequence of this silts and clays are more easily transported in surface runoff and very often compose the major part of the sediments in lakes and estuaries -- particularly those most severly affected by eutrophication. For example 90 per cent of the sediments are in the silt-clay size range in Lake Erie (Lick, 1982).

Numerous qualitative examples exist which illustrate the commonplace nature of sediment resuspension in both deep and shallow lakes. For example Davis (1973), Pennington (1974), and Serruya (1977), have analyzed sediment trap data in several deep, stratified lakes and found substantial quantities of resuspended bottom material present during spring and fall overturn. Davis (1973) and Rosa (1985) have compared sediment trap data from shallow well-mixed water columns with that from stratified water columns and found more frequent and more substantial resuspension in the shallow waters.

It is interesting to note that sediment traps are usually used to quantify the flux of particulate matter settling through the water column and presumably being transported to the sediments. Unfortunately, the interpretation of these data is often made difficult by the need to distinguish between material which is allochthonous, or a new input to the system, and that which is autochthonous, or in this case resuspended. The ability to predict the amount of resuspension which occurs would aid greatly in the routine analysis of these measurements, (Gabrielson and Lukatelich, 1985 and Ovaitt and Nixon, 1975).

Qualitative field evidence suggests suspended sediment has several affects on water quality. Barcia (1974) used in situ enclosures and artificial mixing to show that sediment resuspension could deplete concentrations of dissolved oxygen and increase ammonia concentrations to toxic levels and therefore bring about the collapse of algal blooms in shallow prairie pothole lakes (depths 2.4-5.1m). Lijklema (1977) showed a correlation between wind speed and total phosphorus measurements in Lake Ijsselmeer, (depth 1-2m). Ryding and Forsberg (1977) correlated ammonium and total phosphorus concentrations in Lake Uttran (mean depth 5.7 m) to the daily average speed of winds aligned with the lake's long axis. They also found the July - September average chl-a value, (chl-a is typically used as a measure of algal population), was related to the average wind speed aligned with the lake axis for the four years after the principal external nutrient sources to the lake were diverted. Peters and Cattaneo (1984), made measurements as often as twice daily in waters of 0.5, 1.2, 3, 8, and 100 meters depth in a small cove of Lake Memphremagog. They found total phosphorus concentrations at the three shallowest sites increased on stormy days, but found no trend in the concentration of dissolved reactive phosphorus or the rate of algal phosphorus uptake. Walker and O'Donnell (1981) found a coupling between the chemical and biological processes in the lagoon waters of the Great Barrier Reef and the benthic processes due to the wind driven resuspension of bottom sediment.

In most fresh water systems phosphorus is the limiting element of eutrophication, therefore the following remarks concern it specifically. It is classically held that in aerobic, vertically-mixed lakes there is a net flow of phosphorus into the sediments (Wetzel 1975). The predominant

mechanism for this is the settling of organic and inorganic particulate matter. A significant portion of the mineralization of organic material occurs at the sediment surface, thereby releasing dissolved phosphorus into the interstitial pore water. Gelencser et al (1982) found that the pore water in Lake Balaton, Hungary, had dissolved reactive phosphorus concentrations which were two orders of magnitude larger than the overlying water. The high diffusive flux from the sediments to the overlying water, which would be expected, is drastically reduced by the strong tendency of phosphate to adsorb onto solid phases -- particularly those formed by iron, aluminum and calcium. These act as a phosphorus trap, virtually sealing off the sediments to active exchange with the water column.

However, recent work has shown that phosphorus adsorption/desorption onto calcite and ferric hydroxide occurs rapidly and is highly dependent on the phosphorus concentration of the surrounding water and somewhat dependent on pH, (Gelencser et al., 1982). This suggests a scenario in which particulate organic matter settles to the sediment, is mineralized and releases dissolved phosphorus to the interstitial water which is then adsorbed onto the particulate phase. If the sediment is resuspended a change in pH as well as ambient phosphorus concentration occurs and the phosphorus desorbs into the water.

Gelencser et al (1982) performed laboratory experiments which support this scenario and if extrapolated to Lake Balaton suggest that a moderate storm, leading to 25 mg/l average increase in suspended solids, could cause a release of 250-500 kg P over the whole lake, the same order of magnitude as the daily external load.

Holdren and Armstrong (1980) incubated intact sediment cores from the epilimnion of four Wisconsin lakes to determine the affect of various environmental parameters on sediment phosphorus release. Sediment resuspension was shown to either release or remove phosphorus from the water column depending on the sediment content, the temperature and the redox potential.

Bates and Neafus (1980) obtained a small increase in dissolved phosphorus levels in laboratory cultures which included sediments from Lake Carl Blackwell, Oklahoma, when the sediments were mixed into suspension. The interpretation of these laboratory results should be made with caution, however, since the conditions in the laboratory are not necessarily natural ones.

Ryding and Forsberg (1977) presented nutrient budget calculations for four lakes all of which showed the in lake release of phosphorus from the sediments was substantially greater than that measured in laboratory cultures.

Yousef et al. (1980) found significant phosphorus enrichment can occur when bottom sediments are resuspended by motor boats in shallow lakes.

Suspended sediments also influence the depth of light penetration in a water body. In Lake Balaton, Hungary, (mean depth 3.1 m), suspended solids concentrations range from 5-200 mg/l, and allow the depth of "light penetration" to vary from the entire water depth to tens of centimeters.

The potential importance of resuspension should be contrasted with the ignorance with which sediment interaction is included in water quality models. Typically sediments are treated as a black box into which particulates settle and from which nutrients are exchanged via a diffusive

type process. For example three eutrophication models (Leonov, 1980; Kutas and Herodek, 1986; and Van Straten, 1980) have been developed for Lake Balaton. All three models consider the importance of extinction on light penetration in the water column, yet none include the role of resuspended sediment in extinction. All three models consider nutrient exchange between the sediment and water, but only Leonov (1980) makes any attempt to include the effect of resuspension. This was done by assuming that resuspended particulate inorganic phosphorus (RPIP) and resuspended dissolved inorganic phosphorus (RDIP) were related to wind speed by separate power laws. The implementation of these relations required values to be assigned to four parameters. Leonov (1980) calibrated these parameters along with numerous others based on routine water quality measurements (which do not include measurements of RPIP or RDIP) typically made bi-weekly or monthly within the lake. Considering that the characteristic hydrodynamic forcings in the lake are storms of 12-24 hour duration, it seems difficult to believe that the resuspension effect was accurately represented.

To this point, a case has been presented for the importance of sediment resuspension in affecting lake eutrophication -- particularly in shallow lakes. One potential mechanism for studying this process is to monitor in situ the changes in the aquatic chemistry and biology caused by natural or artificially created resuspension events. Unfortunately, specific cause and effect relationships are difficult to isolate since resuspension can concurrently have opposite effects on a single process, e.g. if resuspension increased the nutrient supply it would tend to increase the algal growth rate but at the same time the decreased light penetration would decrease the growth rate. Also, results gathered from

these experiments are of little use in describing the transport of trace metals, pcb's and other potential toxins which often adsorb to fine sediments in natural water bodies. Finally, these experiments shed little light on the physical process of resuspension of fine sediments -- a topic which until very recently has been studied only in laboratory flumes under steady flow conditions. Therefore, it is assumed that the influence of fine sediment resuspension on water quality can be separated into at least two parts, i.e., the chemical and biological interactions which occur between a suspended particle and its aqueous environment and the hydrodynamical processes which cause that particle to be eroded from its sediment bed. It is the intention of this work to focus on the latter process.

The field study and modeling which comprise the major part of the work described in the remainder of this document were conducted at Lake Balaton, Hungary, which is shown in Figure 1.1. The lake has a maximum length of 77.8 km and an average width of 7.7 km. Two additional unique physical features of the lake are its shallow depths, (mean depth 3.1m), and the Tihany Penninsula, which nearly divides the lake into two parts. The narrow neck of water connecting the two ends of the lake contains the maximum water depth, which reaches 11.6 m. As shown in Figure 1.1, the lake has been arbitrarily segmented into four basins primarily for the purposes of scientific study. These basins are referred to in the remainder of this document in terms of the major city associated with each, i.e. from west to east, Keszthely Basin, Szigliget Basin, Szemes Basin, and Siofok Basin.

The principal tributary to the lake is the Zala River, located at the western end, while the only outflow is the Sio Canal near the eastern end.

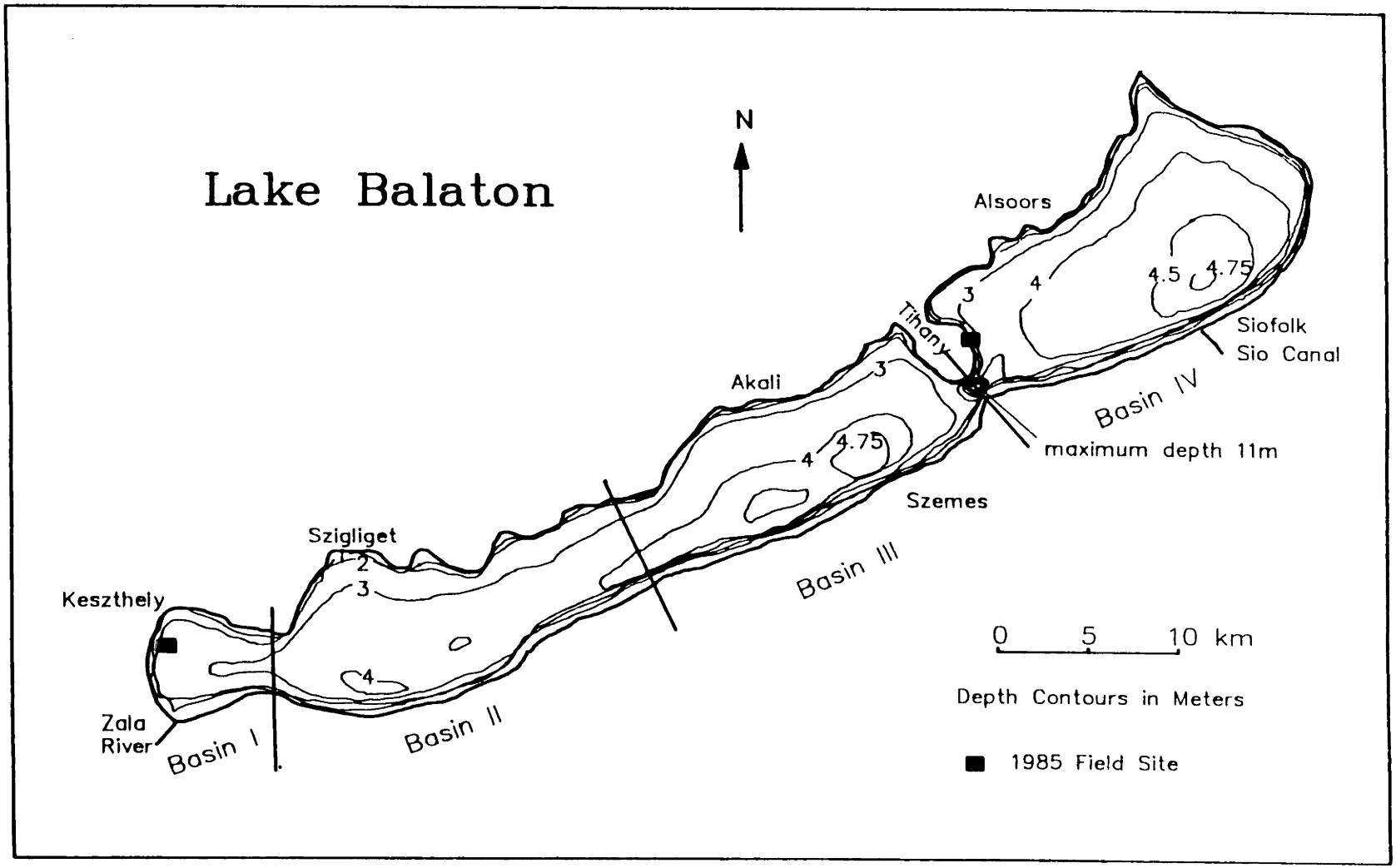

Figure 1.1 Lake Balaton, Hungary

The hydrologic through flow is very low in the lake (~ 0.01 cm/s) and the tributary input is quite closely balanced by evaporative loss. The principal hydrodynamic forcing in the lake is due to storm related wind events. The prevailing wind direction is roughly from the NNW and, therefore, transverse to the lake's long axis.

Until the early 1970's, the lake enjoyed excellent water quality, and this, coupled with the temperate climate, contributed to its immense popularity as a recreational area for much of Central Europe. However, the 1970's saw a rapid decline in the water quality to the point that mid to late summer water at the western end of the lake is aptly described as being "pea soup," and periodic fish kills result from oxygen depletion. Associated with this decline was the development of a water quality gradient along the lake axis, which rougly corresponds to the distribution of external loading. At its worst point, the western end of the lake is severely hypertrophic while the eastern end remains mesotrophic. Throughout this process phosphorus has been the principal limiting nutrient, although in recent years evidence suggests that nitrogen and light penetration may also limit algal growth in certain situations, (S. Herodek, personal communication).

In an effort to reverse this problem, several sweeping steps have been taken to cut off the external nutrient loadings to the lake. These include: (1) re-routing the Zala River through a marshland near its mouth, which will hopefully act as a natural settling basin and remove many of the nutrients before they enter the lake, and (2) constructing an extensive sanitary sewer system to collect and treat domestic waste and ultimately to divert it into the Sio River, which is downstream of the lake.

As a result of these steps, the lake makes an interesting case study into man-made, or so called "cultural" eutrophication, and more importantly into attempts to reverse this situation. It is in this respect that an understanding of the role of sediments, which potentially collect and store many years worth of external loadings, becomes critical. The shallow depths and large open fetches of Lake Balaton suggest that resuspension may play a significant part in this process.

The remainder of this document is broken up into five chapters.

Chapter 2 describes the system of field equipment developed to measure wind events and the resulting hydrodynamic and sediment response. Experiments were conducted at two locations in Lake Balaton in the summer of 1985, and these results are presented as well.

Chapter 3 begins with a conceptual model of the sediment-water column boundary, which is then used as a framework for organizing and interpreting previous theoretical laboratory, field and modeling studies on the response of a cohesive sediment bed to an applied forcing. The chapter concludes with a recommended bottom flux boundary condition for modeling the suspended sediment concentration data collected in the field study.

Chapter 4 discusses the hydrodynamics which are responsible for sediment resuspension. It is shown that waves can be expected to have a dominant role throughout most of Lake Balaton. A wave hindcasting model is presented and then verified using available historical data along with data presented in Chapter 2.

Chapter 5 contains the resuspension model which is calibrated using suspended sediment and simultaneous hydrodynamic data collected in Keszthely basin as a part of this study. Verification is provided over a

15 day period using wind speeds measured at a nearby meteorological station, the wave model developed in Chapter 4 and measured suspended sediment concentrations.

Chapter 6 presents conclusions from this study as well as recommendations for future work.

Chapter 2

Field Study

One of the principal goals of this thesis was to obtain field data detailing the hydrodynamic behavior and sediment response in Lake Balaton to episodic storm events. Previous measurements dating back to the early 1960s have been made in Lake Balaton and have shed some light on these processes. They are briefly reviewed after which the experiments conducted as part of this study are presented.

2.1 PREVIOUS MEASUREMENTS IN LAKE BALATON

At various times wind speed, water level, wave parameters, water velocity, sediment erosion, and suspended sediment concentration have been measured in Lake Balaton. Unfortunately much of these data exist in reports written in Hungarian and therefore are somewhat obscure. However, Somlyody (1979) has summarized the results of much of this work and his report is used as a basis for part of the information presented below.

Wind measurements have been made at seven locations around the lake (Figure 2.1a). Results show that typical wind events are associated with weather fronts and have durations from 12-36 hours and on average blow from the NNW. The terrain to the lake's north is quite hilly, causing generally lower winds along the northern shore in comparison to the southern shore and a substantial variabilty in the wind field along the lake.

Water level measurements have been made at as many as fifteen locations around the lake, (Figure 2.1b), and show that the lake has a characteristic longitudinal and transverse seiching behavior. The maximum

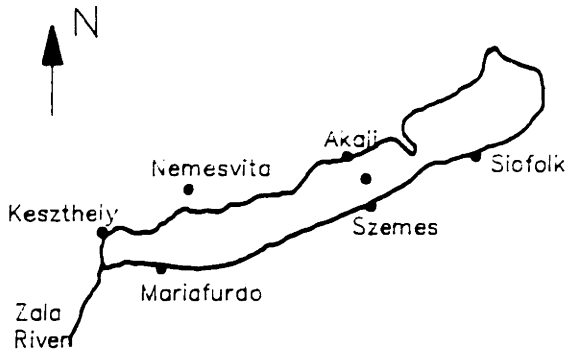

(a) Wind Measurement Stations

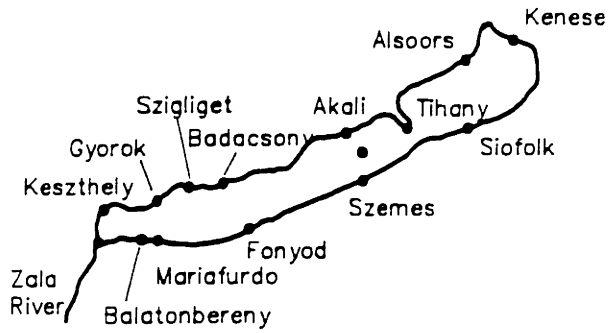

(b) Water Level Measurement Stations

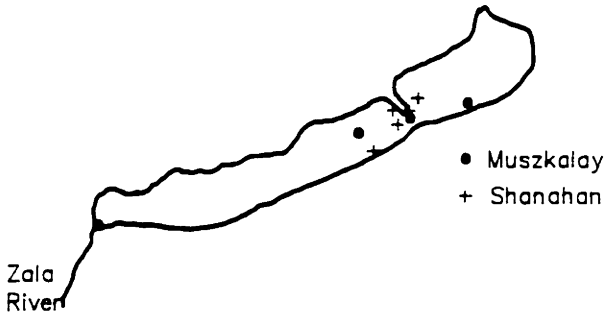

(c) Velocity Measurement Points

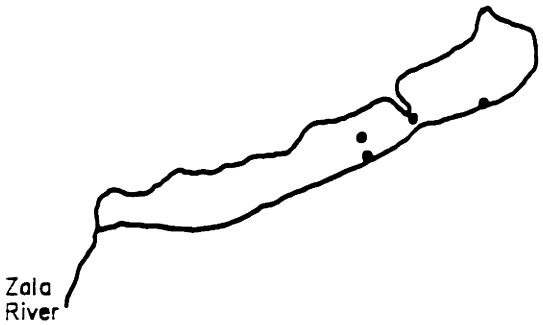

(d) Wave Measurement Points

Figure 2.1 **Summary of Field sites at which wind and/or hydrodynamical data has previously been collected in Lake Balaton, (after Somlyody, 1979).**

longitudinal difference in water level from one end to the other is about 1 m while the maximum transverse difference is about 0.40 m. Muszkalay (1973) found a longitudinal seiche period varying from 10 minutes to 1 day with a mean period of about 5.5 hours, while work done at the turn of the century suggests a longitudinal seiche period of 10-11 hours and a transverse period of about 40 minutes. Muszkalay (1973) proposed empirical relationships for the maximum longitudinal water surface slope from an analysis of typical storms using over a decade of data, (Table 2.1).

Water velocity was measured by Muszkalay (1973) at three locations in the lake and by Shanahan (1981) at several additional locations (Figure 2.1c). Most noteworthy of Muszkalay's measurements were the results obtained from a vertical mooring of four current meters at the narrowest point in the lake, the Tihany Strait. These showed a strong unidirectional current over the depth which was principally due to the lake seiching motion. Again based on his data Muszkalay (1973) defined an empirical relationship between the maximum value of this unidirectional current and the water surface slope, (Table 2.1).

Shanahan (1981) deployed a Marsh-McBirney electromagnetic current meter attached to a 5 m-long pole and visual readout over the side of an anchored ship and made short-term measurements of the vertical distribution of the mean horizontal velocity by raising and lowering the current meter to selected elevations. The measurements were made over three days during which the winds were light ranging up to 3.5 m/s. Shanahan (1981) verified the strong unidirectional currents in the Tihany Strait but at other locations found highly transient values apparently responding to the unsteady turbulent transport of wind shear vertically in the water column as well as the seiching behavior. Rarely did he find the classical

Table 2.1 Empirical Relationships Describing Lake Balaton Hydrodynamics (from Muszalay, 1973)

I. Longitudinal Water Surface Slope

(i) wind directed within 22.5° of the lake's long axis

$$I = 3.8 \times 10^{-7} D^{0.25} (W_{aL} - 2.8) \quad (2.1)$$

(ii) otherwise

$$I = 1.05 \times 10^{-7} D^{0.25} (W_{aL} + 13.5)^{-0.16} \quad (2.2)$$

where:

I = maximum water surface slope (maximum difference in water levels between the extreme ends of the lake divided by the length of the lake).

W_{aL} = longitudinal component of maximum instantaneous wind speed at Szemes. (Somlyody and Virtaen, (1982), found the maximum wind speed typically exceeds the hourly average wind speed by a factor of 1.2 - 1.3.)

D = wind duration in hours (Eqs. 2.1 and 2.2 valid for $D < 12$ hours)

II. Water Velocity at Tihany Strait

$$U_T = 500\ I^{0.5} - 0.5 \quad (2.3)$$

where:

U_T = velocity in Tihany Strait 1 m below the surface

III. Wave Relationships at Szemes

(i) Mid-Lake Station (depth = 4 m)

$$H = 0.0827(W_a - 1)^{0.725} \quad (2.4)$$

$$T = \frac{12 W_a^{1.5}}{29 + 3 W_a^{1.5}} \quad (2.5)$$

Near-Shore Station (depth = 2.5 m, 200 m N of southern shore)

$$H = K_1 (W_a - 2)^{0.725} \quad (2.6)$$

$$T = \frac{60 W_a^{1.5}}{K_2 + 15 W_a^{1.5}} \quad (2.7)$$

Wind Direction	NNW	NW, N	WNW, NNE	W, NE
K_1	0.1125	0.1025	0.0855	0.0685
K_2	168	192	192	192

WSW, ENE	SW, E	SSW, S, SSE, ESE, SE
0.0585	0.0525	0.0470
192	192	192

where:

H = rms of 100 waves (meters)
T = waver period (sec)
W_a = wind speed (m/s)

velocity distribution consisting of a surface current aligned with the wind and a bottom return current in the opposite direction.

Wave measurements have been made at four locations in Lake Balaton (Figure 2.1d). Typically these were conducted three times daily, each over a 5-minute duration. Muszkalay (1973) analyzed the measurements by examining groups of 100 waves. Statistical results for the mid-lake and near-shore station at Szemes are shown in Figure 2.2. Empirical fits made to the data are included in the figures. The relationships are listed in Table 2.1. The effect of varying wind direction, (presumably a fetch effect), was noted in the nearshore measurements and empirical coefficients. Unfortunately neither fetch nor depth were explicitly included in these empirical relationships and therefore it is not possible to extrapolate their predictions to other locations around the lake.

Suspended sediment and erosion measurements have been made at a large number of sites throughout the lake. Characteristic results are that the southern shore is being eroded as rapidly as 1 m/year. Erosion is particulary great during events in which the wind blows from the north across the lake, which is roughly the prevailing direction. Under these circumstances it is believed the soil eroded from the southern shore is transported toward the northern shore by a near-bottom return current. As a result the southern shore has been stripped of its fine sediment and consists mostly of coarse material while the bottom along the northern side is typically fine. This has been qualitatively verified by following marked sediment particles in the field, by a physical model in the laboratory and by observations that particle sizes in suspension along the northern shore after a storm are often larger than those in the sediment.

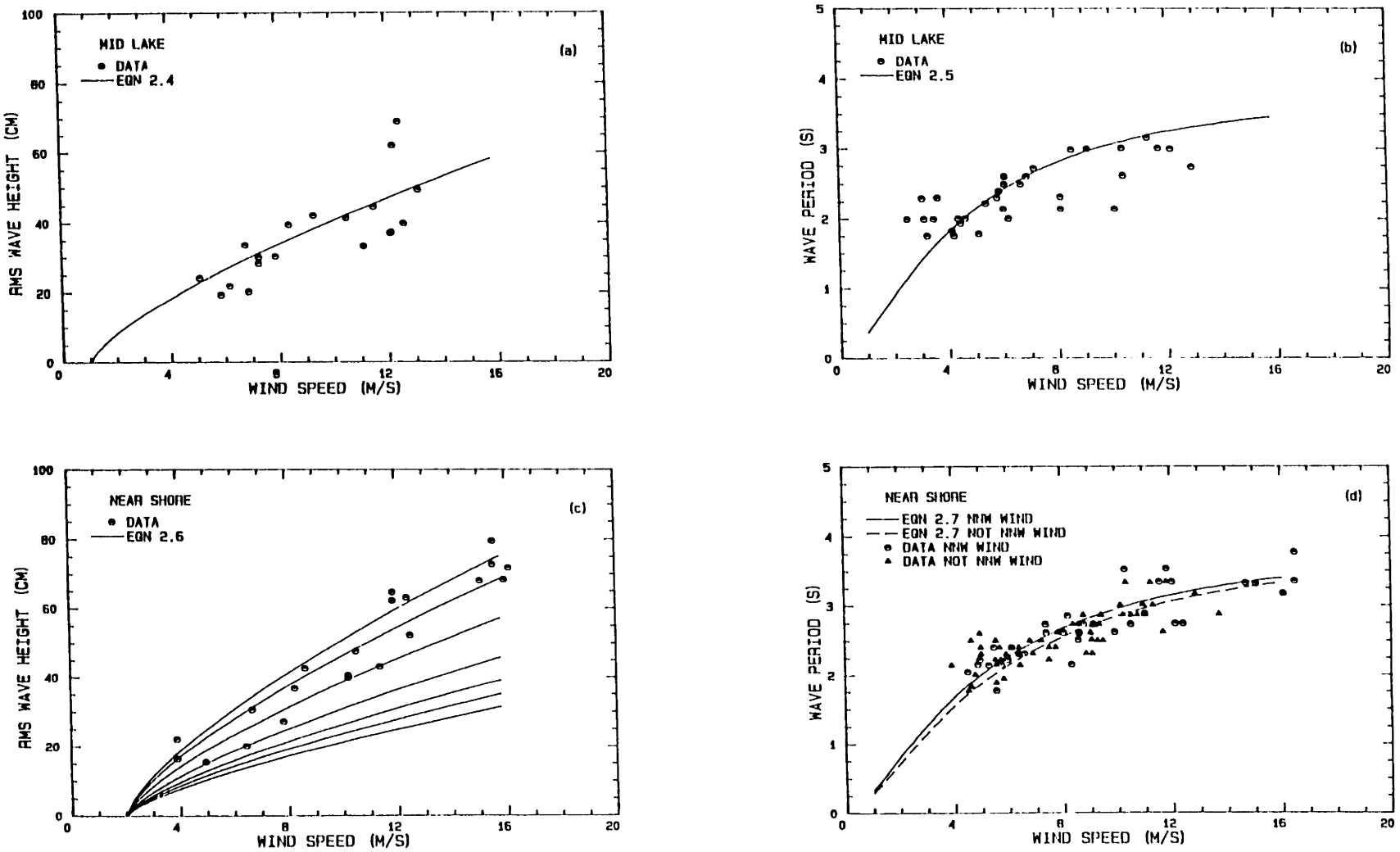

Figure 2.2 Historical wave statistics based on mid-lake and near shore measurements off Szemes in Lake Balaton. Regression Eqs. given in Table 2.1, (modified from Muszkalay, 1973).

The most extensive data set regarding suspended sediment in Lake Balaton has been collected by Somlyody (1980). Daily measurements were made in 4 m-deep water, in the middle of the lake at Szemes for 4½ months during the summer of 1979. Samples taken from five locations over the vertical showed a sediment concentration that was effectively uniform to within 1 m of the bottom. Unfortunately the only other data measured at the time were wind speed and direction at the shore-based meteorological stations. (Note: the station shown in Figures 2.1a-d in the middle of the lake opposite Szemes was destroyed in a storm in the early 1970s.) The daily sampling period makes quantitative conclusions about the sediment response to storm events difficult since frequently these events last for less than a day. Also it is difficult to distinguish the difference between sediment resuspended at the sampling point and sediment resuspended in the near-shore region and transported to the sampling location.

A final data set which is useful in the present context is the recent work of Mate (1985) who has mapped the sediment characteristics in Lake Balaton, taking over 6,000 core samples of the upper sediment layer (at least ten samples/square km). Among the paramters determined were particle size distribution, based on a correlation to hygroscopic moisture, and various chemical contents. Figure 2.3 shows the results of the particle size analysis and is generally consistent with the concept of coarser sediment along the southern shore and finer material toward the north.

Overall, the previous measurements in the lake provide a reasonable qualitative description as well as some quantitative information about the lake behavior under storms and about the behavior of bottom sediment. However, to date there has been no combined effort to measure both types of

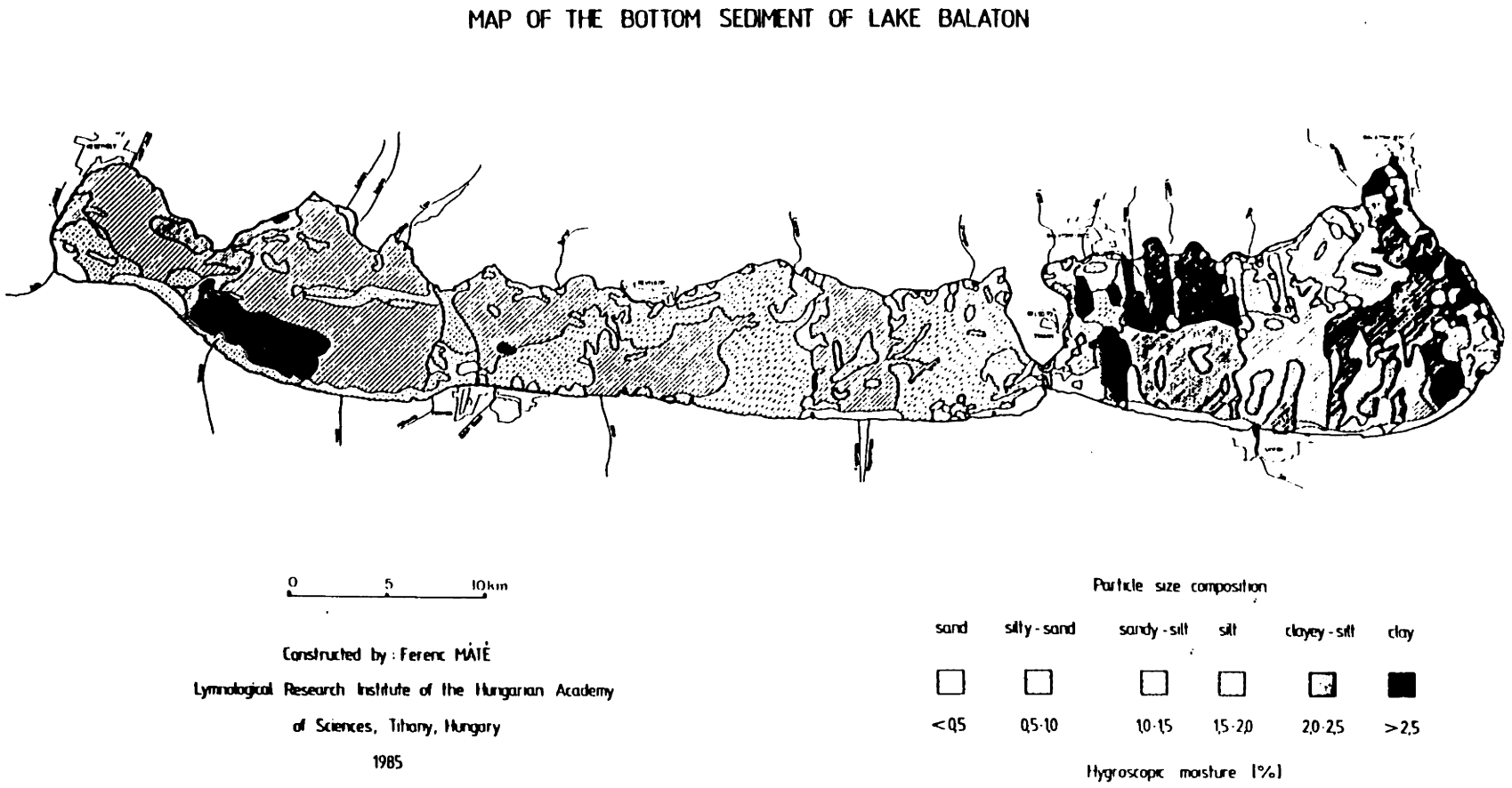

Figure 2.3 Map of bottom sediments in Lake Balaton, (from Máté, 1985).

processes simultaneously and therefore to examine sediment response in detail under measured hydrodynamic conditions.

2.2 EQUIPMENT

It was necessary to assemble a system of equipment that was capable of measuring both the pertinent hydrodynamic processes and the sediment response. The selected system consisted of a wave staff, wind speed and direction equipment, an ABSS particle detector, two BASS current meters, a data logger capable of sampling and recording data from each of these instruments and a remote radio control. The entire package was mounted on an aluminum tripod as shown in Figure 2.4. A large part of this equipment was built by the Sea Data Corporation of Newton, Massachusetts, to meet this project's needs. Specifically, they designed and constructed the data logger and the wave staff. They also constructed part of the two BASS current meters. Each piece of equipment is described below in more detail together with design information and calibrations when appropriate.

For posterity's sake a short note should be included about the Sea Data Corporation. Initial contact was made with this company in the Fall of 1983 leading to design specifications and the awarding of a contract in early 1984. The company gave a completion date of the beginning of June 1984. In reality almost no work was initiated on this equipment before the completion date. A system was not delivered until January 1985 at which time tests showed that none of the instruments worked correctly, if at all. Thereafter, six months of the writer's time was required to work out many of the system's problems. These problems ranged from miswired cables, to inferior workmanship, to faulty design and they ultimately led to the

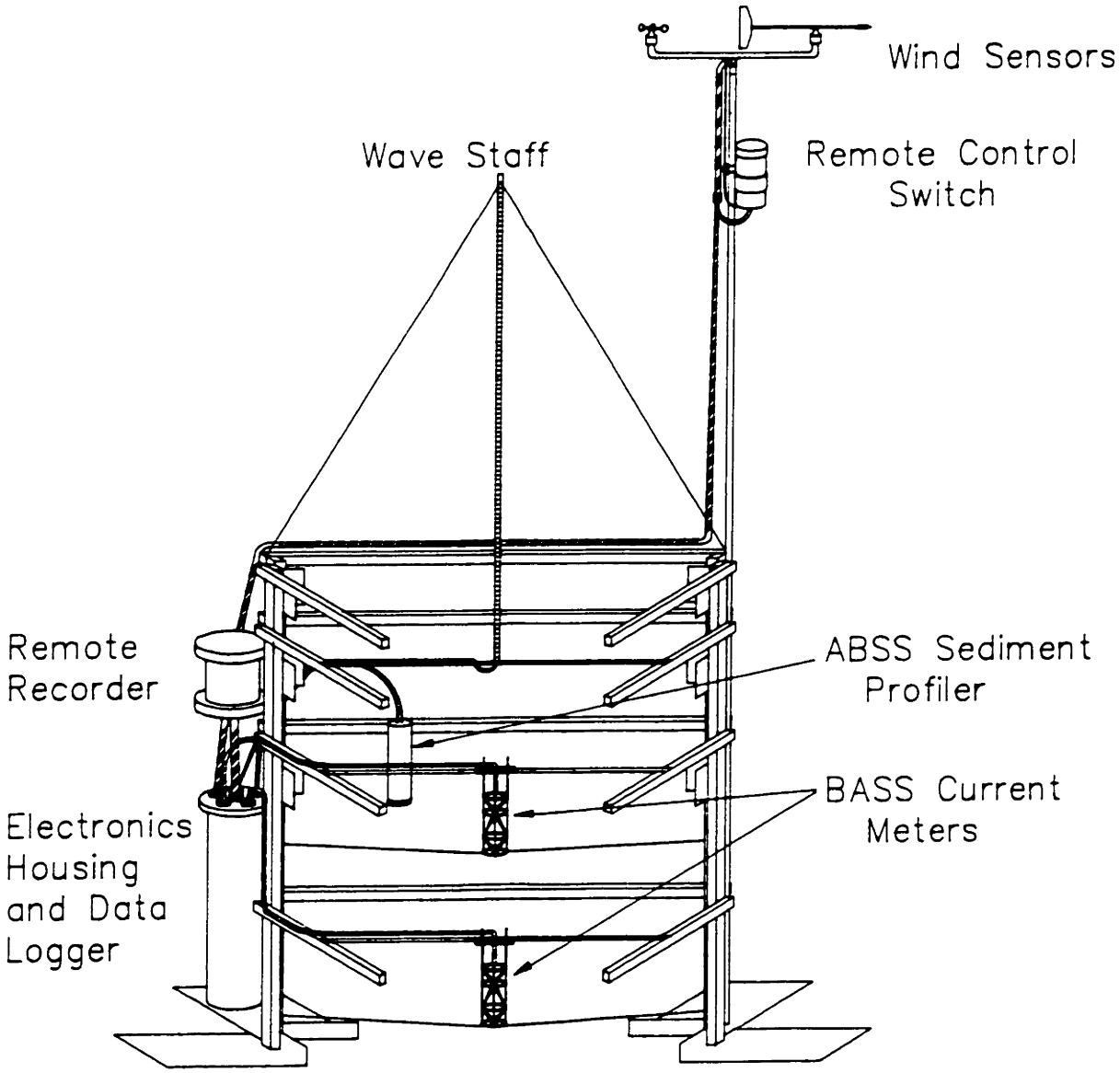

Figure 2.4 **Field equipment and tripod mounting used in the present study. Note, the third leg of the tripod is cut away in this figure.**

premature termination of the experiments as well as to the inability to use data from the wave staff. It was also discovered that at least one of the circuit boards included in the BASS current meters, as delivered by the Sea Data Corp., had actually been loaned to that company by the original designer, Dr. A. J. Williams III of the Woods Hole Oceanographic Institution (WHOI), to be used as a construction guide and for testing.

2.2.1 Data Logger

The data logger was designed to aquire and record data in "bursts." Using such a strategy the instrument was turned on for a specified time, to standby for a specified time, and then on again, etc. This allowed the collection of data at a relatively high frequency without filling up the storage medium (in this case a cassette tape) in an unreasonably short period of time. The on and standby times for which the equipment was set are listed in Table 2.2 together with the total amount of operating time before a cassette tape became filled. Using the remote radio control it was possible to switch between sampling strategies as well as turn the equipment to continuous standby.

During the burst (or the time the equipment was taking and recording data) each instrument could be sampled as rapidly as 2 Hz. This top-end rate was a compromise dictated principally by the available budget. It was accepted as being adequate to define the surface waves which typically have a period of about 2 sec in Lake Balaton. It was assumed that these were the most important high-frequency energy components. Specifically, measurements were taken at 2 Hz from the two BASS current meters, the wave staff, and a vertical sediment profile was taken using the ABSS. The

Table 2.2 Sampling Strategies

Sampling Rate #	On Time (min)	Standby Time (min)	*Deployment time to fill a 450 ft cassette tape (hrs)
1	3	0	6
2	3	2	10
3	6	4	10
4	6	9	15
5	6	14	20
6	6	24	30
7	6	54	60
8	9	21	20
**	0	--	--

*These times assume a sampling frequency of 2hz while the equipment is on

**In this case the instrument was in continuous standby mode

vertical ABSS profile consisted of 128 measurements, each corresponding to the acoustic backscatter from sediments at succeedingly further distances, Δx, from the instrument (in this case $\Delta x \approx 1$ cm). As a result a large amount of data was generated by the ABSS in a very short amount of time and it was not possible to take vertical profiles during the entire burst time. In fact only 40 vertical profiles, one every 0.5 sec, could be taken every 3 minutes. Thus for the first 20 sec of every 3 minutes of on time the ABSS was sampled.

Data from each instrument was recorded on a cassette tape which was located in a remote capsule made of clear Plexiglass outside of the main data logger and electronics housing (Figure 2.4). The remote recorder capsule and main housing were connected by an underwater matable connector so that a diver could remove the remote recorder capsule for the purpose of changing the cassette tape without removing the entire instrument system.

This greatly facilited the equipment's use; however, ultimately it led to the premature termination of data collection since the contacts on the underwater connector corroded rapidly when the capsule was detached. (This was due to the fact that the system design left the main power to the recorder capsule on while the equipment was in standby mode). During the course of the experiments in Lake Balaton twelve cassette tapes full of data were written. However, due to the corroded underwater connector the final three tapes were blank. Also, mysteriously, data on tapes 4 and 7 was unintelligible. This may have been due to improper loading of the cassette into the recorder.

All of the equipment was powered from a battery pack consisting of individual "D"-size batteries wired together to give the desired output voltage and as long an operating life as possible. The battery pack was located in the bottom of the main electronic housing. This turned out to be quite inconvenient since the battery pack life was only 2-3 cassette tapes. Consequently a battery change required a complete new deployment.

The data logger, electronics for each of the instruments, and the battery were encased in a steel pressure housing and comprised the main electronics package, (Figure 2.4).

2.2.2 Remote Radio Control

The sampling strategies shown in Table 2.2 could be set or changed by varying an input voltage to the data logger. This was accomplished remotely using a radio control designed and built by the author. This capability was a crucial part of the instrument system since storms came up often with little advance notice and were separated by prolonged periods of

calm weather. Without this ability little useful data could have been obtained without unreasonably frequent redeployments to change batteries. (A single removal and redeployment took about eight hours and required at least three people.) Thus the irregular, event-based nature of this study necessitated the ability to vary sampling strategies. Since it was often impossible to be physically with the equipment this had to be achieved over short but significant distances. It was accomplished with two Radio Shack 2-watt walkie-talkies, a tone generator similar to that found on Touch-Tone telephones, and a small tone decoding and switching circuit. The circuit diagram is shown in Figure 2.5 while the entire switching assembly is shown in Figure 2.6. The assembly was located in a capsule made of two short lengths of 4"-diameter PVC pipe with two end caps and a threaded coupler. The assembly was mounted on the mast used to support the wind-measuring equipment. The assembly was equipped with an override switch which could be used to manually force the equipment into a continuous sampling mode in the case of the failure of the radio control. Overall the radio-controlled switch functioned quite reliably.

2.2.3 Wind Measurement System

A wind vane and cup anemometer manufactured by the Weather Measure Company were used to determine wind direction and velocity. This equipment seemed quite reliable although tests showed the wind vane's north alignment was initially more than 20° out of line. The wind data was processed in situ and recorded as the 3-min average N and E velocity components, the scalar average velocity, the maximum velocity and direction observed during a 3-min. interval, and the instantaneous velocity and direction observed

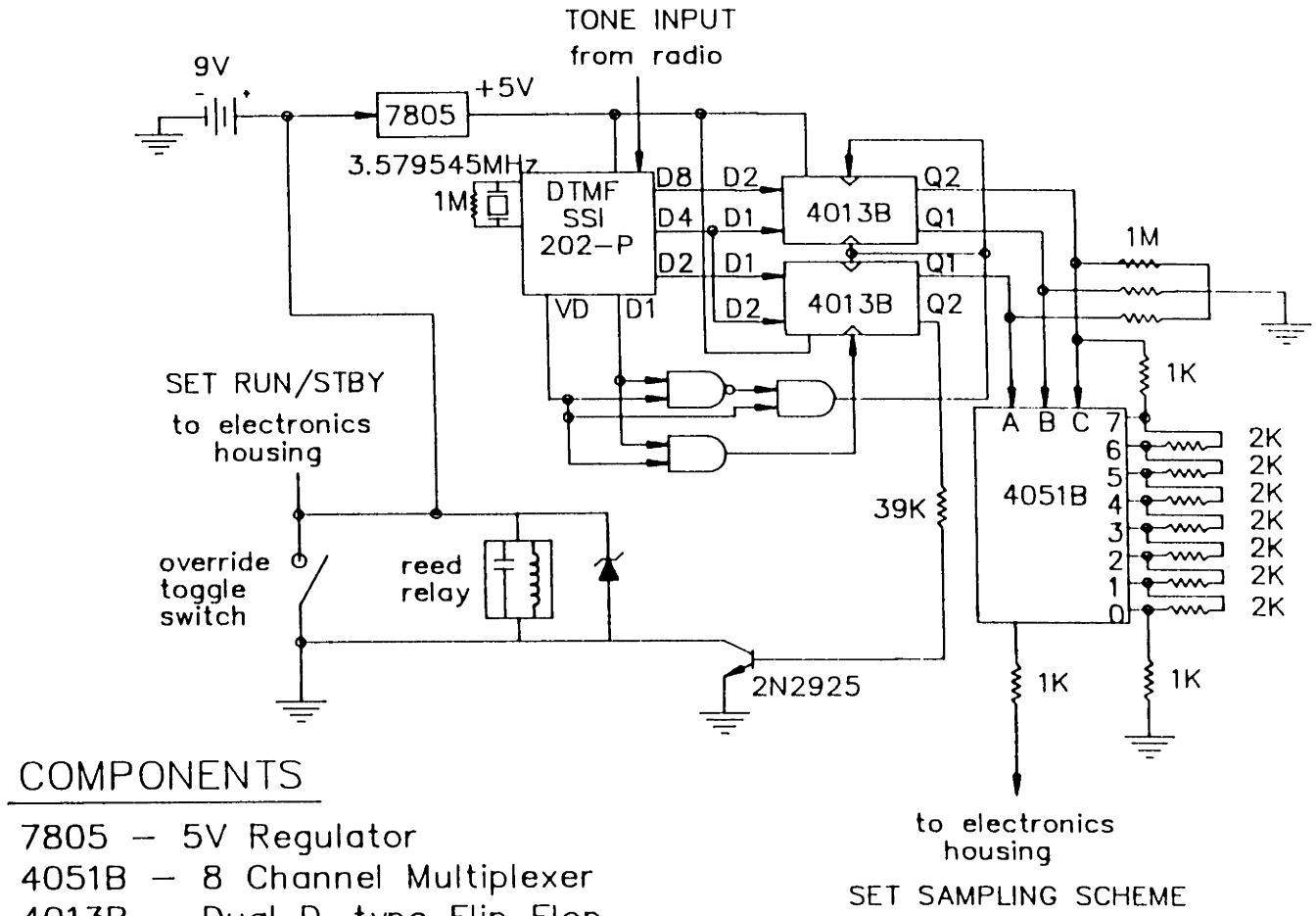

COMPONENTS

7805 – 5V Regulator
4051B – 8 Channel Multiplexer
4013B – Dual D-type Flip Flop
202-P – Dual Tone Multi Freq. Receiver

Figure 2.5 Tone decoding circuit used in the radio control switch.

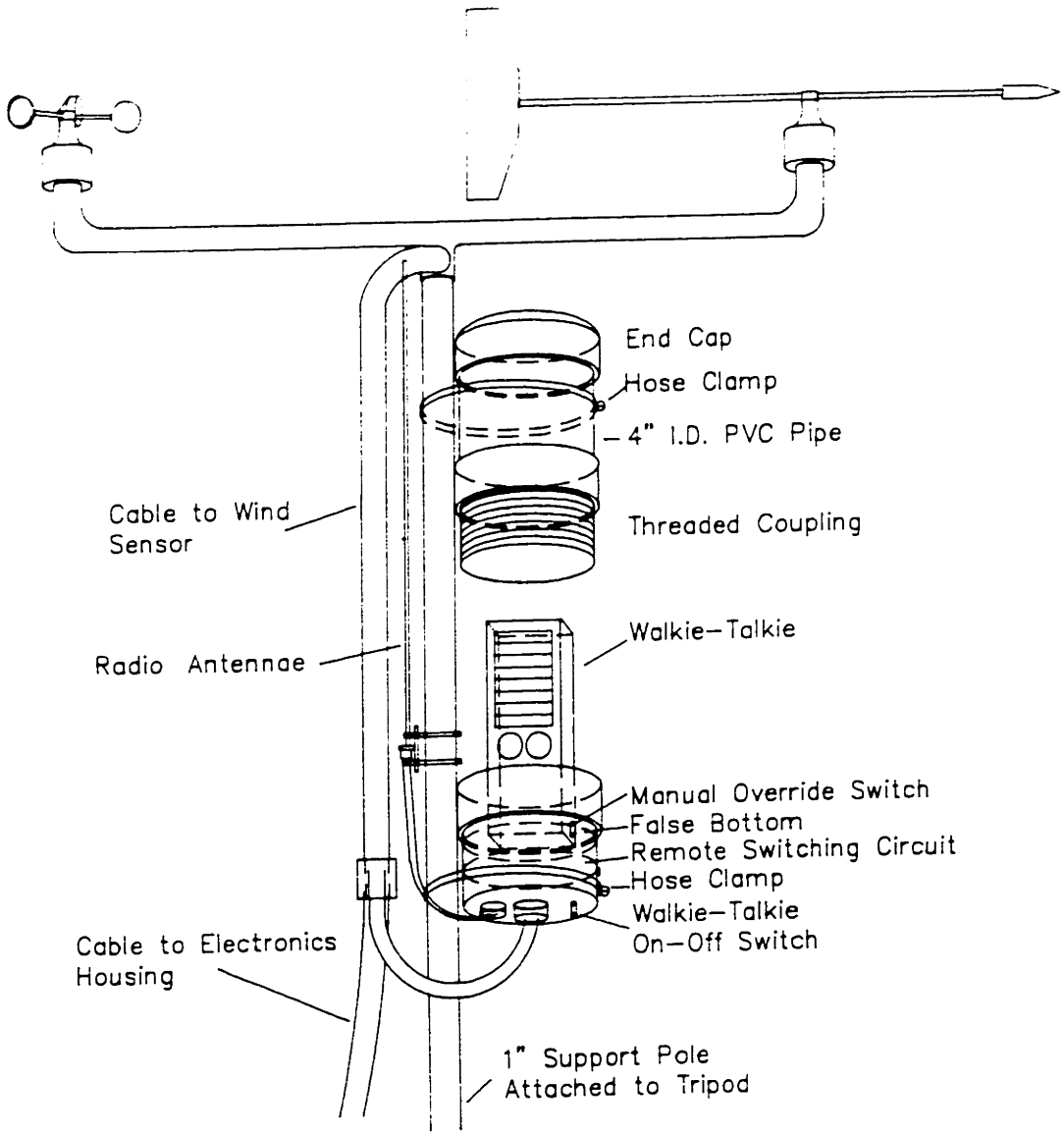

Figure 2.6 **Remote radio control assembly together with mounting and wind sensors.**

every 3 min. (The instantaneous values were later found to be in error.) The equipment was mounted 2 m above the water surface as shown in Figure 2.6.

2.2.4 Wave Staff

The wave staff, (Figure 2.4), was designed and built by Sea Data. It consisted of a 1"-dia PVC pipe approximately 2.2 m long, along 2 m of which were 100 equally spaced rings. The rings were formed by wrapping a wire once around the pipe at each location. Embeded in a groove cut down the side of the pipe were 10 KΩ resistors connecting each adjacent ring. The staff operated on the principle that the resistance in the water over a 2-cm path length was much less than 10 KΩ and therefore the water acted as a short. A voltage difference applied across the entire staff would see effectively a resistance of n × 10 KΩ, where n is the number of rings above the water surface. By Ohm's law this would drive a current which could then be measured. Tests with the staff alone in a wave tank showed it gave a reasonably linear response over that section which fit into the wave tank and responded quite well to passing waves. Later tests both with clip leads and a monotonically rising and falling water column illuminated design problems with capacitance in the connecting cable and the A-D sampling chip which were eventually corrected. The first deployment of the entire system was made in May of 1985, (Section 2.4.1). A review of data from this test showed that the wave staff was giving readings as if completely submerged for the entire deployment. This was due to a design oversight which had the positive voltage applied to the bottom ring of the staff. Therefore, rather than traveling through the staff the current

simply shorted through the water back to the main electronics housing. Unfortunately after this was fixed there was no time for another test field deployment leaving the wave staff unverified in the field. The results from the summer deployment indicated that the response time of the staff during intervals of runoff, i.e., during the trailing half of the wave crest and the leading half of the wave trough, were very poor. As a result wave data from the staff was for all practical purposes useless.

2.2.5 ABSS Sediment Profiler

The Acoustic Backscatter System (ABSS) is an ultrasonic adaptation of classical sonar principles for the purposes of detecting acoustic backscatter from sediment particles over close ranges. The ABSS used in these experiments was loaned by its designer, F. Hess of WHOI. The system emits a 5 MHz pulse having an adjustable duration of about 10 μs and a far-field beam width of about 0.8° (3dB). (Further details can be found in Hess and Bedford, 1985.) Due to the rapid attenuation of sound in water at high frequencies this instrument has an effective range of only a few meters. It was mounted looking vertically downward one meter above the bottom in this study. By monitoring in time the backscattered sound intensity from an emitted pulse, it is possible to obtain a profile of the scatterers as a function of the distance from the instrument. In the present application the response from each pulse was sampled 128 times at intervals of 13 μs yielding measurements separated by about 1 cm in distance.

The potential usefulness of this instrument for determining suspended sediment concentrations is substantial since it can sample unobtrusively in

a nearly continuous fashion in both time and space. There is at least one serious drawback to the use of this method, however. The acoustic backscatter is approximately a linear function of the sediment concentration, and a cubic function of the particle radius. As a result, to be able to determine concentration, it is necessary either to know independently the particle size and shape distribution or to calibrate the backscatter to independent measurements of concentration. To date the only calibration attempts have been made in the laboratory using suspensions having uniform particle sizes (Young et al., 1982).

The present study was conducted as part of an NSF sponsored international cooperative program between MIT and the Hungarian Academy of Sciences. Coincident with the field experiments described herein was a research program in which large in situ enclosures were being used to study biological and chemical processes in the lake. Briefly these enclosures consisted of a 3-m diameter flotation collar to which plastic side walls were attached. The side walls were anchored into the bottom sediment via a large metallic ring, thereby isolating a water column from exchange with the surrounding lake water. These enclosures offered an ideal opportunity to calibrate the ABSS in situ by artificially mixing the enclosed water to entrain different amounts of bottom sediment. ABSS profiles could then be compared to concentration measurements taken concurrently using the multi-port sampler shown in Figure 2.7. The sampler consists of a sliding cover sandwiched between front and back pieces. Five sample bottles could be threaded into the back (at 20-cm intervals). By moving the sliding cover, water was permitted to simultaneously enter and fill each of the sample bottles. Afterward the slide was returned to its original position closing off the sample bottles. This sampler could rapidly take a vertical

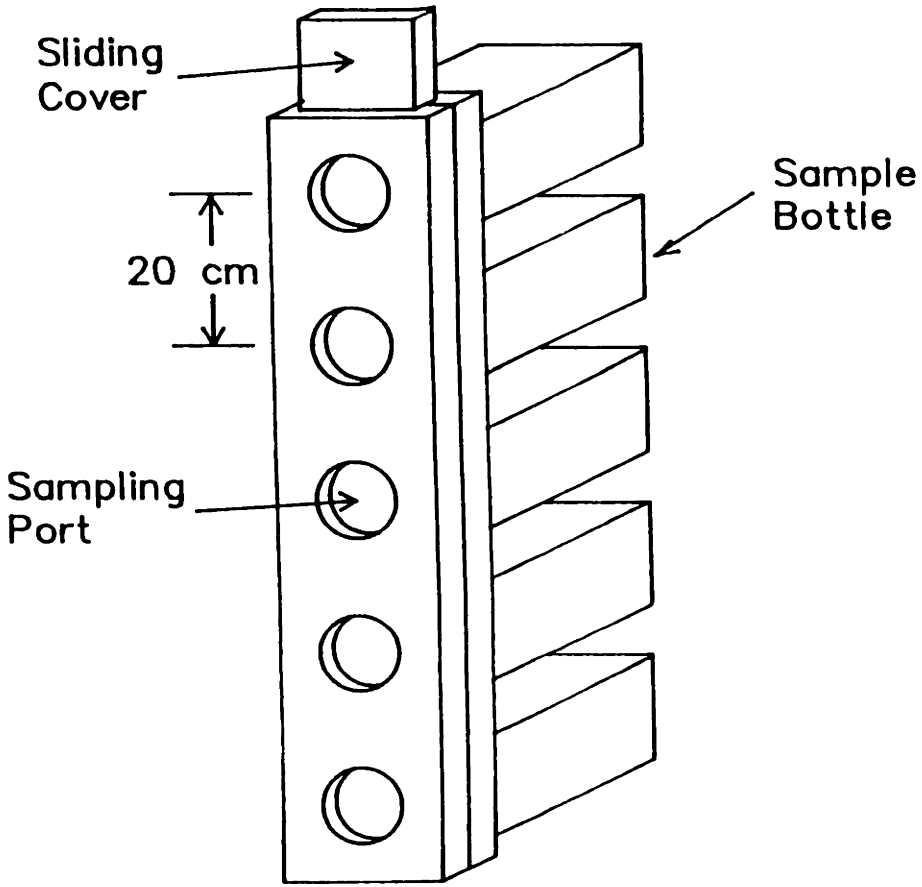

Figure 2.7 Multi-port sampler

profile of water samples over 1 m which could be used to determine concentration gravimetrically and if desired further analyzed for particle size distribution. Laboratory tests in a 1 m-deep tank showed that this system worked quite efficiently.

In the present study the use of ABSS seemed well suited for two reasons: i) it is easily capable of distinguishing between background and significantly higher suspended sediment levels thereby capturing critical conditions required for substantial resuspension, and ii) with the excellent opportunity for in situ calibration, it seemed reasonable that sediment concentration and therefore the resuspension flux could also be determined from the ABSS data.

Tragically, three circumstances combined to eliminate the collection of any useful ABSS data in Lake Balaton. First, the head containing the acoustic pressure transducer and receiver was inadvertently broken during unpacking at Lake Balaton. A spare head had been brought along for such emergencies, but it was an earlier model and had a much higher noise level. The ABSS with its best transducer head responded quite well to particle sizes in the 50μ-100μ range and would also detect scatter from those ranging down to 20μ or smaller by adjusting up the gain. This covers the range of fine sand and much of the silt region as well. Plans were to work largely in the Szemes region due to the large historical data base available there, the intense resuspension events which can be observed simply by the change in water color during storms, and because the sediments were known to fall within the detectable range discussed above. However, this field site was not convenient for the work being conducted by our Hungarian collaborators and striking out alone was totally impossible. As a result deployments were made at Tihany and Keszthely (Section 2.4).

In each location the suspended particle sizes were substantially smaller than at Szemes and combined with the low signal-to-noise ratio of the spare head, no resuspended sediment could be detected over the noise level, even at the peaks of storms. This was very disappointing since it eliminated a major area of emphasis of this work.

A third problem was not discovered until data reduction. Apparently sporadically only the first two complete ABSS profiles were recorded onto the cassette tape. The succeeding 38 recorded profiles were at least partial repeats of the initial two profiles in alternating succession. This behavior was quite difficult to pick out and was not noticed on predeployment tests. It was later determined that this was due to faulty components in the "ping-pong" data storage buffers used to hold the data immediately after it was collected.

2.2.6 BASS Velocity Meters

The Benthic Acoustic Stress Sensor, BASS, is a highly sophisticated velocity meter capable of making measurements in the three coordinate directions with a resolution of 0.3 mm/s and an accuracy typically of about 3 mm/s. It operates on the pulsed time-of-travel principle which is implemented as the time difference required by simultaneously generated acoustic pulses to travel in opposite directions along the same path. In still water the travel time in each direction is identical and is equal to the axis length divided by the speed of sound in water. In moving water a velocity component, vel_{ax}, aligned with the axis can be resolved from

$$vel_{ax} = \frac{L}{\Delta t}\left(-1 + \left(1+\left(\frac{c\Delta t}{L}\right)^2\right)^{0.5}\right) \simeq \frac{c^2\Delta t}{2L} \qquad (2.8)$$

where L is the axis length, Δt is the difference in the travel times of the two pulses and c is the speed of sound in water. (A more detailed description of the methodology and electonics used to implement this procedure can be found in Williams, 1985.) By building three orthogonal axes into one sensor it is possible to determine the velocity component in each coordinate direction. BASS uses four axes on each sensor arranged to form two orthogonal planes as shown in Figure 2.8. The measurement along the fourth axis is redundant, although it offers several interesting opportunities for data processing as discussed below.

The acoustic transducers are mounted on two vertically spaced horizontal rings. Each axis is inclined 45° to the horizontal and has a 15 cm path length. Towing tank tests have shown the horizontal and vertical cosine response has a maximum error of 5% of the speed along any axis until the flow angle comes within 20° of the acoustic axis. At this point wake effects from the mounting ring and the transducers are significant along that axis. In such a case for steady flow the velocity field can be computed from the three unaffected axes (Williams, 1985).

The computation of the flow velocity in the three coordinate directions can be done in several ways due to the presence of the redundant axis. Typically it is desired to resolve the velocity field into a north component, an east component, and a vertical component. It is convenient to define an intermediate coordinate system as shown in Figure 2.8 with the z direction aligned with the sensor's cylindrical axis and the x-y plane parallel to the transducer mounting rings. Once the velocity components in these coordinate directions are determined, they can be rotated into a final system depending on the sensor orientation. In all of the work conducted as a part of this study the sensor was mounted so that the z axis

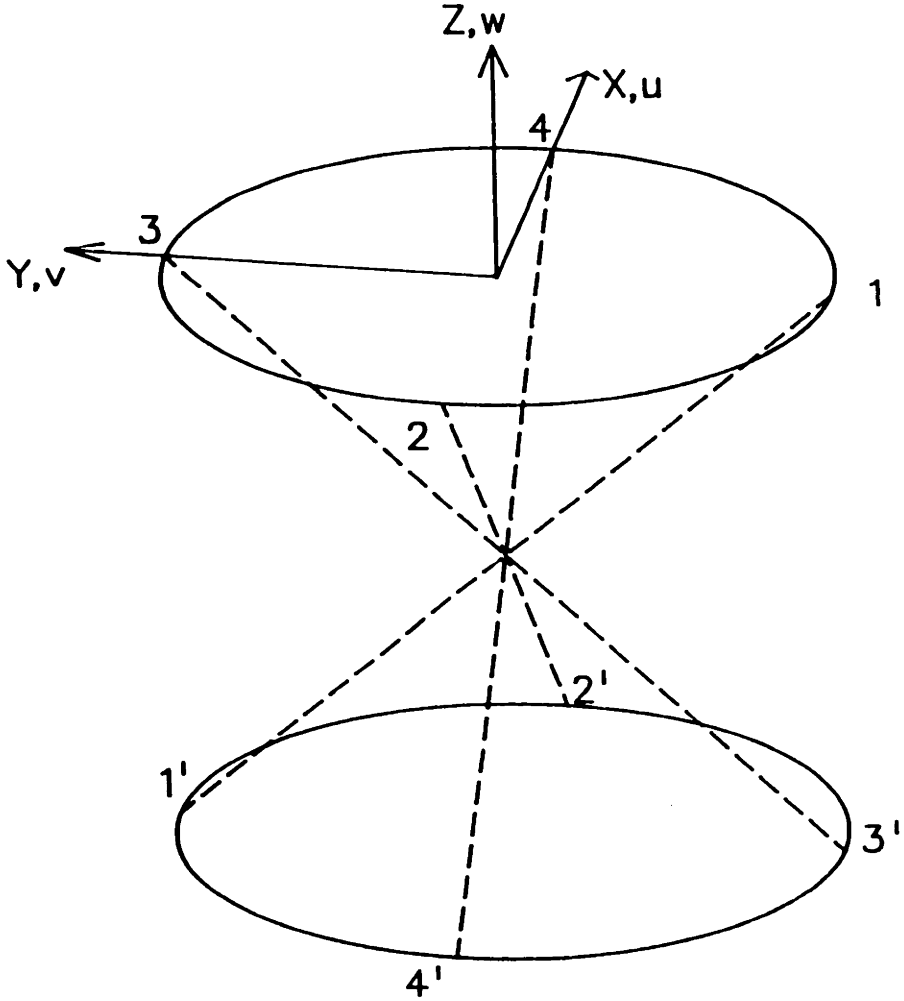

Numbers Denote Locations
of Acoustic Transducers

1–1', 2–2', 3–3', 4–4'
Define the Measurement Axes

Figure 2.8 Schematic of BASS measurement axes and intermediate coordinate system.

was nominally aligned with the vertical. This orientation is assumed throughout.

Making use of the intermediate coordinate system the velocity components are

$$u = \frac{\sqrt{2}}{2}(vel_{ax2} - vel_{ax4}) \tag{2.9}$$

$$v = \frac{\sqrt{2}}{2}(vel_{ax1} - vel_{ax3}) \tag{2.10}$$

$$w = -\frac{\sqrt{2}}{2}(vel_{ax3} + vel_{ax1}) \tag{2.11a}$$

or

$$w = -\frac{\sqrt{2}}{2}(vel_{ax2} + vel_{ax4}) \tag{2.11b}$$

In these definitions the convention has been adopted that a positive axis velocity is oriented in the direction from a transducer on the upper mounting ring toward one on the lower mounting rings. The redundant axis is apparent in the two possible definitions of the w velocity component. Theoretically, the values calculated using Equations (2.11a) and (2.11b) should be equal and therefore

$$vel_{ax2} + vel_{ax4} - vel_{ax3} - vel_{ax1} = 0 \tag{2.12}$$

Thus, theoretically, the velocity component along any one axis can be expressed in terms of the components along the other three axes. This information can then be used in Equations (2.9) or (2.10) allowing all three orthogonal components (i.e., u, v, w) to be computed from any three

of the four axes. This is particularly useful when wake effects are significant along any one axis as discussed before.

Another useful result of the redundant axis is that it offers a gross measure of the sensor's accuracy during use. This comes directly from Equation (2.12) which can be checked in time. A deviation from zero is an indication of possible sensor malfunction (e.g., excessive zero offset drift) or wake effects. This is returned to in Section 2.3.3.

Calibration of the current meter consists of determining the zero offset in still water, due primarily to capacitance in the connecting cables and transducers, and the calibration factor used to convert the voltage output to the along-axis velocity. The zero offsets were measured both in the field and in the laboratory. In the laboratory they were determined by placing the two BASS current meters in a small covered tank in still water.

To distinguish between the two current meters the connectors on each were colored brown and green, respectively. These colors are referred to throughout this thesis. In <u>every</u> field deployment the green BASS was mounted nearer to the bottom while the brown BASS was mounted nearer to the surface.

Histograms of a set of still water outputs for both BASS are shown in Figures 2.9 and 2.10. In these figures the horizontal axis is the 12-bit digitized output voltage in increments of 1 bit, (1 bit $\cong$ 0.03 cm/s), while the vertical axis is the per cent of occurrences of a specific output voltage out of the total number of observations, NRECS. The spread in the distributions around a central output varied significantly depending on where the test was run. Tests in the MIT laboratory typically yielded

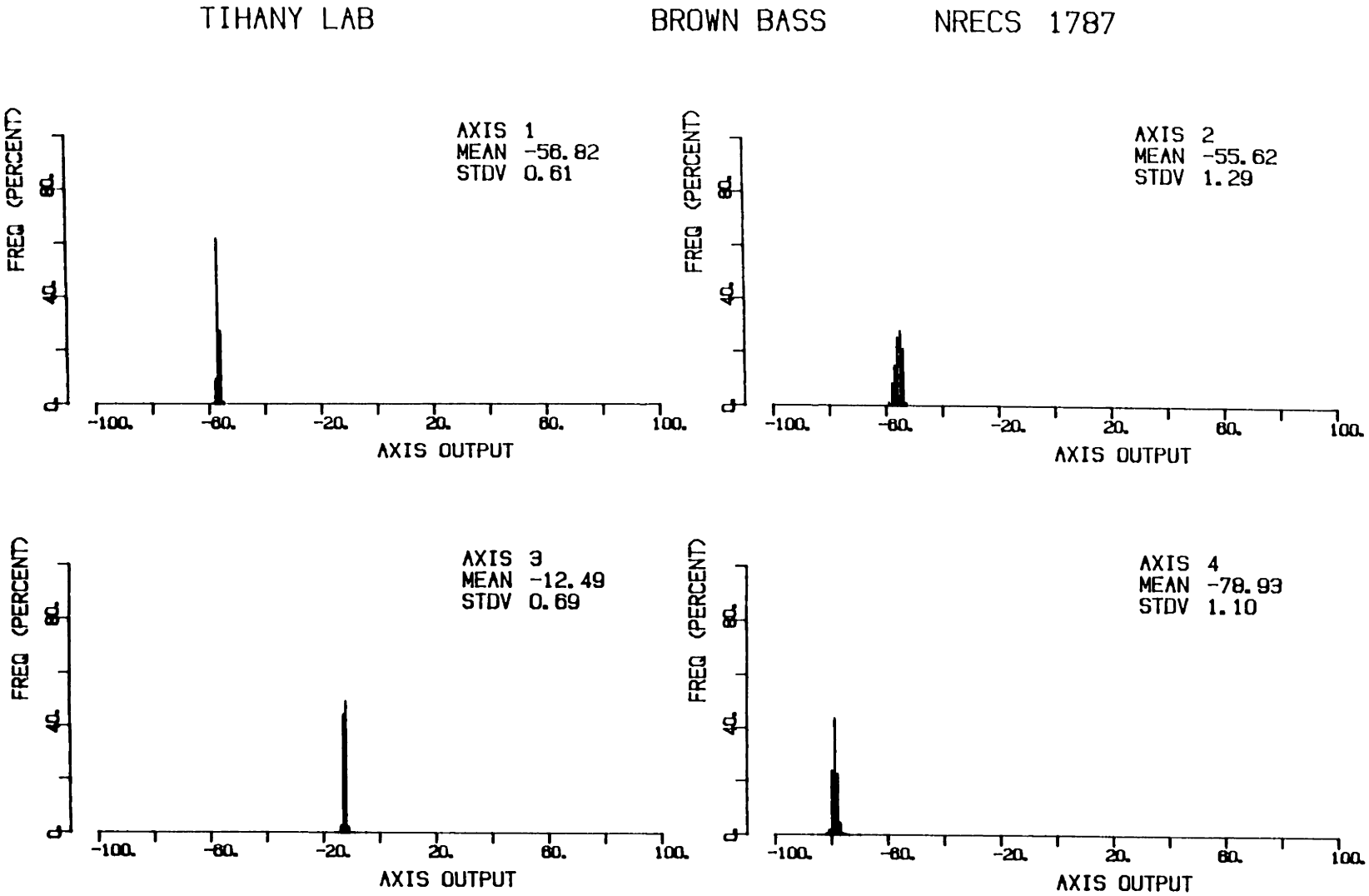

Figure 2.9 Zero calibration (still water) output for the four individual axes on the brown BASS. A total of 1787 samples were taken at 2Hz.

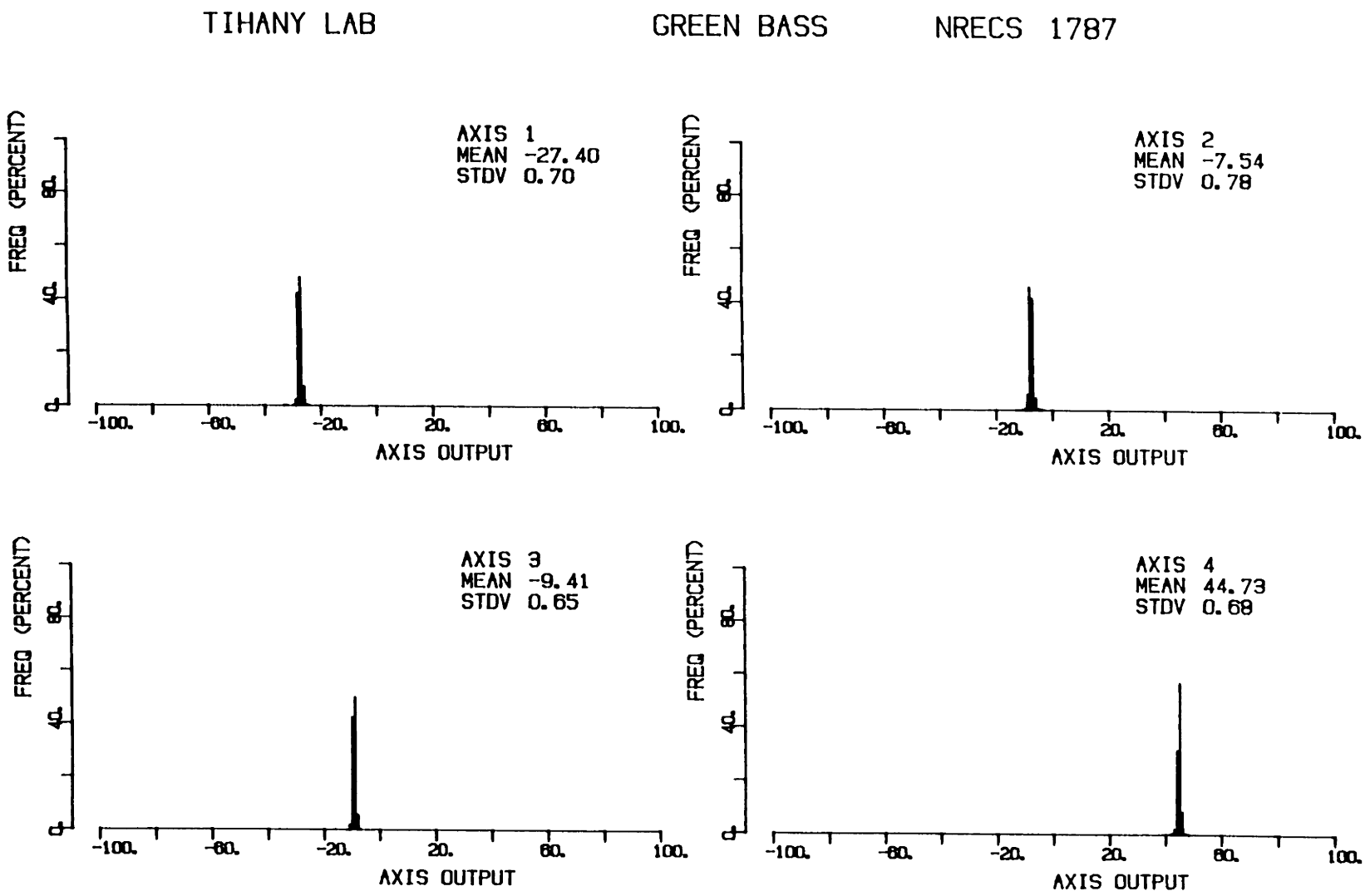

Figure 2.10 Zero calibration (still water) output for the four individual axes on the green BASS. A total of 1787 samples were taken at 2Hz.

larger spreads than those made at Woods Hole or in Hungary, presumably due to higher ambient noise levels at MIT.

In the field zero offsets were measured by enclosing each current meter in a large plastic bag during prolonged calm periods on the lake. This method typically gave slightly wider spreads in the offset distribution than the laboratory measurements, presumably due to small, residual currents within the bags.

A summary of the results of both the laboratory and the field offset measurements over a period of 2.5 months is given in Table 2.3. Between day 21 and 38 the initial Tihany deployment was made at which time the electronics housing flooded. This appears to have caused a jump in the zero offsets. However, the offsets of 7 of the 8 axes before and after this occurance remained constant within a 5 - 10 bit range. The lone exception was axis 2 of the brown BASS whose zero offset varied 22 bits over 33 days. While this variation is poor in relationship to the other axes it still represents an error of only about 0.65 cm/s. Additional field and post deployment laboratory zero offset tests were made. However, due to the corroded connector all of these data were lost. A visual observation of the data after the Keszthely deployment suggested no significant deviations in the offsets had occurred.

The time scale for any significant change in the zero offset is on the order of days. Therefore this should not seriously effect data involving fluctuating components of the velocity field, e.g., wave components, since this offset error would show up as a mean velocity which is removed as a first step in data processing.

Table 2.3 Summary of Zero Offset Results

Date	Time	Axis 1		Axis 2		Axis 3		Axis 4		*Site
		mean	stdv.	mean	stdv.	mean	stdv.	mean	stdv.	
				Brown BASS						
6/1	0:00	-43.0	4.6	-39.2	2.4	-31.4	2.8	-111.4	2.3	1
6/1	19:00	-43.4	3.6	-40.6	2.2	-30.4	2.2	-111.4	2.0	1
6/4	2:10	-42.5	3.6	-53.3	1.3	-31.8	1.5	-107.1	1.7	1
6/4	10:30	-42.5	3.3	-55.0	2.1	-32.0	1.8	-107.7	2.8	1
6/5	19:00	-40.9	4.3	-56.6	3.1	-31.0	4.3	-108.5	4.8	1
6/6	20:00	-41.3	3.4	-45.5	2.0	-31.9	2.1	-110.9	2.6	1
6/6	22:00	-41.4	3.5	-45.7	1.7	-32.0	2.2	-111.0	2.5	1
6/21	15:00	-44.4	1.6	-21.1	1.2	-29.0	1.5	-112.4	1.7	2
7/9	20:20	-56.4	4.6	-43.1	2.0	-11.5	3.4	-79.2	4.4	1
7/9	23:00	-56.2	4.6	-46.7	1.8	-11.2	3.1	-79.1	4.2	1
7/10	8:35	-59.7	3.0	-61.7	1.8	-8.4	2.1	-75.4	3.5	1
7/23	12:00	-56.8	0.6	-55.6	1.3	-12.5	0.7	-78.9	1.1	3
7/27	16:45	-62.2	15.0	-44.1	10.4	-7.4	12.6	-77.0	11.9	4
8/4	12:00	-55.8	0.8	-55.4	1.3	-12.4	1.3	-77.7	1.6	3
8/11	14:15	-55.0	7.0	-33.0	4.5	-13.8	4.6	-75.2	6.9	5
				Green BASS						
6/1	0:00	-36.6	2.2	-21.2	2.1	7.0	1.7	58.7	2.3	1
6/1	19:00	-35.8	2.3	-21.4	2.4	8.1	2.1	60.6	1.9	1
6/4	2:10	-34.8	2.5	-18.2	2.5	9.9	1.7	58.7	2.5	1
6/4	10:30	-35.5	2.9	-18.5	3.1	9.0	1.8	58.4	2.9	1
6/5	19:00	-37.2	2.8	-18.8	1.9	8.6	2.9	52.5	2.9	1
6/6	20:00	-29.9	2.5	-22.1	2.4	8.4	2.5	56.9	1.8	1
6/6	22:00	-29.8	2.5	-22.0	2.3	8.4	2.6	57.5	1.9	1
6/22	11:00	-22.3	1.2	-19.9	0.8	5.2	1.1	54.0	1.3	2
7/9	20:20	-26.9	1.9	-4.9	3.2	-3.8	2.7	49.3	2.5	1
7/9	23:00	-27.2	2.1	-4.0	3.0	-3.4	2.9	49.5	2.5	1
7/10	8:35	-30.5	2.1	4.3	1.7	-8.0	1.4	46.9	2.3	1
7/23	12:00	-27.4	0.7	-7.5	0.8	-9.4	0.7	44.7	0.7	3
7/27	16:45	-30.9	11.5	-3.8	13.3	-10.8	12.4	47.8	11.9	4
8/4	12:00	-27.1	1.2	-3.2	0.7	-4.8	0.6	45.5	0.8	3
8/11	15:00	-27.9	3.4	-2.1	3.3	-3.9	4.1	46.3	4.5	5

*the test sites were as follows:
1 - laboratory at MIT
2 - Hungarian Center for Water Resources Development, Budapest, Hungary
3 - laboratory at Tihany, Hungary
4 - in situ, Tihany field site
5 - in situ, Keszthely field site

It is also necessary to determine by calibration a factor to convert the voltage output to the velocity, i.e., the factor β in the equation

$$vel_{ax} = \beta(B - ZO) \tag{2.13}$$

where B is the digitized output voltage in bits and ZO is the zero offset voltage in bits. Using Eqns. (2.8) and (2.13)

$$\frac{c^2 \Delta t}{2L} \cong \beta(B - ZO) \tag{2.14}$$

Calibration can be performed using nanosecond delay lines, which simulate a velocity measurement by sending a selected Δt into the integrating capacitators of each axis and then recording the digitized output voltage. β can then be determined from the slope of a plot as shown in Figure 2.11. This process is repeated for each axis and the results summarized in Table 2.4.

Table 2.4 BASS Calibration Coefficients

	Axis 1	Axis 2	Axis 3	Axis 4
		Brown BASS		
β (cm/s/bit)	0.0310	0.0311	0.0310	0.0311
		Green BASS		
β (cm/s/bit)	0.0310	0.0310	0.0310	0.0310

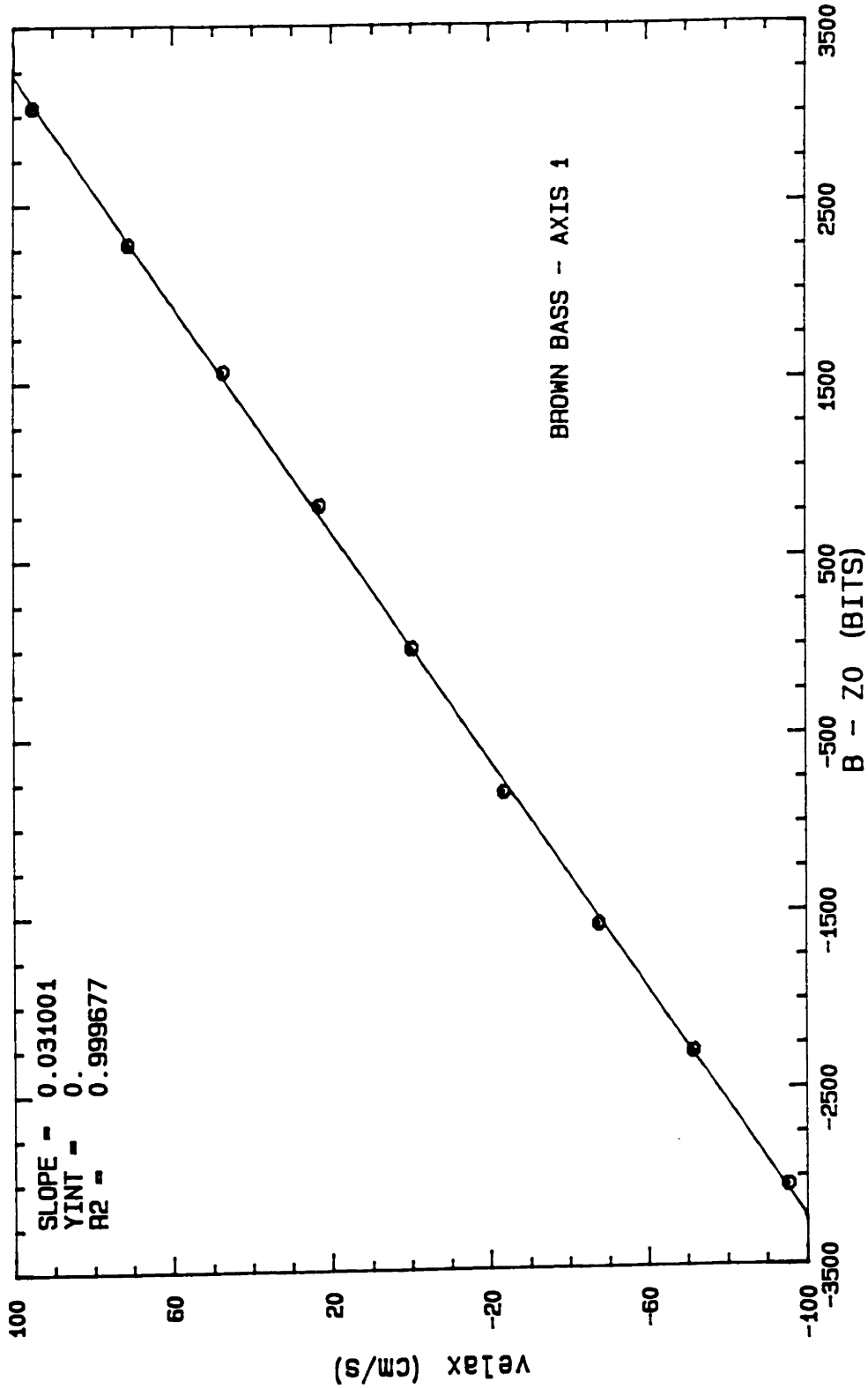

Figure 2.11 Example of a nanosecond delay line calibration curve for one BASS axis. Vel_{ax} is defined in Eq. (2.8).

These values of β were then verified in the towing tank of the Research Center for Water Resources Development in Budapest, Hungary. In this work the precise sensor orientation could not be determined. Therefore, the vector magnitude was computed from the axes' voltage outputs and plotted vs. the carriage speed. The slope was then equal to β. This was done for both sensors using two different orientations. The results are shown in Figure 2.12 and confirm the nanosecond calibrations.

2.2.7 Tripod

The equipment described above was mounted on a 2 m-high × 2 m-on-a-side tripod made of 4 cm × 4 cm square aluminum members, Figure 2.13. Each tripod leg rested on a foot made of 4 mm-thick aluminum plates having an area of 0.13 m^2. Each leg was secured into the bottom using two 1"-dia × 1.8 m-long pipes driven into the mud, one attached to the foot and the other attached about 1.3 m above the foot using a guy wire. The remote switch and wind equipment were mounted on a 1"-diameter steel pipe attached to one of the tripod legs, while the electronics housing and remote recorder capsule were mounted vertically along another leg. The wave staff and two BASS current meters were mounted in a vertical line at the geometric center of the tripod thereby being greater than 1.1 m from any vertical strucuture. None of the horizontal supports were at the same level as the current meters. (The instrument arrangement is shown in Figure 2.4.) The BASS current meters were attached at the top with two vertical rods connected to a crossing piece made of 2 cm aluminum angle. At the bottom they were guyed to each leg using 31-gauge stainless steel

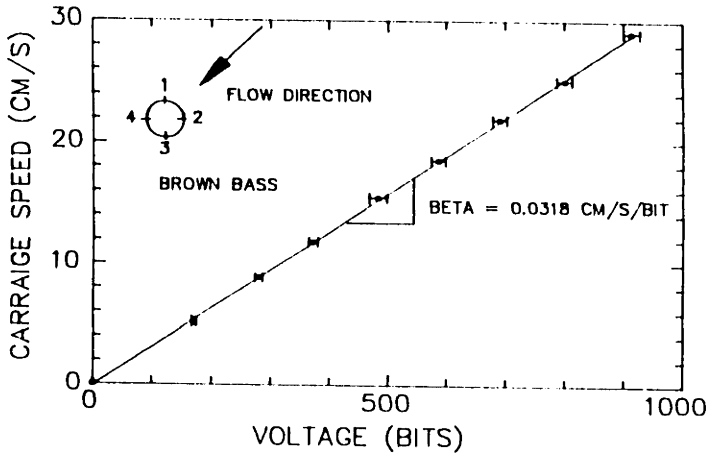

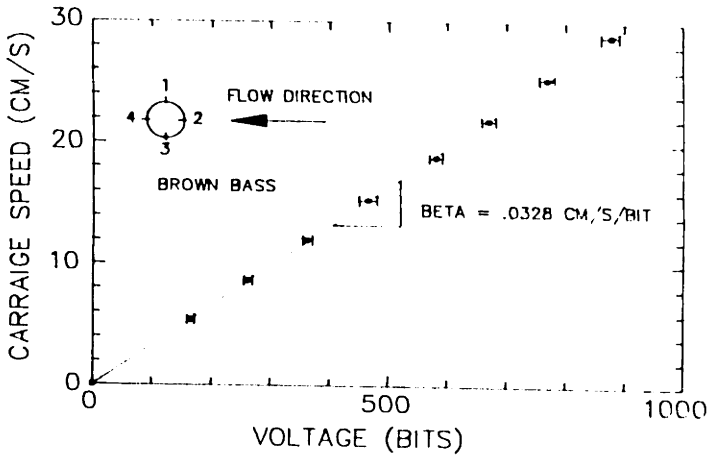

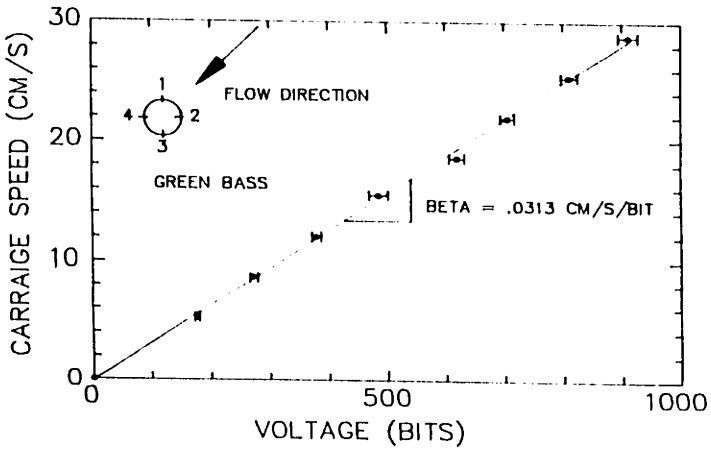

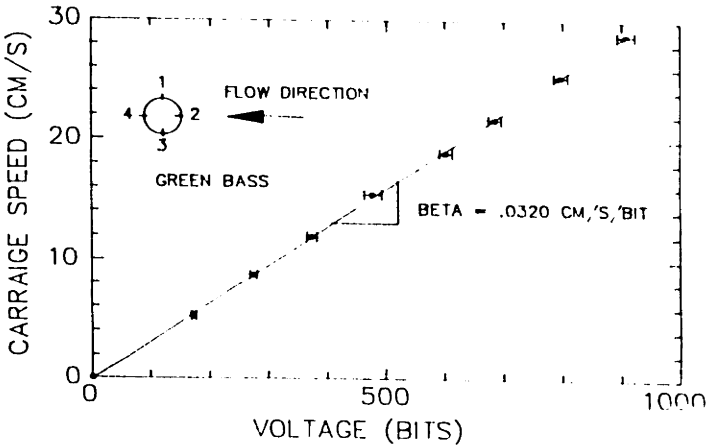

Figure 2.12 **Towing tank calibrations of both BASS using two different sensor orientations.**

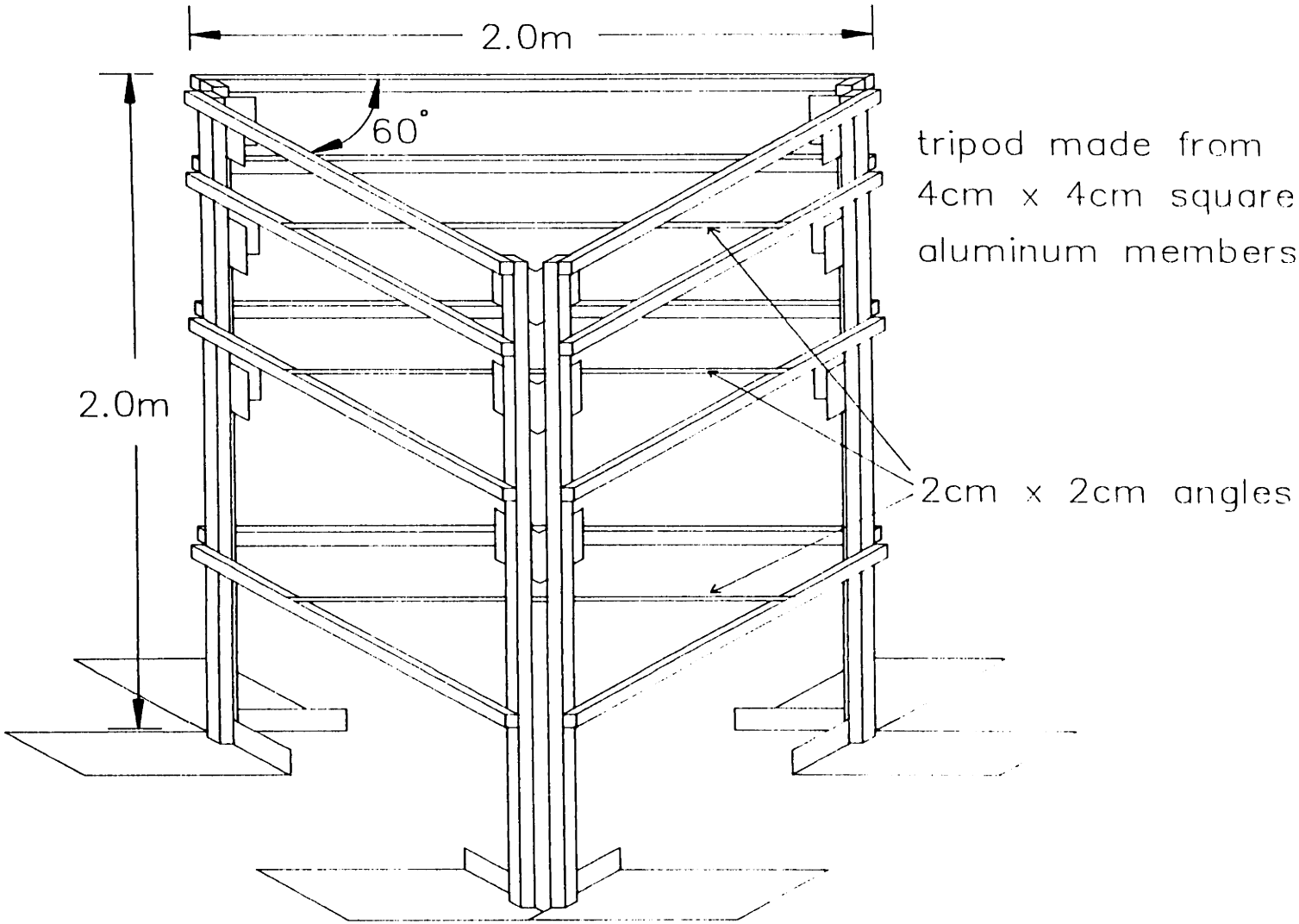

Figure 2.13 **Tripod used for equipment mounting during Lake Balaton deployments.**

wire. A U-shaped arm was used to run the wires connected to the lower acoustic transducers up to join with the wires connecting the upper transducers while causing a minumum amount of flow disturbance.

2.3 DATA ANALYSIS

Due to the problems with the wave staff and sediment profiler the majority of the data analysis that was performed concerned the current meter data. Specifically, this involved determination of a mean velocity and wave properties. The procedure used is outlined below. The redundancy in the velocity measurement also made it possible to check the accuracy of the BASS current meters during the period that measurements were taken.

2.3.1 Mean Velocity Determination

As presented in Table 2.2 samples were usually taken in six-minute "bursts." Therefore averaging to determine the mean velocity was limited to a six-minute period or shorter. Given the typical transverse seiche period of 30-40 minutes this averaging time seemed sufficiently long. Before computing the mean velocity the data was run tested for stationarity of the mean, (Bendat and Piersol, 1971). Both three-minute and six-minute velocity means were computed and typically compared quite closely.

2.3.2 Wave Data Analysis

Wave statistics (height and period) were computed from the vertical velocity component of the upper current meter using linear wave theory.

The use of linear wave theory, which is equivalent to Stokes first-order wave theory, can be justified in two ways. First, Stokes theory in general is valid when

$$\tilde{\epsilon} \equiv \frac{a}{d} \ll 1 \quad \text{and} \quad \tilde{\mu} \equiv \frac{d}{\lambda} \sim O(1)$$

and in particular if

$$\frac{2\tilde{\epsilon}}{\tilde{\mu}^2} < 26$$

where a is the wave amplitude, d is the water depth, and λ is the wave length. Typical values encountered in this field study were d = 2 m, a = 0.10 m, and T = 2 sec (T is the wave period). Using linear theory these yield λ = 6.1 m and lead to the results

$$\tilde{\epsilon} = 0.05$$

$$\tilde{\mu} = 0.33$$

$$\frac{2\tilde{\epsilon}}{\tilde{\mu}^2} = 0.9$$

which easily satisfy the criteria. The appropriateness of using Stokes first-order theory is verified by comparing the magnitude of the first and second terms in higher-order Stokes theory, viz.:

$$\eta(x,t) = \eta^{(1)}\cos(kx-2\pi ft) + \eta^{(2)}\cos 2(kx-2\pi ft) + \ldots\ldots$$

$$\eta^{(1)} \equiv a$$

$$\eta^{(2)} \equiv \frac{ka^2}{4}\frac{(\cosh kd)(3+2\sinh^2 kd)}{\sinh^3 kd}$$

where $\eta(x,t)$ is the surface displacement, $\eta^{(1)}$ and $\eta^{(2)}$ are the magnitudes of the first- and second-order terms, k is the wave number, and f is the frequency. Using the previous typical conditions yields

$$\eta^{(2)} \approx 0.01\eta^{(1)}$$

confirming the use of linear wave theory.

Accepting linear theory, the wave associated vertical velocity, w_w, at any position in the water column given monochromatic waves of frequency f_o is equal to

$$w_w(x,z,t) = \frac{a}{LTF_{wa}}\cos(kx - 2\pi f_o t + \theta) \qquad (2.15)$$

where

$$LTF_{wa}(f_o,h_c) = \frac{\sinh kd}{2\pi f_o \sinh kh_c} \qquad (2.16)$$

h_c is the elevation above the bottom at which w_w is to be determined and θ is a phase angle. A Fourier decomposition of the vertical velocity time series from such a wave train yields a single, complex set of Fourier coefficients, the magnitude of which is equal to a/LTF_{wa}. In a real water

body waves are not monochromatic but rather are a combination of waves of many frequencies. Thus a Fourier decomposition of a real vertical velocity time series will yield many sets of Fourier coefficients each being valid at a different frequency. Denoting $W_w(f,h_c)$ as the magnitude of the Fourier coefficients for a given frequency computed from measurements at an elevation h_c, the wave amplitude at the corresponding frequency can be computed as

$$a(f) = W_w(f,h_c) \cdot LTF_{wa}(f,h_c) \tag{2.17}$$

Using Equations (2.16) and (2.17) it is also possible to define a transfer function $LTF_{ww}(f,h_{c1}, h_{c2})$ relating the vertical velocities at two different elevations in the water column through their Fourier coefficients, viz.

$$W_w(f,h_{c1}) = LTF_{ww}(f,h_{c1},h_{c2})W_w(f,h_{c2}) \tag{2.18}$$

where

$$LTF_{ww}(f,h_{c1},h_{c2}) = \frac{\sinh(kh_{c1})}{\sinh(kh_{c2})} \tag{2.19}$$

The frequency dependence in Equation (2.19) is implicit through the dependence of k on f since

$$f^2 = \frac{gk}{4\pi^2}\tanh\ kh \tag{2.20}$$

In summary Equations (2.16) and (2.17) provide a method for computing wave amplitides from measured vertical velocities, while Equations (2.18) and (2.19) allow a further check on the assumption of linear wave theory since $W_w(f,h_{c2})$ can be computed from $W_w(f,h_{c1})$ and $LTF_{ww}(f,h_{c1},h_{c2})$ and compared with the $W_w(f,h_{c2})$ determined directly from vertical velocity measurements at elevation h_{c2}. The same comparison can also be made using the power spectral density defined as

$$S_{ww}(f) = \frac{W_w^2}{2\Delta f} \tag{2.21}$$

where Δf is the frequency bandwidth (Δf^{-1} = sampling duration).

Complete vertical velocity time series were not recorded in this study. Rather discrete samplings of these time series were taken for finite durations. Specifically, all sampling was done at 2 Hz and unless otherwise noted for 6-minute durations. Nominally this yielded 720 points for each spectral computation. However, due to the redundancy in the current meter two vertical velocity measurements were actually made every 0.5 sec (i.e., Equations 2.11(a) and 2.11(b)). Before processing these measurements were averaged together. This doubled the number of degrees of freedom in the spectral estimate as noted below.

The spectral computation procedure was to first average the two simultaneous vertical velocity measurements, run test the data for stationarity (Bendat and Piersol, 1971), divide the time series into several equilength segments (typically 4 or 6), apply a 10% cosine window to each segment, remove the mean and any linear trend from each segment, FFT and compute an estimate of the power spectral density for each segment,

average the estimates for each segment together, and finally smooth the estimate in the frequency domain using a running average. The stability of the resulting estimate is defined in probabilistic terms as

$$P\left[\frac{NDF}{\chi_2} \cdot \hat{S}(f) < S(f) < \frac{NDF}{\chi_1} \cdot \hat{S}(f)\right] = 0.90 \qquad (2.22)$$

where P( ) stands for probability of, $\hat{S}(f)$ is the spectral estimate computed as described above, S(f) is the true power spectrum, NDF is the number of degrees of freedom in the system, and χ_1 and χ_2 are the values of a chi-squared distribution for NDF degrees of freedom and $\chi = 0.05$ and $\chi = 0.95$ respectively. Equation (2.22) means that there is a 90 per cent chance that the true spectrum falls within the computed upper and lower limits. Note: for large numbers of degrees of freedom (NDF > 100)

$$\frac{NDF}{\chi_2} \approx 10^{-NDF^{-0.5}} \qquad (2.23a)$$

$$\frac{NDF}{\chi_1} \approx 10^{NDF^{-0.5}} \qquad (2.23b)$$

It is apparent that the spectral estimate is more stable and hence known to within a smaller interval for larger NDF. In the present application

$$NDF = 4 \cdot NSEGS \cdot NBAND \qquad (2.24)$$

where NSEGS is the number of segments the orginal data set is broken into and NBAND is the number of bands used for smoothing in the frequency domain. The coefficient four is twice that in the normal definition of NDF

reflecting the fact that two measurements of the vertical velocity (i.e., Eqs. 2.11a and 2.11b) were averaged to get the "original" data set.

Typical results of the check on linear theory discussed above are shown in Figures 2.14 and 2.15, which were computed with data from the Keszthely and Tihany field sites, respectively. In Figures 2.14a and 2.15a the solid line is the power spectral density, hereafter called simply the power spectrum, computed from the data from the upper current meter. The dashed line is the power spectrum computed at the elevation of the lower current meter using the linear theory transform, $LFT_{ww}(f,h_{c1},h_{c2})$, and the upper current meter power specturm. The dotted line is the power spectrum computed from data from the lower current meter. Figures 2.14b and 2.15b show a comparison of the latter two lines at an expanded vertical scale. In both cases agreement is excellent, being within about 5 percent over the frequency range from 0.30 to 0.80 Hz, which as discussed below corresponds to the linear surface wave region. The low-frequency energy is most likely associated with the mean current while any energy associated with surface waves at high frequencies is filtered out by attenuation in the water column. In all cases the predicted and measured spectra have almost identical shapes with the predicted spectra usually being slightly larger than the measured. It is quite likely that this discrepancy is due to imprecise measurement of the current meter elevations above the bottom. Trials showed that a change in this distance of 1 to 2 cm could easily account for the difference.

As discussed above wave amplitude spectra were computed using Equations (2.16) and (2.17) together with the vertical velocity spectra obtained from the upper current meter. The shape of the transfer function

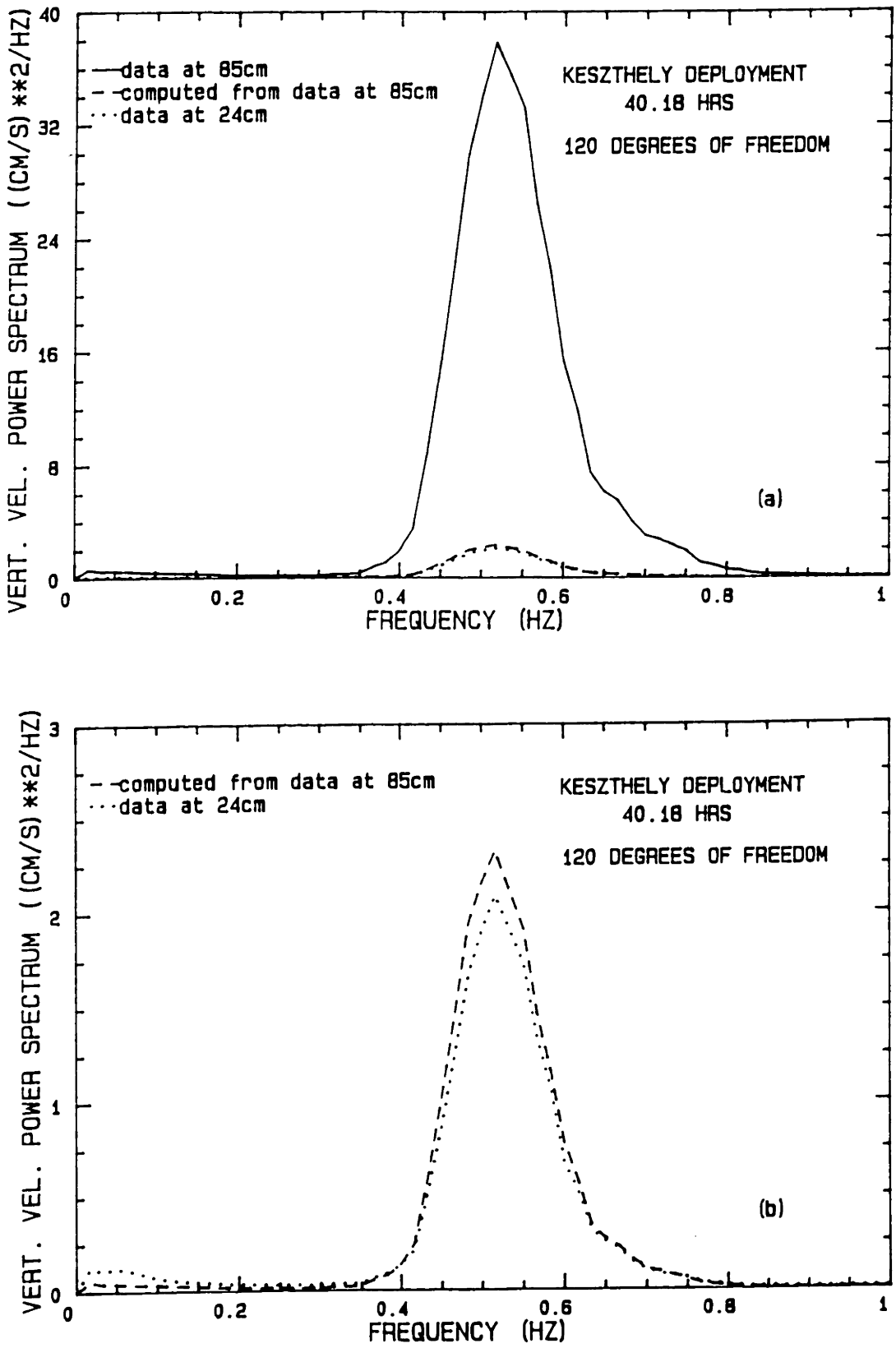

Figure 2.14 Test of the applicability of linear wave theory at the Keszthely deployment site using velocity measurements at two depths and the linear transfer function defined in Eq. (2.19).

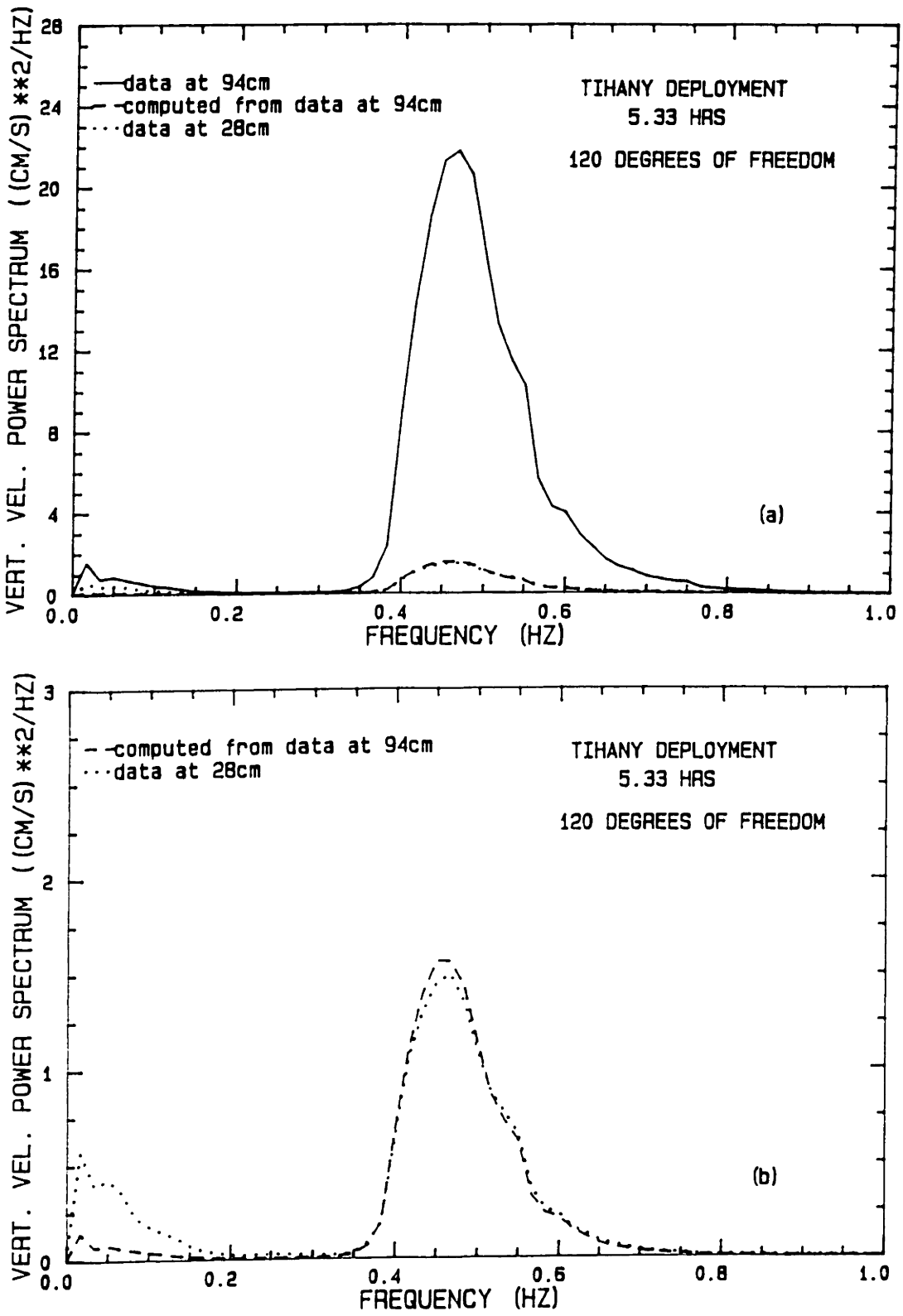

Figure 2.15 Test of the applicability of linear wave theory at the Tihany deployment site using velocity measurements at two depths and the linear transfer function defined in Eq. (2.19).

$LTF_{wa}(f,h_c)$ is shown in Figure 2.16 for the values of total depth and measurement height used in the Tihany and Keszthely deployments. It is evident that attenuation of the vertical velocity signal in the water column overlying the upper current meter becomes substantial at frequencies above about 0.8 Hz. Figure 2.17a (as well as Figures 2.14 and 2.15) indicates the existence of a large concentration of energy from about 0.35 to 0.75 Hz and a much smaller amount below 0.05 to 0.1 Hz. Visual observations on the lake yielded a characteristic wave period of approximately 2 seconds and suggest that the energy around 0.5 Hz is associated with surface waves. During the calm period Figure 2.17b shows that the energy in the 0.5-Hz region is very small particularly in comparison to that in the low-frequency region. This growth and decline of energy around 0.5 hz characteristically corresponded to observation of the presence or absence of surface waves and was independent of the mean flow velocity. Thus it was assumed to be solely due to surface waves. This assumption is strengthened further by the applicability of linear wave theory in this frequency range as shown previously. As a wave field decayed and during calm periods the energy associated with the surface waves decreased to the point where it was not significantly distinguishable from the energy being cascaded from the mean flow and/or other sources of turbulence. This typically occurred at significant wave heights of about 4 cm (see below). Therefore 4 cm was used as a cutoff point below which wave properties were not computed.

Figure 2.18 shows the amplitude spectra obtained using $LTF_{wa}(f,h_c)$ on the vertical velocity spectra in Figure 2.17a. Assuming that the amplitude spectrum decreases monotonically on either side of the spectral peak

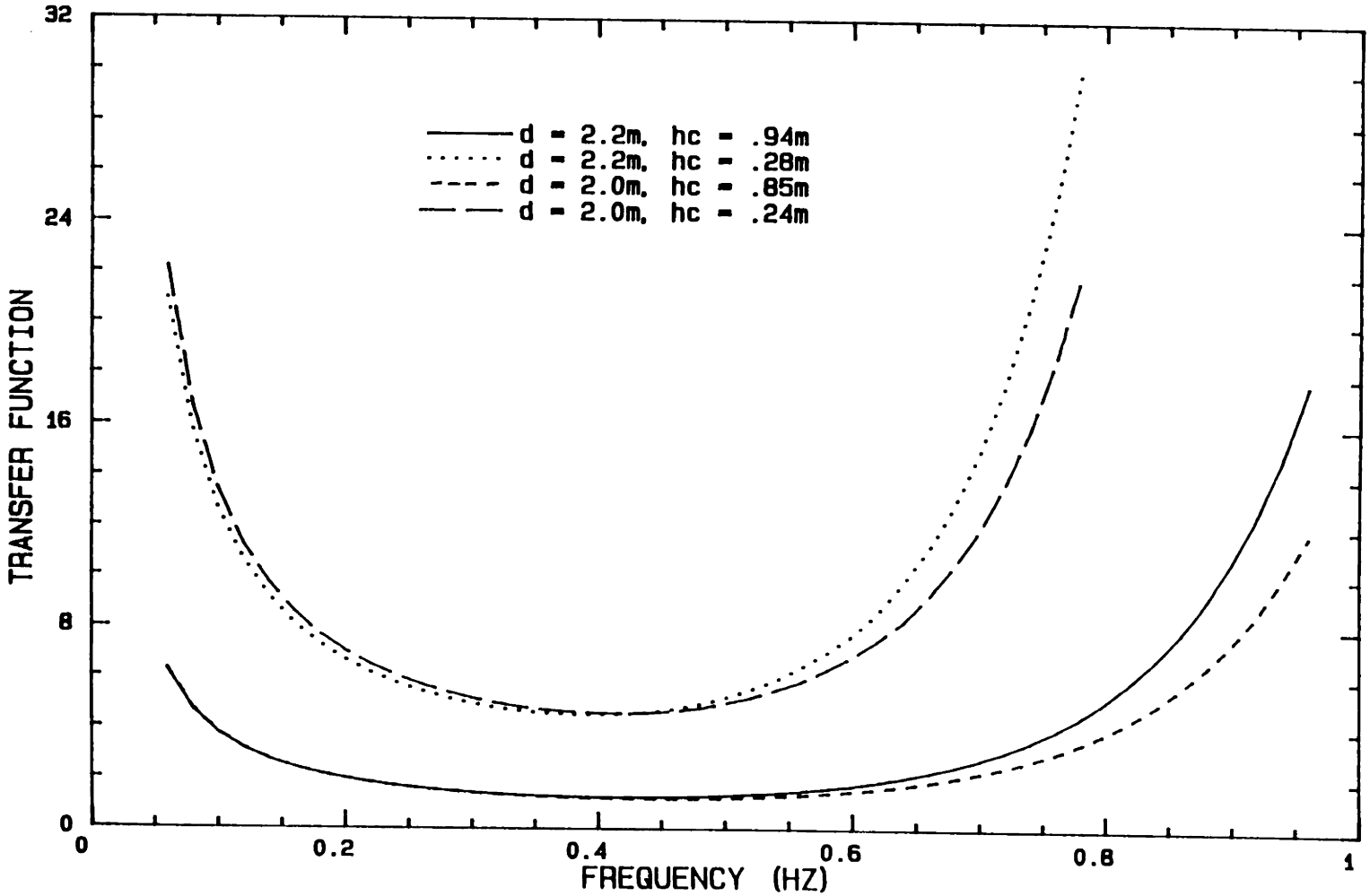

Figure 2.16 Linear transfer functions between wave amplitude and vertical velocity, Eq. (2.16), as a function of wave frequency for the depth and measurement height combinations used at the Tihany and Keszthely deployments.

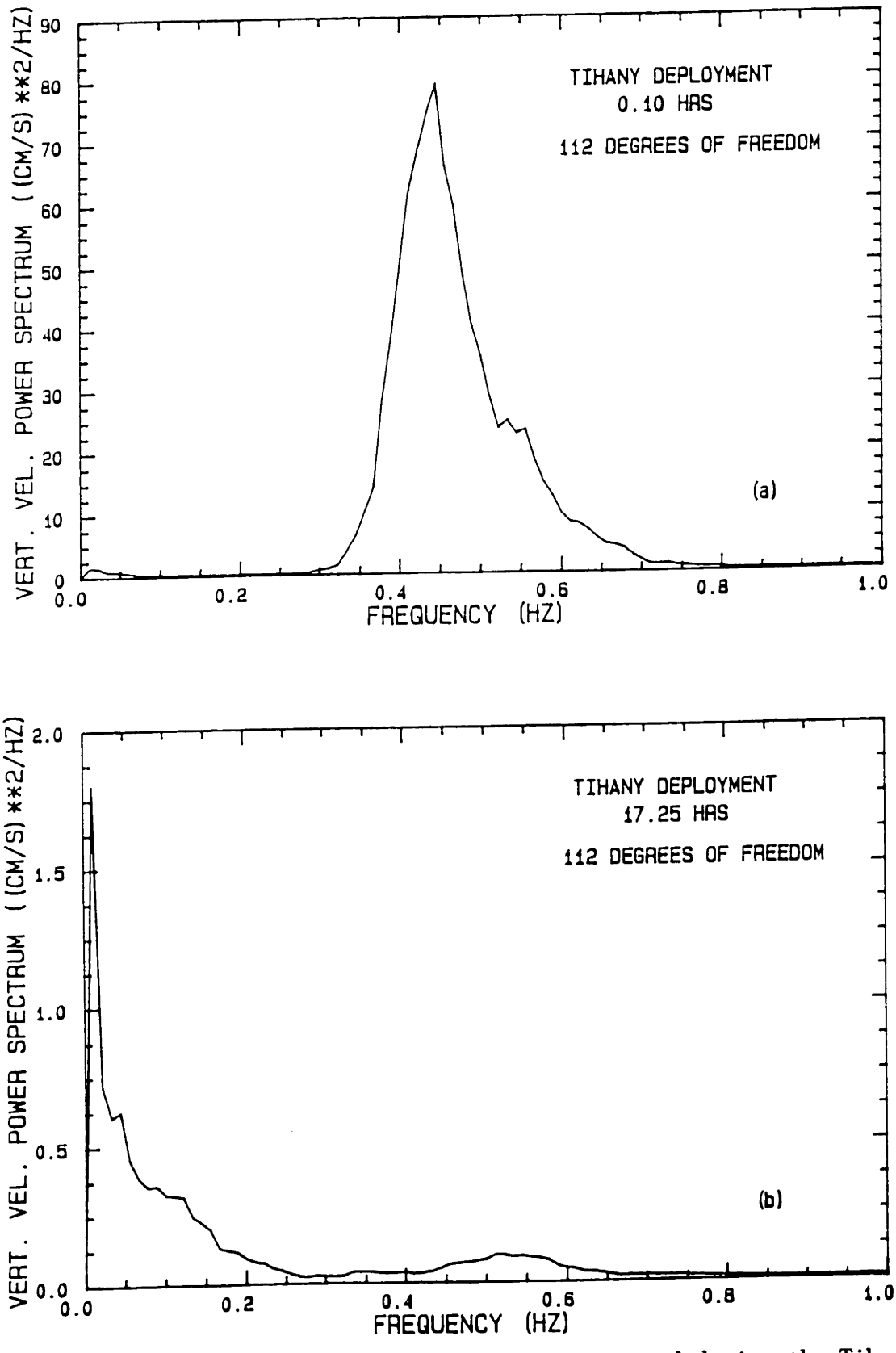

Figure 2.17 Vertical velocity power spectra measured during the Tihany deployment during intervals of (a) substantial surface waves and (b) near calm.

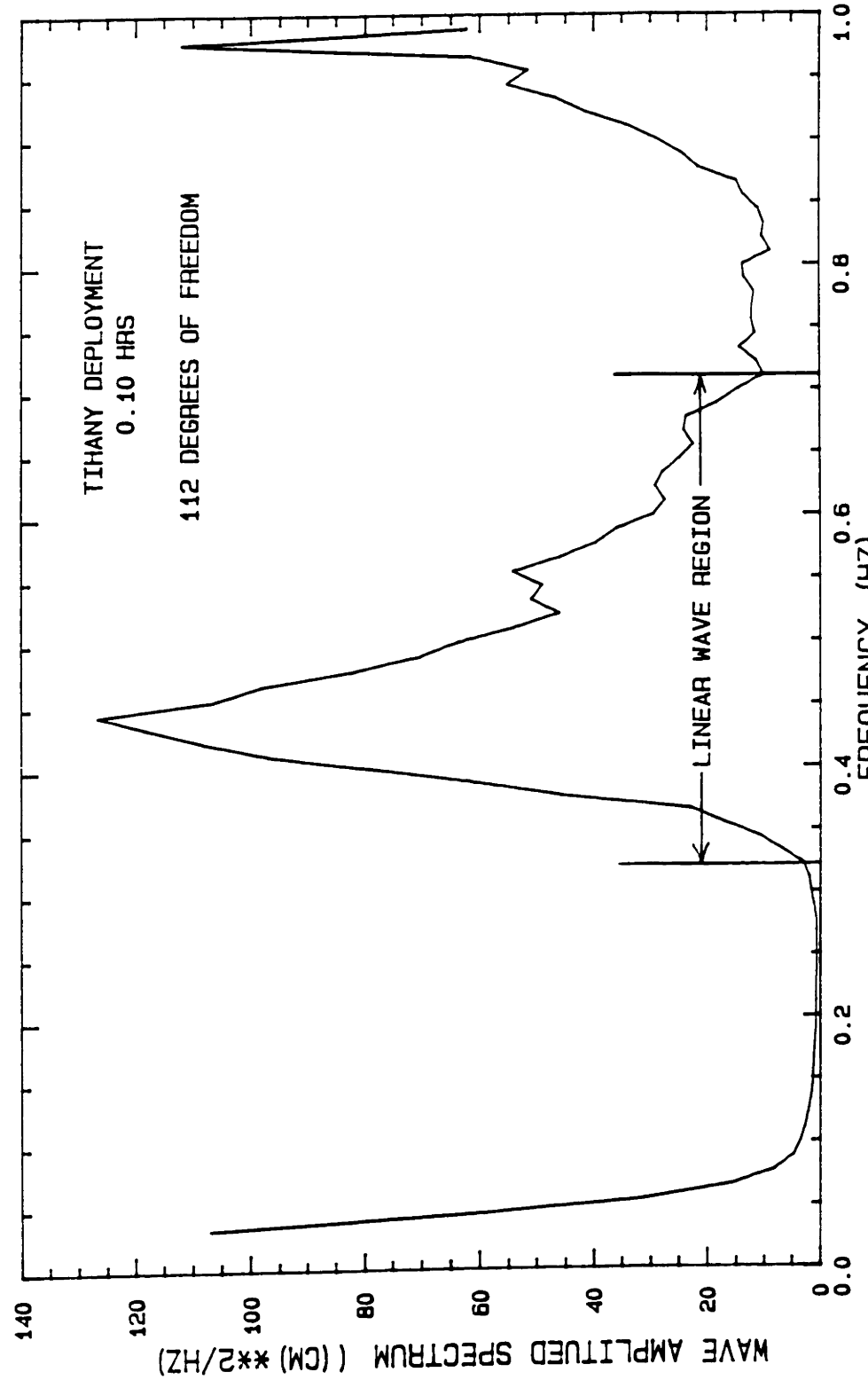

Figure 2.18 Wave amplitude power spectrum obtained from vertical velocity spectra in Figure 2.17a and Eq. (2.16).

(except for possible local "bumps" presumably due to spectral instability) it can be truncated at the upper and lower frequency where this ceases to occur. The included frequency range was treated as the "linear wave region." To confirm this result a comparison was made between the measured spectra at each elevation and the linear transfer function. Typically the two methods agreed within 5-10 per cent. The frequencies within the linear wave region were used to compute the statistical wave properties.

Considering waves to be a weakly steady-state, ergodic random process, (and in particular a normal process with zero mean), with a narrow-banded spectrum and statistically independent peaks, it can be theoretically derived that the wave heights follow the Rayleigh probability law (Ochi, 1982). Thus, various statistical properties of wave heights are most commonly estimated based on the Rayleigh probability assumption. In particular the significant wave height, defined as the mean height of the one-third highest waves, can be computed as:

$$H_s = 4.01\sqrt{M_o} \tag{2.25}$$

where M_o is the zeroth-order moment of the wave amplitude spectrum which is equivalent to the area under the spectrum. Note, an arbitrary-order spectral moment is defined as

$$M_n = \int_0^\infty f^n S(f)df \tag{2.26}$$

Where S(f) is the power spectrum. The most often violated of the assumptions behind the Rayleigh probability distribution is the narrow

bandedness condition and therefore it is useful to have a criterion for when this condition holds. At least two may be used. Ochi (1982) shows that

$$H_{s_{true}} \leq H_{s_{Rayleigh}} \leq 1.08 H_{s_{true}} \qquad (2.27a)$$

$$\text{if} \quad \epsilon \equiv (1 - M_2^2/M_0 M_4)^{1/2} < 0.8$$

Longuet-Higgins (1983) found that a wave spectrum can be considered narrow banded if

$$\upsilon^2 \equiv (M_0 M_2/M_1^2) < 0.36 \qquad (2.27b)$$

Thus these criteria may be checked to determine the suitability of using Eq. (2.25). All of the data taken as a part of this study was screened using Eqs. (2.27) and (2.28) and found to satisfy the narrow-banded criterion.

Based on Eq. (2.22) the significant wave heights are known to within

$$P[(NDF/\chi_2)^{1/2} \cdot \hat{H}_s < H_s < (NDF/\chi_1)^{1/2} \cdot \hat{H}_s] = 0.90 \qquad (2.28)$$

where $\hat{H}_s$ is the estimate obtained from Eq. (2.25) and H_s is the true value.

Several measures are commonly used for the wave period. Among them are

$$T_p \equiv (f_p)^{-1} \tag{2.29}$$

where f_p is the frequency of the wave amplitude spectral peak,

$$T_m \equiv M_0/M_1 \tag{2.30}$$

which is the mean period and

$$T_{zc} \equiv \sqrt{M_0/M_2} \tag{2.31}$$

which is the expected zero-crossing wave period.

2.3.3 Dynamic BASS Error Analysis

The redundancy in the BASS current meter leads to Eq. (2.12) as derived in Section 2.2.6

$$vel_{ax2} + vel_{ax4} - vel_{ax1} - vel_{ax3} = 0 \tag{2.12}$$

which can be checked during the course of the measurement program and therefore yield some information in a dynamic sense about the current meter performance. Clearly, it is possible that simultaneous errors in more than one axis could compensate one another in Eq. (2.12) and give a falsely low result; however, the possibility of even a gross performance check is unique in field instrumentation and can be exploited to yield a substantial amount of information.

There are two principal sources of error in the current meter measurement. One is due to the sensor electronics and would most likely show up as drift in the zero offset (Section 2.2.6) due to changes in the capacitance of the sensor cables or the circuitry itself. Also it was discovered that as the battery weakened the third axis of the green BASS frequently gave zero readings during the first 40 records (20 seconds) of each 3-minute on cycle due to the extra power drain on the system by the ABSS. A second source of error is due to turbulent eddies in the water column having a characteristic length scale smaller than the size of the sensor sampling area (each axis length = 15 cm). In particular these eddies could be the result of flow disturbances induced by the cage, rings, or transducers of the current meter itself.

To check for the possibility of such errors the deviation from zero of Eq. (2.12), hereafter called the residual value of Eq. (2.12) or just the residual, was solved for in time for each of the current meter data sets. The results from the Keszthely data set of August 15 to August 18, 1985 are illustrative of the typical BASS behavior and are presented below. The residual was broken down into its 3- or 6-minute mean value, the variance from the mean value, and the Fourier decomposition of the fluctuations from the mean value.

Figures 2.19a and 2.19b are comparisons between the 6-minute mean residual and the 6-minute mean components along the two vertical measurement planes from each BASS. The outputs have been left in bits and can be converted to cm/s using Eqs. (2.11) and (2.13). The brown BASS shows substantial variability in its mean residual which ranges over 65 bits. This variability was not correlated to the mean output or variance along any one axis or to the horizontal velocity components in either

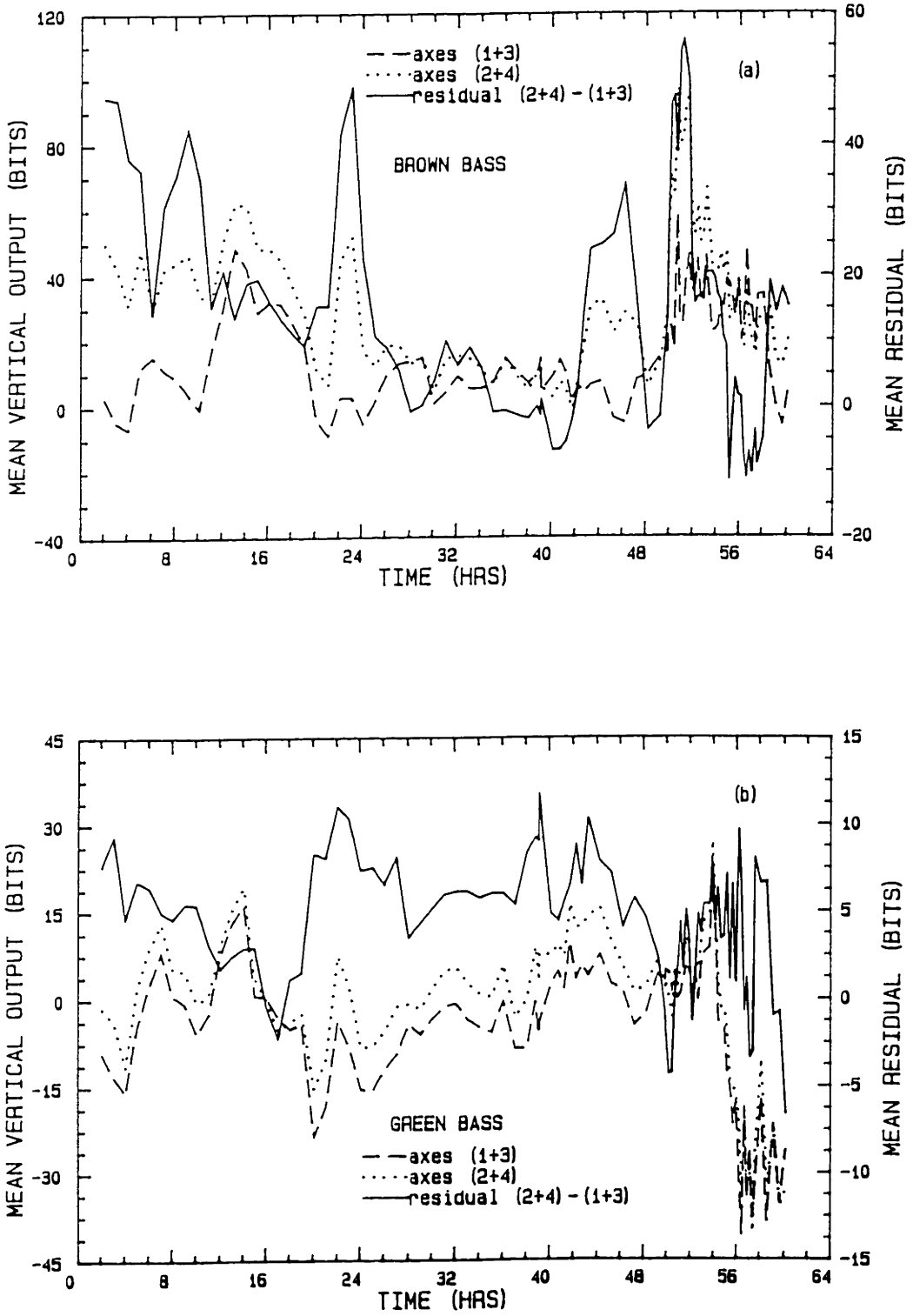

Figure 2.19 Comparison between the 6-minute mean residual, Eq. (2.12), and the 6-minute mean vertical velocity components along the two measurement planes, Eq. (2.11) from the two BASS current meters. Note the differences in vertical scales.

plane. It was, however, somewhat correlated to the vertical velocity component in the axis2, axis4 plane. A sense of this can be gained from Figure 2.19a but is shown more clearly in the form of a scatter plot by Figure 2.20. Throughout most of the Keszthely deployment any mean current was oriented in a shore-parallel or North-South direction. Due to the sensor orientation the axis2, axis4 plane was aligned within about 15° of this direction. The magnitude of the mean residual is roughly 50 percent that of the mean vertical velocity along the axis2, axis4 plane suggesting that the source of the residual could be the same as the source of the vertical velocity. This may be due to flow disturbance by the sensor which is only important when there is a signficant mean vertical velocity component. Another possibility is the drift noted in the zero offset on axis 2 of the brown BASS. This error would be correlated with any velocity component using axis 2. While the mean residual is large in comparison to the mean vertical velocity, it is much smaller in comparison to the mean horizontal velocity and typically ranges from 5 to 10 per cent of this component.

Figure 2.19b indicates that the mean residual varies over a much smaller range (~ 15 bits) on the green BASS. It was found that this mean residual did not correlate well against any of the flow parameters and thus is probably due to small, random drifts in the zero offsets of each axis. The green BASS was mounted below the brown BASS and very near to the bottom. This may have led to a decrease in the mean vertical velocity and therefore a decrease in any associated flow disturbance. The mean horizontal velocity was usually about the same size or slightly larger than that at the brown BASS.

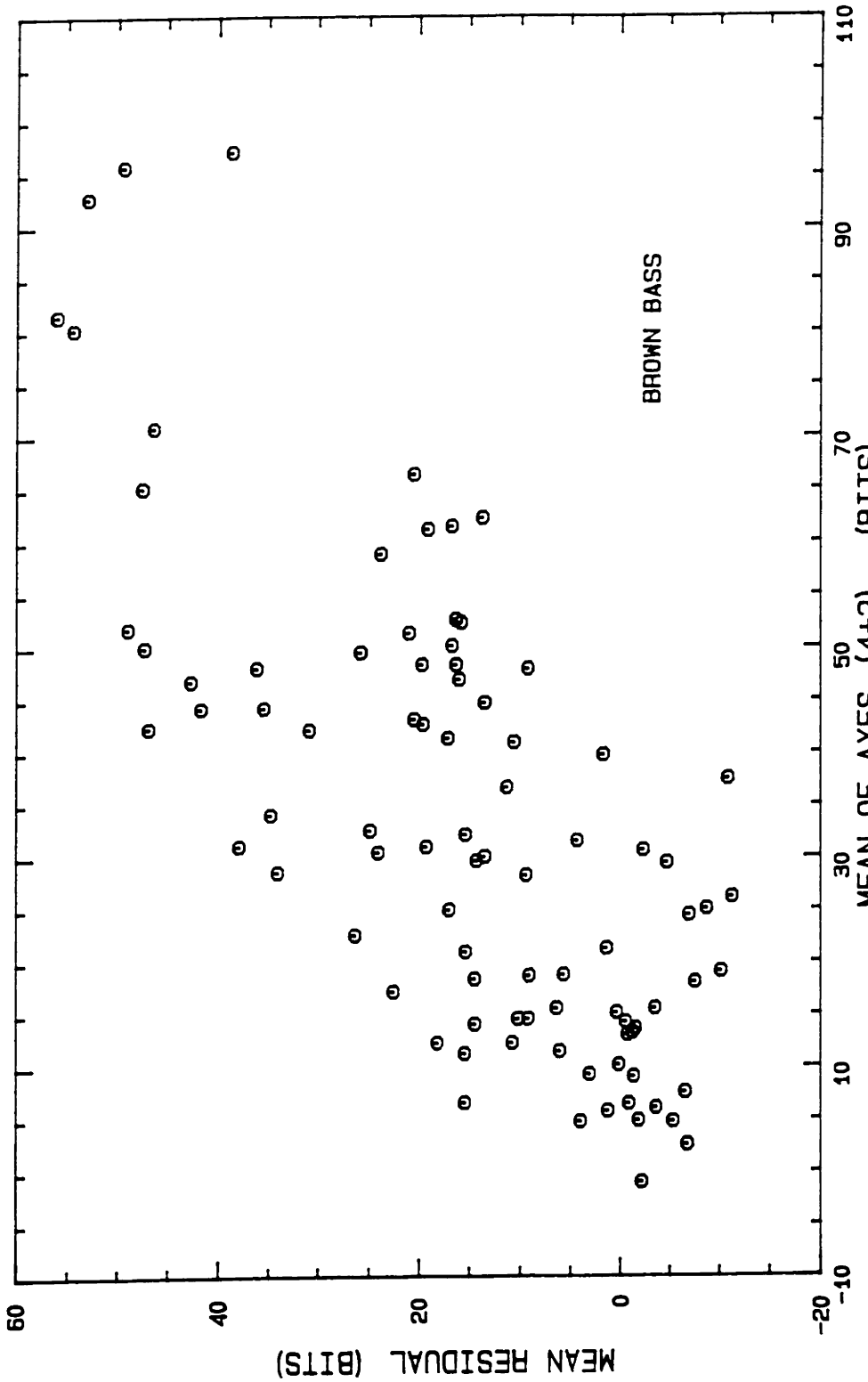

Figure 2.20 Scatter plot of 6-minute mean residual and 6-minute mean vertical velocity in the axis 2, axis 4 plane.

The variance of the residual is compared in Figure 2.21 to variances computed in the two vertical measurement planes. For both BASS it is clear that the residual variances correspond closely to flow variances and have no axis alignment in the vertical direction. This is shown further in Figure 2.22 where scatter plots are presented of the residual variance vs. the average vertical velocity component variance. For both BASS they are well correlated, although the residual variance is about 6 per cent of the vertical variance for the brown (upper) BASS while it is about 25 per cent for the green (lower) BASS. A similar scatter plot of the residual variance vs. the average horizontal variance also shows a good correlation (Figure 2.23). In this case the residual variance changes from 1.1 per cent to 1.9 per cent of the horizontal variance for the brown and green BASS, respectively.

Figures 2.24 and 2.25 show the power spectrum of the residual variance at four different times for both BASS. Often these spectra have a peak in the surface wave band although they typically have substantial energy throughout the entire resolvable frequency range. In some cases the spectra are almost "white."

These results together with the dominance of the horizontal and vertical velocity variances by surface waves (see previous section) suggest that the residual variance is also surface wave related. Most likely it is due to turbulent wakes forming around the transducer heads in the oscillatory flow. Turbulence so generated could be relatively broad-band as indicated in Figures 2.24 and 2.25. These wakes appear more nearly related to the horizontal rather than the vertical oscillations since the residual variance is more nearly a constant fraction of the horizontal variance from one BASS to the other.

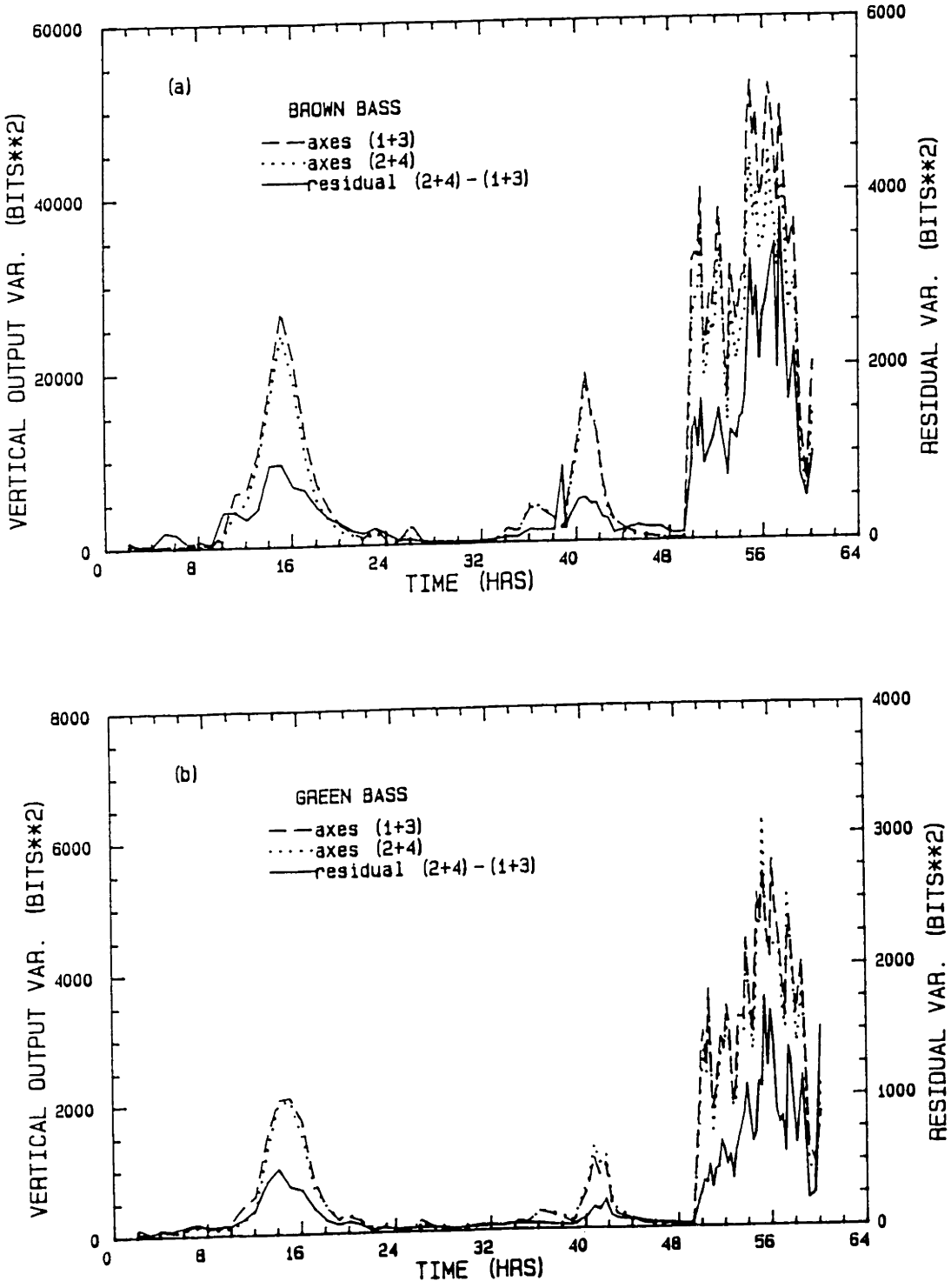

Figure 2.21 Comparison between the variance of the residual and the variances of the vertical velocity components along the two measurement planes for 6-minute sampling intervals.

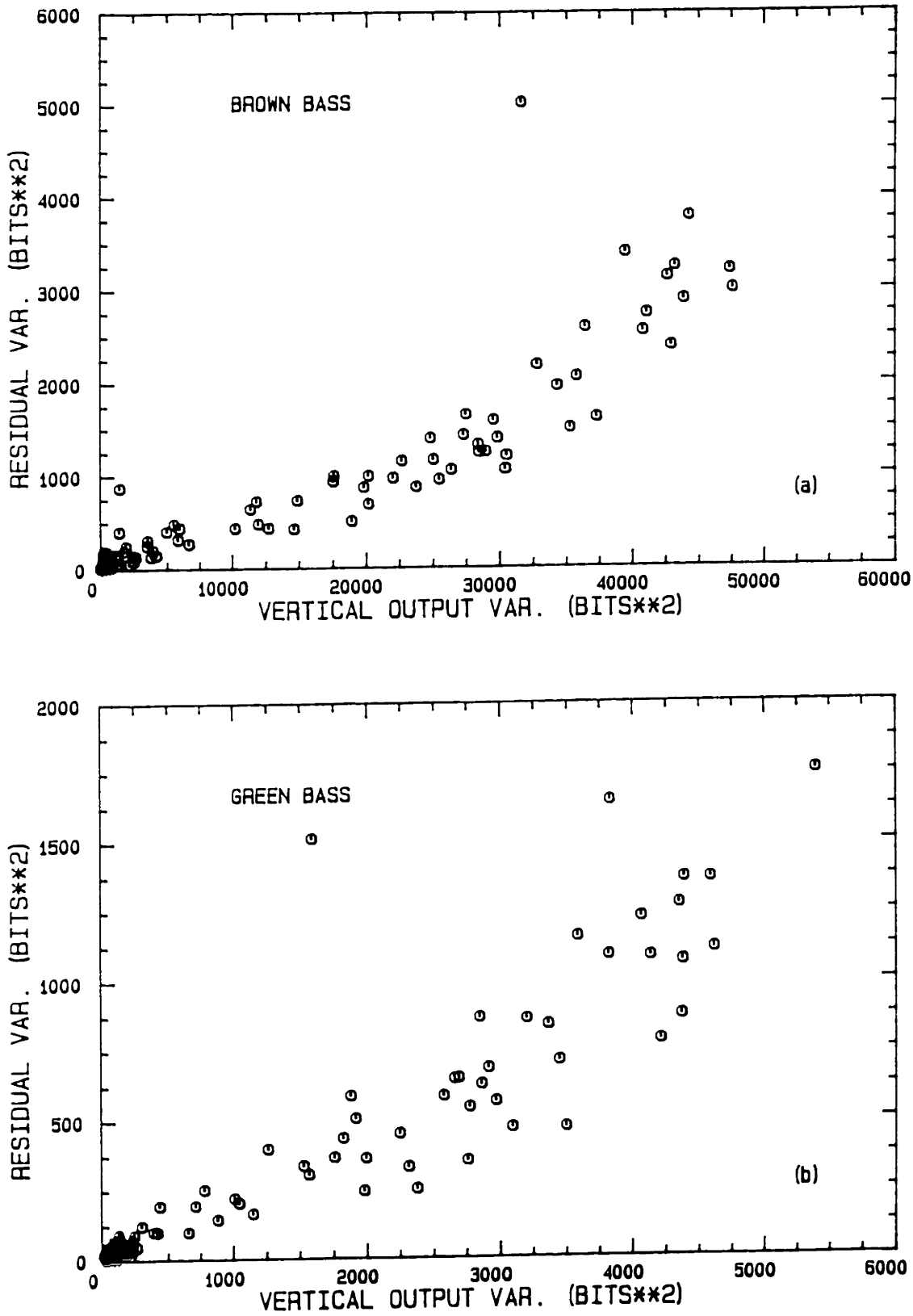

Figure 2.22 Scatter plot of the residual variance and the average vertical velocity variance from the two measurement planes for 6-minute sampling intervals.

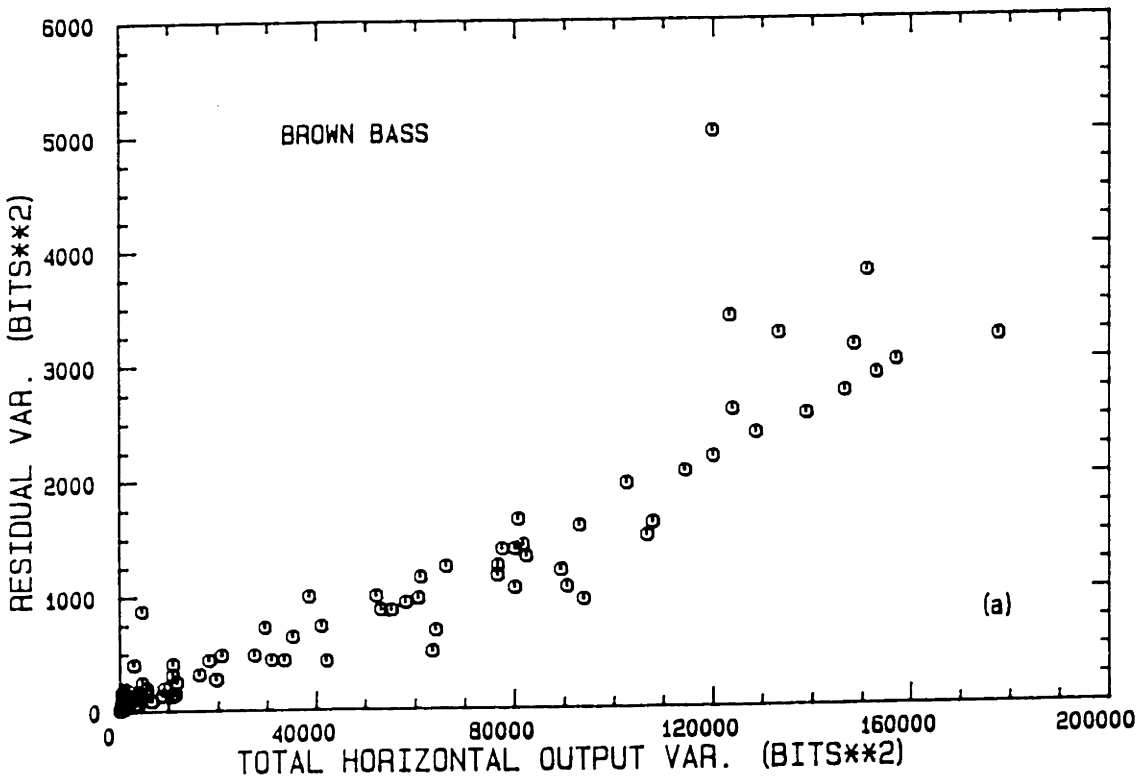

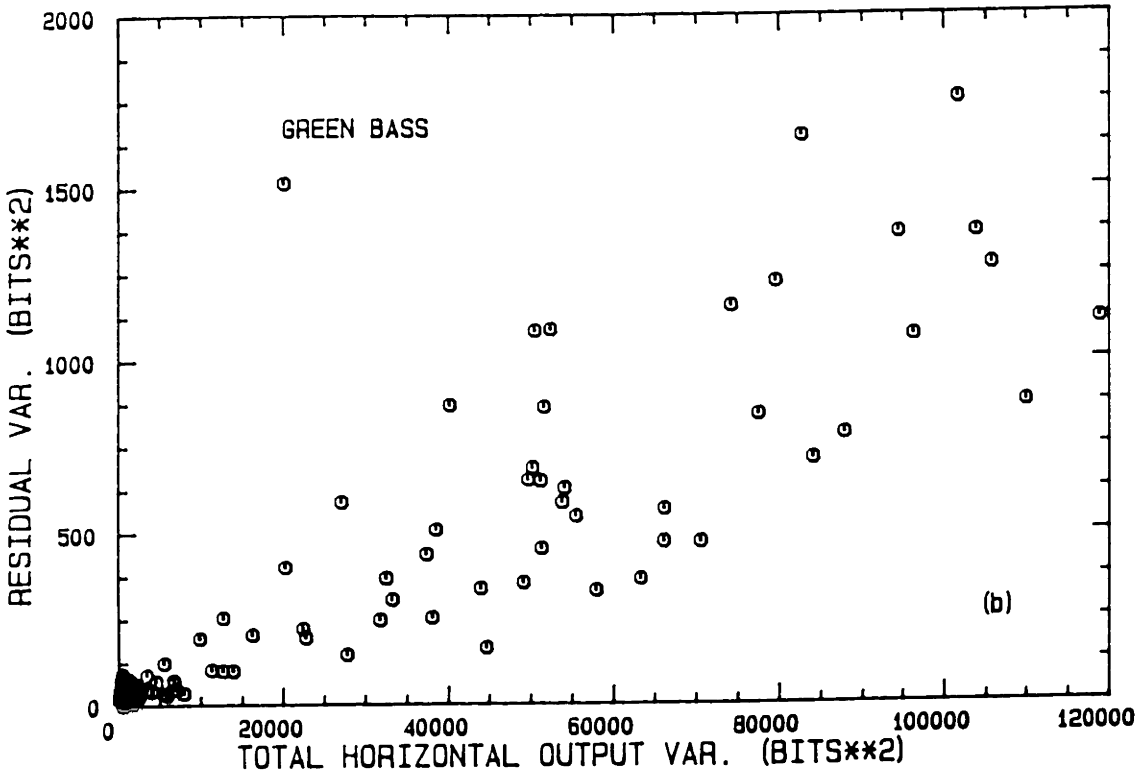

Figure 2.23 Scatter plot of the residual variance and the horizontal velocity variance for 6-minute sampling intervals.

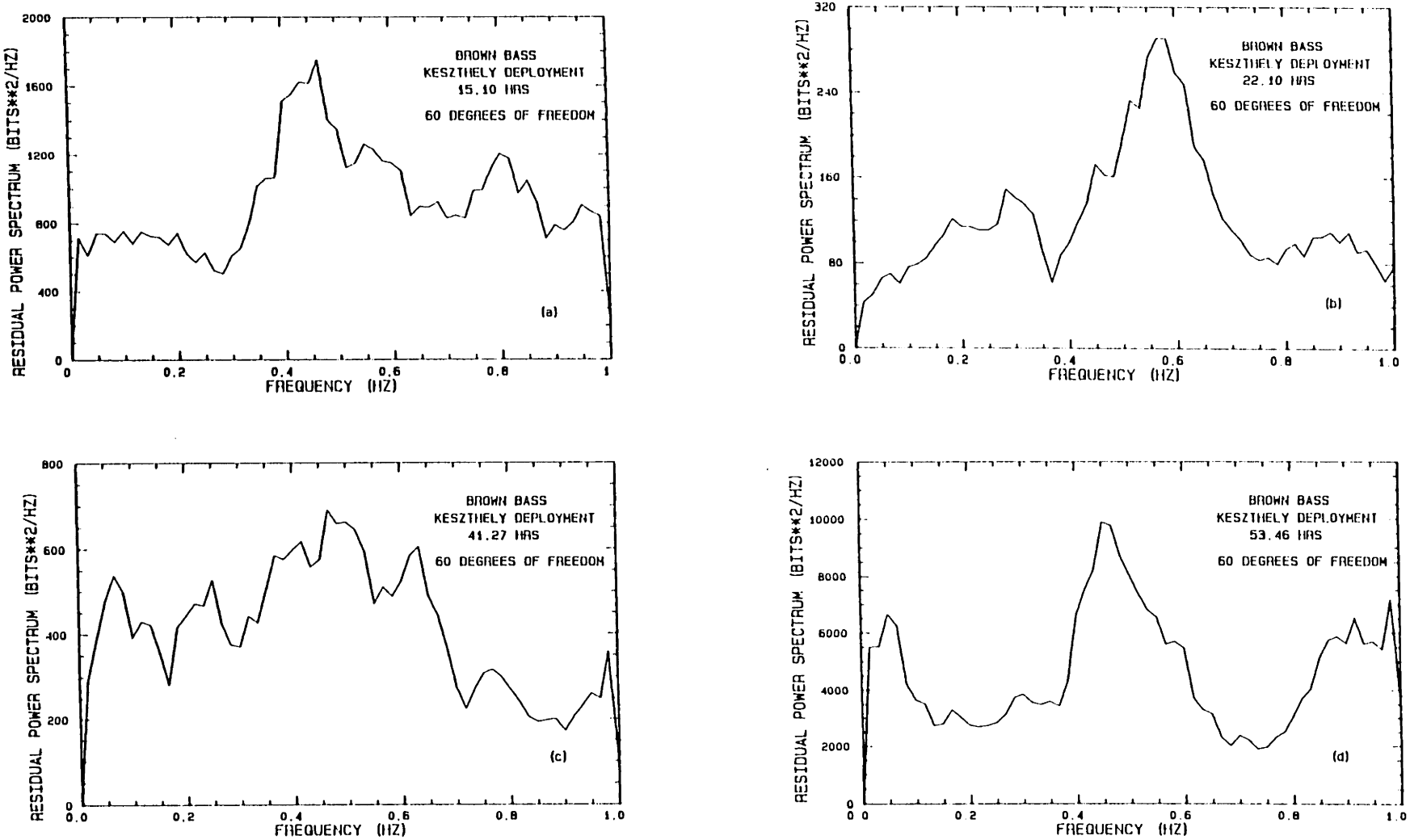

Figure 2.24 Power spectrum of the brown BASS residual during four, 6-minute measurement intervals at the Keszthely field site.

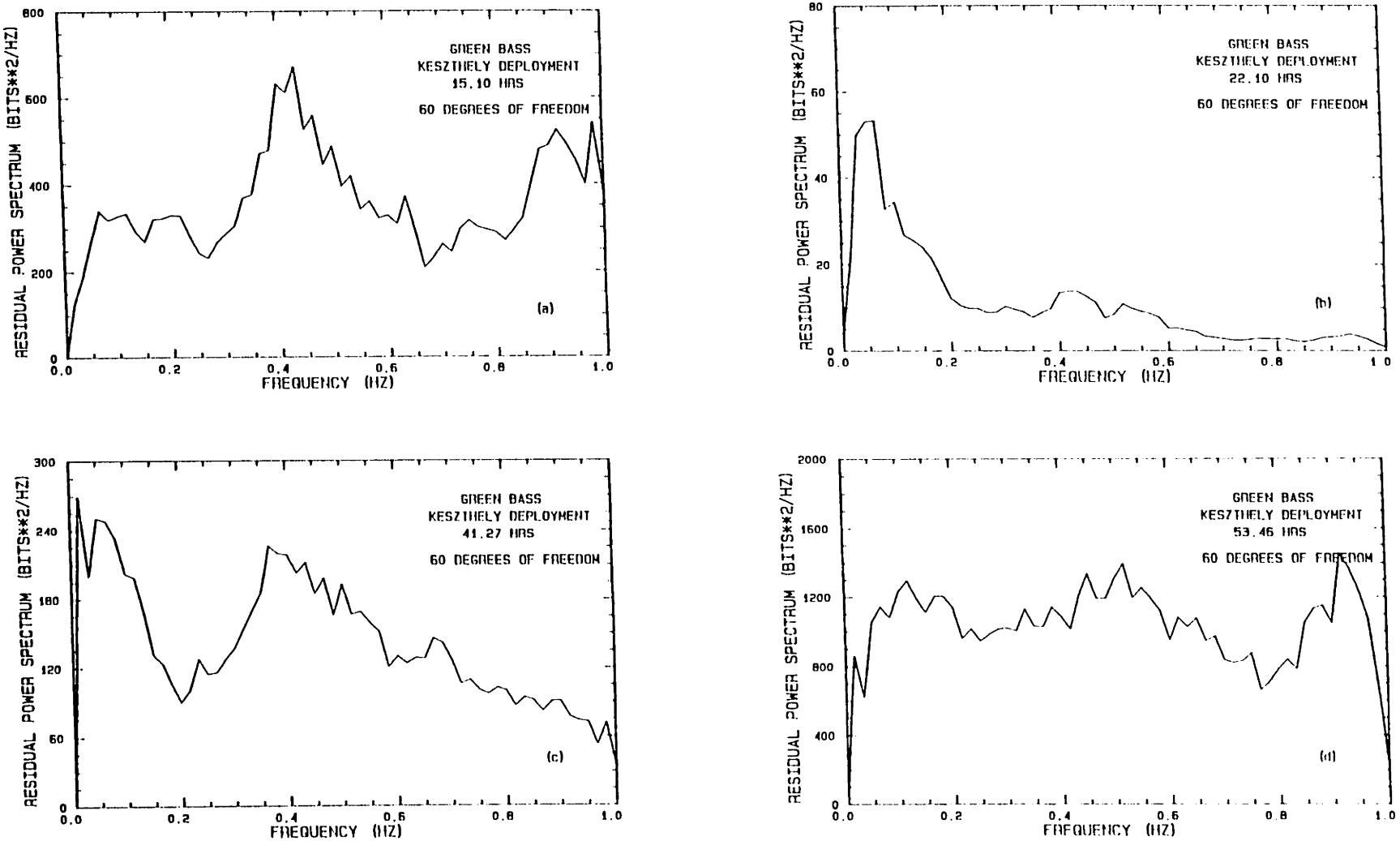

Figure 2.25 Power spectrum of the green BASS residual during four, 6-minute measurement intervals at the Keszthely field site.

To conclude, the information gained from the redundant BASS axis has suggested that mean horizontal current measurements are probably good to within 5-10 percent. Due to their much smaller magnitude mean vertical velocities are known with much less accuracy. The horizontal velocity variance is known to within about 1-2 percent while the vertical variance is known less accurately, again due to its decreased magnitude. The variance error appears to be most closely related to the horizontal velocity component of the surface waves. The error in the variance translates to a 0.6 and 1 per cent error in the fluctuating horizontal velocity and a 3 and 14 per cent error in the fluctuating vertical velocity at the upper and lower current meters, respectively.

Recent attempts have been made to compute Reynolds stress terms directly from the fluctuating componets of measured vertical and horizontal velocities. The BASS current meters used in this study are among the most accurate current meters presently available for use in field studies. In comparison with the sphere of an electromagnetic current meter, BASS should also be superior in minimizing the induced flow disturbance. The dynamic error analysis presented above provides some indication of how well this may be done using BASS in the presence of a substantial surface wave component. Judging from the spectra presented in Figures 2.14 and 2.15, it is likely that the energy directly associated with the surface waves is 90 per cent or more of the total energy of the fluctuating components. This energy must be removed, (e.g., using linear filtration, Lumley and Terray, 1983), before the Reynolds stresses can be computed. Therefore, while the residual variances presented above are small compared to the total energy in the system, they may be quite significant compared with that energy which is only associated with the Reynolds stresses.

2.4 DEPLOYMENT LOCATIONS

The system of equipment described above was deployed in three different locations as a part of this study, the first being a test deployment in the United States and the other two in Lake Balaton, Hungary.

2.4.1 Test Deployment Site

The equipment was initially deployed in water of 2.4 m depth in Long Pond, Belgrade, Maine, to test the overall system under field conditions. During this deployment several problems with the equipment were discovered. Among them were an incorrect wiring of the cable connecting the electronics housing to the wind equipment. This resulted in wind output being sent down wires intended for the remote switch and a change in the equipment's sampling rate or on/standby status every time the wind speed changed. Also the design flaw in the wave staff which resulted in the fully sumberged readings discussed in Section 2.2.4 was discovered. Both the ABSS and BASS seemed to work, although there were no significant resuspension events so that the ABSS did not vary significantly from background.

2.4.2 Lake Balaton Site 1—Tihany

The initial Lake Balaton deployment was made off the east side of the Tihany peninsula as shown in Figures 2.26 and 2.27. This location was convenient because of the presence of the Limnological Research Institute of the Hungarian Academy of Sciences which was participating in the cooperative study.

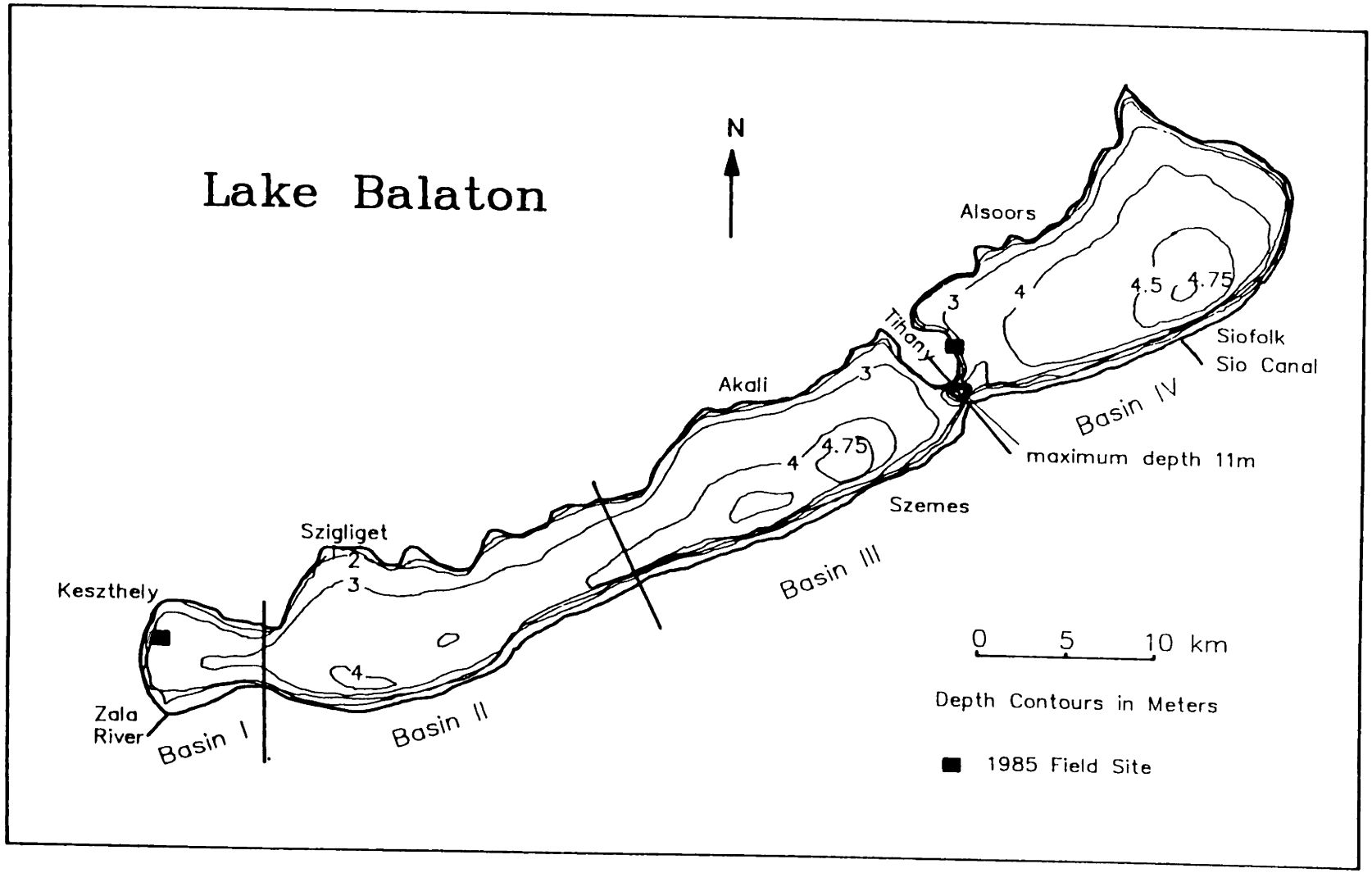

Figure 2.26 **Lake Balaton including 1985 field sites.**

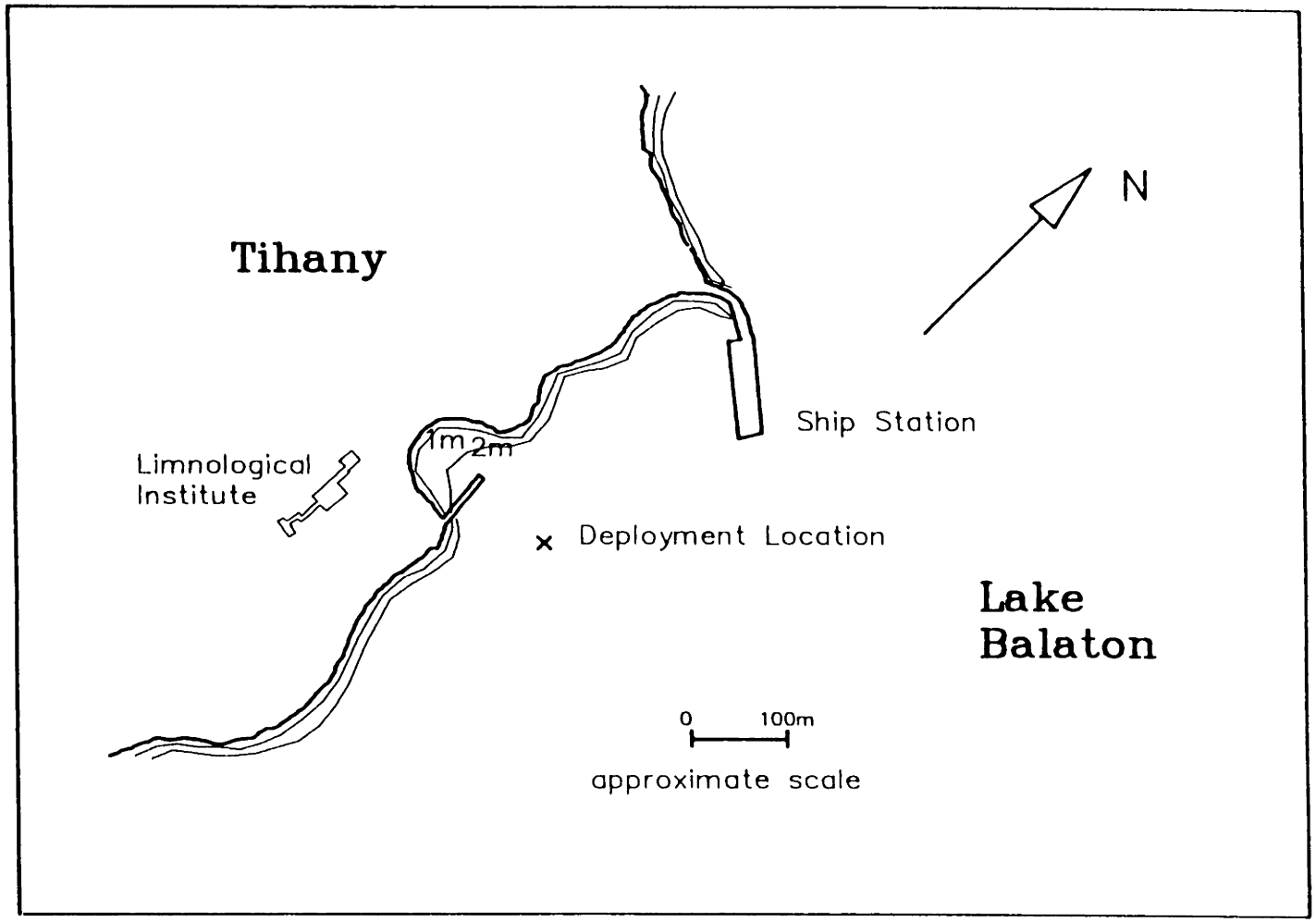

Figure 2.27 Detail of Tihany field site.

The still-water depth at this location was 2.2 m. Figure 2.3 indicates the bottom sediment was typically a silty sand which was confirmed by the fact that almost no settling of the tripod feet into the sediment was observed over the 1.5-month-long period that the tripod was in place at this site.

Figure 2.27 shows that the deployment site was sheltered from winds blowing from the north by the cement pier and breakwater associated with the ship station. Orignally, it was intended to make the deployment farther from shore to avoid this effect; however, such a location was abandoned in favor of one that afforded more protection for the equipment from interference by the large number of people using the lake for recreational purposes.

The first installation turned out to be disastrous as the electronics package flooded with lake water due to a loose connector in the end cap of the pressure housing. It was then necessary to return the electronics package to the United States where each of the boards was carefully cleaned and the equipment restored to working order. It was during the return trip that the ABSS was broken contributing to its failure during the ensuing experiments. A second installation was made at Tihany which was more successful and lasted from July 23 to August 4, 1985.

Two substantial storms occurred during this period which are described in Section 2.5.1.

2.4.3 Lake Balaton Site 2—Keszthely

A second Lake Balaton deployment was made at the western end of the lake as shown in Figures 2.26 and 2.28. This location was chosen because

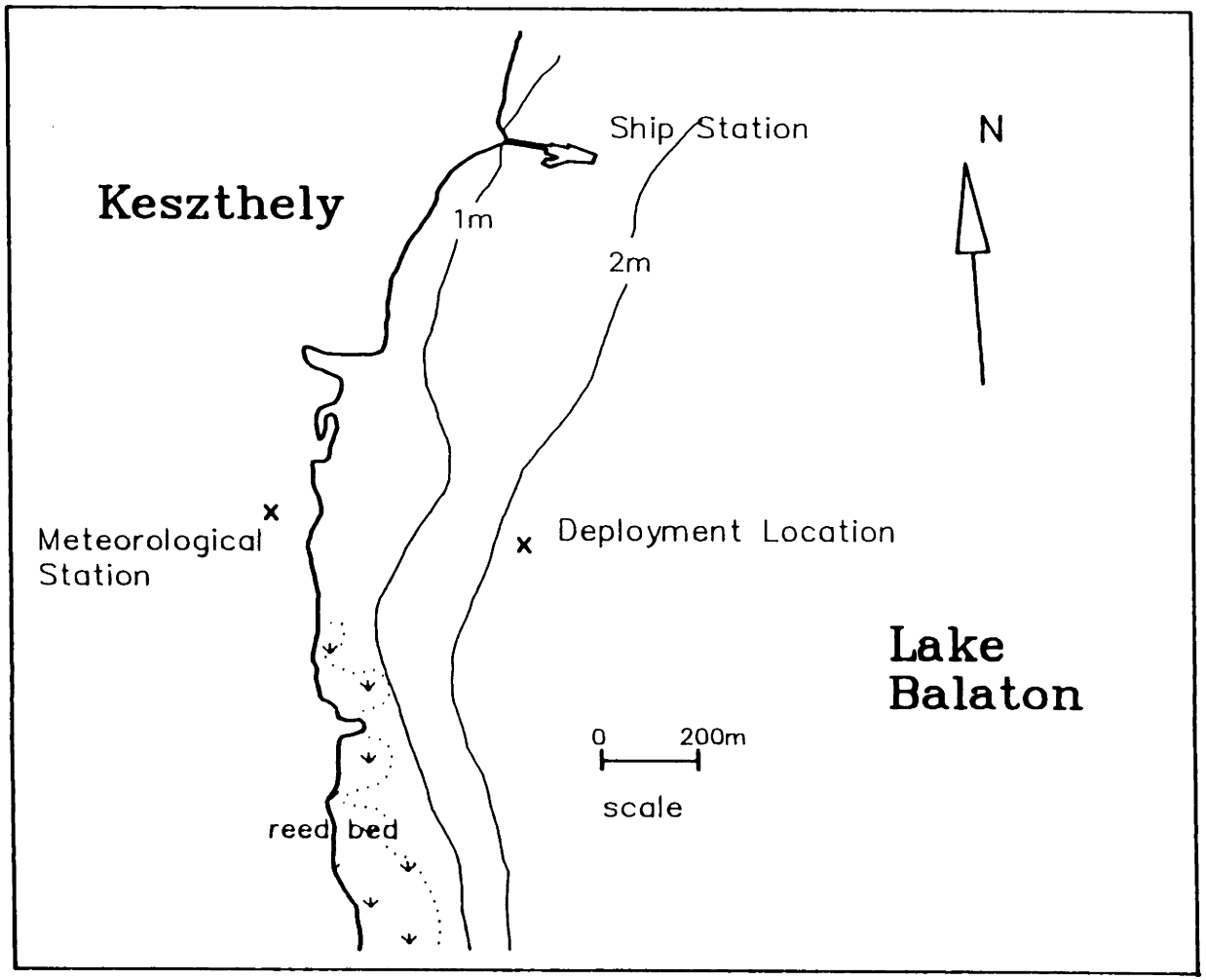

Figure 2.28 Detail of Keszthely field site.

it was known that resuspension was substantial during storms and because simultaneous work was being conducted there by the Hungarian Center for Water Resources Development which was also participating in the cooperative study. This group intended to anchor a research vessel and make measurements of wind velocity, suspended solids, light penetration, and various other chemical and biological parameters as often as every two hours. Thus their work complemented the measurements planned for this study.

The deployment was made in water of 2.0 m depth and as shown in Figure 2.3 in an area of clayey-silt bottom material. Upon installation the tripod rapidly sank about 15 cm into the bottom whereafter no further settling was measured throughout the deployment. In general the bottom in this region was much more like a thick mud than a solid boundary.

Two deployments were made here covering the periods August 8 to August 13, 1985, and August 15 to August 22, 1985. During the second deployment a substantial storm event occurred which caused significant amounts of resuspension. Unfortunately the underwater matable connector corroded to the point that no data continued to be passed from the electronics package to the recorder after about 8:00 A.M. on August 18, 1985.

Additional sources of data which are available during this study period are wind speed and direction from a nearby, shore-based meteorological station and wind speed measured with a hand-held gauge on ship board as often as every two hours. Mid-depth suspended sediment concentrations measured at least every 2-3 hours are also available.

2.5 RESULTS

The results presented below are for significant storm events during the Tihany and Keszthely deployments. For much of the deployment periods the weather was calm resulting in minimal water movement. During such periods the equipment was turned to standby to conserve battery power. From the two Lake Balaton deployments seven casette tapes full of good data were obtained, corresponding to about 42 hours of continuous sampling at 2 Hz. About 70 percent of this data is presented below. The remainder was taken during periods of minimal hydrodynamic activity.

2.5.1 Tihany Deployment

Two data sets from this deployment are presented. In each case the current meters were located at elevations of 28 cm and 94 cm above the bottom while the wind speed and direction was measured 2 m above the water surface.

July 27 - July 28, 1985

Data was taken over a 20-hour period beginning at 10:00 a.m. on July 27. It was collected using the sampling schemes listed in Table 2.5.

The average wind speed and direction over each 6-minute period are shown in Figure 2.29. The equipment was initially turned on during a period of sustained on-shore wind from across the lake. This gradually diminished and in the process turned to almost shore parallel and from the north. Approximately 6 hours of calm was broken by a sudden storm having

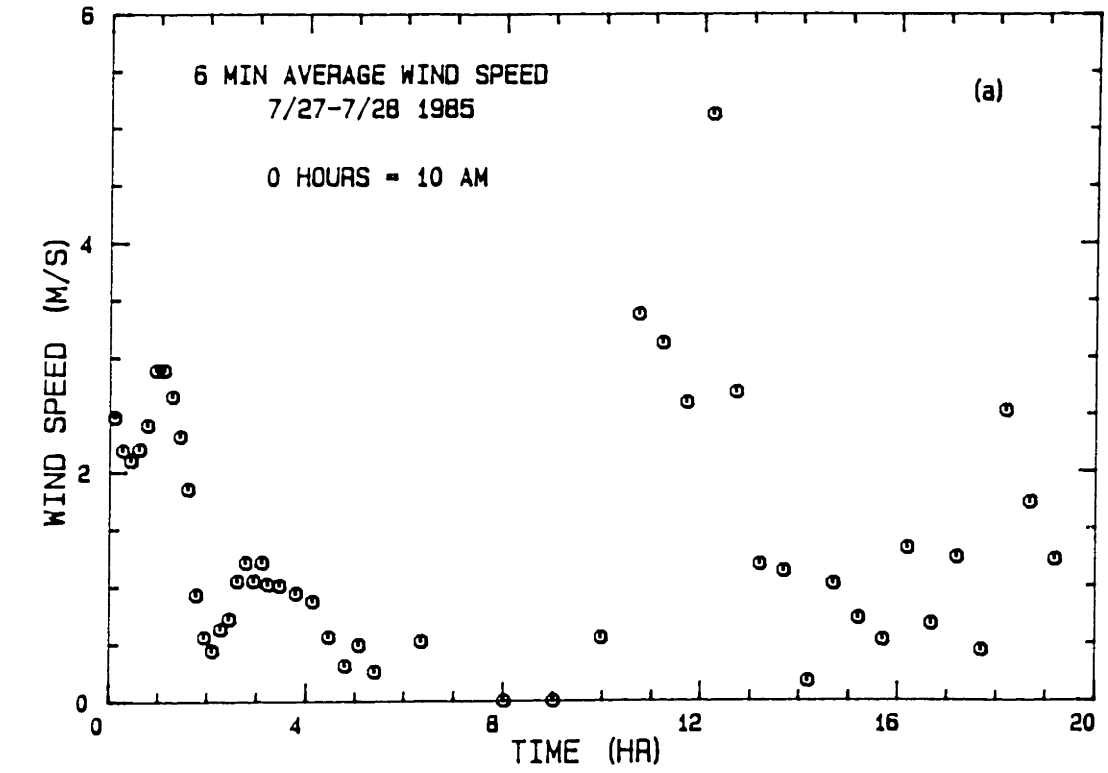

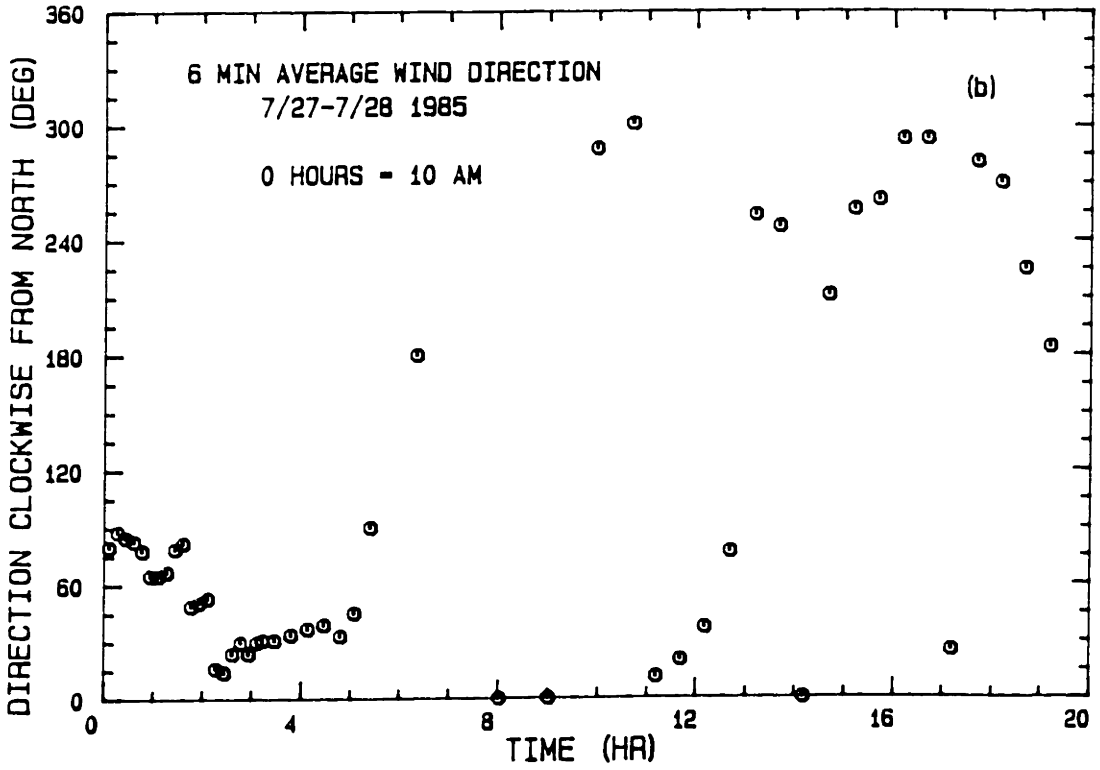

Figure 2.29 6-minute average wind speed and direction, Tihany deployment, event #1.

Table 2.5 Event #1 Sampling Rates

Time (hrs)	On Time (min)	Standby Time (min)
0 - 3.3	6	4
3.3 - 5.3	6	14
5.3 - 6.5	6	54
6.5 - 7.9	in situ zero calibrations	
7.9 - 10.6	6	54
10.6 - end	6	24

intense wind gusts. This is illustrated by the large difference in the 6-minute maximum wind speeds shown in Figure 2.30 and the average values in Fig. 2.29. During this period the average wind came predominantly from the north while gusts came mostly across the lake from the east.

The significant wave heights and mean wave periods are shown in Figure 2.31. As discussed in Section 2.3.2 the surface wave activity was assumed negligible for significant wave heights below 4 cm. The data set begins during a period of established waves that diminish with the wind. The intense storm does not produce larger waves primarily due to the wind direction which casts the deployment site partially in the shadow of the ship station breakwater, particulary in the initial stages of the storm. A brief period follows of substantial wave action which rapidly dimishes as the wind direction rotates back through north until it blows from the shore. The wave periods shown in Figure 2.31b exhibit a characteristic behavior found in all the data collected in this study, namely a mean wave period of between 1.9 and 2.2 seconds during significant wave events.

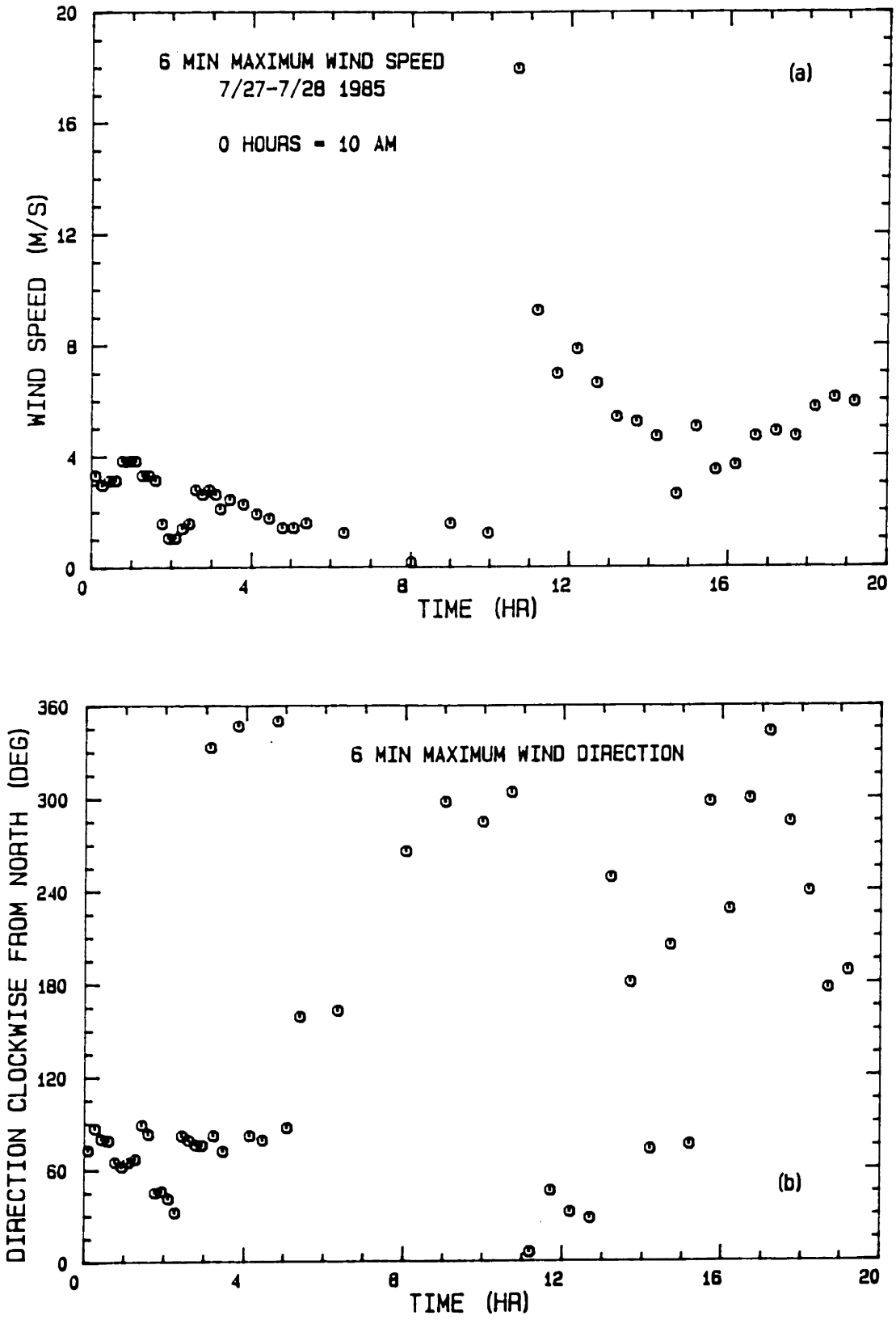

Figure 2.30 6-minute maximum wind speed and direction, Tihany deployment, event #1.

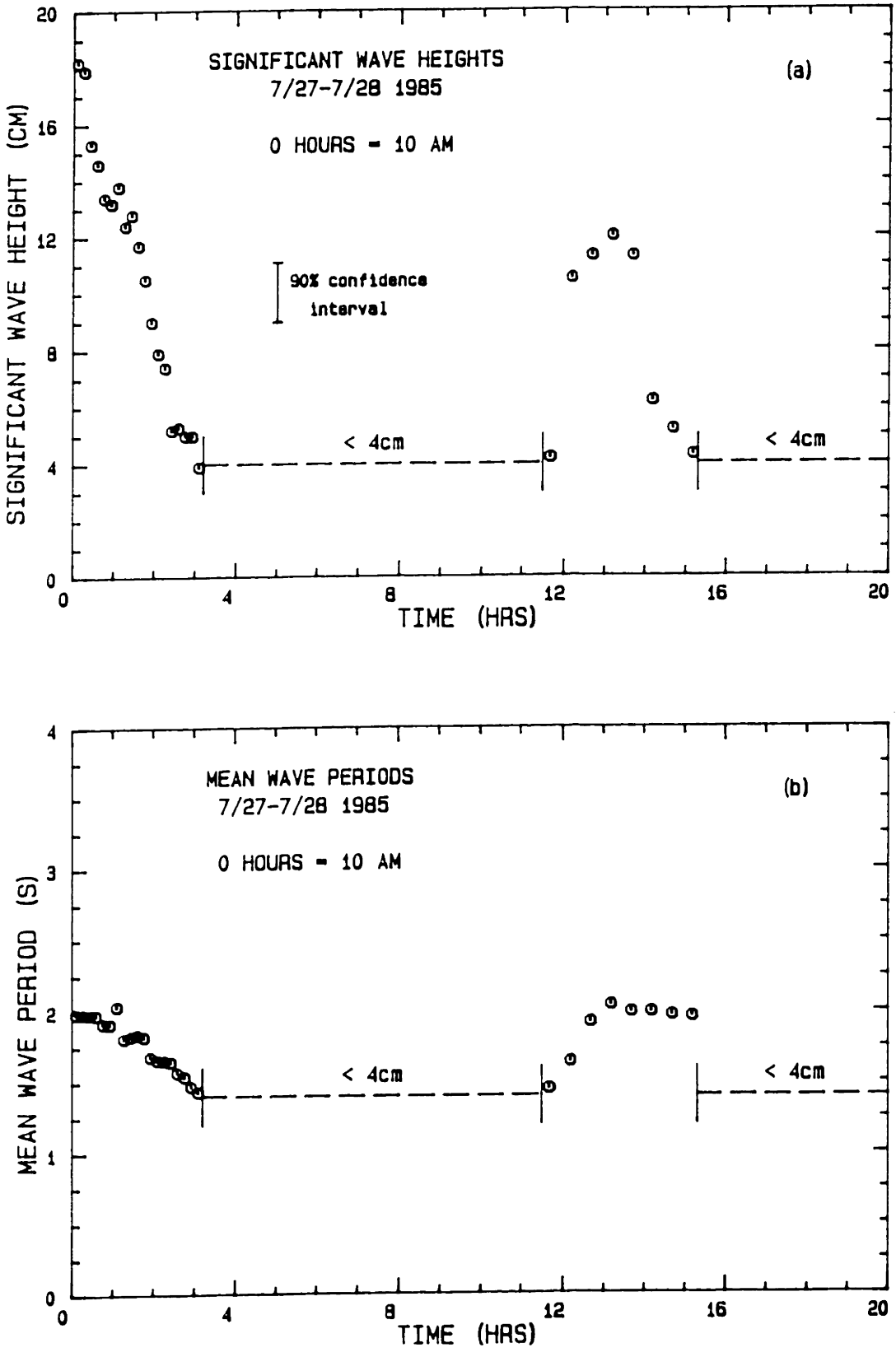

Figure 2.31 Significant wave heights and mean wave periods, Tihany deployment, event #1.

Figure 2.32 shows the 3-minute average current speeds and vector velocities. The response to the sustained onshore wind and the intense storm are dramatically different. During the earlier period flow was generally toward the south to southeast. A wind blowing from east to west would be roughly aligned with the lake axis and cause a longitudinal setup at the western end. Associated with this would be a westward flow in the Tihany Strait and in the eastern basin a flow that was generally toward the strait. Thus a southerly flow along the Tihany peninsula would be expected. The eastward component is probably a near-bottom return current due to a minor local setup against the Tihany peninsula. At about 2 hours the east-west wind diminished substantially and shortly thereafter the current direction reversed, consistent with a west-to-east flow through the Tihany Strait brought about by the first cycle in a longitudinal seiche. The current direction reversed again at about 6 hours and again at about 10 hours, although this last reversal may have been influenced partly by the approaching storm. To summarize the east-to-west wind probably initiated a longitudinal seiche with a period of 6-8 hours and velocities at the deployment site of 2-6 cm/s.

The storm event beginning at about 10.5 hours resulted in mean velocities double those measured at any other time during the entire field study and 4-5 times those associated with the earlier longitudinal event. Figure 2.32b shows that for the first part of the storm the mean velocity at both current meters was against the wind indicating a near bottom return flow. This includes the interval during which the extremely high velocity was recorded. Thereafter, a seiche is initiated which appears to dominate the observed velocities. Based on the propagation speed of a shallow water gravity wave and typical dimensions of the Siofok basin, a transverse

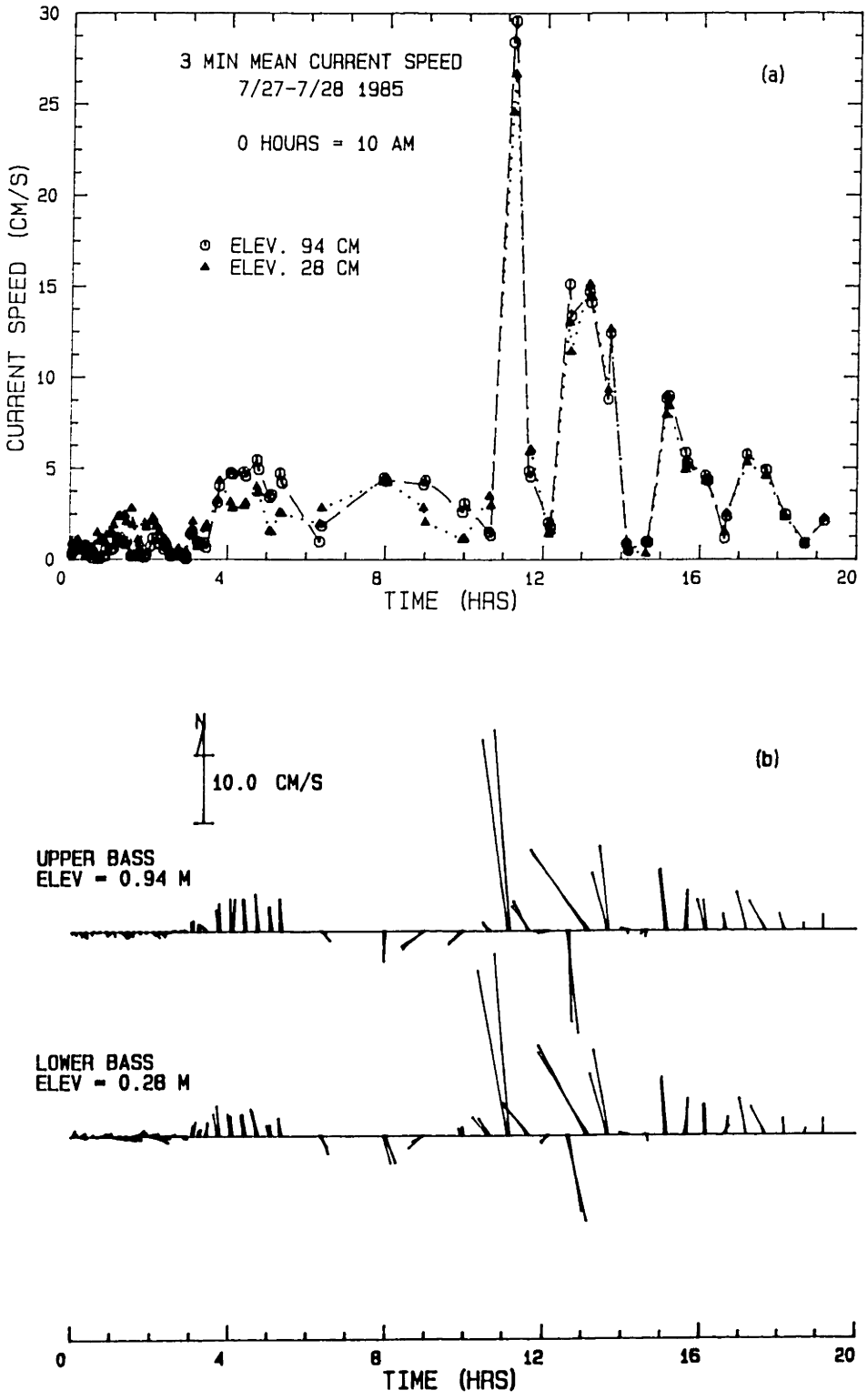

Figure 2.32 3-minute mean velocity summary, Tihany deployment, event #1. (a) Current speed plot (b) Vector velocity plot.

seiche would have a period of about 50 minutes while a longitudinal seiche would have a period of about 2 hours. The latter corresponds to the periodicity observed in the velocity measurements. However, the dominating north-south components in both the water velocity and the wind forcing suggest a transverse seiche. The Tihany field site would have been near the nodal point of such a seiche which would account for the high velocity magnitudes which were observed.

Figure 2.33 shows suspended solids concentration measurements made gravimetrically from bottle samples during the first 6 hours of the sampling period. The data indicate concentrations a little bit higher than typical background levels, which range from 5 to 10 mg/ℓ, suggesting some resuspension occurred. They provide no evidence of a significant suspended sediment gradient over the depth.

July 30 - July 31, 1985

Data were taken over a 12-hour period beginning at 6:40 p.m. on July 30 using the sampling schemes listed in Table 2.6.

Table 2.6 Event #2 Sampling Rates

Time (hrs)	On Time (min)	Standby Time (min)
0 - 1.0	6	24
1.0 - 1.4	6	4
1.4 - 4.9	6	0
4.9 - end	6	24

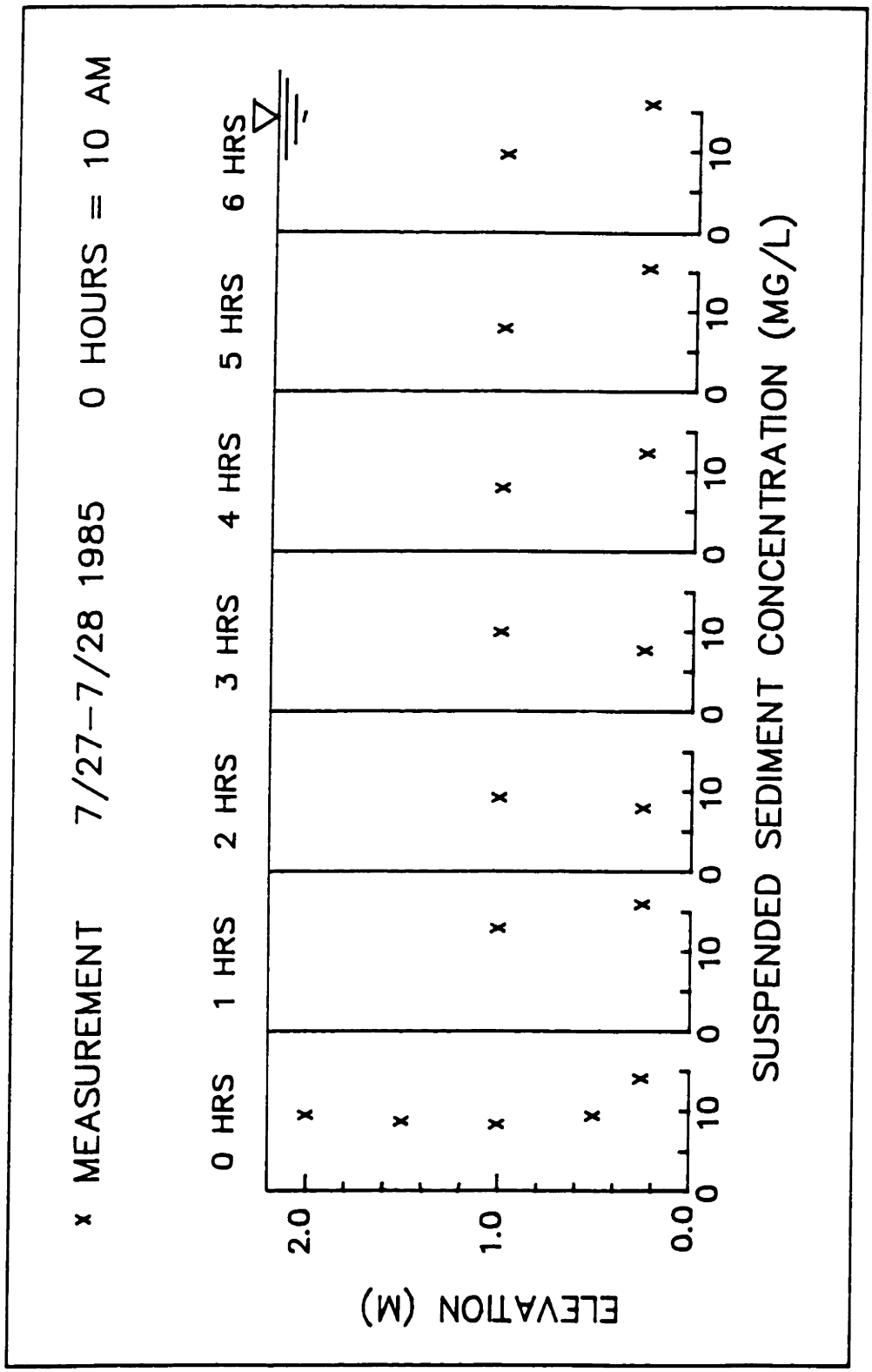

Figure 2.33 Suspended sediment concentrations, Tihany deployment, event #1.

The average wind speed and direction over each 6-minute on period are shown in Figure 2.34. Data collection began at an average wind speed of about 2.5 m/s where after the wind speed approximately doubled for a couple of hours. It then decreased to below 1 m/s over about 3 hours and remained at this level for the remainder of the time. During the majority of the event the wind was directed across the lake assuring nearly the maximum possible fetch.

Significant wave heights and mean periods are shown in Figure 2.35. The significant wave heights increase roughly in proportion to the wind speed and reach a maximum value of about 22 cm. Thereafter they decrease as the wind dies. The mean periods show the characteristic value of about 2 seconds.

Plots of the mean current speed and vector velocities are shown in Figure 2.36. The current behavior is quite similar to the initial hours of the previous event when there was also an on-shore wind. They again suggest the existence of a longitudinal seiche with a period of 6-8 hours and associated velocities of 2-6 cm/s. The water surface elevation data obtained from the wave staff showed no significant deviation of the mean water level during the entire period.

Figure 2.37 shows the suspended sediment concentration 50 cm above the bottom determined gravimetrically from bottle samples during the major part of the wind event. It indicates an approximate doubling of the suspended sediment concentration over the period. A linear regression of all but the final point gives a resuspension rate of 3.6 mg/ℓ/hr. Considering the scatter in the measurements they appear to indicate slightly larger amounts of sediment in suspension than observed in the previous data set (Figure 2.33). Assuming an average current of 2 cm/s the horizontal transport

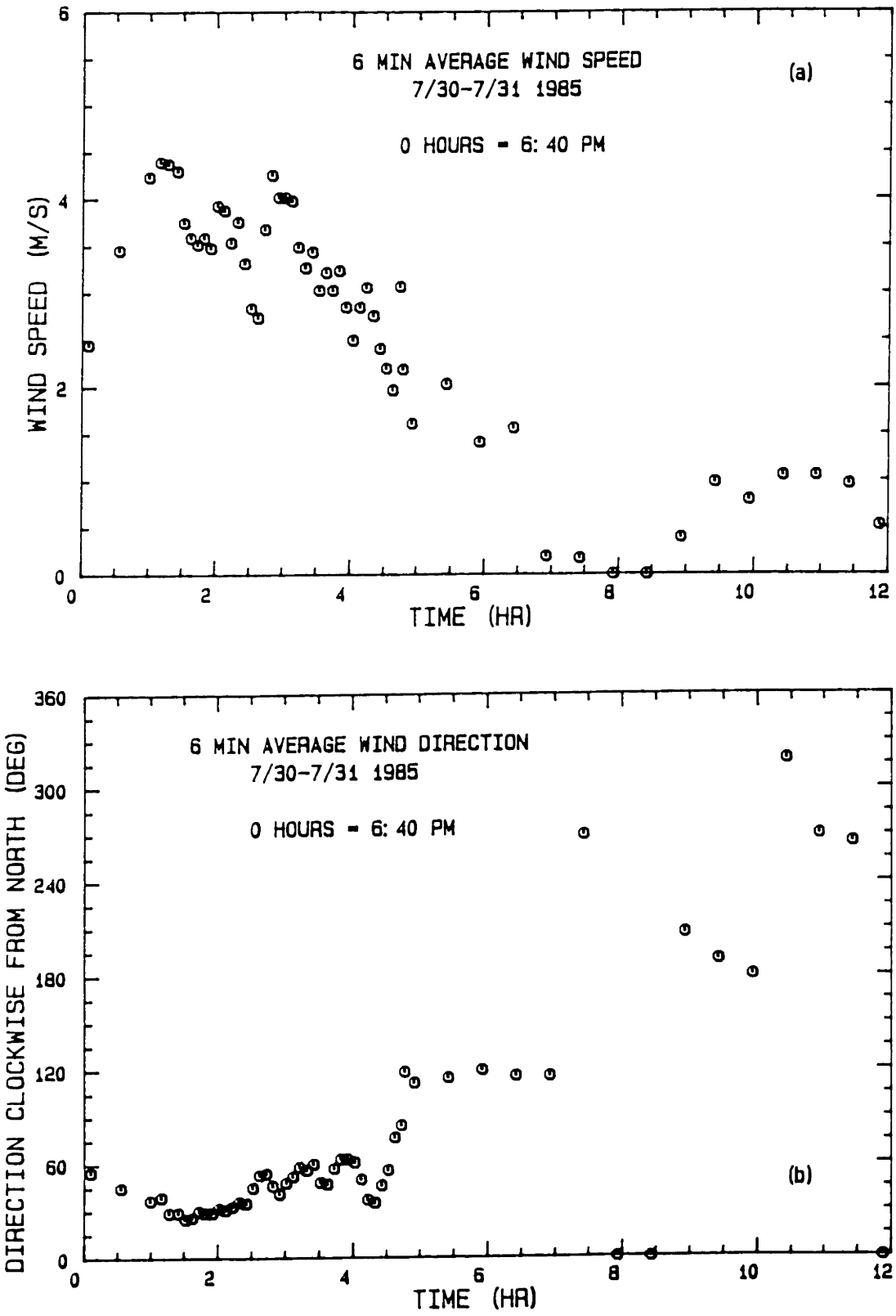

Figure 2.34 6-minute average wind speed and direction, Tihany deployment, event #2.

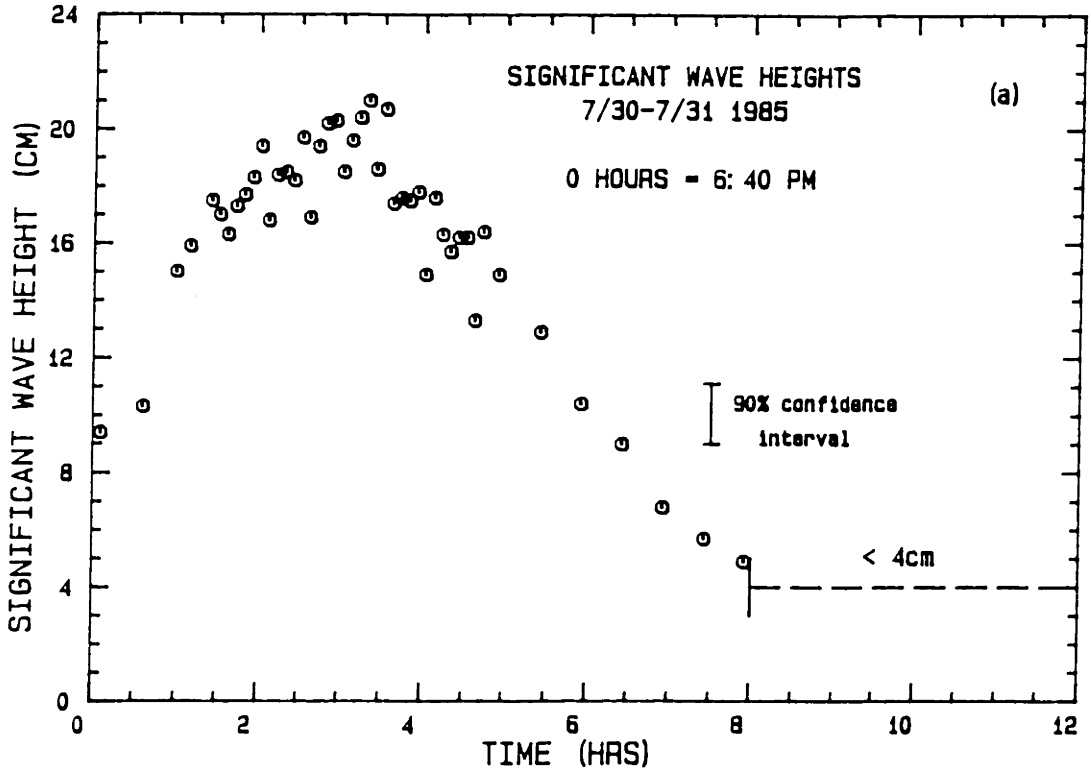

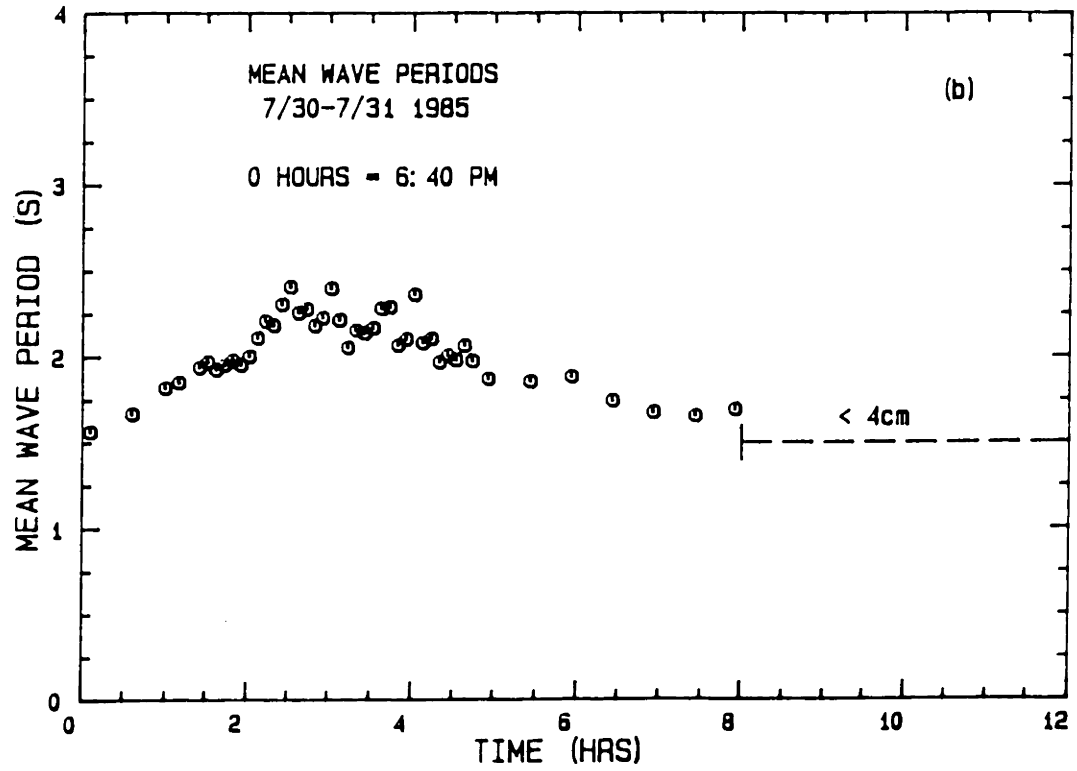

Figure 2.35 Significant wave heights and mean wave periods, Tihany deployment, event #2.

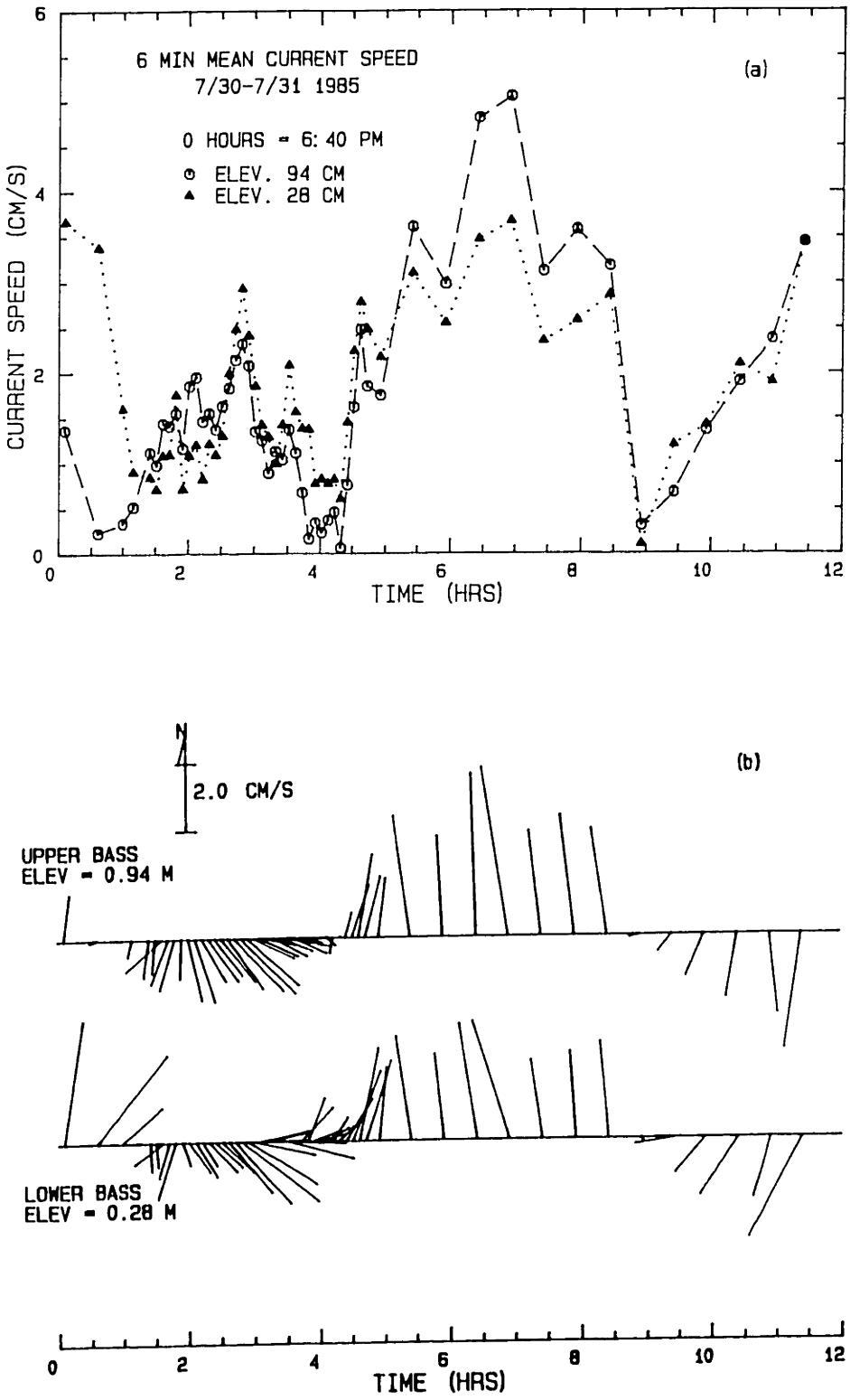

Figure 2.36 6-minute mean velocity summary, Tihany deployment, event #2. (a) Current speed plot (b) Vector velocity plot.

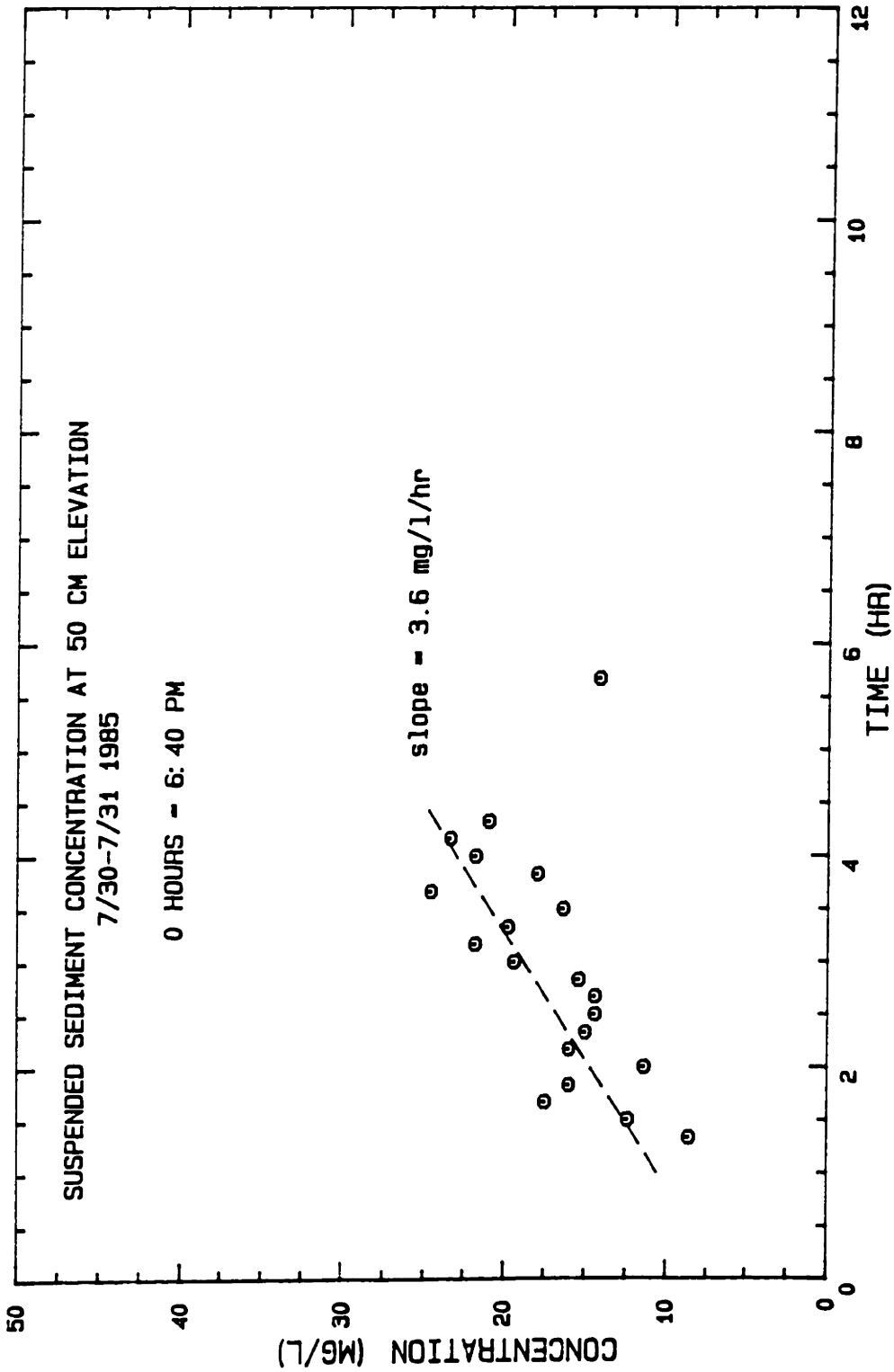

Figure 2.37 Suspended sediment concentrations, Tihany deployment, event #2.

distance during the three-hour measurement period would be about 200 m suggesting that the response given in Figure 2.37 is most likely representative of local resuspension rather than distant resuspension and horizontal transport.

2.5.2 Keszthely Deployment

One data set covering about 2.5 days from this deployment is presented below. The current meters were located at elevations of 24 cm and 85 cm above the bottom while the wind speed and direction were measured 2 m above the water surface. Additional suspended sediment concentration and wind measurements made over 15 days including the deployment period are also presented.

August 15 - August 18, 1985

Data was taken over a little more than 60 hours beginning at 8:00 p.m. on August 15 using the sampling schemes listed in Table 2.7.

Table 2.7 Event #3 Sampling Rates

Time (hrs)	On Time (min)	Standby Time (min)
0 - 40.1	6	54
40.7 - 42.7	6	24
43.2 - 49.2	6	54
49.9 - 57.4	6	9
57.6 - 60.2	6	24

The average wind speed and direction over each 6-minute on period are shown in Figure 2.38. It indicates two small wind events during which the wind blew from east to west along the lake's long axis and one larger event with almost twice the wind speeds blowing from north to south across the lake. At the end of this data set the underwater connector between the recorder and the electronics housing became sufficiently corroded that no further data could be collected. Fortunately this occurred at the tail end of the latter storm.

Figure 2.39 shows the significant wave heights and mean wave periods. The peak significant wave heights during the two early events are about 75 per cent of those in the latter event due to the increased fetch along the lake vs. across the lake.

As in the Tihany deployment the mean wave period exceeded 2 seconds during substantial waves.

The 6-minute average currents shown in Figure 2.40 appear to behave quite differently than those measured at Tihany. While the Tihany currents seemed often driven by seiching those measured at Keszthely do not show significant periodicity and rather follow changes in the wind field much more closely. The onshore wind of the first event enhances an existing northward flowing current apparently the result of a previous forcing. The resulting flow reaches a magnitude of 8-12 cm/s at about peak winds and decreases in close correspondence to the wind speed. The second event is quite similar to the first in magnitude and eventual wind direction; however, in the beginning of the event the wind is oriented toward the south and is strong enough to initiate a southerly current. As the wind shifts to onshore the direction is maintained and the current enhanced. After the wind dies the current begins to rotate around to the north,

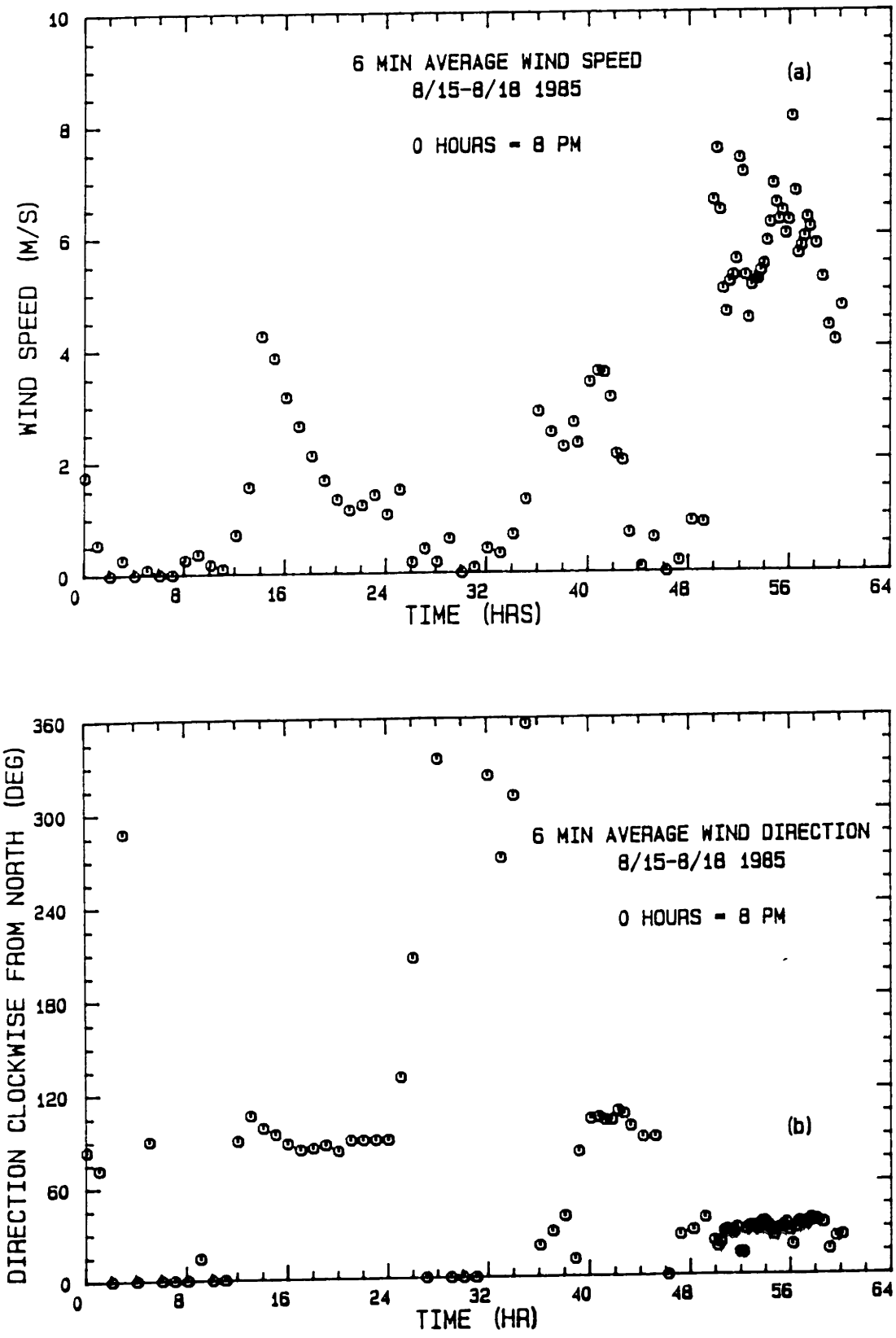

Figure 2.38 6-minute average wind speed and direction, Keszthely deployment.

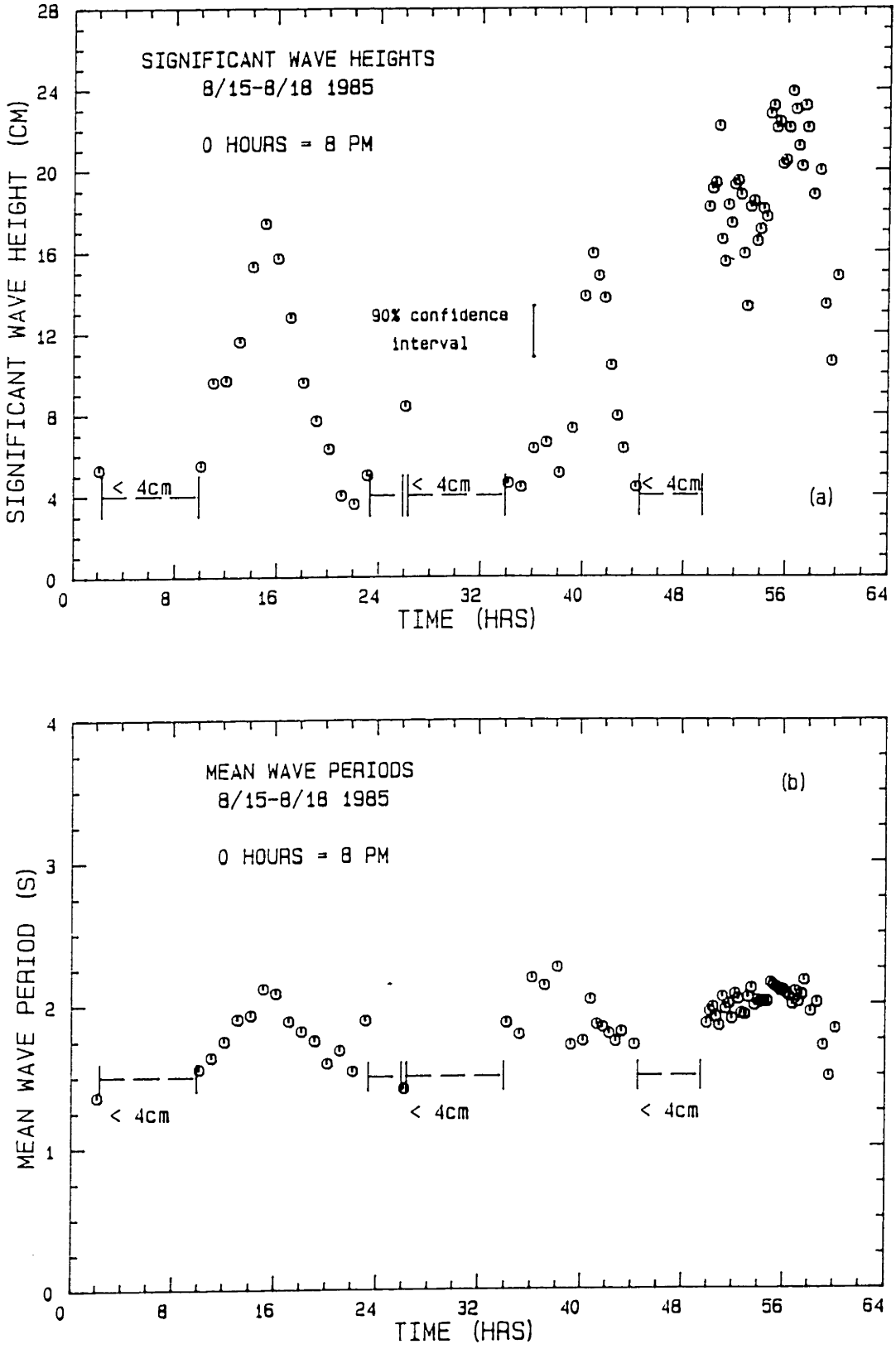

Figure 2.39 **Significant wave heights and mean wave periods, Keszthely deployment.**

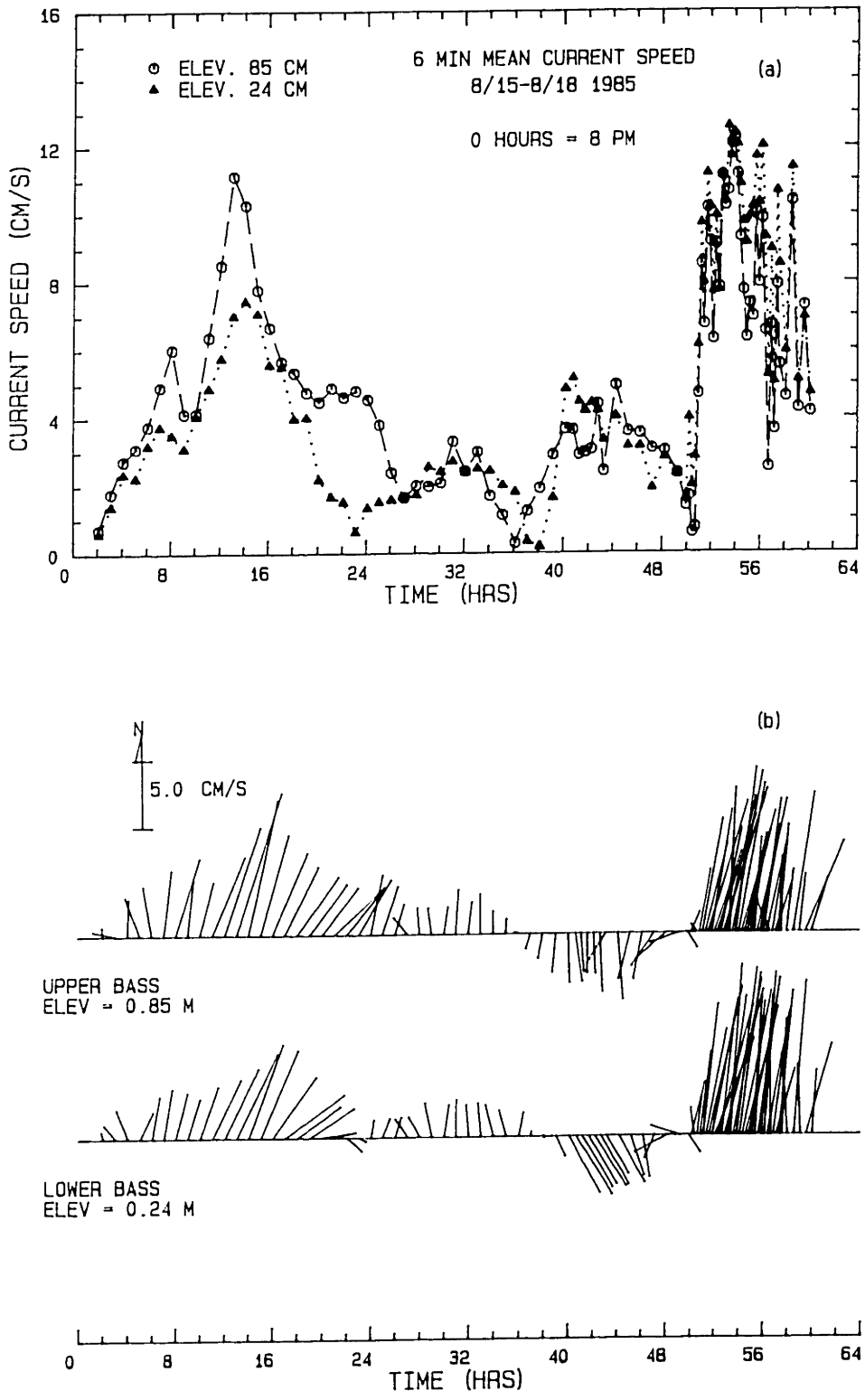

Figure 2.40 6-minute mean velocity summary, Keszthely deployment. (a) Current speed plot (b) Vectory velocity plot.

although this is interrupted by the final storm. The initial mean current measurement during the storm, at about hour 50, is southward and roughly aligned with the wind. However, by the next measurement it has shifted to northward indicating a return current against the wind. The remainder of the mean current data indicates a dynamic balance between a surface layer aligned with the wind and a bottom return current against the wind. This is indicated by decreases in the return velocity, particulary at the upper current meter, at times of increased wind speed (e.g., ~56.5 hours) and increases in the velocity with decreased wind speed (e.g., ~53 hours).

In summary an onshore wind at Keszthely was capable of driving a current at the deployment site which was oriented either to the north or south depending on the residual flow field or an initial shore-parallel wind direction. There is no evidence of a shore-normal return circulation and data from the wave staff indicate no set up of the mean water surface elevation during any events for which data was collected at this time. A transverse wind does result in a substantial return circulation with slightly larger near-bottom than mid-depth velocities, both of which respond dynamically to variations in the wind speed.

Figure 2.41 shows the suspended sediment concentration measured gravitimetrically from bottle samples taken at mid-depth during this period. It indicates a small concentration increase during the two early events and a very large increase during the latter storm. A rapid drop off occurs at the tail end of the big storm. The disproportionate concentration increase of the latter storm suggests either a very non-linear sediment response to the forcing or the existence of a threshold value below which resuspension is minimal and above which resuspension

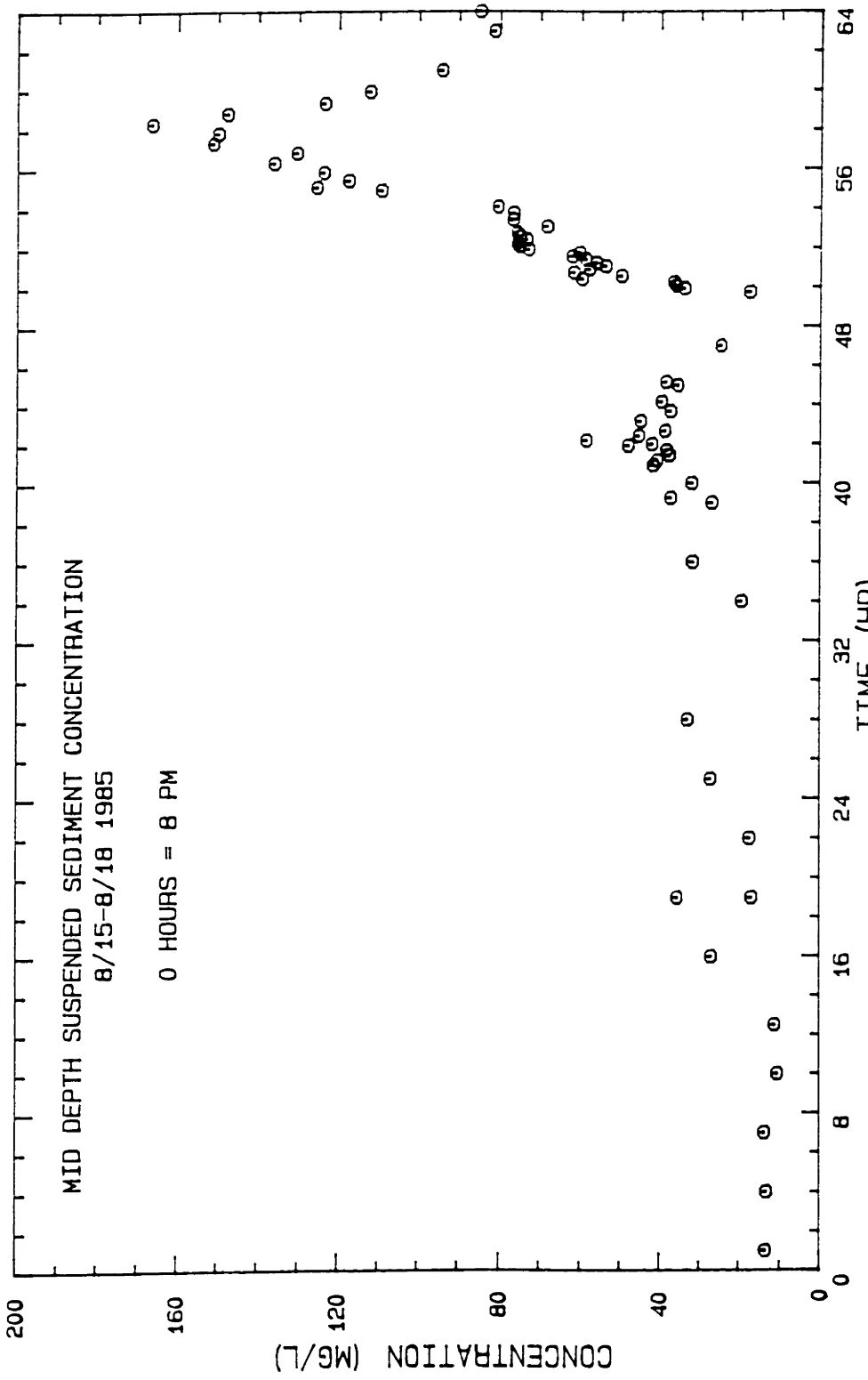

Figure 2.41 Suspended sediment concentrations, Keszthely deployment.

occurs rapidly. Both the mean current and the wave height were higher during the latter event.

A less evident feature of the concentration data is the apparent stair stepping or steady-state values reached around hour 52 and hour 54 during the larger period of concentration increase associated with the big storm. This would not have been evident from hourly sampling, but because samples were taken every 10 minutes the trends are well established.

Using a typical measured velocity of 10 cm/s sediment could have been transported horizontally a distance of almost 3 km during the 8 hours of suspended sediment increase measured during the latter storm.

Additional Data

Although not as complete as the data set presented above, longer-term concentration and wind speed measurements provide further useful information about sediment resuspension at the Keszthely site. The concentration measurements are shown in Figure 2.42 while the 30-minuite average wind speed and direction measured at the nearby meteorological station (see Figure 2.28) is given in Figure 2.43. The concentration data indicate that there were two major resuspension events during this period--one at the very beginning (before the field equipment could be completely deployed) and one included in the data set discussed above. Interspersed over the remainder of the period are several minor resuspension events in which concentrations reached about 40 mg/l.

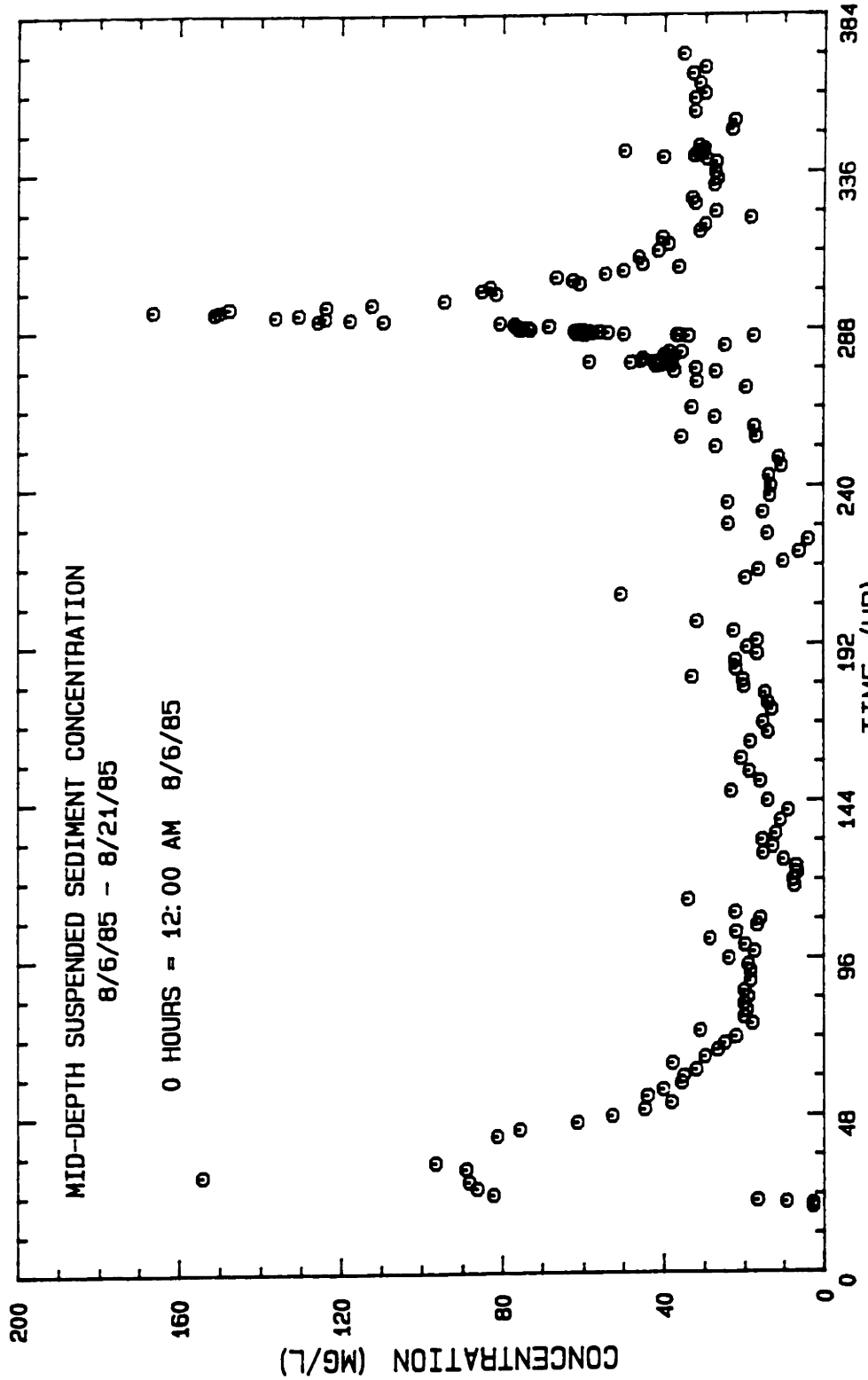

Figure 2.42 Suspended sediment concentrations during the 15-day field experiment at the Keszthely field site. Figure 2.41 covers the period of 235-296 hours.

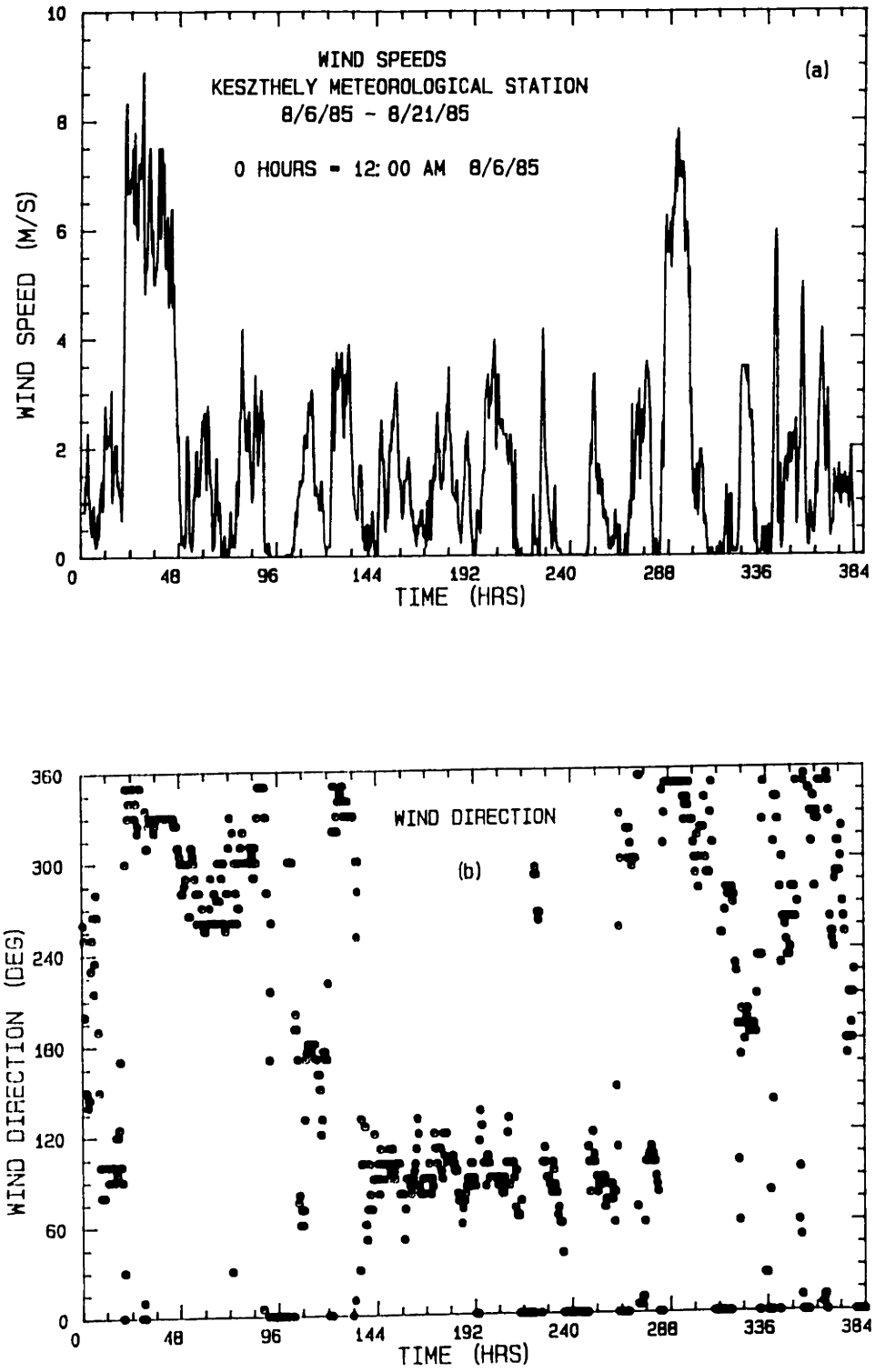

Figure 2.43 30-minute average wind speed and direction measured at the Keszthely meteorological station during the 15-day field experiment at the Keszthely field site. Figure 2.38 covers the period of 235-296 hours.

2.5.3 Discussion

Mean current and suspended sediment measurements at two locations on Lake Balaton showed significantly different behaviors, while waves observed at each location had quite similar characteristics. The significant wave height was strongly related to the wind speed and fetch, while the mean wave period was at or a little above 2 seconds during substantial wave events. The mean current at Tihany seemed often dominated by the flow through the Tihany Strait which in turn was mainly controlled by the lake's longitudinal seiching activity. However, these currents were generally small (reaching values of only 4-6 cm/s) and unlikely directly the cause of resuspension. A short but intense event with winds oriented across the lake produced currents several times as large as any others measured during either deployment. It is much more likely that these contributed to resuspension although concurrent concentration measurements were not made. It is not completely clear what these large currents are attributable to, although it is most likely they are associated with a transverse seiche in Siofok basin. At Keszthely longitudinal winds were accompanied by a more sustained northerly or southerly flow probably indicative of a horizontal eddy in the Keszthely basin. Again these mean currents seemed unable to resuspend sediment on their own. A stronger wind from north to south resulted in a return flow against the wind at the deployment site which was closely coupled to variations in wind intensity. Due to the final equipment failure it is unknown how much of a seiching motion was set up by this wind.

Resuspension at Tihany was smaller than at Keszthely probably due to the finer particle sizes making up the Keszthely sediment. However, during

the periods for which suspended sediment concentration was measured at Tihany, no events having current speeds and wave heights as large as those of the major resuspension event at Keszthely were observed.

Despite the failure of the ABSS the data set presented in Section 2.5.2 is one of the best obtained to date for the purposes of understanding the resuspension of fine, presumably cohesive, lake sediments during a storm event. To proceed it is desirable to model the hydrodynamic response of the lake to a wind event and the sediment response to the resulting hydrodynamic forcing. The data in Section 2.5.2 offer an opportunity to evaluate the components in such a model while the longer-term wind and sediment concentration data provide an opportunity for model verification.

Chapter 3

Cohesive Sediment Response to an Applied Hydrodynamic Forcing

To study the erosion and deposition of cohesive sediments, it is necessary to understand both the hydrodynamical processes occurring in the water column and the resulting sediment response. Most of the data collected as a part of this study, (Chapter 2), were oriented toward quantifying the hydrodynamical processes occurring in the water column at the study sites in Lake Balaton. Chapter 3 is devoted to understanding the cohesive sediment response.

Fine or cohesive sediments are considered to be any mixture consisting predominantly of silt and clay and possessing some degree of cohesion when in a wet dense state, (Partheniades 1972). Because of their small size and low settling velocities these particles are transported in suspension and constitute much of the "wash-load" of many streams, (Krone 1983). They can be contrasted with coarse or non-cohesive sediments, which consist mainly of sand and gravel. The major distinction between the two groups comes from the importance of physico-chemical attractive and repulsive forces in affecting their behavior. This is typified by the structure of clay particles which are small thin plates with negatively charged faces and positively charged edges. These particles attract positively charged ions (cations) from the surrounding water which form a cloud around the negative faces. Aggregation can occur as a result of attraction between the positive edge and negative face of two particles, forming a open "cardhouse" arrangement, or in a parallel stacking in which a layer of cations is "sandwiched" between two clay faces. The latter structure is encouraged when the surrounding water has a high concentration of salt and

therefore positive ions, when there is an overburden pressure, or when the temperature is decreased, since in each case the ability of the repulsive electro-chemical forces to keep the particles apart is reduced. Depending on the favorability of the chemical environment aggregation may occur when particles collide. Such collisions are a result of Brownian motion, differential settling, turbulent fluctuations and velocity gradients in the surrounding water.

To date the response of a cohesive sediment bed to an applied stress has been considered to occur using either of two theories. These will be called previous theories 1 and 2 or just PT1 and PT2 and are defined as

PT1 - The sediment flux consists exclusively of either erosion from the sediment bed to the water column or deposition to the sediment bed from the water column.

PT2 - The sediment flux consists of simultaneous erosion and deposition between the sediment bed and the water column.

The distinction between PT1 and PT2 is clearest at conditions of steady state when

Erosion - Deposition = 0

Using PT1 at steady state

Erosion = 0 and Deposition = 0

while using PT2 at steady state

Erosion = Deposition

From a physical perspective PT1 assumes that erosion will only occur when the applied stress is greater than the cohesive strength of the

sediment bed. Similarly, deposition can not occur unless the applied stress is less than the bed strength. On the other hand PT2 assumes that the sediment bed-water column exchange occurs in a fashion analogous to that observed with cohesionless sediment.

Conflicting experimental evidence exists in support of both PT1 and PT2, although the majority of the results have been interpreted using PT1. Rather than reviewing these results strictly in terms of PT1 and PT2, a new, more general, conceptual model of the exchange process is proposed in Section 3.1 which includes the physical processes encompassed both by PT1 and PT2. It leads to two equally valid approaches, DIM A1 and DIM A2, for specifying the sediment flux into or out of the water column. To conclude Section 3.1, a simple analytical model is proposed and yields a general expression for the sediment flux into or out of the water column using DIM A2.

In Section 3.2 previous laboratory experiments are interpreted using the proposed conceptual model while the inability of either PT1 or PT2 to explain these results is exposed along the way. Results of these experiments are used to provide quantitative verification of the conceptual model presented in Section 3.1 and to specify an empirical expression for DIM A2.

In Sections 3.3 and 3.4 previous field and modeling studies of cohesive sediment transport are presented.

In Section 3.5 a bottom boundary condition following DIM A2 is recommend for use in Chapter 5.

3.1 A CONCEPTUAL MODEL OF THE EXCHANGE BETWEEN A COHESIVE SEDIMENT BED AND THE OVERLYING WATER COLUMN IN RESPONSE TO A HYDRODYNAMIC FORCING.

The general conceptual model is presented in Figure 3.1 and includes the sediment bed, a surface zone and the water column. Because of the presence of two theoretical interfaces, it will be called a double interface model, (DIM). The definition of the water column and the sediment bed are obvious ones with the latter consisting of sediment particles that are bound together cohesively. The surface zone is considered to consist of sediment particles or flocs which are in contact with the bed surface but which are either not cohesively bound to the bed or are bound at a very low cohesive strength. Sediments in the surface zone may be those which have recently settled out of the water column and have not had enough time to bond with the bed, or those whose cohesive bonds with the bed have been broken but which have not been suspended.

When sufficient stress is available across the sediment bed-surface zone boundary to overcome the cohesive bonds and frictional forces between sediment particles as well as their submerged weight, sediments will be ripped from the bed yielding a non-zero rip-off rate, ($E_1 > 0$). (It is convenient to define the combined cohesive bonding strength, inter-particle friction force, and submerged weight of a particle in the bed as the "bed strength." When the stress applied at the boundary, τ_b, becomes equal to the bed strength and rip off first begins to occur, the applied stress is defined to be equal to the critical stress of the sediment bed, denoted τ_{csb}. Therefore, the bed strength and τ_{csb} can be used interchangeably and if $\tau_b > \tau_{csb}$ then $E_1 > 0$). Any particle undergoing the process of consolidation into the bed when $E_1 > 0$ must also be ripped away because it

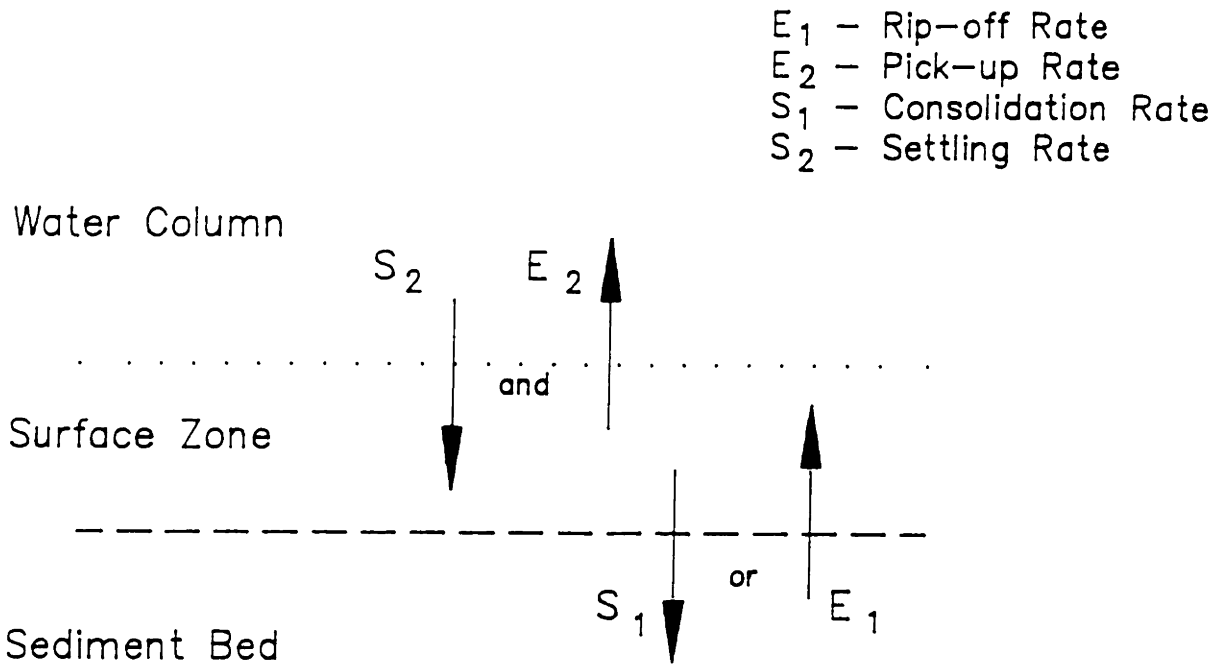

Figure 3.1 Conceptual double interface model of the physical processes involved in cohesive sediment exchange at the sediment-water column boundary.

would not have reached full bed strength. Therefore if $E_1 > 0$, then $S_1 = 0$. By the same argument, if τ_b is small enough that particles can successfully consolidate into the bed, ($S_1 > 0$), then τ_b must be less than τ_{csb} and therefore $E_1 = 0$. Thus the exchange process at the surface zone-sediment bed interface is expected to be exclusively in one direction or the other.

A stress applied at the water column-surface zone interface which is strong enough to overcome any minimal cohesive bonding, the inter-particle friction forces and a particle's submerged weight will result in a non-zero pick-up rate, ($E_2 > 0$), provided there are sediments in the surface zone to pick up. (In a manner similar to before, the surface zone strength is defined and is quantitatively equal to the critical stress of the surface zone, τ_{csz}.) Pick up will indiscriminantly include recently settled particles, those existing in the surface zone from previous times and those recently ripped from the sediment bed, since cohesive bonding is minimal and a particle entering the surface zone becomes equivalent to all other particles instantaneously. As a result, there is a concurrent exchange in both directions across this interface. It can be anticipated that this process is very similar to the exchange between coarser particles and a non-cohesive bed. In the latter case classical experiments by Dobbins (1943) using grid generated turbulence have shown qualitatively that the amount of sediment brought into suspension is dependent on the rate of turbulence generation. Therefore, it may be presumed that the pick-up rate is some function of the applied stress in excess of the critical stress of the surface zone.

For the purposes of determining the net sediment flux into or out of the water column, it is only necessary to know quantitatively what is

happening at the surface zone-water column interface since this is in direct contact with the water, i.e.,

$$\phi = E_2 - S_2 \tag{3.1}$$

As long as the surface zone remains populated with sediment, E_2 can occur at its maximum possible rate for the given sediment and applied stress and ϕ can be expressed without any consideration for processes occurring at the sediment bed-surface zone interface. As a result under this condition ϕ is independent of what has been defined herein as the bed strength.

When the surface zone becomes depopulated, Eq. (3.1) will still be valid, however E_2 can no longer occur at its maximum possible rate. Rather E_2 will be restricted by the rate at which sediments are supplied either by S_2 or by E_1. Therefore

$$\phi = E_2 - S_2 = E_1 \qquad \tau_b > \tau_{csb} \tag{3.2a}$$

It can be anticipated that when the applied stress is very much larger than the surface zone strength but only slightly larger than the bed strength the surface zone will become depopulated and Eq. (3.2a) will be valid. In this case the flux can be called bed strength limited. The limiting case of this occurs when the applied stress is equal to the bed strength and the rip-off rate is zero. In this case

$$\phi = E_2 - S_2 = E_1 = 0 \qquad \tau_b = \tau_{csb} \tag{3.2b}$$

In summary, the conceptual double interface model has suggested the bottom flux of cohesive sediments under an applied stress is effected by two types of exchanges, one being unidirectional and the other bidirectional. Given an infinite availability of sediment in the surface zone, E_2 should behave like the erosion rate of a non-cohesive sediment and the net flux would depend only on $\tau_b - \tau_{csz}$. However, when the surface zone becomes depopulated the net flux will be a function of the applied stress in excess of τ_{csb} and therefore will be bed strength limited. Regardless of the case, Eq. (3.1) will be correct, while if the flux is bed strength limited Eq. (3.2) will be valid as well.

The general applicability of Eq. (3.1) using the DIM suggests two <u>equally valid</u> approaches may be taken in specifying the bottom flux, ϕ. These are

DIM approach 1, (DIM A1) - Try to quantify ϕ directly. In particular determine two relationships, one for ϕ_e and one for ϕ_d such that

$$\phi = \phi_e \quad \text{if} \quad \frac{d\bar{c}}{dt} > 0 \tag{3.3a}$$

$$\phi = \phi_d \quad \text{if} \quad \frac{d\bar{c}}{dt} < 0 \tag{3.3b}$$

DIM approach 2, (DIM A2) - Try to quantify E_2 and S_2 and compute ϕ from Eq. (3.1).

A comparison between these two approaches and the previous theories illustrates several interesting features of PT1 and PT2.

First, the expression in Eq. (3.3) for DIM A1 could be used to express the physics contained in PT1. Likewise, an expression for DIM A2 could be

used to express the physics contained in PT2. The equivalence of DIM A1 and DIM A2 suggests that two investigators, one using an expression based on PT1 and the other an expression based on PT2, could both reproduce the same observed cohesive sediment behavior even though the physics of PT1 and PT2 may not be correct.

Second, the definition of erosion and deposition in PT1 and PT2 are significantly different. In PT1 erosion has a meaning analogous to ϕ_e in Eq. (3.3a) while deposition is analogous to ϕ_d in Eq. (3.3b). In PT2 erosion is represented by E_2 and deposition is represented by S_2. The equivalence of DIM A1 and DIM A2 indicates that an erosion rate determined using experiments interpreted with PT1 is valid in a DIM A1 boundary condition but not in a DIM A2 boundary condition. The same is true with the interchangeability of the other terms. For this reason the terminology used throughout the remainder of this text is as presented in Figure 3.1 along with $\phi_e \equiv$ net erosion and $\phi_d \equiv$ net deposition.

The purpose of determining ϕ in the present study is to solve for the concentration of sediment suspended in the water column. In one dimension, this is governed in the fluid by the transport equation

$$\frac{\partial c}{\partial t} = \frac{\partial}{\partial z}\left(w_s c - \overline{w'c'}\right) \tag{3.4}$$

where c is the suspended sediment concentration, w_s is a particle settling velocity, t is time, z is the vertical coordinate and $\overline{w'c'}$ is the vertical transport due to turbulent fluctuations in the vertical velocity and the concentration. In this equation, all horizontal transport terms, molecular diffusion and vertical advection by the fluid have been neglected. The remaining terms indicate that the temporal change is due to

the vertical flux divergence associated with settling and turbulence. Appropriate boundary conditions for Eq. (3.4) are zero vertical sediment flux at the top of the water column and a specified vertical flux at the bottom, i.e.,

$$w_s c - \overline{w'c'} = 0 \qquad \text{at} \qquad z = h \quad \text{(free surface)} \tag{3.5a}$$

and

$$- w_s c + \overline{w'c'} = \phi \qquad \text{at} \qquad z = 0 \quad \text{(bottom)} \tag{3.5b}$$

An alternate form of Eq. (3.4) which will be considered in this study comes from the integration of Eq. (3.4) over the depth of the water column, h, making use of Eqs. (3.5a) and (3.5b) as boundary conditions. This yields

$$h \frac{d\bar{c}}{dt} = \phi \tag{3.6}$$

where $\bar{c}$ is the depth-averaged suspended sediment concentration defined as

$$\bar{c} \equiv \frac{1}{h} \int_o^h c \, dz \tag{3.7}$$

At this point to solve either Eq. (3.4) or (3.6), an analytical expression must be given for ϕ. One analytical model of ϕ is suggested by Eq. (3.5b) which can be written as

$$- w_{so} c_o + \overline{w'c'} \Big|_o = \phi \tag{3.8}$$

where the subscripts "o" indicate evaluated at the bottom. However, the

use of this equation requires a parameterization of the turbulent transport term. Two possible choices are presented below.

Defining a reflectivity parameter, α, as

$$\alpha \equiv \frac{\overline{w'c'}}{w_{so}c_o} \tag{3.9}$$

Eq. (3.8) becomes

$$\phi = w_{so}c_o(\alpha - 1) \tag{3.10}$$

In this case for $\alpha = 0$ the bottom completely absorbs any particles reaching it while for $\alpha = 1$ the bottom reflects all incident particles. This parameterization has found use in modeling suspended concentrations in settling tanks.

Alternitively, defining

$$\beta \equiv w_{so}\frac{c_o}{\bar{c}} \tag{3.11}$$

and

$$c_{ss} \equiv \frac{\overline{w'c'}}{\beta}\Big|_o \tag{3.12}$$

Eq. (3.8) can be written as

$$\phi = \beta(c_{ss} - \bar{c}) \tag{3.13}$$

Given enough turbulence in the water column for the sediments to be

relatively well mixed over the depth, i.e., if $\bar{c} \approx c_o$, then

$$\beta \approx w_{so} \tag{3.14}$$

For obvious reasons c_{ss} can be interpreted as a steady-state suspended sediment concentration.

A comparison between Eq. (3.13) and DIM A2 suggests that

$$E_2 = \beta c_{ss} \tag{3.15a}$$

$$S_2 = \beta \bar{c} \tag{3.15b}$$

Note, the parameterization in Eqs. (3.10) and (3.13) are equivalent. To maintain as much consistancy as possible with previous studies of cohesive sediment transport, the latter parameterization will be used below.

For two idealized cases, the form of the suspended concentration in time expressed by Eq. (3.6) can be solved for explicitly.

Case 1 is when the flux is controlled by the bed strength. As expressed in Eq. (3.2a) this means $\phi = E_1$. If the stress applied at the surface zone-sediment bed is constant in time and the bed strength is constant with depth into the bed, E_1 must also be constant in time. In this situation integration of Eq. (3.6) yields

$$\bar{c} = \bar{c}_i + \frac{E_1}{h}(t - t_i) \tag{3.16}$$

where $\bar{c}_i$ and t_i are the initial conditions. Eq. (3.16) suggests that the

concentration will increase linearly in time as long as the assumed conditions are maintained.

Case 2 makes use of Eq. (3.13) to express ϕ. In addition, it is assumed that β and c_{ss} are constant in time. Integration of Eq. (3.6) gives

$$\bar{c} = c_{ss} + (\bar{c}_i - c_{ss}) \cdot \exp(-\frac{\beta}{h}(t - t_i)) \qquad (3.17)$$

showing that the concentration changes exponentially in time.

Further use is made of both Eq. (3.16) and (3.17) in Section 3.2

Summarizing the content of this section, a conceptual double interface model was first presented to aid in the understanding and quantification of the net exchange flux, ϕ, occurring at the water column-sediment boundary for a given hydrodynamic forcing. It suggested this flux is dependent on a unidirectional exchange between the cohesive sediment bed and a surface zone (E_1, S_1) and a bidirectional exchange between a surface zone and the water column (E_2, S_2). While ϕ is always equal to the difference between E_2 and S_2, it can be controlled by processes at the other interface in which case the flux is bed strength limited. An expression for ϕ may be posed directly in terms of appropriate variables, DIM A1, or expressions may be posed separately for E_2 and S_2, and ϕ computed with Eq. (3.1), DIM A2. An analytical expression based on a parameterization of the suspended sediment transport equation led to general expressions for E_2 and S_2, Eqs. (3.15a) and (3.15b).

3.2 THEORETICAL AND LABORATORY RESULTS FOR COHESIVE SEDIMENTS

The psysico-chemical interactions so complicate the behavior of cohesive sediments that historically very little purely theoretical progress has been made in quantifying ϕ. Rather, most of the exisiting relationships are empirically based on experimental data obtained in the laboratory. Early erosion studies were invariably conducted to correlate either the erosion rate under a specified flow condition, or the critical flow conditions required to initiate sediment erosion, i.e., the critical velocity or the critical shear stress, to gross sediment properties such as vane shear strength, Atterberg limits, particle size, voids ratio and per cent silt and clay. Unfortunately, the range of test equipment and sediment conditions makes it very difficult to quantitatively compare the results of many of these studies or to extrapolate the findings to field conditions. For example, Dunn (1959) and Moore and Masch (1962) subjected sediment samples to scour from vertically pointing submerged jets. Moore and Masch (1962) developed an apparatus in which a cylindrical sample of cohesive soil was placed concentrically into a slightly larger cylindrical container with water filling the space between the two. A stress was created by rotating the outer cylinder. Christensen and Das (1974) studied erosion rates using a constant flow of water through a brass tube lined with clay. Carlson and Enger (1963) tested soil samples set into a well, flush with the bottom of a circular tank, using stress generated in the overlying water by a rotating impeller. Various other researchers conducted flume studies using either sediment filled trays set into a drop section in the channel bottom (e.g. Kamphius and Hall, 1983; Southard et al., 1971) or sediment beds covering the entire flume bottom, (e.g.,

Grissinger, 1966; Abdel-Rahman, 1962; Krone, 1962). Krishnamurthy (1983) found substantial differences in the critical shear stress of identically pepared samples subjected to erosion by a submerged jet and steady flow in a flume. Partheniades (1972) concluded that small scale tests give higher critical shear stresses than tests in open rectangular flumes.

Adding to this uncertainty is the lack of standardization in the preparation of sediment samples. Early experiments were often conducted using placed beds which might be anything from a thick slurry, (Mehta and Parthenaides 1979), to a bed which was consolidated in a soil press, (Abdel-Rahman 1962; Kamphuis and Hall 1983; Ariathurai and Arulanandan 1978; Krishnamurthy 1983).

More recently deposited beds have been proposed as more representative of beds being found in nature. (Southard et al. 1971; Fukuda and Lick 1980; Lee et al. 1981; Mehta et al. 1982; Parchure and Mehta 1985 and many others.) A deposited sediment bed is created by bringing a large amount of sediment into suspension and then allowing it to settle in place for a specified time period. However, Lee et al. (1981) noticed that when creating a deposited sediment bed in the laboratory, a thin layer of very fine sediments frequently formed at the sediment surface. They felt that this was not representative of the structure of a natural bed and, therefore, homogenized the upper 5mm of the sediments by resuspending them and allowing them to deposit a second time. This procedure resulted in a factor of four decrease in the erosion rate and a factor of five to ten decrease in the steady-state suspended sediment concentration when compared with the once deposited bed.

The careful analysis of the more rigorous experiments suggested that gross soil properties did not characterize the erosion resistance of a fine

sediment, Partheniades (1972). Raudkivi (1976) concluded: "In general, the shear strength of a soil (i.e. as measured by a vane) has little bearing on its erodability. Critical shear stresses have been found to be orders of magnitude lower than corresponding soil shear strength and the same flow conditions may initiate erosion in cohesive soils which differ in shear strength by orders of magnitude."

3.2.1 Qualitative Results

Observations of the interaction between a cohesive sediment bed and its overlying water column indicate that it may be characterized by several types of behavior. Very soft muds can have properties similar to a viscous fluid, in which case a distinct interface develops between the water and the sediment, and interfacial waves may form. If the water velocity is larger than the phase velocity, these waves break and cause mixing between the mud and water, (Migniot, 1968). A substantial flow may also be developed in the sediment bed itself, particularly in the presence of surface waves with lengths which are large compared to the depth and with large amplitudes. In turn, the mud often acts as a substantial source of damping for the waves, (Yamamoto et al. 1986). At increased strength the sediments cease to behave like a fluid. Migniot (1968) reported that surface wrinkles or ripples appeared in steady flow experiments, which retracted as if they were elastic when the flow was stopped. This is the only report of such behavior, however.

Typically, erosion occurs as a random removal of surface particles and flocs, defined as "surface erosion," which often leaves small holes or ridges aligned with the flow direction. (Southard et al. 1971; Partheniades 1972; Talebbeydokhti and Klingeman 1984.) Less often a

massive scouring of large bed portions, termed "bulk or mass erosion", has been observed. In no case has any type of bed load layer been reported. Rather, all of the particles or flocs which have eroded from the bed have been immediately incorporated into suspension. Based on a bed strength limited flux, Partheniades (1977) has presented arguments for why a bed load layer does not exist for cohesive sediments.

Bulk erosion is characterized by a large scale failure along a fault plane located some depth below the bed surface. Dixit (1982) found that kaolinite deposited in tap water was entrained via bulk erosion for deposition times less than two hours, after which surface erosion occurred. The erosion rate associated with bulk erosion is theoretically infinite since, as defined, this process consists of an instantaneous entrainment of a large quantity of sediment. Because its occurrence is infrequent and is dependent on the location of fault planes in the bed, few attempts have been made to characterize this process experimentally.

Laboratory experiments investigating surface erosion have yielded erosion rates having the general form:

$$\phi = \phi\,(\tau_b,\ \eta_1, \eta_2, \ldots\ \eta_n)$$

where ϕ is the erosion flux (erosion rate/area) and η_1, η_2, $\ldots\eta_n$ are physico-chemical parameters specifying the bed resistivity. Some of the parameters on which entrainment has been shown to depend are: (i) bed consolidation, often expressed via the bed density or the bed water content, (ii) bed make-up including mineralogy, particle size, and organic content, (iii) temperature, (iv) chemistry of the overlaying and pore fluid, particularly its salinity, (v) bioturbation from benthic organisms and (vi) the presence of cementing agents such as iron oxide or mucus excreted by benthic organisms.

Almost all of the laboratory studies into cohesive sediments have been conducted under steady flow conditions. However, various investigators have emphasized the importance of waves on cohesive sediment transport in shallow lacustrian and coastal water bodies. (Anderson 1972; Lick 1982; Hakanson 1977). Sleath (1984) suggests that the critical stress for the initiation of motion will be the same for wave-induced motion and steady flow. This is due to the small size of cohesive particles and the negligible effects of acceleration at such low Reynolds numbers.

The only experimental evidence is a comparison study by Talebbeydokhti (1984) on the initiation of motion caused by waves and a steady flow using deposited beds consisting of sediments from Sturgeon Lake, Oregon. All the runs were characterized by the formation of a skin layer at the sediment surface, which was resuspended via a local "peeling off" accompanied by the formation of narrow groves or pit marks and streaks on the bed surface. Once the skin layer was removed, underlying sediments were eroded in a particle by particle fashion. The skin layer re-formed overnight in the absence of continued eroding stress. This layer seemed to be the single most important factor constraining erosion; that is, no significant difference existed in the behavior of beds deposited for 71 days in comparison to those deposited for a week. The organic content of sediments which were resuspended was significantly larger than the average organic content of the bed suggesting that the skin layer was partially formed by bacteria and other bottom dwelling organisms. Initiation of motion was observed in steady flow at bottom stresses from 5.1 - 6.1 dynes/cm^2 and in waves at maximum shear stresses of 3.7 - 5.5 dynes/cm^2. Artificially roughened beds showed motion at lower bottom stress than smooth beds. All

of the erosion which occurred did so via surface erosion. Bulk erosion could not be induced regardless of the applied flow conditions.

3.2.2 Quantitative Results

Quantitatively some progress has been made toward expressing ϕ from specific sediment samples under systematic, well-defined variations in applied stress and a limited number of physico-chemical parameters. These results are organized into three categories. The first is in terms of a single interface model (SIM), while the second and third are the two different approaches which are possible using the DIM. Reviewing briefly, the latter two are:

DIM A1 - Try to quantify ϕ directly. In particular determine two relationships, one for ϕ_e and one for ϕ_d such that

$$\phi = \phi_e \quad \text{if} \quad \frac{d\bar{c}}{dt} > 0 \tag{3.3a}$$

$$\phi = \phi_d \quad \text{if} \quad \frac{d\bar{c}}{dt} < 0 \tag{3.3b}$$

This has been done by conducting two separate types of experiments, one being an "erosion" experiment ($\frac{d\bar{c}}{dt} > 0$) and one being a "deposition" or settling experiment ($\frac{d\bar{c}}{dt} < 0$).

DIM A2 - Try to quantify E_2 and S_2 and compute ϕ from Eq. (3.1). Typically, this has been done through "erosion" experiments.

Although the SIM will be shown to be a special case of the DIM, the body of data which has been interpreted using it is large enough to warrant considering it separately.

3.2.2.1 Single Interface Model

The conceptual model presented in Section 3.1 was, for obvious reasons, labeled a double interface model. Using a similar line of reasoning, PT1 can be interpreted as a single interface model (SIM). This SIM is identical to the DIM except that the surface zone is not included. As a result, ϕ is always equal to E_1 or S_1, and the SIM corresponds to the bed strength limited case of the DIM. Therefore, during a period of net erosion, i.e., ($\frac{d\bar{c}}{dt} > 0$), ϕ is dependent on the applied stress in excess of the bed strength. If a steady-state concentration is reached after a period of net erosion, it indicates $\tau_b = \tau_{csb}$. During a period of net deposition, ($\frac{d\bar{c}}{dt} < 0$), ϕ consists of particles whose fall velocity is greater than the flow induced lift forces and whose internal bond strength is strong enough to withstand the shear stresses near the bed. If a steady-state concentration is reached after a period of net deposition, it indicates all particles in suspension meeting the above criteria have reached the bottom.

In general, at the attainment of a steady-state concentration, the bottom stress is less than or equal to the bed strength, prohibiting further erosion, while at the same time, the flocs in suspension are too weak and small to be able to withstand the shear stresses near the bed and, therefore, are not deposited.

Much of the data used by this group has come from studies in the rotating annular flume at the University of Florida (Mehta 1973), hereafter referred to as the UF flume, a smaller version at M.I.T. (Partheniades 1972), and a straight recirculating flume also at the University of Florida (Dixit 1982). Briefly, the UF flume consists of an annular fiberglass

channel (0.20m wide, 0.46m deep, and 1.52m in mean diameter) containing sediments, a fluid and an annular ring of slightly smaller width positioned within the channel and in contact with the fluid surface. A simultaneous rotation of the two components in opposite directions generates a uniform turbulent shear flow free from external floc-disrupting elements such as pumps and diffusers. By a proper adjustment of the speeds of the two components, an effort was made to minimize rotation-induced secondary currents near the bed. Typically, experiments were conducted with water depths of 15cm to 30.5cm.

The choice of a SIM stemmed from experimental observations both over placed and deposited beds. Experiments over deposited beds were conducted by Partheniades et al. (1968) and Parchure (1984). The latter is described below.

Parchure (1984) allowed an initially well-mixed suspension of kaolinite and tap water to deposit in the UF flume for one day. This procedure yielded a deposited bed which was assumed to have increasing density and strength as a function of depth due to the longer deposition time and higher overburden pressure at deeper depths. The bed was then eroded at a bottom stress of 2 dynes/cm^2. The suspended concentration quickly reached a steady state, Figure 3.2a. After five days of erosion, the turbid water was replaced by clear water over a four hour period, while maintaining the 2 dynes/cm^2 bottom stress. This resulted in a drop in the suspended sediment concentration to 0.03 g/ℓ. Continued erosion for 24 more hours yielded a small concentration increase to 0.1 g/ℓ. These observations were interpreted to indicate that erosion proceeded to a depth in the bed where the sediment erosive strength equaled the bottom stress.

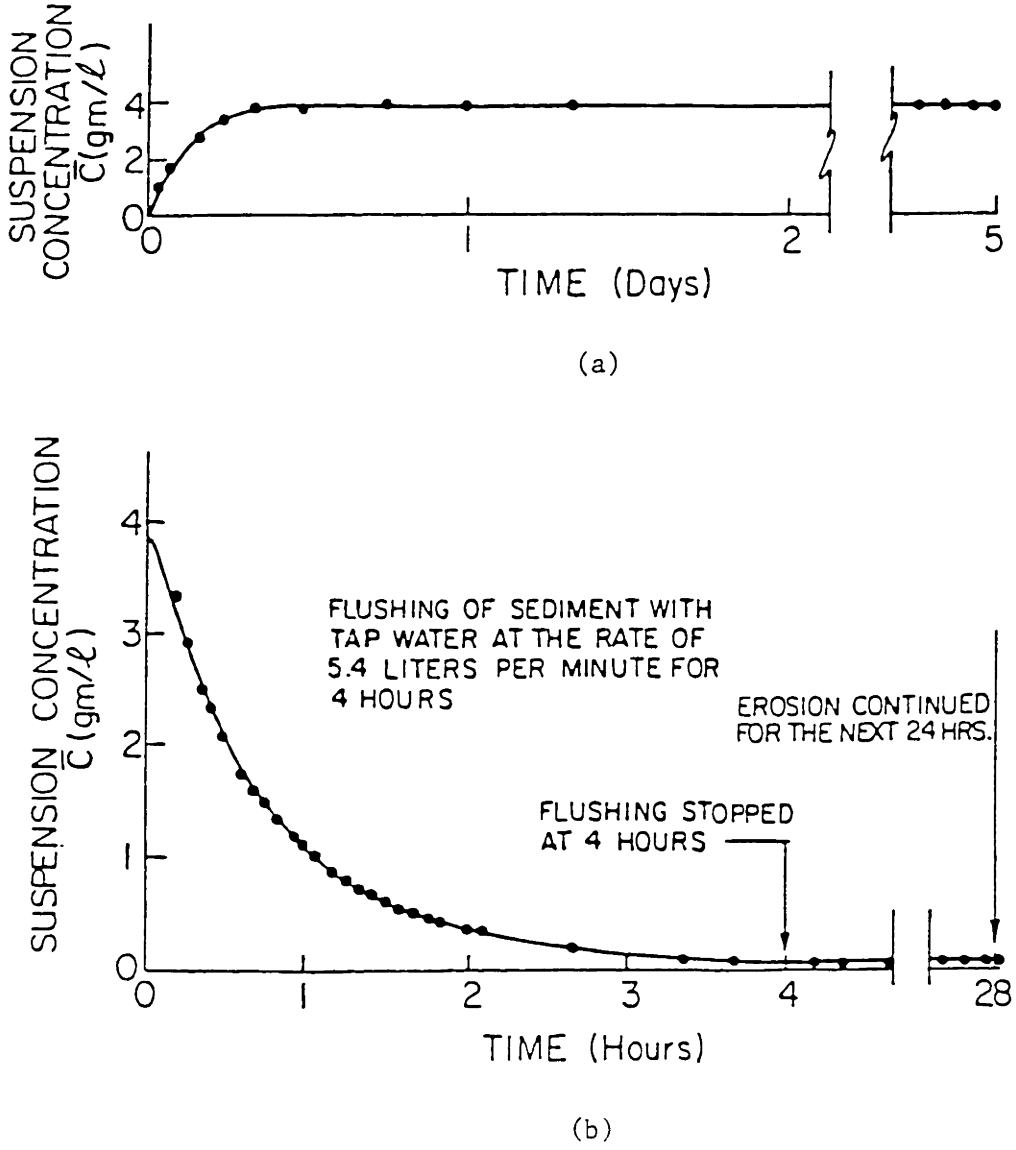

Figure 3.2 Erosion of kaolinite in tap water; Deposition time = 1 day; Bottom stress = 2.0 dynes/cm^2.
(a) Time history of suspended sediment concentration during initial erosion, (b) Suspended sediment concentration time history during and after flushing. (from Parchure, 1984)

Once the sediments were flushed out, minimal additional erosion occurred because the bed was stronger than the bottom stress.

Experiments over a placed bed are described by Mehta and Partheniades (1979). They were conducted using a procedure similar to that of Parchure (1984), except that the bed was prepared by creating, outside the channel, a slurry of kaolinite in tap water, at a density close to that of the deposited bed of Parchure (1984), and subsequently placing and leveling it in the flume. This procedure yielded a placed bed whose density and erosive strength were hypothesized to be uniform with depth. Erosion at 4.13 dynes/cm^2 produced the results shown in Figure 3.3, indicating a depth averaged concentration which increased linearly in time over the two days. Partheniades (1962) obtained similar results in experiments of up to 8 days duration, also using placed beds. This is exactly the result predicted in Eq. (3.16) which was derived for a flux which is controlled by the bed strength when the bed strength is uniform over the depth.

To summarize, the two experiments just described both indicate systems which behave like bed strength limited cases of the DIM and for this reason are adequately described using a SIM.

However, this does not mean that all cases can be treated using a SIM. This is illustrated by work was conducted in an annular flume at Case Western University, hereafter called the CW flume, which is similar to the UF flume, but with shear stress produced by a rotating top only. The flume was 0.15m wide, 0.305m deep and 1.17m in mean diamter, (58% of the surface area of the UF flume), and was typically operated at a shallower water depth than the UF flume. Because the bottom was stationary, secondary circulation was probably more significant than in the UF flume.

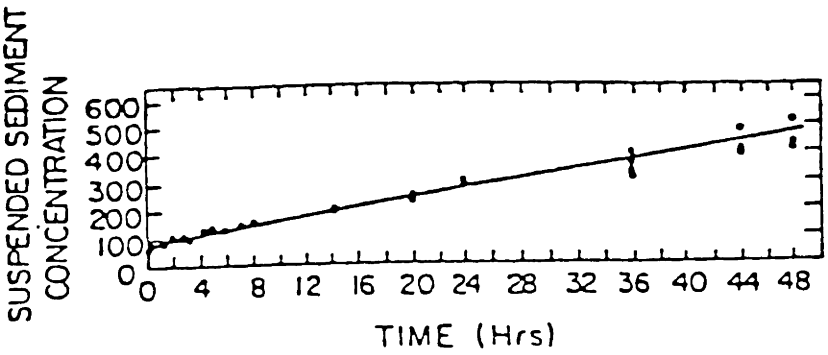

Figure 3.3 Time history of suspended sediment concentration during erosion from a uniform bed of kaolinite in distilled water. Bottom stress = 4.13 dynes/cm^2. (from Mehta and Partheniades, 1979)

Lick (1982) discusses an experiment using a deposited bed of Lake Erie sediments in the CW flume in which sediment was resuspended under a constant applied stress until a steady-state concentration was reached. By continuously withdrawing the turbid water and replacing it with clear water, up to three times the amount of sediment in suspension at steady state was entrained. This result cannot be explained using the SIM. The DIM suggests that during the initial steady states the surface zone remained populated. However, after several flushings it became depleted and a bed strength limited condition was reached.

Partheniades (1965, 1977) used the SIM to propose an erosion rate expression based on the arguments presented by Einstein and El-Samni (1949) for non-cohesive sediments and obtained Eq. (3.18) in Table 3.1. Unfortunately, the general use of the equation is made quite impractical by the difficulty associated with determining the constants and coefficients which are required.

On a more empirical basis, assuming a SIM is valid for all systems, any change in the flux during net erosion under a constant applied stress must be due to a change in the bed strength. Therefore, any expression for the flux must explicitly include the bed strength profile. To determine the bed strength profile for an arbitrary bed, the following procedure was proposed: (i) erode the bed at a constant bottom stress until a steady-state suspended sediment concentration is reached. (ii) Compute the depth of bed which is eroded, based on a mass balance. (iii) The erosive strength of the bed at that depth is equal to the bottom shear stress under which the erosion was conducted. (iv) Repeat this process with incrementally increasing bottom shear stresses to obtain the bed's strength profile.

Table 3.1. Cohesive Sediment Flux Relationships Assuming a SIM

$$E_1 = \frac{A' D_s \gamma_s}{t(\tau_b)} \left[1 - \frac{1}{\sqrt{2\pi}} \int_{\frac{-c}{k\,\bar{\tau}_b\,\eta_o} - \frac{1}{\eta_o}}^{\frac{c}{k\,\bar{\tau}_b\,\eta_o} - \frac{1}{\eta_o}} \exp\left(-\frac{\omega}{2}\right) d\omega \right] \qquad (3.18)$$

$$E_1 = E_{1o1} \cdot \exp\left[\alpha_1 \left(\frac{\tau_b - \tau_{csb}(z)}{\tau_{csb}(z)}\right)\right] \qquad (3.19)$$

$$E_1 = E_{1o2} \cdot \exp\left[\alpha_2 (\tau_b - \tau_{csb}(z))^{\delta}\right] \qquad (3.20)$$

$\delta = 1.0$ rate process theory
$\delta = 0.5$ Parchure and Mehta (1985)

Variable Definition:

α_1, α_2 - internal energy constants
γ_s - unit weight of solids
η_o - a constant
ω - dummy variable
τ_b - shear stress at sediment bed surface (force/area)
$\bar{\tau}_b$ - time-averaged bed shear stress
$\tau_{csb}(z)$ - critical stress, function of depth (force/area)
A' - dimensionless shape factor
c - macroscopic strength of the clay
D_s - average diameter of eroded clay particle or cluster
E_1 - flux during net erosion (mass/area·time)
E_{1o1}, E_{1o2} - erosion rate constants (mass/area·time)
k - dimensionless constant
$t(\tau_b)$ - time required for the breaking of a particle by τ_b

Measurements of the strength profiles of deposited beds of kaolinite and of sediment from Lake Francis, Nebraska, were conducted in water of varying salinity and with varying deposition histories in the UF flume and in a recirculating flume also at the University of Florida by Parchure (1980), Dixit (1982), and Parchure (1984). An example of the experimental procedure is shown in Figure 3.4a and the resulting bed strength profile is shown in Figure 3.4b. Each stress value was applied for a one-hour duration, which in most cases was long enough to reach an approximate steady state. Figure 3.5 shows a summary of the suspended sediment concentrations at the end of each one hour increment vs. the bottom shear stress for three experiments in which the deposition conditions that the bed was created under were varied. The dominant feature is the bilinear form of each curve. This was interpreted as indicating a rapidly increasing strength profile with depth near the bed surface and a more slowly increasing profile below. The difference between each curve shows a concentration decrease, due to the bed strength increase associated with increasing the time of deposition.

These same experiments, i.e., by Parchure (1980), Dixit (1982), and Parchure (1984), yielded erosion relationships given in Eqs. (3.19) and (3.20) in Table 3.1. A plot of Eq. (3.20) to data from Parchure (1984) for experiments using Lake Francis mud in water of varying salinity (LM), kaolinite in tap water (KT), and kaolinite in salt water (KS), the latter two with varying periods of deposition, is shown as Figure 3.6. Parchure and Mehta (1985) proposed that α_2 and E_{102} may be independent of the period of bed consolidation and the salinity of the eroding fluid, however a substantial scatter in the data is evident. A summary of the average paramater values found for each class of experiments (i.e., LM, KT, KS) is

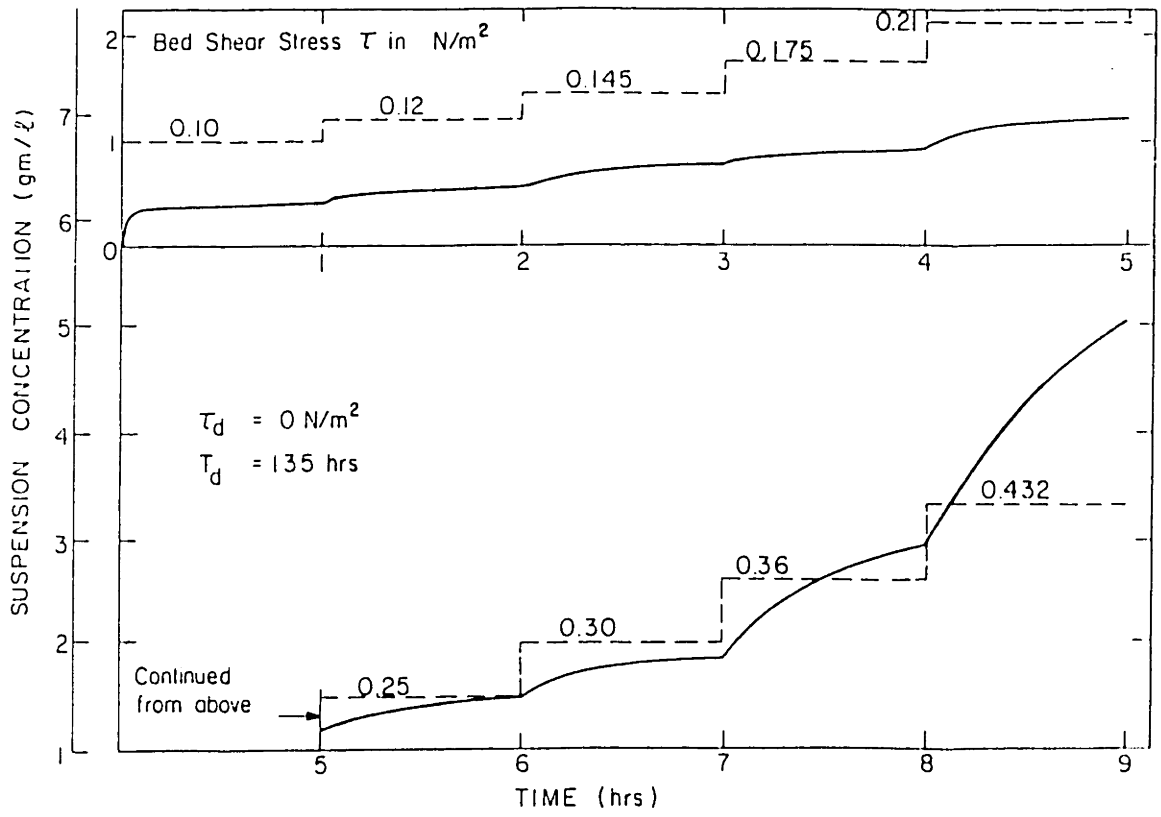

(a)

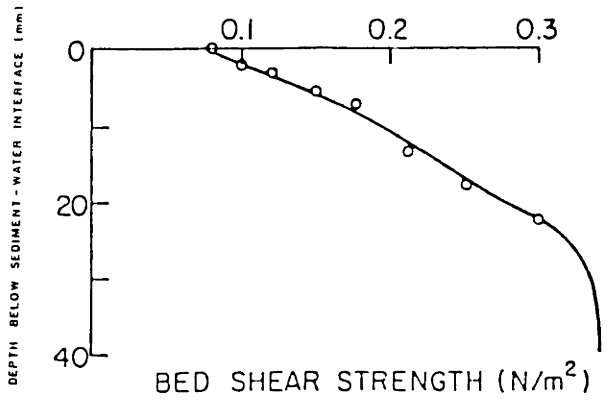

(b)

Figure 3.4 (a) Time history of applied stress and suspended sediment concentration in a bed strength experiment. T_d is the deposition time and τ_d is the stress applied during deposition. (b) Bed strength profile from experiment in (a). Note, only the first seven values were plotted. (from Parchure, 1980)

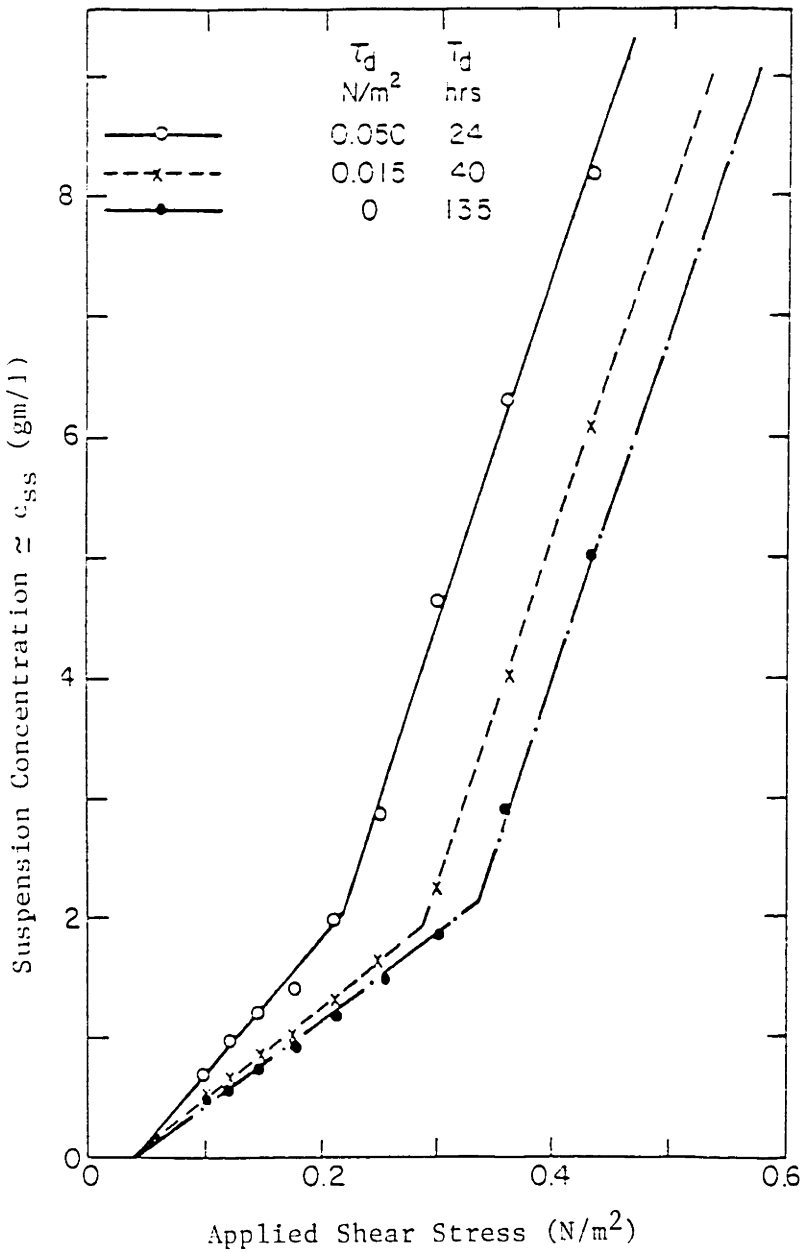

Figure 3.5 Suspended sediment concentration after 1 hour vs. applied bottom stress for three experiments having deposition time, T_d, of 24, 40 and 135 hours. The applied bottom stresses during deposition, τ_d, were 0.05, 0.015 and 0.0 N/m^2 respectively. The beds consisted of kaolinite in tap water. (from Parchure, 1980)

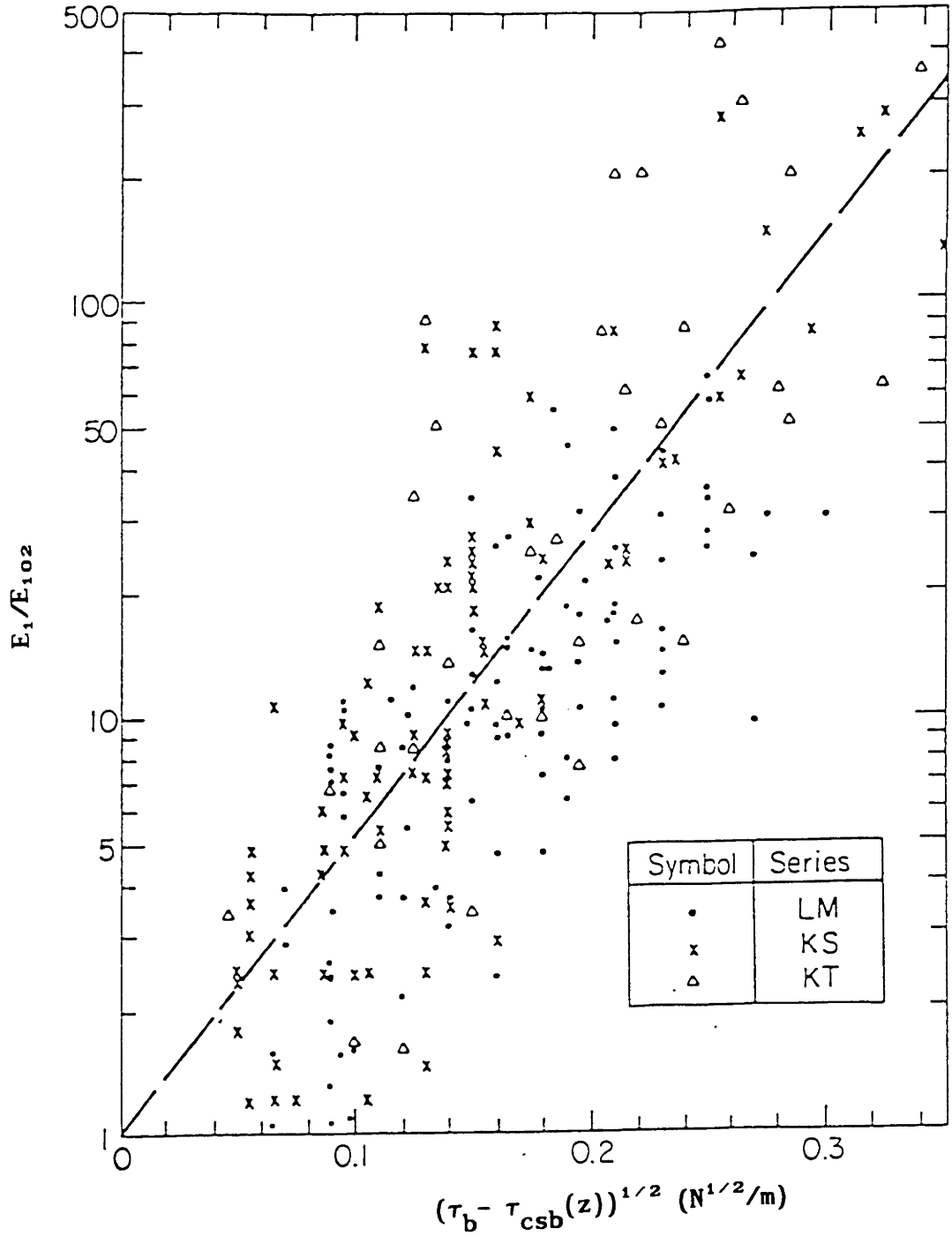

Figure 3.6 Plot of non-dimensional erosion rate vs. excess bottom stress as given by Eq. 3.20. LM = Lake Francis sediment; KS = kaolinite in salt water; KT = kaolinite in tap water. (From Parchure, 1984)

given in Table 3.2 along with values obtained from the re-analysis of experimental data from other investigators.

Table 3.2. Erosion Rate Parameters
(from Parchure, 1984)

Bed	Investigator	α_2 ($m/N^{1/2}$)	$E_{102}x10^5$ ($g/cm^2 \cdot min$)	Correlation Coefficient
Kaolinite & tap water	Parchure (1984)	18.4	0.5	0.70
Kaolinite & salt water	Parchure (1984)	17.2	1.4	0.75
Lake mud & salt water	Parchure (1984)	13.6	3.2	0.65
Bay mud	Partheniades (1965)	8.3	0.04	
Lake Erie mud	Lee et al., (1981)	8.3	0.42	
Estuarial mud	Thorn and Parsons (1977)	8.3	0.42	
Estuarial mud	Thorn and Parsons (1979)	4.2	1.86	
Kaolinite	Dixit (1982)	25.6	0.60	

Parchure (1984) argued the plausibility of an erosion rate which is exponential in shear stress using a heuristic interpretation of chemical rate process theory. These arguements uield an exponent, δ, in Eq. (3.20), of unity, although, the regression in Figure 3.6 yields $\delta = 0.5$.

To summarize the results of this section, a SIM was presented along with two supporting experiments using different types of beds. The major feature of this model is that erosion continues until the bed strength equals the applied stress. Based on the assumed validity of the SIM, experiments were conducted to characterize the bed strength profile. These resulted in expressions for the rip-off rate, which in this case equals the net erosion rate, which are exponential in the excess applied stress. The

SIM was shown to be the bed strength limited verson of the DIM. Additional experimental evidence showed that the SIM may not be generalized to all systems.

Net deposition experiments have also been conducted and interpreted with the SIM. However, the resulting relationships are appropriate for all cases of the more general DIM and, therefore, are presented in the next section under DIM A1.

3.2.2.2 DIM Approach 1

Using this method an effort is made to quantify ϕ directly. As noted before, Eq. (3.3), this typically involves two separate equations, one valid during net erosion, $(\frac{d\bar{c}}{dt} > 0)$ and one valid during net deposition, $(\frac{d\bar{c}}{dt} < 0)$. A criterion must also be determined for switching between the two.

Quantitatively, the only efforts to determine ϕ_e have been interpreted using the more restrictive SIM and were presented in the previous section.

Qualitatively, several investigators have noted that ϕ_e decays exponentially in time for a constant applied stress, eventually approaching zero at steady state, (Parchure, 1984; Fukuda and Lick, 1980; Lee et al., 1981).

On the other hand, most deposition experiments have been interpreted directly in terms of ϕ_d. (Note, clearly during quiescent settling $\phi_d = S_2$). These experiments are typically conducted by bringing a high concentration of sediment into steady-state suspension at a large applied stress. The stress is then lowered, and a time history of the sediment in suspension is determined. Several characteristic results are:

(i) Initially, a period of rapid deposition occurs lasting from a few minutes to a few hours. This is followed by a leveling off of the suspended sediment concentration to a new steady state value. Figure 3.7a shows several time histories obtained by Mehta (1973) using suspensions of kaolinite in distilled water in the UF flume. For a given sediment type, water salinity and temperature, and bottom stress, the final steady-state concentration depends only on the initial suspended sediment concentration, Figure 3.7b.

(ii) There exists a well-defined limiting bottom stress, τ_{bmin}, below which no sediment remains in suspension indefinitely. Mehta (1973) reported this to be 1.8 dynes/cm^2 (see Figure 3.7b) for kaolinite in distilled water. Krone (1962) and Mehta (1973) found values from 0.6 - 0.8 dynes/cm^2 for suspensions of San Francisco Bay muds.

(iii) A substantial hysteresis develops in the curve of steady-state suspended sediment concentration vs bottom stress depending on whether erosion or deposition takes place. If a specified stress is applied to clear water overlying a sediment bed, the steady-state suspended sediment concentration which results from the ensuing erosion will be smaller than if the same stress is applied to a suspension of depositing sediments. This is shown clearly by a combined erosion-deposition experiment in the CW flume by Lee et al (1981). Their experiment started with a deposited bed to which an incrementally increasing applied stress was added. After each stress increment constant conditions were maintained until a steady-state concentration was reached. After

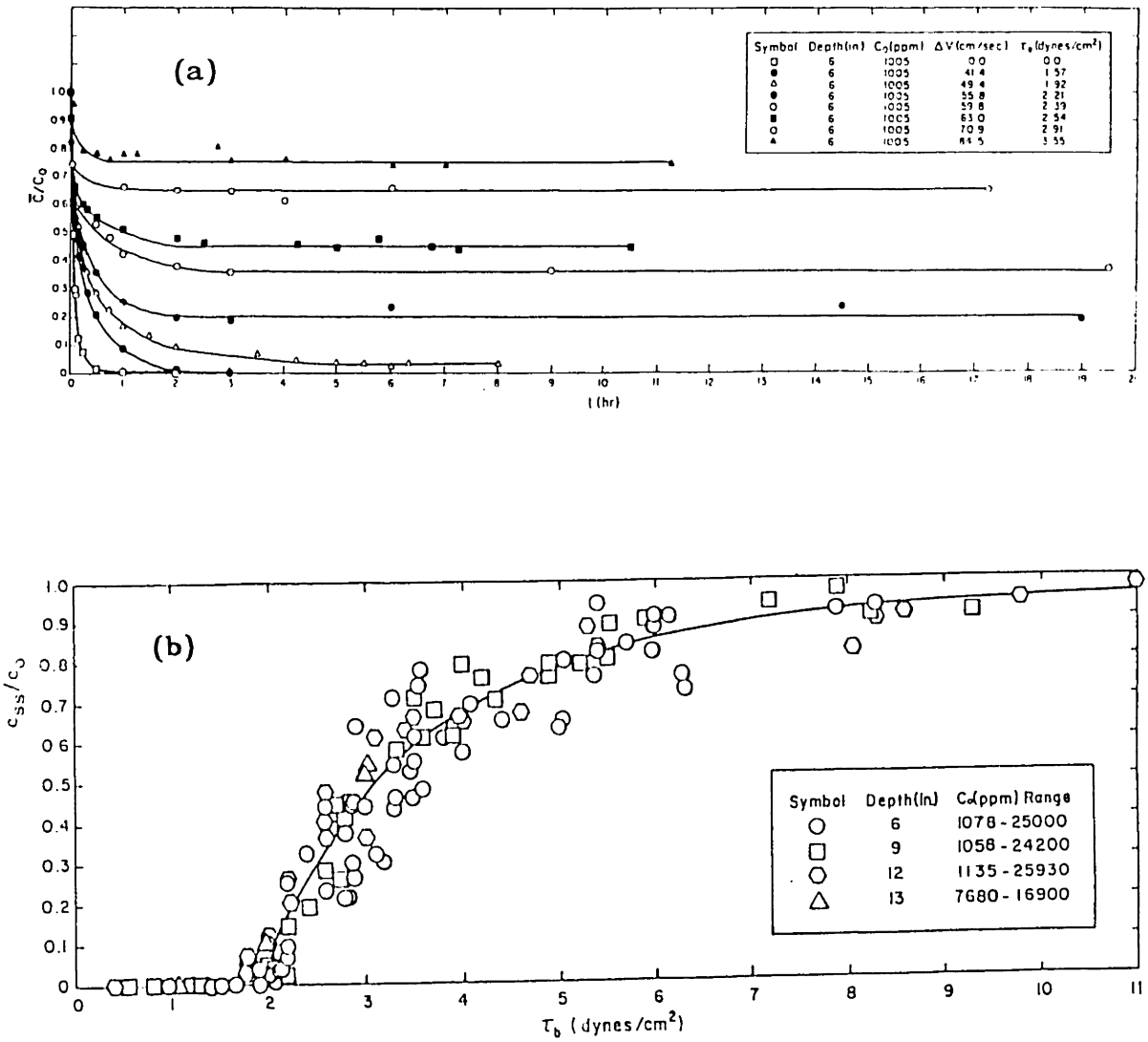

Figure 3.7 Deposition of kaolinite in distilled water. (a) Time history of dimensionless concentration for different applied stresses; (b) summary of dimensionless steady-state concentration for various initial concentrations and applied stresses. Note, in this figure c_o is the initial concentration. (from Mehta, 1973)

reaching the highest stress the stresses were then decreased incrementally, again allowing steady-state concentrations to occur at each stress level. The resulting steady-state concentrations are shown in Figure 3.8 plotted against the applied stress. They demonstrate the hysteresis effect dramatically.

(iv) The depositional process is sensitive to changes in water temperature and salinity, and sediment chemical content.

Mehta and Partheniades (1975) interpret these results by proposing that for a floc to deposit it must have a submerged weight which is larger than the flow induced lift forces and an internal strength which is strong enough to withstand the shear stresses near the bed. These properties would allow the floc to reach the bed without being broken apart and mixed back up into the flow. They concluded that the steady-state concentration is dependent on the initial concentration because a constant fraction of any suspension is capable of forming large and strong enough flocs to deposit under the prevailing stress. The hysteresis occurs because the bed strength is greater than the internal strength which can form during settling. An alternate explanation for the steady-state concentration being dependent on the initial concentration is provided by Lee et al. (1981). They assume the sediments initially in suspension consist of large particles that cannot be maintained in suspension, fine particles which remain almost entirely in suspension and intermediate sized particles which actively participate in the entrainment and deposition (i.e., E_2 and S_2). The steady state concentration is made up primarily of the fine material, which is a certain fraction of the initial sediment concentration and also by the entrainment and deposition of the

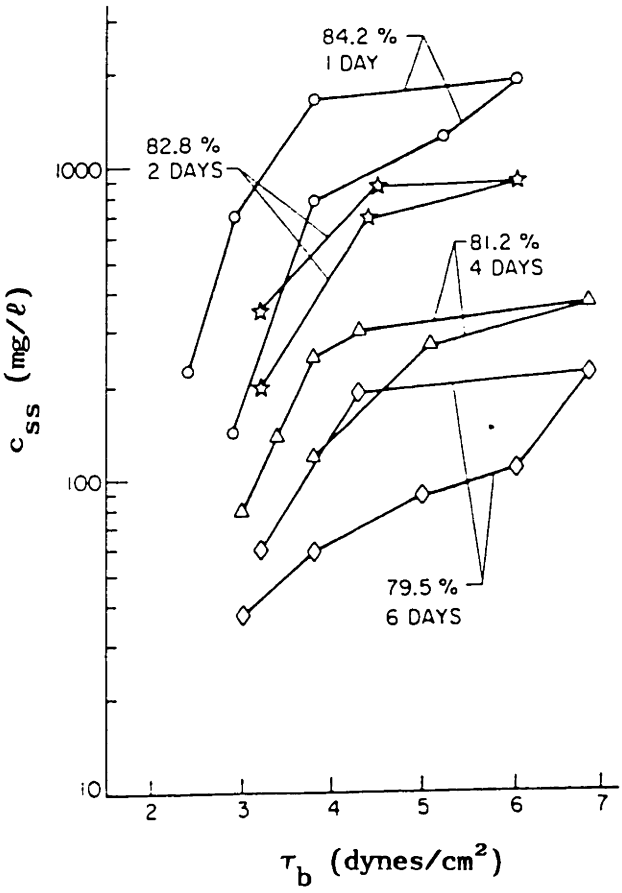

Figure 3.8 Steady-state concentration vs. bottom stress in combined erosion-deposition experiments with sediment water content as a parameter.

intermediate particles. This effectively yields a steady-state concentration which is proportional to the initial concentration. An alternate explanation for the hysteresis suggested by the DIM is the existence of a depleted surface zone during erosion which is repopulated during deposition. As a result E_2 is greater during deposition leading to a higher steady-state suspended sediment concentration.

Attempts to quantify the deposition process via the DIM A1 have led to the equations listed in Table 3.3. They were obtained from deposition in steady flow experiments or in quiescent water columns.

Krone (1962) suggested that at bottom stresses above τ_{bmin} no deposition would occur and that deposition was linearly related to the stress below this limit, Eq. (3.21). He also identified three settling regions, (i) no mutual interference, (i.e., no particle interactions), at low concentrations, ($c < 100$–700 mg/ℓ), (ii) mutual interference at higher concentrations, (300 mg/ℓ $< c <$ 10,000 mg/ℓ), and (iii) hindered settling at very high concentrations, ($c >$ 10,000 mg/ℓ). He obtained good experimental agreement for Eq. (3.21e) describing flocculation at high suspended sediment concentrations, under conditions of free as well as hindered settling.

Migniot's (1968) results, Eq. (3.22), were mostly for very high sediment concentrations and therefore are mainly appropriate for bed consolidation.

Partheniades (1972) and Mehta and Partheniades (1975) explicitly included the steady-state concentration in their deposition expressions, although Partheniades (1972) expression does not give a concentration which asymptotically approaches the steady-state concentration, c_{ss}, as time becomes infinite. Both expressions are substantially complicated by the

Table 3.3 Cohesive Sediment Flux Relationships Using a DIM Approach 1

Krone (1962)

$$\phi_d = P\, w_s\, \bar{c} \qquad (3.21a)$$

$$P = (1 - \tau_b/\tau_{bmin}) \qquad \tau_b < \tau_{bmin} \qquad (3.21b)$$

$$P = 0 \qquad \tau_b \geq \tau_{bmin} \qquad (3.21c)$$

$w_s \neq$ function of $\bar{c}$ $\qquad \bar{c} < c_1$ no mutual interaction (3.21d)

$$w_s = -K\, \bar{c}^{4/3} \qquad \bar{c} \geq c_1 \qquad (3.21e)$$

$K = K_1$ $\qquad c_1 \leq \bar{c} \leq c_2$ mutual interaction

$K = K_2$ $\qquad \bar{c} \geq c_2$ hindered settling

where,

ϕ_d - net deposition flux (mass/area·time)
τ_b - bottom stress (force/area)
τ_{bmin} - bottom stress above which no sediments are deposited
w_s - settling velocity (length/time)
P - probability that a particle that hits the bed will stick
$\bar{c}$ - depth-avg. suspended sediment concentration (mass/vol)
$c_1 \simeq 300$ mg/ℓ
$c_2 \simeq 10{,}00$ mg/ℓ
K_1, K_2 - constants

Migniot (1968)

$$\phi_d = \frac{-\alpha}{t} \qquad (3.22)$$

where,

α - constant (mass/area) (function of particle size)
t - time

Partheniades (1972)

$$\phi_d = P\, w_s\, \bar{c} \qquad (3.23a)$$

$$P\, w_s = \frac{-\alpha(c_o - c_{ss})\, h}{2.3\, t\, \bar{c}} \qquad (3.23b)$$

$$c_{ss} = \frac{c_o}{2}\,(1 + \mathrm{erf}(y_a/\sqrt{2})) \qquad (3.23c)$$

$$y_a = \frac{1}{\sigma_1}\log_{10}\left(\frac{(\tau_b^* - 1)}{(\tau_b^* - 1)_{50}}\right) \qquad (3.23d)$$

$$\tau_b^* = \tau_b/\tau_{bmin} \qquad (3.23e)$$

where,

c_{ss} - steady state suspended sediment conc. (mass/vol)
c_o - initial suspended sediment conc. (mass/vol)
τ_{bmin} - bottom stress below which no seds. stay suspended
$(\tau_b^* - 1)_{50}$ - geometric mean
h - flow depth
σ_1 - geometric standard deviation of τ_b
α - constant (length^{-1})
erf - error function
all other variables as defined above

Mehta and Partheniades (1975)

$$\phi_d = P\, w_s\, \bar{c} \qquad (3.24a)$$

$$P\, w_s = \frac{h\,(c_o - c_{ss})\; 0.434}{\bar{c}\; t\; \sigma_2\sqrt{2\pi}}\exp\left(-\frac{T^2}{2}\right) \qquad \tau_b^* > 0.25 \qquad (3.24b)$$

$$T = \frac{1}{\sigma_2}\log_{10}\left(\frac{t}{t_{50}}\right) \qquad (3.24c)$$

where,

σ_1 = 0.49 independent of material
σ_2 - standard deviation
t_{50} - geometric mean
all other variables are as defined above

need to determine the parameters of log-normal distributions for c_{ss} and in Mehta and Partheniades (1975) for ϕ_d as well. Mehta and Partheniades (1975) found that for their deposition experiments the parameters in Eq. (3.23d) were related, i.e., σ_1 was constant over all the experiments while $(\tau_b^* - 1)_{50}$ could be expressed in terms of τ_{bmin}, thereby reducing the number of parameters needed to apply this relationship. However, no general verification of these results has been made. Also no similar success was obtained in expressing the parameters in Eqs. (3.24b) and (3.24c).

Each of the equations in Table 3.3 implicitly includes effects of coagulation, erosion from the surface zone, hindered settling, etc. However, Lee et al (1981) found that in quiescent water column tests the settling characteristics of Lake Erie sediment in tap water for initial concentrations less than 500 mg/ℓ were almost identical to those of dispersed sediment in de-ionized water. This suggests coagulation may not substantially affect the settling process in fresh water at sediment concentrations typically observed in nature. It is not clear how this effect might be eliminated from Eqs. (3.23) and (3.24).

To summarize the results falling into the category DIM A1 and not already discussed in the previous section, qualitative observations of ϕ_e suggest it typically decays exponentially in time for a constant applied stress. Deposition experiments also under constant applied stress have shown that the resulting steady-state concentration is a function of the initial concentration, the applied stress and a suite of physico-chemical parameters, e.g., salinity, temperature, etc., which can be expected to influence coagulation. In addition, a hysteresis is observed between the

steady-state concentration during erosion and during deposition for the same applied stress. The dependence on initial concentration has been explained both by coagulation and fracture in the water column and by the particle size distribution. The hysteresis can be attributed to differences in the bed strength and the strength of flocs in suspension or to a population of the surface zone during deposition. Several quantitative expressions have been developed for ϕ_d; however, the more recent ones are substantially complicated by the need to know the parameters of several log-normal distributions. It may be appropriate to combine these expressions for ϕ_d with expressions for E_1 obtained in the previous section for use in a general erosion-deposition model since the SIM is a subset of the DIM A1, although, this model would only be valid in cases for which erosion was bed strength limited, (i.e., $\phi_e = E_1$). To apply such a model, it would be necessary to set $\phi = E_1$ when $\tau_b > \tau_{cbs}$ and to set $\phi = \phi_d$ when $\tau_b \leq \tau_{cbs}$ and the system is not at steady state .

In a separate quiescent water column study, it was shown that it may not be necessary to include coagulation effects in fresh water at the typical suspended sediment concentrations observed in nature.

3.2.2.3 DIM Approach 2

Using this method an effort is made to quantify E_2 and S_2 independently and then compute ϕ from the difference, Eq. (3.1). To date this has been done exclusively using erosion experiments. Recalling the results of Section 3.1,

$$E_2 = \beta c_{ss} \tag{3.15a}$$

$$S_2 = \beta \bar{c} \tag{3.15b}$$

Together with Eq. (3.1) they suggest that $\phi \approx E_2$ when $\bar{c} \approx 0$. This is the basis for a number of early determinations of E_2, most of which were conducted over placed beds. Typically these tests yielded relationships which were linear in stress either in the form of Eq. (3.25) or Eq. (3.26) in Table 3.4 (Partheniades, 1962; Christensen and Das, 1974; Ariathurai and Arulanandan, 1978). Eq. (3.25) considers erosion to be a function of the excess bottom stress above a critical value. Eq. (3.26) considers erosion to be bilinear in bottom stress since the erodability constant, M, increases when the bottom stress reaches a characteristic value, τ_{ch}, at which time the erosion is also a characteristic value, E_{2ch}. The coefficients N, τ_c, M_1, M_2, τ_{ch}, and E_{2ch} are all expected to be related to the physico-chemical properties of the sediment and water. Ariathurai and Arulanandan (1978) obtained values of N ranging from 0.003 to 0.03 g/cm^2•min for over 200 natural and made-up soil samples. Note Eq. (3.25) is a subset of Eq. (3.26) if $M_1 = 0$, $M_2 = N/\tau_c$, and $E_{2ch} = 0$. Eq. (3.26) may reflect nonuniformities in the stress field and the sediment bed since it allows a small amount of erosion, ($M = M_1$), due perhaps to the stochastic nature of bottom stresses and bed properties, when the mean values might otherwise indicate that none should occur. Erosion increases more rapidly, ($M = M_2$), for larger mean stresses. Alternatively the bilinear relationship may indicate a change in the erosive strength of the bed.

Mehta and Partheniades (1979) proposed that a linear change in the erosion rate with applied stress indicated an erosive strength which was

Table 3.4 Cohesive Sediment Flux Relationships Using DIM Approach 2

$$E_2 = 0 \qquad \tau_b < \tau_c$$
$$E_2 = N\left(\frac{\tau_b - \tau_c}{\tau_c}\right) \qquad \tau_b \geq \tau_c \qquad (3.25)$$

$$E_2 = M(\tau_b - \tau_{ch}) + E_{2ch} \qquad M = M_1 \quad \tau_b < \tau_{ch}$$
$$M = M_2 \quad \tau_b \geq \tau_{ch} \qquad (3.26)$$

$$E_2 = \beta\, c_{ss} \qquad (3.15a)$$

$$S_2 = \beta\, \bar{c} \qquad (3.15b)$$

$$\beta = w_s \frac{c_o}{\bar{c}} \qquad (3.11)$$

$$E_2 = \xi(\tau_b)^{\eta} \qquad (3.28)$$

Variable Definition:

η - erosion rate exponent
ξ - erosion rate constant (mass/area•time)
τ_b - shear stress at sediment bed surface (force/area)
τ_c - critical shear stress (force/area)
τ_{ch} - "characteristic" shear stress (force/area)
c_o - bottom concentration (mass/volume)
$\bar{c}$ - depth average concentration (mass/volume)
E_2 - erosion flux (mass/area•time)
E_{2ch} - "characteristic" erosion rate (mass/area•time)
M_1, M_2 - erodability constants (mass/force•time)
N - erodability constant (mass/area•time)
S_2 - deposition flux (mass/area•time)
w_s - settling velocity (length/time)

constant over the depth. They further proposed that this was a characteristic of placed beds and was due to the aritificial procedures used in their creation. They felt the results in Eqs. (3.25) and (3.26) would not be generally applicable to deposited beds or conditions found in nature.

In more recent studies efforts have been made to recreate a sediment bed which is representative of conditions likely to exist in the field. Typically this involves the use of a deposited bed as described previously. Fukuda and Lick (1980), Lee et al (1981) and Lick (1982) proposed the use of the relationships given by Eq. (3.15), although they defined a slightly different β. Values of c_{ss} and β were determined using incrementally applied stresses in the CW flume following a procedure similar to that described before, (e.g., Figure 3.4a), and the assumption that β and c_{ss} were constant over each period of constant stress. These assumptions correspond exactly to those under which Eq. (3.17) was derived suggesting the concentration should vary as a decaying exponential in time. An example of a measured concentration vs. time curve obtained under a constant applied stress by Fukuda and Lick (1980) using Lake Erie sediment in tap water is shown in Figure 3.9 along with a fit of Eq. (3.17).

Results from Fukuda and Lick (1980) are summarized in Figure 3.10. Values of β are typically spread over a factor of 3-4 for a given sediment type and appear to be independent of applied stress and bed water content. Also listed are the median settling velocities measured in tap water which compare reasonably well, (i.e., as suggested by Eq. 3.14), considering the two order of magnitude range in settling velocities present, Figure 3.10b. Values of c_{ss}, Figure 3.10c, appear to vary exponentially with applied stress, although many of the tests were only run at two stresses. In each

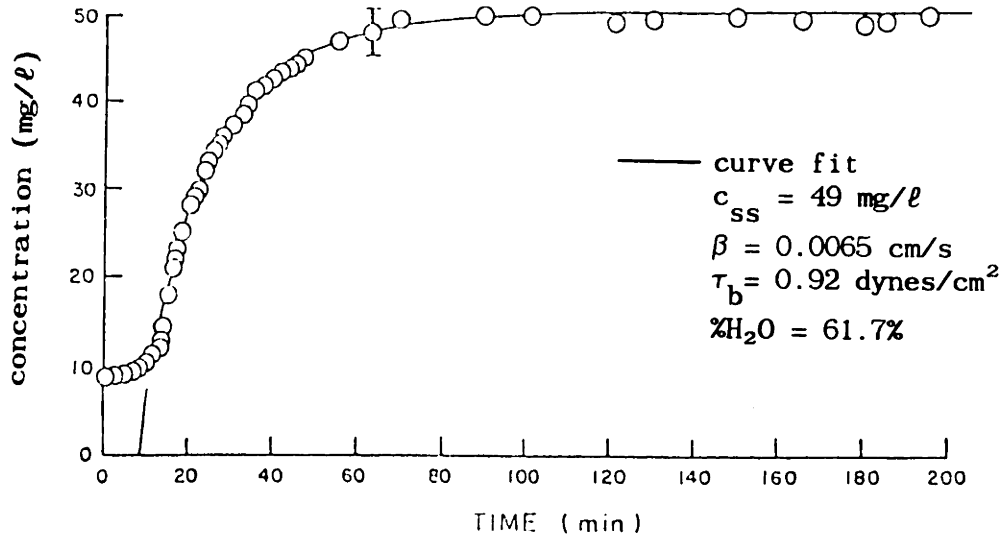

Figure 3.9 Concentration vs. time history for erosion of Lake Erie sediment under a constant applied stress. The solid line is a fit of Eq. 3.17 to the data points. (From Fukuda and Lick, 1980)

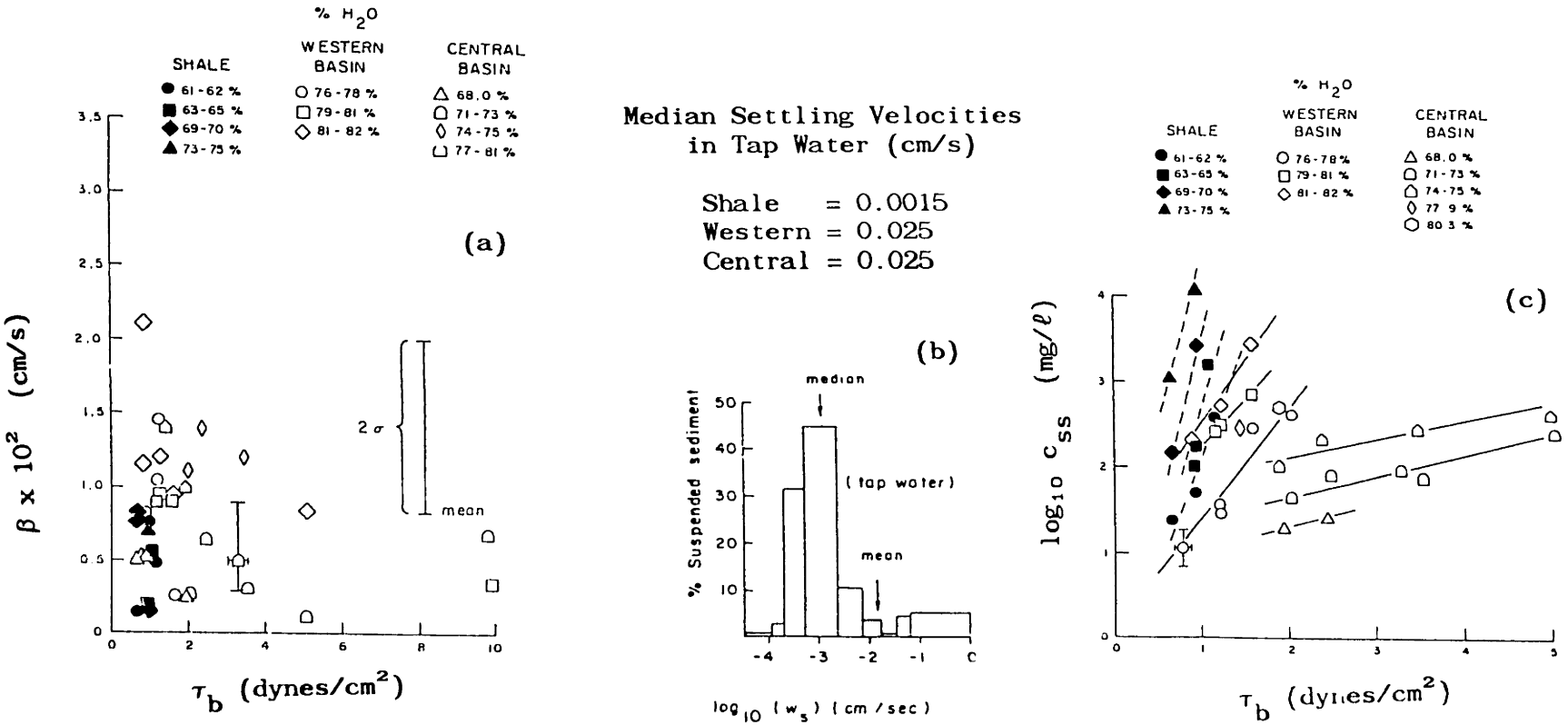

Figure 3.10 (a) Variation of β with applied stress using three different Lake Erie sediments at varying water contents (b) Distribution of settling velocities for shale based sediment in quiescent water column tests. (c) Variation of the steady-state concentration with applied stress for the three sediments from Lake Erie. (from Fukuda and Lick, 1980)

case c_{ss} decreases with decreased bed water content and therefore increased bed strength.

Lee et al. (1981) found similar results, Figure 3.11, although the variation of c_{ss} with applied stress in Figure 3.11c is closer to linear.

Parchure (1984) also fit exponential curves to data from incremental erosion studies in the UF flume using deposited beds of sediments from Lake Francis, Nebraska, in water of varying salinity. However, he discarded the significance of these results in favor of the SIM erosion relation given by Eq. (3.20). Results of a re-analysis of these data are given in Table 3.5. The values of β are remarkably constant and appear to be independent of both salinity and applied stress. Figure 3.12a shows available data from Hayter (1983) on the measured settling velocity of sediment from Lake Francis. The average values at each salinity from Table 3.5 agree closely with the direct measurements made at the University of Florida.

Table 3.5 c_{ss} and β values computed from a fit of Eq. (3.17) to data from Parchure (1984) Lake Francis sediment experiments

τ_b	Salinity									
	0.5 ppt		1.0 ppt		2.0 ppt		5.0 ppt		10 ppt	
	c_{ss}	β	c_{ss}	β	c_{ss}	β	c_{ss}	β	c_{ss}	β
dynes/cm^2	gm/ℓ	mm/s	gm/ℓ	mm/s	gm/ℓ	mm/s	gm/ℓ	mm/s	gm/ℓ	mm/s
1.4	0.62	.38								
1.7	0.75	.29								
2.1	1.33	.28								
2.5	1.97	.34	0.92	.18	0.47	.28			0.67	.30
3.0	3.12	.28	1.42	.26	0.82	.17	0.92	.29	0.79	.24
3.6	4.44	.24	2.32	.19	1.53	.27	1.91	.07	1.21	.26
4.3	6.00	.19	3.14	.20	2.38	.21	2.99	.21	1.87	.38
5.2			5.00	.11	3.61	.22			2.33	.12
6.2			6.32	.12						
mean		.29		.18		.23		.19		.26

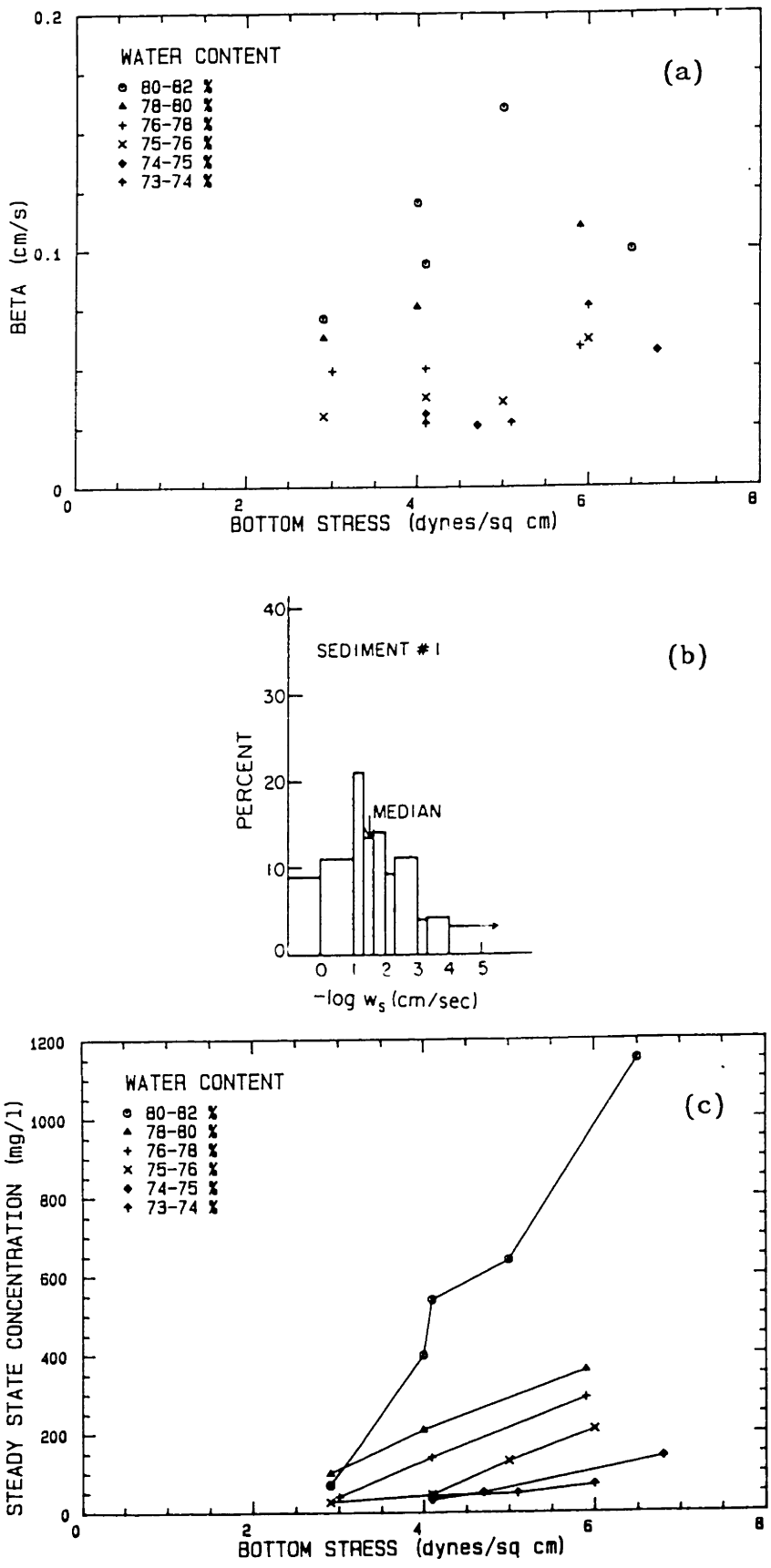

Figure 3.11 (a) Variation of β with applied stress for Lake Erie sediments. (b) Distribution of settling velocities in quiescent water column tests. (c) Variation of the steady-state concentration with applied stress. (after Lee et al. 1981)

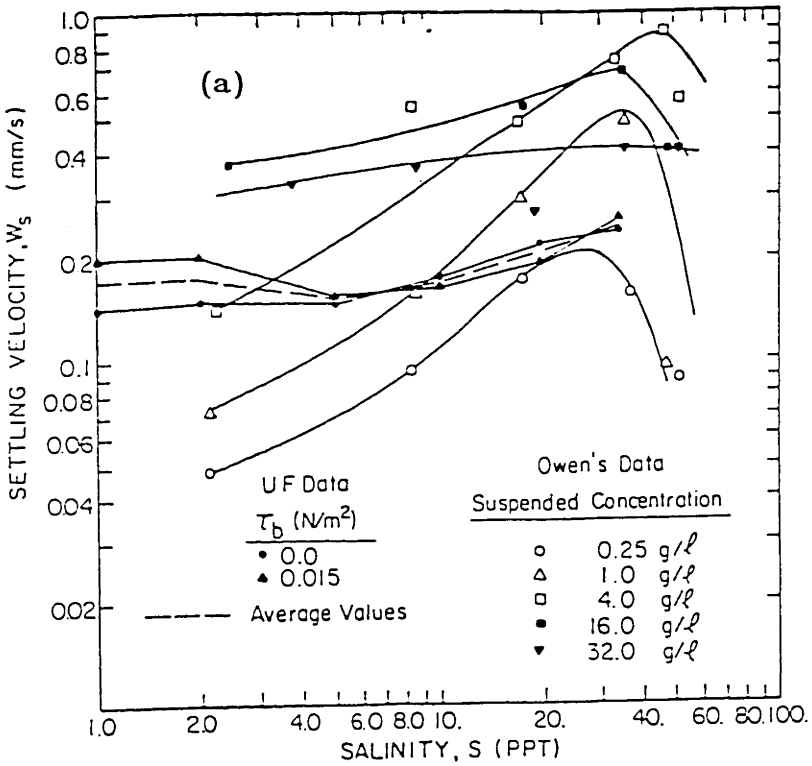

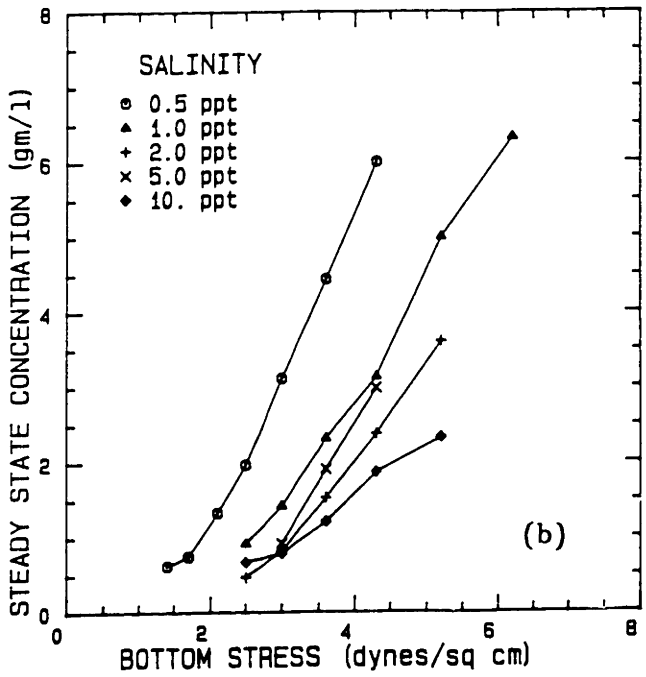

Figure 3.12 (a) Settling velocity of Lake Francis sediment as a function of water salinity and applied stress. (after Hayter, 1983)
(b) Steady-state concentration vs. applied stress for erosion experiments using Lake Francis sediment. (data from Parchure, 1984)

The behavior of c_{ss} is shown in Figure 3.12b. It indicates an approximate linear relationship between c_{ss} and τ_b, the slope and intercept of which are functions of salinity. This linear trend is similar to the results from Parchure (1980) presented previously in Figure 3.5, in which deposition time was a parameter, although the results in Figure 3.12b do not have a clear bilinear trend. In each of these results, as well as in the work of Fukuda and Lick (1980) and Lee et al. (1981), increases in the bed cohesive strength result in lower values of c_{ss} for a given applied stress, thereby indicating that each run was bed strength limited.

Quantifying these results suggests that

$$c_{ss} = K(\tau_b - \tau_{csbo})^n \tag{3.27a}$$

and

$$E_2 = \beta\, c_{ss} = \beta K(\tau_b - \tau_{csbo})^n \tag{3.27b}$$

where τ_{csbo} is the value of τ_{csb} when $c_{ss} = 0$. Both K and τ_{csbo} are functions of the bed cohesiveness. The results of Parchure (1980), (1984) and Lee et al. (1981) indicate an exponent $n \approx 1$. (This is particularly true since the slope change in the curves in Figure 3.5 did not occur until after about 2cm of the bed had eroded. A 100 mg/ℓ increase in the suspended sediment concentration of a 2m deep water column is equivalent to the removal of less than 1mm of a sediment bed having a 90 per cent water content.) Results from Fukuda and Lick (1980) suggest $n > 1$.

Lavelle et al. (1984) proposed Eq. (3.28), Table 3.4, which has a form similar to Eq. (3.27), based on the re-analysis of previous laboratory studies. Eq. (3.28) does not include a critical stress criterion. The authors cite evidence that some transport, predominantly due to the stochastic nature of the bed material and the stress, occurs down to the

smallest stresses. Also it is not clear when the critical stress is reached, (i.e., when one particle moves, when a few particles move, etc.) or that laboratory preparation procedures do not minimize bed inhomogeneity and therefore artificially induce a critical level of stress. A summary of some of the parameter values they obtained is given in Table 3.6.

Table 3.6. Erosion Rate Parameters
(from Lavelle et al., 1984)

Bed	Investigators	Water content %	ξ (mg/cm^2·min)	η
Lake Erie mud	Fukuda and Lick (1980)	81-82[a]	0.222	5.0
Lake Erie mud	Fukuda and Lick (1980)	74-75[a]	0.043	1.3
Lake Erie mud	Sheng and Lick (1979)	76-77[a]	0.138	1.2
Lake Erie mud	Sheng and Lick (1979)	78-80[a]	0.038	2.1
Lake Erie mud	Lee et al (1981)	80-82[a]	1.3×10^{-3}	3.6
illitic silt	Gularte et al. (1980)	60[a]	5.0×10^{-3}	2.0
dredge spoil Thames River	Gularte et al. (1977)	113-222[b]	0.011	1.6
San Francisco Bay mud	Partheniades (1965)	110[b]	5.6×10^{-4}	1.7
San Francisco Bay mud	Partheniades (1965)	120[b]	1.1×10^{-4}	2.0

a - water content computed as the weight of water divided by the total weight of a unit volume of bed.

b - water content computed as the weight of water divided by the weight of solids in a unit volume of bed material.

To summarize these results, early erosion relationships from experiments using placed beds were presented that were linear or bilinear in excess bottom stress. Experimental data of Fukuda and Lick (1980), Lee et al. (1980) and Parchure (1984), analyzed using the analytical model presented in Section 3.1 together with the assumption that β and c_{ss} are constant for a constant applied stress, yielded values of β which were independent of applied stress and bed strength. Values from Parchure (1984) agree very closely while those of Fukuda and Lick (1980) and Lee et al. (1981) are in reasonable agreement with independent measurements of settling velocity. Values of c_{ss} decreased as the bed strength increased suggesting each experiment was bed strength limited. Assuming that these experiments were bed strength limited, c_{ss} reflects the amount of bed material which can be removed before reaching a bed strength that is equal to the applied stress. In experiments by Lee et al. (1981), and Parchure (1980, 1984), c_{ss} varied approximately linearly with applied stress while the variation obtained by Fukuda and Lick (1980) was more rapid. A power law relationship was proposed for c_{ss}, Eq. (3.27a), as a function of excess bottom stress. Lavelle et al. (1984) proposed an expression similar to Eq. (3.27) excluding the critical stress.

Unfortunately as it stands, the use of Eq. (3.15a) together with relationships for c_{ss} derived from erosion experiments is not entirely correct since it will not reproduce the hysteresis effect observed during deposition experiments if the values of c_{ss} reflect bed strength limited conditions. As deposition occurs the surface zone will become repopulated with sediment and the exchange will no longer be bed strength limited. As a result the use of c_{ss} values determined from erosion experiments would predict deposition to occur too rapidly. This problem will be minimized as

the cohesive strength of the bed decreases or if erosion is not bed strength limited.

In addition the use of a constant value for β will not reproduce the fact that c_{ss} is a function of the initial concentration. Evidence does suggest, however, that the role of coagulation in affecting this process may be negligible in fresh waters at naturally occurring suspended sediment concentrations.

Both of these problems have been overlooked by those conducting experiments into E_2 and S_2, perhaps because of the lack of a consistent framework like the DIM for interpreting these processes and also because of the difficulty of isolating the effects.

3.2.2.4 Summary of Quantitative Results

The wide range of experimental procedures and conditions which have been used to study cohesive sediment behavior make quantitative comparisons amoung most of this work impossible. Recent attempts to recreate conditions representative of those expected in nature have led to the use of deposited sediment beds in recirculating or annular flumes. These studies have been emphasized in this review. The DIM presented in Section 3.1 suggested that two approaches can be used to specify the bottom boundary condition for cohesive sediment transport. These two approaches, DIM A1 and DIM A2, were used to catagorize previous experimental results. A third catagory, SIM, was also added, although it was pointed out that this was really just a bed strength limited version of the DIM A1.

Tables 3.1, 3.3 and 3.4 present expressions which have resulted, along with Eq. (3.27) proposed in this study. Expressions classified as DIM A1

and those classified as DIM A2 will ideally be equally valid. This equivalence was illustrated by the re-analysis of DIM A1 data from Parchure (1984) using DIM A2 expressions with the results shown in Table 3.5 and Figure 3.12. Interestingly, Parchure (1984) also showed this equivalence, although it was not presented with this purpose in mind, by expressing DIM A2 results from Lee et al. (1981) using the DIM A1 expression, Eq. (3.20). (The coefficients he obtained are listed in Table 3.2.)

From a practicle standpoint, the choice of whether to use DIM A1 or DIM A2 depends on what is known about the application. If enough information is given to definitively determine all of the parameters associated with DIM A1, this approach may be best. Ideally, it has the advantage of being able to capture the hysteresis observed between erosion and deposition, and the fact that c_{ss} depends on c_i during deposition. On the other hand if it is known that the hysteresis effect and flocculation are not important, it may be more realistic to use DIM A2 which, using Eqs. (3.27) and (3.15), has fewer parameters. In addition at least two of the parameters, β and τ_{csbo}, have physically intuitive meanings.

Finally, it should be pointed out that the expressions for ϕ_e and E_2 presented above are all based on bed strength limited conditions. Therefore, there is no direct evidence for expressing either ϕ_e or E_2 under conditions of a populated surface zone. The DIM suggests that exchange with a populated surface zone is similar to exchange with a cohesionless sediment bed and as a result it is anticipated to depend on the excess applied bottom stress, $\tau_b - \tau_{bsz}$. Unfortunately it is difficult to extract erosion rates from many of the cohesionless sediment transport studies since most of these results are summarized in terms of discharge relationships. This subject is returned to in Chapter 5.

3.3 FIELD EXPERIMENTS

Suspended sediment concentration is a routinely measured water quality parameter suggesting that a large field data base is potentially available. Unfortunately, most of these data are collected on time scales of weeks or months which are quite large compared to the time scales of hydrodynamic forcings, (hours or days). Thus there is very little field data which shows the transient response of a cohesive sediment bed to a hydrodynamic forcing event. This paucity of field data becomes particularly severe when accompanying hydrodynamical measurements of the forcing event are also desired.

Anderson (1972) measured resuspension of cohesive sediments in approximately 2 m deep water over a tidal flat in a small coastal cove. Observations were also made of wave heights and nearby wind speed and directon. Results showed a cyclic resuspension-deposition process driven by the flood and ebb tide. Superimposed on this were substantial suspended sediment increases which were closely correlated to increased wave heights, particularly during the flood tide. A linear regression between suspended sediment concentration and wave height gave a correlation coefficient of $r = 0.8$, (total of 56 observations).

Carper and Bachmann (1984) measured suspended sediment concentrations at two locations in a small prarie lake (mean depth = 1.3 m). Three to four fold concentration increases occurred over background when the predicted surface wave length, (computed using the shallow water SMB method), was more than twice the depth.

Krone (1972) measured vertical profiles of suspended sediment concentration along with velocity and tidal elevation at 3 positions in the

Savannah River estuary over a 13.5 hour period. Results from one site are shown in Figure 3.13. Particularly notable is the rapid decrease in the suspended sediment concentration at the onset of decelerating flow and the absense of the hysteresis effect described in Section 3.2.2.2.

Lavelle et al (1984) measured mean velocity and turbidity 5 m above the floor of Puget Sound in 202 m water depth. Results indicated a rapid rise in suspended sediment concentration that was nearly simultaneous with increasing currents, (Figure 3.14). They reported three to four fold concentration increases over a single 15 min. sampling interval and favored a local resuspension arguement vs substantial horizontal transport. There is no evidence of a hysteresis in this data either.

Somlyody (1982) and Aalderink et al (1984) have conducted studies in which detailed suspended sediment measurements have been made at sampling intervals ranging from two hours to daily for extended time periods. In each case these were correlated with wind data after making assumptions about the mechanisms thru which wind energy is available to cause sediment resuspension. This work is considered more fully in Section 3.4.

3.4 MODELING OF COHESIVE SEDIMENT TRANSPORT

The ultimate usefulness of the laboratory and field studies which have been conducted to understand the behavior of cohesive sediments is the development of quantitative relationships which can be used to predict the erosion and deposition of these sediments in natural water bodies. To date the work which has been tried has mostly been focused toward estuarine studies, presumably because the shoaling of cohesive sediments has had a major impact on navigation. Briefly, shoaling occurs when the fine but

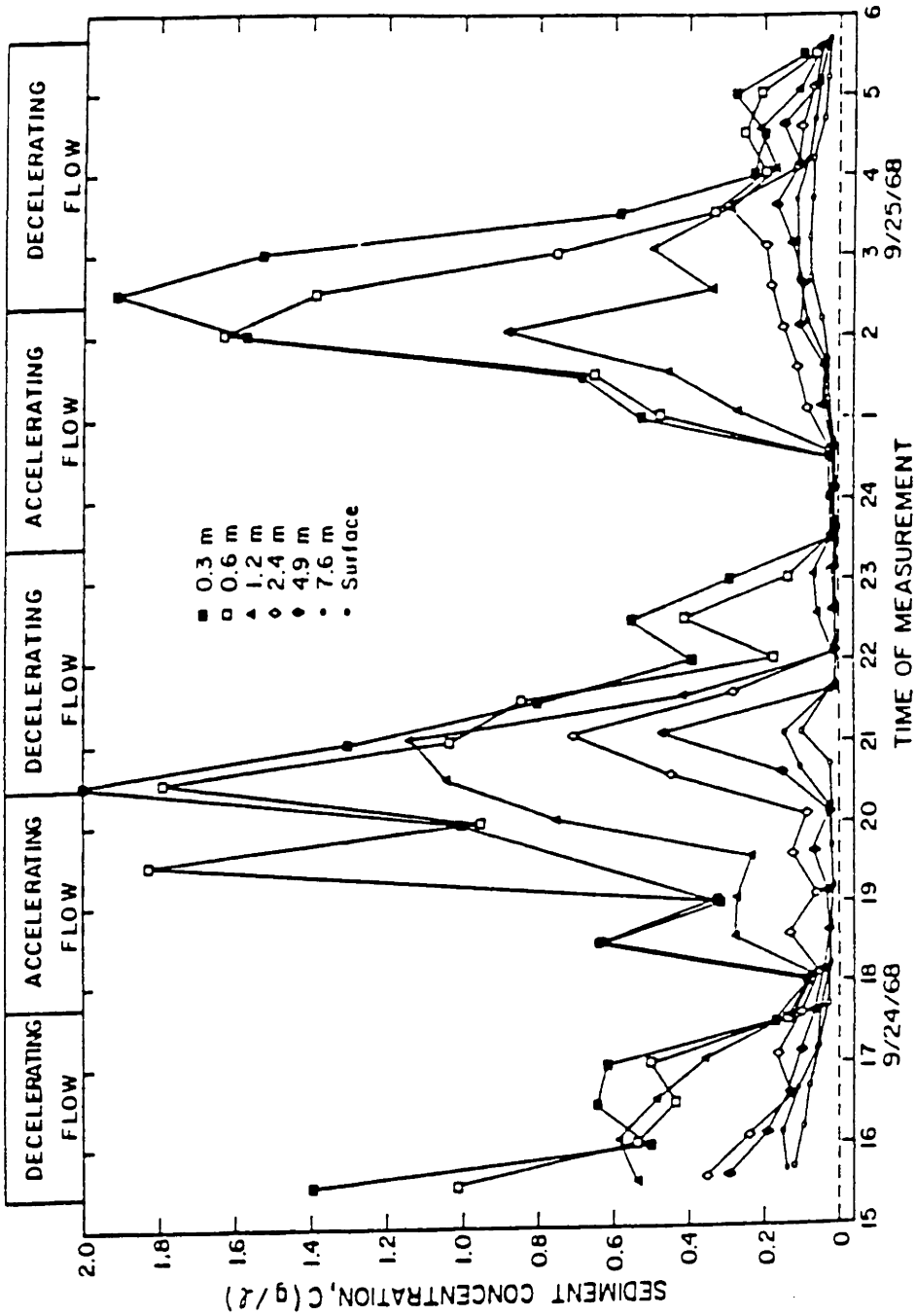

Figure 3.13 Time history of suspended sediment concentration at 7 vertical positions over 13.5 hours in the Savannah River estuary. (from Krone, 1972).

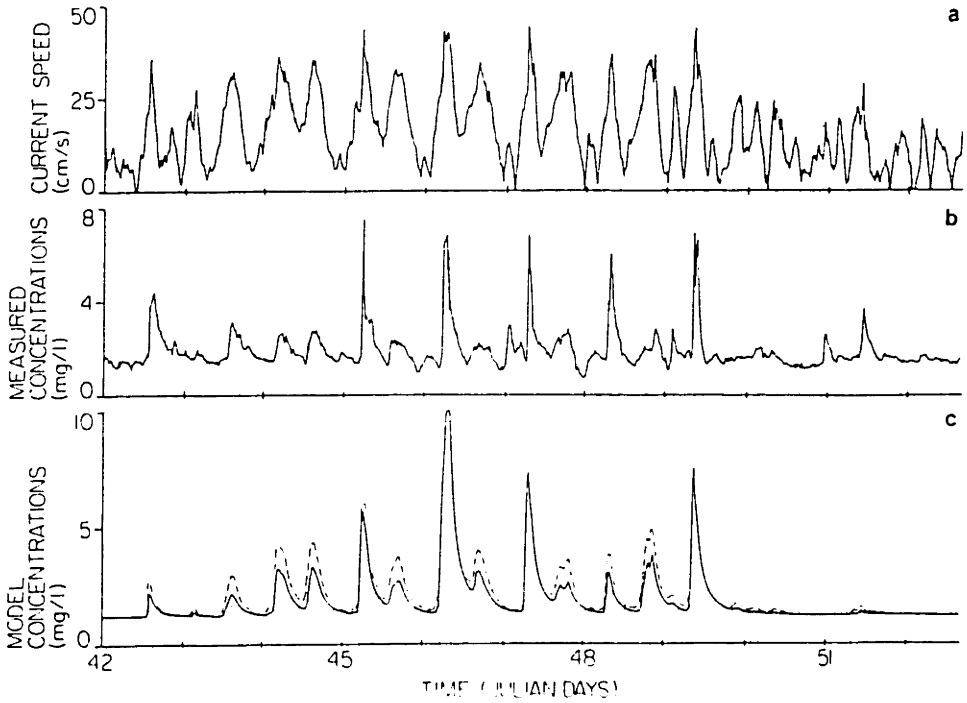

Figure 3.14 Time histories of current speed and measured and modeled suspended sediment concentration 5 m above the bottom in Puget Sound. In figure (c), the solid, dashed and dotted lines indicate $\eta = 3$, $\eta = 4$ and $\eta = 5$, respectively. η is the exponent of the erosion term, Eq. 3.28, Table 3.4. (from Lavelle et al. 1984)

relatively dispersed wash load carried by many fresh water rivers reaches the increased salinity of an estuarine or coastal water body. This encourages flocculation resulting in increased sizes and settling velocities and increased deposition. In this context, deposition is of initial importance, although resuspension and transport also factor into the ultimate fate of the cohesive sediments. All of the modeling of cohesive sediment behavior in estuaries has assumed that mean currents, typically tidally induced, dominate the hydrodynamic processes. Therefore, it has been assumed that bottom stress, vertical turbulent transport and horizontal transport can be characterized by these currents.

A substantially smaller effort has been extended to the modeling of cohesive sediment behavior in fresh water. This is due to the relative unimportance of shoaling in fresh water and our only recent appreciation of water quality issues and the influence of cohesive sediments upon them. From a water quality standpoint the investigator is usually more concerned with the resuspension of sediments and the resulting impact they have on the water column, although clearly transport and deposition also are important parts of the total picture. Lakes do not usually have the large mean flow velocities characteristic of estuaries and therefore the role of currents in causing erosion remains a matter of some debate. On the other hand, waves have received substantial attention because of the large shear stresses they are capable of exerting on the sediment bed. (This is illustrated in Section 4.1 by a comparison of the shear stress associated with surface waves and the mean current in Lake Balaton.)

Model verification must be conducted both in time and in space. Due to the difficulty in making spatially synoptic measurements which are of sufficient detail in time, the only practical alternatives are either to

select a field location at which spatial variations can safely be assumed to be small and then verify the model in time, or to model an event with a sufficiently long time constant that a non-synoptic spatial sampling program will give a meaningful verification.

As mentioned above attempts to model the erosion and deposition of cohesive sediments have mostly been oriented toward estuarine studies. One of the first of these models was by Odd and Owen (1971) and applied to the Thames Estuary. Erosion and deposition were treated using early equations proposed by Partheniades (1962) and Krone (1962, 1963).

O'Connor and Zein (1974) implimented a two-dimensional, laterally averaged, cohesive sediment transport model. Erosion was modeled using the linear relationship in shear stress given by Eq. (3.25), while deposition was modeled with Eq. (3.29), Table 3.7. Erosion was assumed to occur at bottom stresses greater than a critical stress while deposition occurred at stresses below the same critical stress, (DIM A1). Variations of this model were applied to field studies on sewage sludge dumping in the Irish Sea, sediment spoil disposal on the Potomac Estuary and sediment intrusion into a tidal lock in the Mersey Estuary.

Ariathurai and Krone (1976) developed a two-dimensional, depth integrated, finite element model for cohesive sediment transport based on a DIM A1. The sediment bed was assumed to consist of a specified number of layers of known thickness, density, critical shear stress for erosion, erodability constant, criterion for surface or bulk erosion, and consolidation rate. In addition a critical shear stress for deposition was necessary. At each time step the bed shear was computed assuming a logarithmic velocity profile. Erosion was computed using a linear relationship in shear stress, Eq. (3.25), for bottom stresses greater than

Table 3.7 Boundary Conditions for Cohesive Sediment Transport Models

O'Connor and Zein (1974)

erosion: Eq. (3.25)

deposition:

$$\phi_d = w_s c_o \qquad \tau_b \le \tau_c \qquad (3.29)$$

$$\phi_d = 0 \qquad \tau_b > \tau_c$$

where

τ_b - bottom stress (force/area)
τ_c - critical bottom stress (= 0.205 dynes/cm^2)
w_s - settling velocity (length/time)
c_o - suspended sediment concentration at the bottom (mass/vol)

Ariathurai and Krone (1976)

bulk erosion: ϕ_e = entire layer eroded $\qquad \tau_b \ge \tau_{cbe}$

surface erosion: Eq. (3.25)

deposition: Eq. (3.21)

where

τ_{cbe} - critical shear stress for bulk erosion (force/area)

Scarlatos (1981)

erosion:

$$\phi_e = 0 \qquad \tau_b \le \tau_c$$

$$\phi_e = c_{ss}\, \alpha \cdot \exp(-\alpha \cdot t) \qquad \tau > \tau_c \qquad (3.30)$$

deposition: Eq. (3.24)

where

τ_{bmin} = 1.2 dynes/cm^2
τ_c = 1.6 dynes/cm^2
$\alpha = 3.6 \times 10^{-6}$ s^{-1}

Cole and Miles (1983)

erosion: not considered

deposition: Eq. (3.21)

Hayter (1983)

erosion:

UND: bulk erosion.

PCND: Eq. (3.29), $\ell = 1$

SB: Eq. (3.25)

deposition:

$$\phi_d = P\, w_s\, \bar{c} \qquad (3.31a)$$

$$0 \le \tau_b^{**} < \tau_{bc}^{**} < 1$$

$$P = (1 - \tau_b^{**}) \qquad (3.31b)$$

w_s = median particle settling velocity $\qquad \bar{c} < c_1 \qquad (3.31c)$

$$w_s = K\, \bar{c}^{\,n} \qquad c_1 \le \bar{c} < c_2 \qquad (3.31d)$$

$$w_s = \frac{250}{D^{1.8}} \frac{g\, D^2 \left(\frac{\rho_s}{\rho} - 1\right)}{18\, \nu} \left(\frac{\bar{c}}{c_2} - 1\right)^{\ell} \qquad \bar{c} \ge c_2 \qquad (3.31e)$$

$$\tau_{bc}^{**} < \tau_b^{**} < \tau_{bmax}^{**}$$

$$P\, w_s = \text{Eq. (3.24b)} \qquad (3.31f)$$

$$c_o = \bar{c} = c_1 \text{ and } c_{ss} = 0 \qquad \bar{c} < c_1$$

$$c_{ss} = 0 \qquad \bar{c} \ge c_1$$

where

$\tau_b^{**} = \tau_b / \tau_{bmin}$
$\tau_{bmax}^{**} = \tau_{bmax} / \tau_{bmin}$
$\tau_{bc}^{**} = 1 - (P\, w_s$ from Eq. 3.24b$)/(w_s$ from Eq. 3.31c$)$
$\tau_c(z)$ - critical erosion stress (force/area)
τ_{csb} - critical bottom stress in settled bed zone (force/area)
τ_{bmin} - stress below which all sediment deposits (force/area)
τ_{bmax} - stress above which no sediment deposits (force/area)
c_1 = 100 - 700 mg/ℓ
c_2 = 10,000 - 15,000 mg/ℓ
ℓ = - 0.6
K,n - settling constants
ρ_s - density of sediment particle (mass/vol)
$\rho_b(z)$ - dry density of sediment bed (mass/vol)
ρ - density of water (mass/vol)
ν - kinematic viscosity of water (area/time)
g - acceleration of gravity (length/time^2)
D - particle diameter (length)
ζ, m - shear strength constants
z - vertical coordinate
other variables as defined above

Table 3.7 (cont.)

Lavelle et al. (1984)

erosion — Eq. (3.26)

deposition $\Phi_d = w_s c_o$ (3.32)

where,

$\xi = 1.7 \times 10^{-6}$ g/cm²·min
$\eta = 4$
$w_s = 0.1$ cm/s

Lam and Jaquet (1976)

$$E_2 = (6.4 \times 10^{-4})\left(\frac{\rho \cdot \rho_s}{\rho_s - \rho}\right)\left(\frac{U_a}{U_{cr}}\right)(U_m - U_{cr}) \quad (3.33)$$

where,

size class (μm)	U_{cr} (cm/s)
1000 - 63 (noncohesive)	20
63 - 4 (partially cohesive)	3
< 4 (cohesive)	2

U_m - maximum bottom wave orbital velocity (cm/s)
U_{cr} - threshold velocity for sediment movement (cm/s)
U_a - refrence velocity (1 cm/s)
ρ_s - dry density of a particle of sediment (2.6 g/cm³)
ρ - density of water (g/cm³)

Sheng and Lick (1979)

erosion $E_2 = 0$ $\tau_b \leq 0.5$ (3.34a)

$E_2 = M(\tau_b - 2) + 1.2 \times 10^{-4}$ $\tau_b > 0.5$ (3.34b)

$M = 4.0 \times 10^{-5}$ g/dyne·min $\tau_b \leq 2$; $M = 1.24 \times 10^{-4}$ g/dyne·min $\tau_b > 2$

deposition Eq. (3.15b) $\beta = 0.008$ cm/s

Somlyody (1980,1982,1986)

erosion $E_2 = A U_{wind}^n$ $1 \leq n \leq 3$ (3.35)

deposition Eq. (3.15b)

Szemes Basin, 1979 $\beta = 4.4 \times 10^{-5}$ m/s, $A = 2.7 \times 10^{-7}$, $n = 0.93$
Keszthely Basin, 1985 $\beta = 26.4 \times 10^{-5}$ m/s, $A = 15.6 \times 10^{-7}$, $n = 1.1$

where,

E_2, S_2 - (kg/m²·s)
A, n - erosion constants
U_{wind} - wind velocity (m/s)

Mulderink et al. (1984)

$$S_2 = \beta(\bar{c} - c_b) \quad (3.39)$$

$$E_2 = K\rho\left(\frac{\rho_s}{\rho_s - \rho}\right)\left(\frac{U_m - U_{cr}}{U_{cr}}\right) \quad (3.40)$$

$$E_2 = B\, U_{wind}^m \qquad 1 \leq m \leq 3 \quad (3.41)$$

$$E_2 = K_1\, \omega^n\, U_m^p \qquad n = 1.125, \quad p = 1.875 \quad (3.42)$$

$$E_2 = K_2\, U_{wind}^q \qquad q = 2.75 \qquad U_{wind} \leq 5.67 \text{ m/s} \quad (3.43a)$$

$$E_2 = K_3\, U_{wind}^r \qquad r = 3.5 \qquad U_{wind} > 5.67 \text{ m/s} \quad (3.43b)$$

Calibrated Parameter Values
(3.40) $K = 0.19$, $U_{cr} = 0.01$ cm/s, $\beta = 0.10$ m/hr, $c_b = 28.7$ mg/ℓ
(3.41) $B = 1.63$, $m = 0.40$, $\beta = 0.15$ m/hr, $c_b = 13.3$ mg/ℓ
(3.42) $K_1 = 1.63$, $n = 3.91$, $p = 0.94$, $\beta = 0.22$ m/hr, $c_b = 26.8$ mg/ℓ
(3.43) $K_2 = 1.63$, $q = 0.4$, $K_3 = 1.63$, $r = 0.4$, $\beta = 0.15$ m/hr
$c_b = 13.3$ mg/ℓ

where,

c_b - background concentration (mass/volume)
ρ - density of wate
ρ_s - dry density of the sediment
U_m - maximum bottom wave orbital velocity (length/time)
U_{cr} - critical velocity for erosion (length/time)
ω - wave frequency (1/s)

Kang et al (1982)

Resuspension Criteria

bottom stress (dynes/cm²)	size entrained (μm)
< 1	none
1 - 2	4
10	250

Paul et al (1982)

$$T = c_1 + c_2 F(\tau_b) + c_3 F(\tau_b)\, I(L) + c_4 D(L) \quad (3.44)$$

where,

T - turbidity (NTU)
τ_b - bottom stress due only to waves
c_1 - background turbidity
$c_2 F(\tau_b)$ - Erosion of particles characteristic of the area
$c_3 F(\tau_b) I(L)$ - erosion of very fine particles transported into the area by the Maumee River
$c_4 D(L)$ - direct transfer of Maumee River sediments past observation point

the critical stress of the exposed layer, although, for large enough stresses bulk erosion could entrain the layer instantaneously. This was repeated for each layer exposed during a time step. Deposition occurred if the bottom stress was less than the critical stress for deposition and was computed from Eq. (3.21). The model was tested with data from a shoaling experiment in a laboratory flume using mud from San Francisco Bay whose erosive and depositional properties were previously studied by Krone, (1962). Good agreement between the predicted and observed shoaling patterns were obtained when the model was provided with transient upstream sediment concentrations and a measured velocity field.

Scarlatos (1981) applied a one-dimensional transport equation to the Savannah River estuary which was assumed to be vertically and laterally well mixed. The expressions used for erosion and deposition follow a DIM A1 and are given in Eqs. (3.30), Table 3.7 and (3.24), respectively. In particular the equations developed by Mehta and Partheniades (1975) were used to describe depostion, although the meaning of τ_{bmin} was changed. Originally this was defined as the bottom stress value below which no sediments remain in suspension, (see Table 3.3). In the present use τ_{bmin} is defined to be the bottom stress value above which no sediments will deposit. Since τ_{bmin} is the normalizing factor used in the deposition equation this difference in defintion is potentially quite important. None the less the parameter values determined in the laboratory experiments by Mehta (1973) were used in this model. The value of the longitudinal dispersion coefficient was artifically increased to maintain numerical stability. A comparison of the model results, (which were computed using measured upstream and downstream boundary conditions and measured velocities), with a depth-average of the measured suspended

sediment concentrations of Krone (1972), (the vertical profiles have been presented previously in Figure 3.13), is shown in Figure 3.15. The author claims this agreement is "satisfactory" and is a "promising factor of the validity of the model".

Cole and Miles (1983) developed a two-dimensional, vertically-averaged, cohesive sediment transport model to study shoaling in estuaries. They concluded it was pointless to include erosion in their model due to the present state of the art in defining appropriate relations. Deposition was modeled using Eq. (3.21). The model was used to predict areas of expected shoaling in two estuary applications.

Without question the most extensive model development effort has been made by Hayter (1983) working with the group at the University of Florida. The principal effort of this work was a systematic quantification and parameterization, consistent with the SIM and/or the DIM A1, of sediment erosion, deposition and bed consolidation processes and the influence of changing salinity on each. The bed was partitioned into three major zones (i) unconsolidated new deposits (UND), (ii) partially consolidated new deposits (PCND), and (iii) settled bed (SB). Zones UND and PCND have stratified properites with depth while zone SB is uniform. Each zone was split into a specified number of layers. Erosion was assumed to occur only during accelerating flows or steady flows preceeded by a period of acceleration. Deposition occurred during decelerating flows or steady flows preceeded by a period of deceleration. Erosion occurred from each zone (if exposed to the water) as follows:

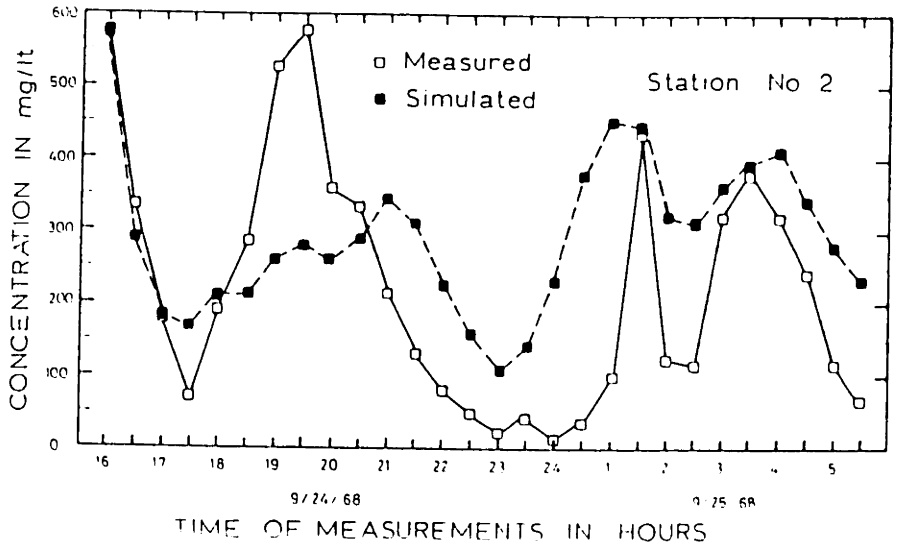

Figure 3.15 Comparison of model predictions with the depth-average of concentration measurements made by Krone (1972) in the Savannah River estuary. (from Scarlatos, 1981)

(i) UND - instantaneous bulk erosion to a depth where the bottom stress equals the erosive strength of the UND deposit (maximum erosion was to the bottom of this zone),

(ii) PCND - surface erosion at an exponential rate, Eq. (3.20) with $\delta = 1$,

(iii) SB - surface erosion at a linear rate, Eq. (3.25).

To use this algorithm it was necessary to know the erosive strength and dry density of each layer in UND, the erosive strength, dry density, coefficients α_2 and E_{1o2} for each layer in PCND, and the erosive strength, dry density and the erodability constant, N, for each layer in SB.

Deposition was computed using Eq. (3.31), Table 3.7. Based on laboratory experiments reported in the literature and some performed in his study, Hayter empirically included the effect of varying salinity on the parameters required in these equations. (In general he found that changes in salinity become unimportant at salinities above 2-3 ppt.) To apply the deposition equations it was necessary to specify more than 20 parameters.

Bed consolidation was also considered in this model by increasing the bed density and shear strength with time. Newly deposited sediments were assumed to remain as UND for two hours after all deposition stopped. (The choice of two hours was based on observations by Dixit, 1982.) After this period they became PCND. The consolidation of PCND was empirically represented using an exponential increase in the dry density with time, while the density increase with depth was computed using an empirical power law relation. Finally, the shear strength of the bed was assumed related to the dry density thru a power law. To use the consolidation algorithm 11 more parameters had to be specified.

Verification of the model was performed by simulating several laboratory erosion-deposition experiments. Three of the tests were conducted in an 18.3 m long recirculating flume at the University of Florida using kaolinite clay in tap water subject to several different erosion and deposition periods. Figure 3.16 shows the bottom stresses used and the concentration time history which was obtained in one of these tests. (The bed was deposited for 240 hours before the experiment was started.) Evident from this figure is a characteristic result observed in all three tests. The model underpredicted the rate of erosion soon after a stress increase which followed a period of depositition, although in time the suspended concentration caught up. Hayter (1983) proposed that the model was underpredicting the quantity of material undergoing bulk erosion. By themselves these tests provide questionable verification since the model equations were empirically developed to describe kaolinite behavior under almost identical experimental conditions, (e.g. Parchure,1980,1984; Dixit, 1982 and Mehta, 1973).

Another experiment was conducted in the rotating annular UF flume using bottom sediment from Lake Francis and 10 ppt NaCl solution. The rotation speed was varied approximately sinusoidally with a period of 6 hours to simulate the erosion and deposition expected in a tidal cycle. Figure 3.17 shows the velocity and the measured and predicted suspended sediment concentrations as a function of time. It is interesting to note that there is no hysteresis in the suspended sediment concentration before and after the intervals of maximum velocity. The model is able to capture this by switching off erosion and starting deposition as soon as deceleration begins and by proper combinations of the parameter values. Strictly speaking, however, this is inconsistant with the SIM/DIM A1 in which

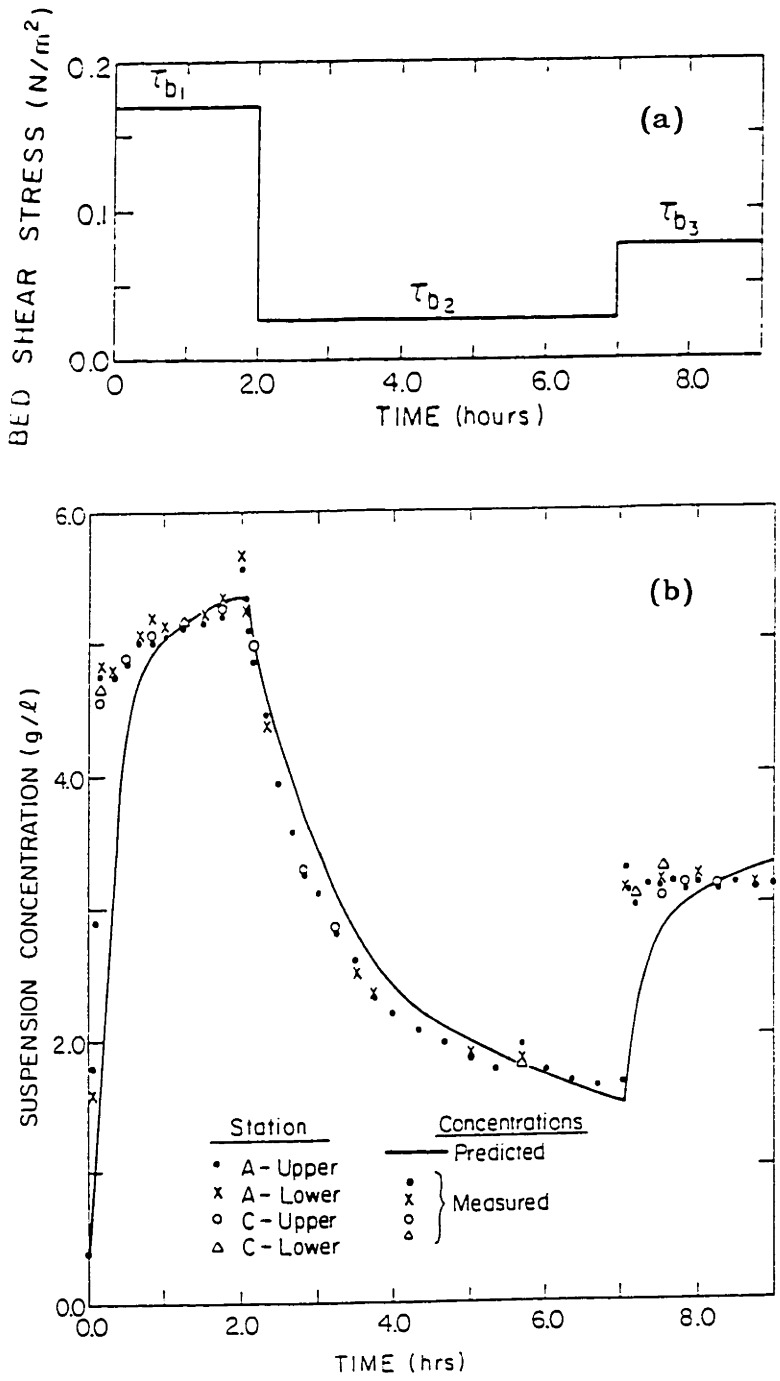

Figure 3.16 (a) Time history of applied stress used for model test. (b) Comparison between measured concentration and model predictions. (from Hayter, 1983)

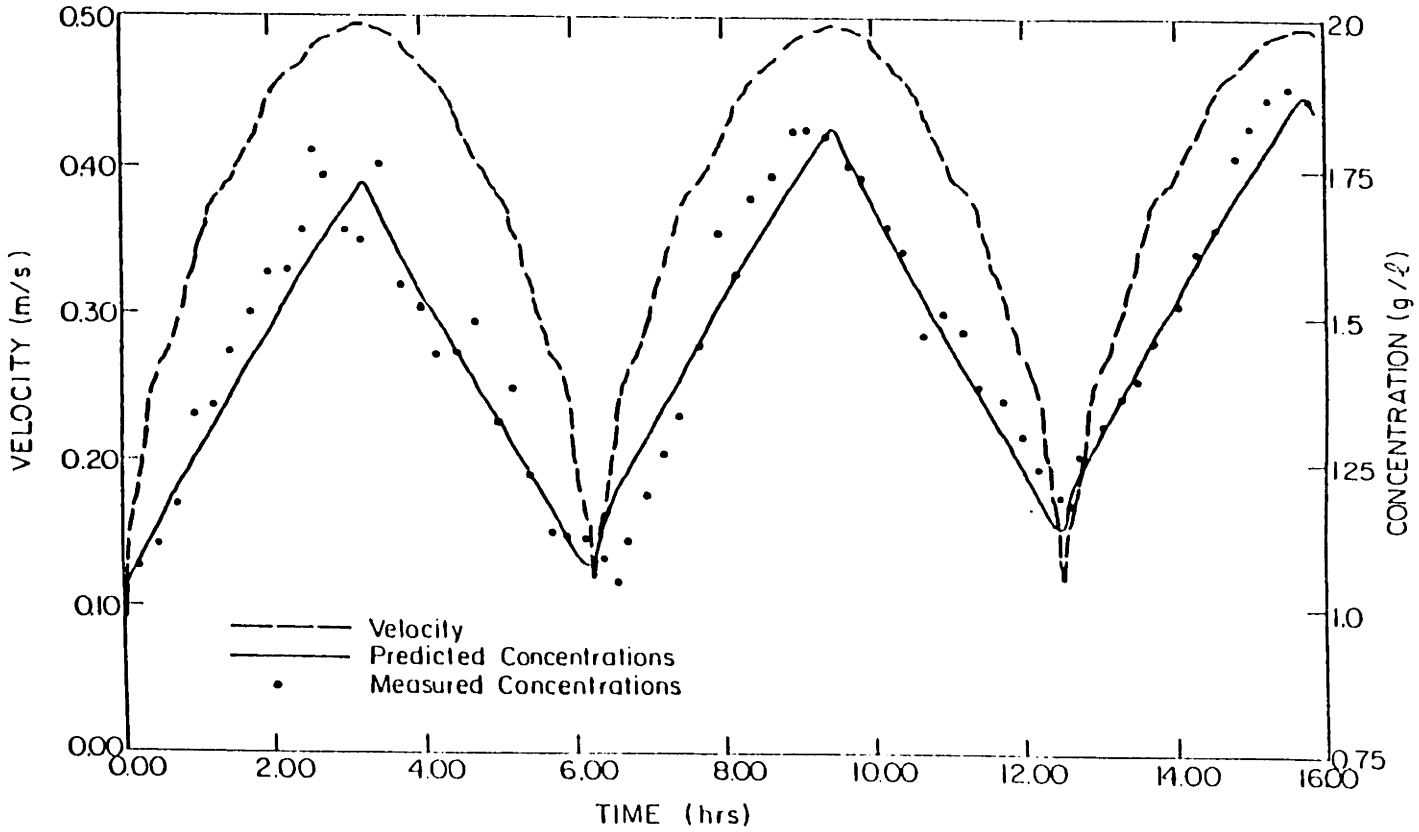

Figure 3.17 Companison between applied velocity and measured and predicted suspended sediment concentrations in a laboratory simulation of estuarine conditions. (from Hayter, 1983)

erosion continues until the bottom stress is less than or equal to the bed erosive strength. The occurance of erosion should be a functon of the bed strength profile and not the flow conditions. Therefore the model has abandoned a central concept associated with the DIM A1 or SIM, leaving one suspicious that it is accomplishing little more than curve fitting.

An application of this model to a field study would be quite difficult due to the extremely large number of parameters which must be specified. Mehta (1983) describes the field and laboratory measurements necessary to evaluate some of these parameters, but the equipment (e.g., a flume suitable for erosion and deposition experiments) and the effort needed to conduct these experiments makes their wide spread usage somewhat unrealistic. Also there is still a question of how representative laboratory deposited beds are in comparison to the natural field beds. For example it is not clear whether bioturbation or residual turbulence in the water column are enough to keep the erosive strength of the upper part of the sediments relatively homogeneous, particularly since resuspension typically involves only the upper 1 cm of the bed or less.

Lavelle et al. (1984) developed a model of the bottom boundary layer and used it to predict bottom stresses in a tidally driven flow. Using this boundary layer model and a DIM A2 boundary condition, Eqs. (3.28) and (3.32), Table 3.7, they also modeled the one-dimensional vertical transport of fine sediment. The coefficients in the bottom boundary condition, i.e., w_s, ξ, and η were calibrated using a time series of horizontal current and turbidity measurements taken 5 m above the bottom in 202 m deep water in Puget Sound. A small difference in current speeds produced a large difference in suspended sediment concentration suggesting a non-linear

sediment response to bottom stress. Good comparison was obtained between the model and measurements with a range of parameter values, Figure 3.14.

Gabrielson and Lukatelich (1985) measured resuspension at five locations in the Peel-Harvey Estuary, Australia. Resuspension at four of the five sites was found to be correlated with the third power of wind speed in combination with a fetch factor and the number of hours of winds greater than 5 m/s. The only exception was a site which had a cover of benthic algae.

Although less extensively, models have also been applied to describe cohesive sediment transport in strictly fresh water. Hakanson and Jansson (1983) classify lake bottoms into three catagories: (i) accumulation areas in which fine materials can be deposited continuously, (ii) transportation zones in which periods of accumulation are interrupted by periods of resuspension, and (iii) erosion areas where there is no deposition of fine materials. They point out that in large shallow lakes the resuspension activity due to wind/wave action will dominate many aspects of the limnological "character" (e.g. transparency). Hakanson (1977) quantifies the potential for sediment entrainment by wind/waves using the maximum effective fetch (CERC, 1977) as a measure of energy input and the depth as an indication of the ability of the energy to reach the bottom.

Lam and Jaquet (1976) considered the transport of cohesive sediment indirectly thru its effect on the regeneration of total phosphorus in Lake Erie. They calculated wave statistics using the deep water SMB method, and used linear wave theory to determine maximum bottom orbital velocities. Based on dimensional analysis, laboratory data and "After a few trials with the model," they obtained an empirical expression for the resuspension flux, (Eq. 3.33, Table 3.7). A further empirical relation for the amount

of phosphorus regenerated from the resuspended sediments was determined and together these expressions were used in a two-dimensional transport model to predict total phosphorus levels in Lake Erie. The form of the resuspension expression, values of all empirical coefficients, (which included transformations between various chemical components), and validation were all determined using total phosphorus data obtained on a series of three cruises over a two month period. Sheng and Lick (1979) point out that typical resuspension and deposition events in Lake Erie have time scales of about 2 - 3 days. Each cruise took 5 - 7 days and therefore the lake-wide data lacked synoptic nature. Since the time between cruises ranged from 25 - 35 days it is unreasonable to expect that initial conditions generated with data from one cruise would be relevant to model predictions at the time of the next cruise. Considering also the uncertainty in all of the other model parameters the model results are unconvincing.

Sheng and Lick (1979) constructed both a two-dimensional and a three-dimensional model of the cohesive sediment transport in the shallow western basin of Lake Erie, (mean depth = 24 ft). Erosion and deposition were modeled following a DIM A2, as described by Eqs. (3.34), Table 3.7, and (3.15b), respectively. The equation coefficients were selected from laboratory tests, made by Fukuda and Lick (1980) using a sediment sample from the western basin in tap water. The bottom stress, τ_b, was determined by adding the computed component due to the current to that computed for the waves and averaging over a wave period. The wave stress was computed using the shallow water SMB wave hindcasting model, linear wave theory and assuming a smooth bottom. The current stress was determined from an accompanying hydrodynamic model. Both the 2-D and the 3-D models were used

to simulate lake response to a 3-day storm event. Visible light band remote sensing photographs taken approximately every day were used as a source of data on the suspended sediment concentration in the lake. Commparisons between the photos and the models were mixed presumably because of spatial inhomogeneities in the bottom sediment properties and because of a finite availability of cohesive sediments which may be entrained, (Lick 1982). Unfortunately, no data was taken to allow verification in time, making it more difficult to conclude exactly what was wrong. Also, remote sensing inherently only picks up the surface concentrations. These depend not only on the bottom boundary condition but also on the parameterization of the vertical turbulent diffusion.

Somlyody (1980,1982,1986) developed a simple ordinary differential equation to describe the depth-average suspended sediment concentration in Lake Balaton, Hungary, based on the depth-integrated transport equation, the neglect of horizontal transport terms, and a flux bottom boundary condition. The resulting equation expresses the change in the depth-average suspended sediment concentration per unit depth as being equal to the bottom sediment flux, ϕ, and is exactly that presented in Section 3.1

$$h \frac{d\bar{c}}{dt} = \phi \qquad (3.6)$$

where h is the water depth. A DIM A2 was used for the bottom flux with erosion given by Eq. (3.35), Table 3.7, and deposition given Eq. (3.15b).

The form of Eq. (3.35) along with the expected range of the exponent, n, were determined via a loose analogy to the turbulent kinetic energy

(TKE) budget which has commonly been used in modeling entrainment in a two-layer, thermally stratified system, (e.g., wind-induced entrainment across the thermocline in a stratified water body or entrainment near the top of an atmospheric inversion). In each application the terms in the TKE equation are parameterized and the resulting expression solved for an entrainment velocity. The entrainment flux can then be computed knowing the bed density. Following this methodology two limiting cases result

$$\frac{U_e}{U_*} \sim \frac{\rho U_*^2}{\Delta\rho\, g\, h} \equiv R_i^{-1} \tag{3.36a}$$

and

$$\frac{U_e}{U_*} = \text{constant} \tag{3.36b}$$

where $\Delta\rho$ is the density difference in the present case between the sediment bed and the water column, (which is assumed to be fully mixed), U_* is the shear velocity which is taken to be the characteristic velocity scale for turbulence, h is the water column depth, g is the acceleration due to gravity, and R_i is the Richardson number. Equation (3.36a) implies a balance exists between the TKE input and the buoyant entrainment. It leads to an entrainment velocity and therefore an entrainment/erosion flux of the form:

$$\phi_e \sim U_*^3 \tag{3.37a}$$

Eq. (3.36b), as introduced by Zilitinkevich (1975) and Ottesen-Hansen (1975), arises from a balance between the transient change in the TKE and the TKE input due to shear production. In a deep, weakly or unstratified

fluid, at small times after a shear loading, a transient change in the TKE caused by shear production is associated with an increase in the depth over which the shear profile extends and an "entrainment" of unsheared lower fluid into the upper shear layer. This leads to an entrainment velocity and therefore an entrainment/erosive flux of the form:

$$\phi_e \sim U_* \tag{3.37b}$$

Somlyody (1980, 1982, 1986) assumed that since the principal source of turbulent input was the wind

$$U_* \sim U_{wind} \tag{3.38}$$

where U_{wind} is the wind velocity. Combining this with Eq. (3.37) yields

$$E_2 = A\, U_{wind}^n \qquad n = 1 - 3$$

where A is an unknown coefficient. This is the basis for Eq. (3.35) in Table 3.7.

Using data from Lake Balaton, Hungary, Somlyody (1986) applied four parameter estimation techniques to verify the form of the expressions for E_2 and S_2, and to determine the parameter values. Figure 3.18 shows results obtained using a Global Optimization Procedure (GOP) with hourly wind speed and daily suspended sediment measurements made in 4.3 m deep water in the center of the Szemes basin, (see Figure 1.1). (Actual measurements were made at five points over the vertical and showed no significant concentration gradient to within at least 1 meter of the

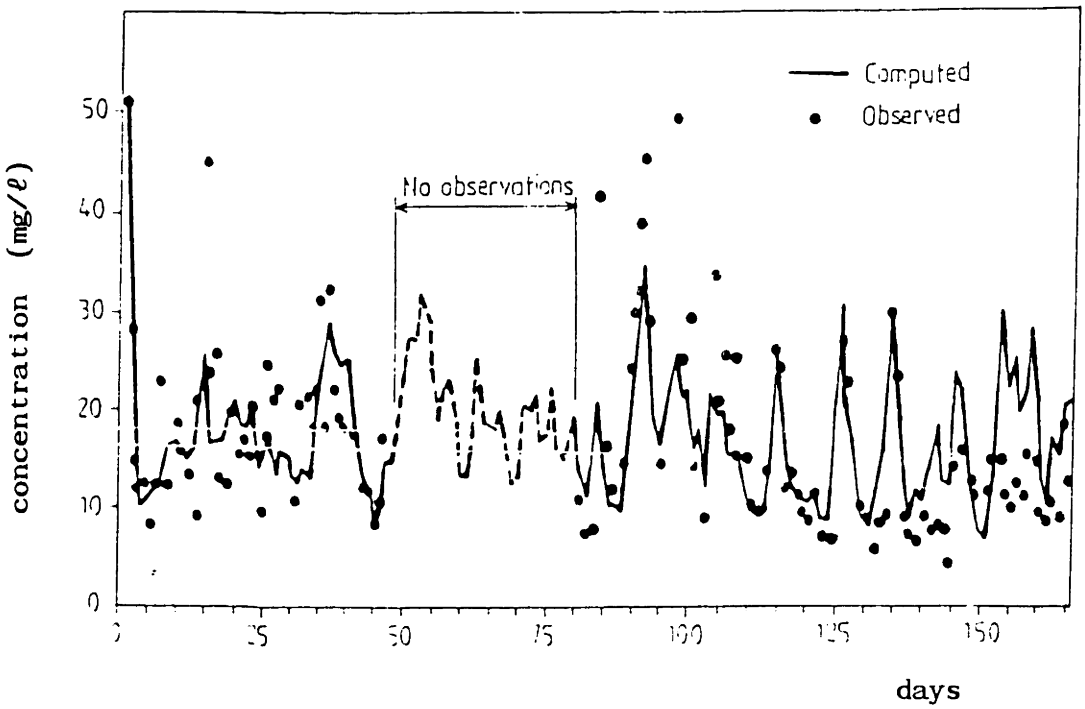

Figure 3.18 Comparison of observed and modeled suspended sediment concentrations in Szemes Basin, Lake Balaton, Hungary. (from Somlyody, 1986)

bottom.) The parameter values which resulted are given in Table 3.7. A value of $n \approx 1$ was rationalized based on a presumed small density difference between the water and the surface sediments, which can have a water content in excess of 90 per cent. This model does a reasonable job of predicting the observed suspended sediment concentrations particularly during days 105 - 140. At other times peak concentrations are underpredicted, (days 85 - 100), and over predicted, (140 - 165).

Somlyody (1982) used the Extended Kalman Filter (EKF) method and recursively estimated the parameter values for each time step using the suspended sediment data. He obtained reasonably constant values for each parameter and considered this to be a verification of the model structure. However, Beck (1985) performed a similar analysis holding $n = 1$ and concluded that the model structure was "relatively good" but that fluctuations in the parameter values did "exhibit the non-stationarity that is an essential indication of the failure of a component in the model structure".

Additional suspended sediment and wind speed data were taken in Keszthely basin, (see Figure 1.1), in 1985. In this instance the parameter values found to fit the data were substantially different from those found in the Szemes basin, (Table 3.7). Specifically, the parameter β, (which is related to the settling velocity, see Section 3.2), increased by a factor of six. This is curious since the sediment particle sizes are 2 - 3 times smaller in the Keszthely basin than in the Szemes basin.

In a shallow lake light extinction is closly related to suspended sediment concentration and therefore similar equations should govern both. In addition, the parameters β and n should theoretically remain unchanged for each. Somlyody (1986) performed parameter estimations on extinction

data covering the same period as shown in Figure 3.18 and obtained values of β and n which were unchanged from the suspended sediment data and a value of A which decreased by a factor of 10. He also used a year long set of bi-weekly observations of light extinction in the Siofok basin together with hourly wind speeds to further test the model. He obtained the same parameter values as found in the Szemes basin for extinction. Figure 3.19 shows the excellent comparison between the model and the measurements.

As mentioned previously in each of these results a value of the exponent, $n \approx 1$ was found. This was rationalized by assuming that the sediments and water column approximate a weakly stratified, two-layer system. In this case Eq. (3.37b) might be expected to apply. However, it is not clear that the conditions under which Eq. (3.37b) were derived, i.e., a deepening, wind driven shear layer, are in any way analogous to the conditions prevalent at the bottom of a shallow lake. In particular this implies that no bottom boundary layer exists and that there is no contribution to the near bottom flow due to any setup of the lake. Clearly in the data measured at Keszthely, Figure 2.40, where the bottom current was oriented against the wind, this is not true. It is also not certain how valid the assumption expressed by Eq. (3.38) is. In parameterizing the entrainment in a deep lake, the characteristic turbulent velocity scale is assumed to be associated with the surface boundary layer, i.e., eddies scale with a free surface length scale. Therefore it is reasonable to expect that the turbulent velocity scale is related to the wind velocity. However, the entrainment of bottom sediments takes place in the bottom boundary layer and therefore the appropriate velocity scales may no longer be those associated directly with wind input at the surface. Rather, if waves dominate resuspension the turbulent velocity would scale with the

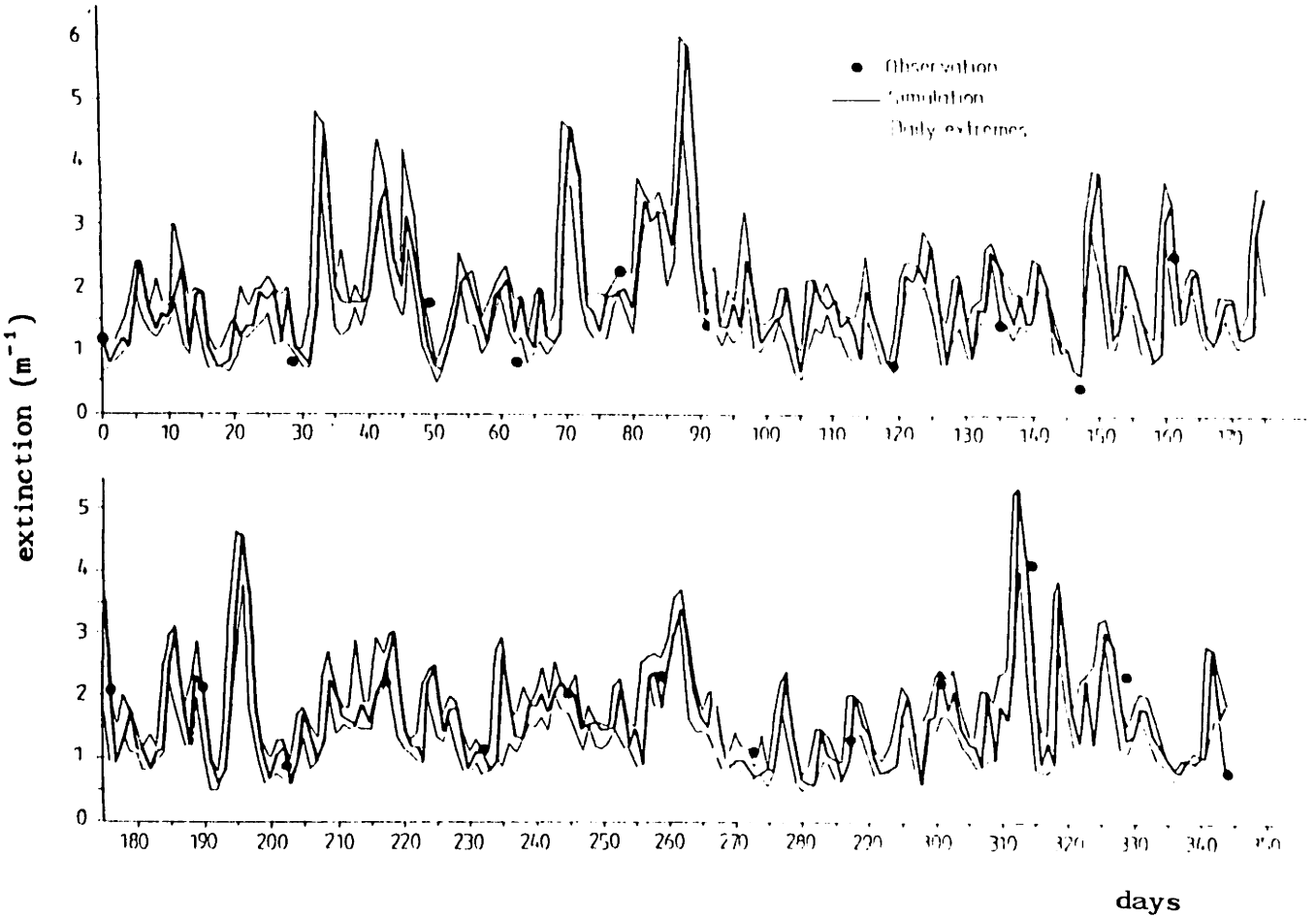

Figure 3.19 Comparison of observed and computed light extinction measurements in Siofok Basin, Lake Balaton, Hungary. (from Somlyody, 1986)

bottom wave orbital velocity. If resuspension is due to the mean current it is not clear a priori what the appropriate scaling velocity should be. Finally, the two-layer fluid entrainment analogy allows no provision for erosion to be affected by the presence of the bed. While the water content of the surface sediments are high, dives made during the field study described in Chapter 2 always indicated the existence of a relatively distinct interface. Therefore, it is not clear that the value of n = 1 can be generalized in any way using the "weak interface" arguement nor is it clear that Eq. (3.35) derives any physical basis from the entrainment analogy. On the other hand Eq. (3.35) may give reasonable results simply because the wind ultimately provides the energy for the hydrodynamic forcing and therefore erosion is expected to be related to wind speed in some fashion.

Aalderink et al. (1984) have conducted a similar study in a shallow Dutch lake, (10 km x 1-3 km x 1 m). Suspended sediment samples were collected as often as hourly for periods of at least two weeks in the fall of 1981 and the spring of 1982. During one session samples were taken at different horizontal positions in the lake and showed some sensitivity to effective fetch illustrated in Table 3.8.

Table 3.8. Fetch Effect on Observed Suspended Sediment Concentrations (after Aalderink et al 1984)

Sampling Station	Average effective fetch (m)	Average S.S. conc. (mg/ℓ)	Range (mg/ℓ)
1	1100	23.2	15 - 35
2	1430	30.2	21 - 41
3	1890	33.1	22 - 45

The deposition flux was parameterized as done by Somlyody, although a background concentration was also included, (Eq. 3.39, Table 3.7). Four expressions were proposed to quantify the resuspension flux and are listed in Table 3.7. Briefly Eq. (3.40) was from Lam and Jacquet (1976), Eq. (3.41) was from Somlyody (1980, 1982, 1986), while the other two were obtained by assuming a kinetic energy - potential energy balance as quantified by Eq. (3.36a). The difference between these final two relationships was that one assumed U_* could be characterized by turbulence generated in the boundary layer associated with the mean current while the other considered turbulence in the wave boundary layer. A loose parameterization of U_* for each case led to Eqs. (3.42) and (3.43) in Table 3.7. A set of hindcasting equations with the same form as the shallow water SMB equations were used to determine the wave properties. Resuspension and deposition were assumed to occur simultaneously.

The Marquard parameter estimation technique was used to estimate parameter values for the four different equations from the field data measured in the fall of 1981, (about 185 points taken over 16 days).

The results are shown in Table 3.9 in terms of the root mean square error and suggest that Somlyody's model performed the best having an average error of ± 3.6 mg/ℓ, Figure 3.20.

Table 3.9. Mean Square Error Results
(after Aalderink et al 1984)

Data Set	Entrainment eqn. number	RMS Error (mg/ℓ)
Fall 1981 - calibration	3.40	4.3
Fall 1981 - calibration	3.41	3.6
Fall 1981 - calibration	3.42	4.0
Fall 1981 - calibration	3.43	3.6
Spring 1982 - verification	3.40	3.8

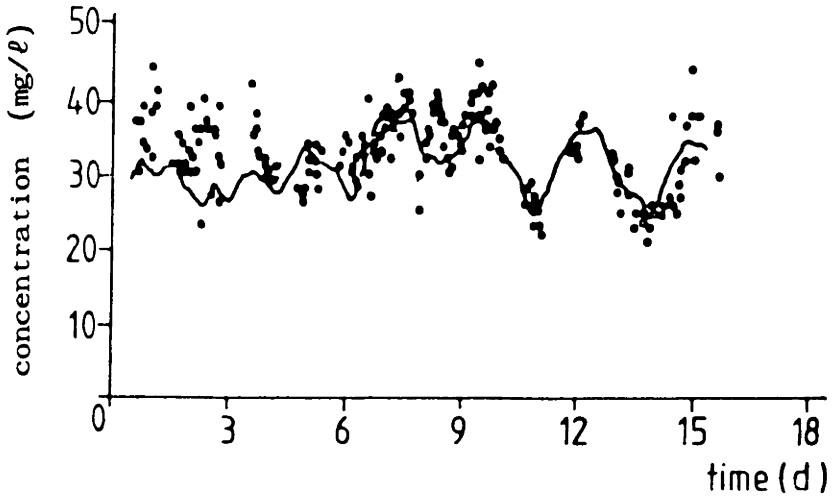

Figure 3.20 Comparison of calibration of Somlyody's model to suspended sediment concentrations measured in a shallow Dutch lake. (from Aalderink et al. 1984)

Kang et al (1982) used the shallow water SMB method to calculate wave statistics in Lake Erie. Assuming that the bottom stress was due only to waves, they computed the stress distribution at the sediment surface throughout the lake using linear theory and the relationships for a smooth wave boundary layer as proposed by Kajiura (1968). They assumed a general resuspension criterion based on particle size and compared the distribution of sediments which should not be resuspended in typical storms with measurements by Thomas (1976) of the sediment characteristics along the lake. The results suggested qualitative correspondence between areas of high shear and larger grain sizes and low shear and finer grain sizes.

Paul et al (1982) correlated turbidity data measured every two hours at a municipal water intake in the western basin of Lake Erie from 1976 through 1979 to predicted bottom stress due to waves and the loading from a nearby river. After some experimentation they obtained Eq. (3.44) in Table 3.7. The wave characteristics were computed using measured wind speed and the shallow water SMB method. Results over all were good, although it appears that the model responded mostly to the loading terms as indicated by the magnitude of terms shown in Table 3.10. Therefore, minimal verification is provided for the resuspension terms themselves. In spite of this the authors conclude that, "The turbidity is directly related to wave action and the resulting bottom stress".

Table 3.10. Contributions of the Terms in Equation (3.44) in 1977 (from Paul et al 1982)

Time	Turbidity observed	Turbidity predicted	C_1	$C_2F(\tau)$	$C_3F(\tau)I(L)$	$C_4D(L)$
113 days, 16 hours	150	141	4	4.3	21.8	110.7
252 days 2 hours	20	19.4	4	3.4	1.5	10.5
282 days 4 hours	5	5.3	4	0.5	0.1	0.6

To summarize the results of previous attempts at cohesive sediment transport modeling, a distinction is first made between models applied to laboratory tests and those applied to field sites. Inherently, the potential for verification of those models applied in the laboratory is much greater due to the more controlled conditions and the smaller area over which measurements must be made. On the other hand, it is difficult to devise an experiment which is different enough from the experiments on which the general model formulation and the parameter calibrations are based to provide a statistically significant verification. This may be the case with the work of Hayter (1983). The fact that in some tests he appeared to underpredict bulk erosion but the surface erosion rates made the predicted concentrations eventually "catch up" with observations is of concern. Also the absence of any hysteresis and the need to abandon one of the central principles associated with the SIM in the simulated tidal experiment, cast substantial doubt on the quality of verification being provided.

The amount of data required for field verifications of cohesive sediment transport models is so extensive that most of the applications to

date are at best intuitive guesses. This is particularly true for situations in which both the transient response and horizontal transport are significant, since it is then necessary to perform verification in time and space simultaneously.

Generally DIM approach 1 has been applied in much more detail than DIM approach 2. Typically the former models have involved breaking the bed into numerous layers each of which has several parameters which must be specified to characterize the erosive process. The deposition expressions also require the specification of several parameters which can only be done directly through extensive laboratory testing. These models end up with so many parameters to be calibrated that their verification is almost impossible.

The most definitive applications of the DIM approach 2 have been in cases in which horizontal transport has been neglected and verification in time conducted. In each case four or less calibrated parameters were used. The results of Lavelle et al. (1984) are quite good although a range of parameter values was found and the results offer only a calibration. The studies of Somlyody (1980, 1982, 1986) and Aalderink et al. (1984) give mixed results. While trends are often reproduced they are also missed completely. It is difficult to conclude whether problems are due to the grossness with which the forcing is represented, the neglected spatial variability or an inadequate model formulation.

3.5 SELECTION OF A BOTTOM FLUX BOUNDARY CONDITION FOR FIELD APPLICATION IN A COHESIVE SEDIMENT TRANSPORT MODEL

The conceptual double interface model presented in Section 3.1 has suggested that two approaches can be followed in specifying the bottom flux for a cohesive sediment transport model; specify the net flux directly, (Eq. 3.3) or specify both components of the simultaneous exchange between the water column and the surface zone, E_2 and S_2, and then compute the net flux with Eq. (3.1). Theoretically either of these methodologies are equally valid.

From a modeling perspective, the choice must be made based on achieving the best representation of the physics using relationships which can be calibrated and verified with the available data. At present there is no indication that parameter values can be generalized from one application to another, and therefore the calibration and verification process must be repeated for each. In this respect a model which has so many parameters that it cannot be verified is no better than one which is known to fail. In fact, the failing model may be more useful if information can be gained about why it failed and therefore be used to identify a higher level of complexity which must be considered. A model is also much more useful if physical meanings can be attached to calibrated parameter values since this lends confidence to the calibrations and provides insight into the implications of simplifying assumptions or approximations that are being made.

Currently, the best field data available to calibrate and/or verify a dynamic model of cohesive sediment transport are time histories of suspended sediment concentration and some measure of the forcing. As

presented in Chapter 2, at least 60 hours of such data was collected in Keszthely Basin of Lake Balaton along with an idea of the particle sizes found there. In particular this data set is unique because of the amount of information available defining the hydrodynamic forcing.

Given this much information, it seems unlikely that a model in which the sediment is discretized into multiple layers having different erosive properties can be applied in a meaningful way. Although useful for purposes of interpretation, there appears to be no indication that the conceptual DIM can be quantified directly, i.e. by specifying E_1, E_2, S_1 and S_2 and then modeling the population/depletion of the surface zone. Therefore, the modeler is left to specify ϕ using the fewest and most meaningful parameters possible, in a physically realistic way, which hopefully has a general enough form to represent exchange with a populated surface zone or bed strength limited conditions depending on the calibrated values determined for the parameters.

A model based on a DIM A1 might express the net erosive flux using either Eqs. (3.19) or (3.20) and require some specification to be made of the bed strength profile. This would involve 2-3 parameters plus those associated with the bed strength and would only be realistic for the bed strength limited erosion. The deposition would be computed using Eqs. (3.23) and (3.24) and require the specification of 4 more parameters. Unfortunately, it is quite difficult to associate a physical meaning with the resulting parameters. In addition the expressions themselves are so empirical that it is difficult to know whether their form is sufficiently general to ensure that just the parameter values will change from one application to another.

A model based on a DIM A2 can express E_2 and S_2 using Eq. (3.15) and c_{ss} using Eq. (3.27a). This yields an expression for ϕ of

$$\phi = -\beta\bar{c} + K(\tau_b - \tau_c)^n \tag{3.45}$$

At least two of the four parameters in this model have clear physical meanings, β, (Eq. 3.11) and τ_c. In addition, they are potentially measurable in the field, i.e., by measuring the settling velocity, concentration gradient and conditions under which erosion is initiated. For the latter two measurements, the ABSS described in Chapter 2 would be particularly useful since it is capable of yielding a profile measurement and at the same time "seeing" when erosion begins.

It can be expected that K, τ_c and possibly n are functions of the bed strength, if the exchange is bed strength limited, or at least of the particle size distribution (as is β). Clearly, the simplest assumption would be that each of these is constant in time yielding a model with four parameters to calibrate. The nice feature about such a model is that if it fails, physically meaningful improvements can be made in a relatively straight forward (albeit not simplistic) manner. For example, if the bed is highly cohesive and the model overpredicts the deposition rate during periods of decreasing concentration, it may be necessary to alter the coefficients in the expression for c_{ss}. If an indication is obtained that the concentration is not well-mixed over the depth or a significant change occurs in the particle size distribution in time, each of these effects can be modeled explicitly. If it is possible to make bed strength measurements in the laboratory, as discussed in Section 3.2.2.1, these results are also fairly easily included in the model.

In conclusion the DIM approach 2 model gives a very simple starting point, i.e., Eq. (3.45) with constant parameters, and a lot of flexibility for improvement in a straight forward, physically meaningful way. Therefore this model was selected for implementation in Chapter 5.

Chapter 4

The Hydrodynamics Controlling Resuspension

Depending on their relative magnitudes, the bottom stresses due to the current and due to the waves have similar effects on resuspension, i.e., being responsible either for the "pick up" or "rip off" of sediment. The bottom stress associated with the waves varies in time within each wave cycle, and it is useful to select a single value to describe the wave effect. For this purpose the maximum stress associated with the bottom wave orbital velocity is used.

The maximum bottom stress can be computed from

$$\tau_{bw} = \frac{f_w}{2} \rho U_b^2 \tag{4.1}$$

where U_b is the maximum bottom orbital velocity, ρ is the density and f_w is a wave friction factor. The friction factor has been related to the bottom roughness and a wave Reynolds number by Jonsson, (1966) as shown in Figure 4.1.

The wave Reynolds number, RE_w is defined as

$$RE_w = \frac{U_b A_b}{\upsilon} \tag{4.2}$$

where A_b is the bottom excursion amplitude, and υ is the kimematic viscosity. The bottom roughness is expressed in terms of k_s, which is a measure of the physical bottom roughness height, normalized by the bottom excursion amplitude. Using linear wave theory, the following are true:

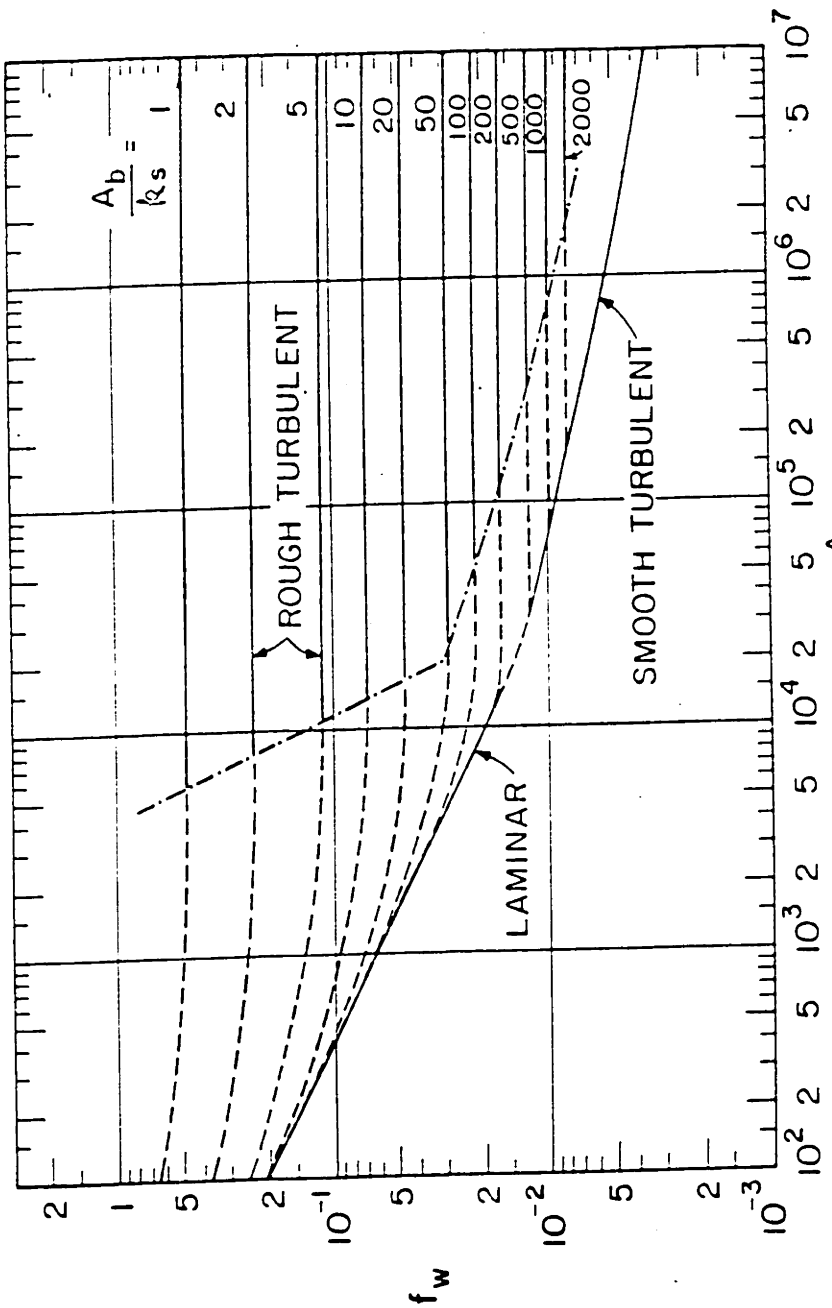

Figure 4.1 Wave friction factor diagram after Jonsson, 1966. (Figure taken from Madsen and Grant, 1976.)

$$A_b = U_b/\omega \tag{4.3a}$$

$$U_b = \frac{a\omega}{\sinh kh} \tag{4.3b}$$

where ω is the radian frequency, a is the wave amplitude, k is the wave number and h is the mean water depth.

Throughout all of the measurements made as a part of this study, the wave Reynolds number rarely reached 1000 and never surpassed 2000. This yields a laminar wave boundary layer for a physical bottom roughness less than about 0.3mm and one in the transition region between laminar and rough turbulence for larger roughnesses. A roughness of 0.3mm is more than 10 times the particle size at either of the measurement sites suggesting a turbulent boundary layer would not exist in the absence of some type of bed form.

It is evident that the particular values of frequency and wave amplitude used in Eqs. (4.1) - (4.3) will affect the predicted maximum bottom stress. A reasonable choice for the wave amplitude would be one-half of the significant wave height based on the fact that linear wave theory has been shown to be applicable and also anticipating the eventual use of a model to hindcast significant wave heights, (Section 4.1). However, the choice for the wave period is not as straight forward. None of the values presented in Chapter 2, Eqs. (2.29) - (2.31), correspond to the significant wave period, which in itself is somewhat illusively defined as discussed further in Section 4.1, and none have gained the wide acceptance for representing a wave field the way the significant wave height has. There is also no reason to believe that any one of these definitions of the period together with the significant wave height will

provide the correct combination of frequency and amplitude to accurately reproduce the bottom orbital velocity and therefore the bottom stress.

For these reasons the equivalent velocity period, T_{ev}, is defined. This is the period, when combined with the significant wave height, that yields a bottom rms orbital velocity equal to the total bottom rms velocity in the surface wave band of the measured velocity spectrum. For a monochromatic, unidirectional, linear wave train

$$U_b = \sqrt{2}\, U_{rms} \tag{4.4}$$

Therefore, given T_{ev} and H_s, a maximum bottom velocity and therefore a maximum bottom stress can be computed which are eqivalent to a unidirectional, monochromatic, linear wave train having the same energy in the wave amplitude and velocity spectra as that which was measured.

T_{ev} is computed implicitly from the linear wave relationship

$$U_b = \frac{\pi H_s}{T_{ev} \cdot \sinh kh} \tag{4.5}$$

together with the definition of k, Eq. (2.20), using the significant wave height as determined in Chapter 2, Eq. (2.25), and U_b from Eq. (4.4). U_{rms} is defined here as

$$U_{rms} = \left[\int_0^{\pi}\int_0^{\infty} S_{uu}(f,\theta,0)\ df\ d\theta\right]^{1/2} \tag{4.6}$$

where $S_{uu}(f,\theta,0)$ is the directional, horizontal velocity power spectrum at the bottom. An equivalent expression for linear waves is

$$U_{rms} = \left[\int_0^\infty S_{ww}(f,h_{c1})\cdot LTF^2_{wu}(f,h_{c1},0)\ df\right]^{1/2} \tag{4.7}$$

where

$$LTF_{wu}(f,h_{c1},0) = \frac{1}{\sinh(kh_{c1})} \tag{4.8}$$

$S_{ww}(f,h_{c1})$ is the measured vertical velocity power spectrum at height h_{c1} and $LTF_{wu}(f,h_{c1},0)$ is the transfer function.

For the data presented in Chapter 2, T_{ev} is generally about 10 per cent less and has a more compressed peak to peak range than alternate definitions of the period. A comparison is provided in Figure 4.2 between the mean period, M_o/M_1, and the equivalent velocity period for each data set presented in Chapter 2.

The bottom stress due to the mean current can be related to the current friction velocity, U_{c*}, as

$$\tau_{bc} = \rho U^2_{c*} \tag{4.9}$$

and can be determined from a known velocity at a known elevation above the bottom assuming the current boundary layer is logarithmic with constant stress. If the bottom is hydrodynamically smooth

$$\frac{U(z)}{U_{c*}} = \frac{1}{0.4}\ln\left\{\frac{zU_{c*}}{\nu}\right\} + 5.5 \tag{4.10a}$$

$$\frac{k_s U_{c*}}{\nu} < 4 \tag{4.10b}$$

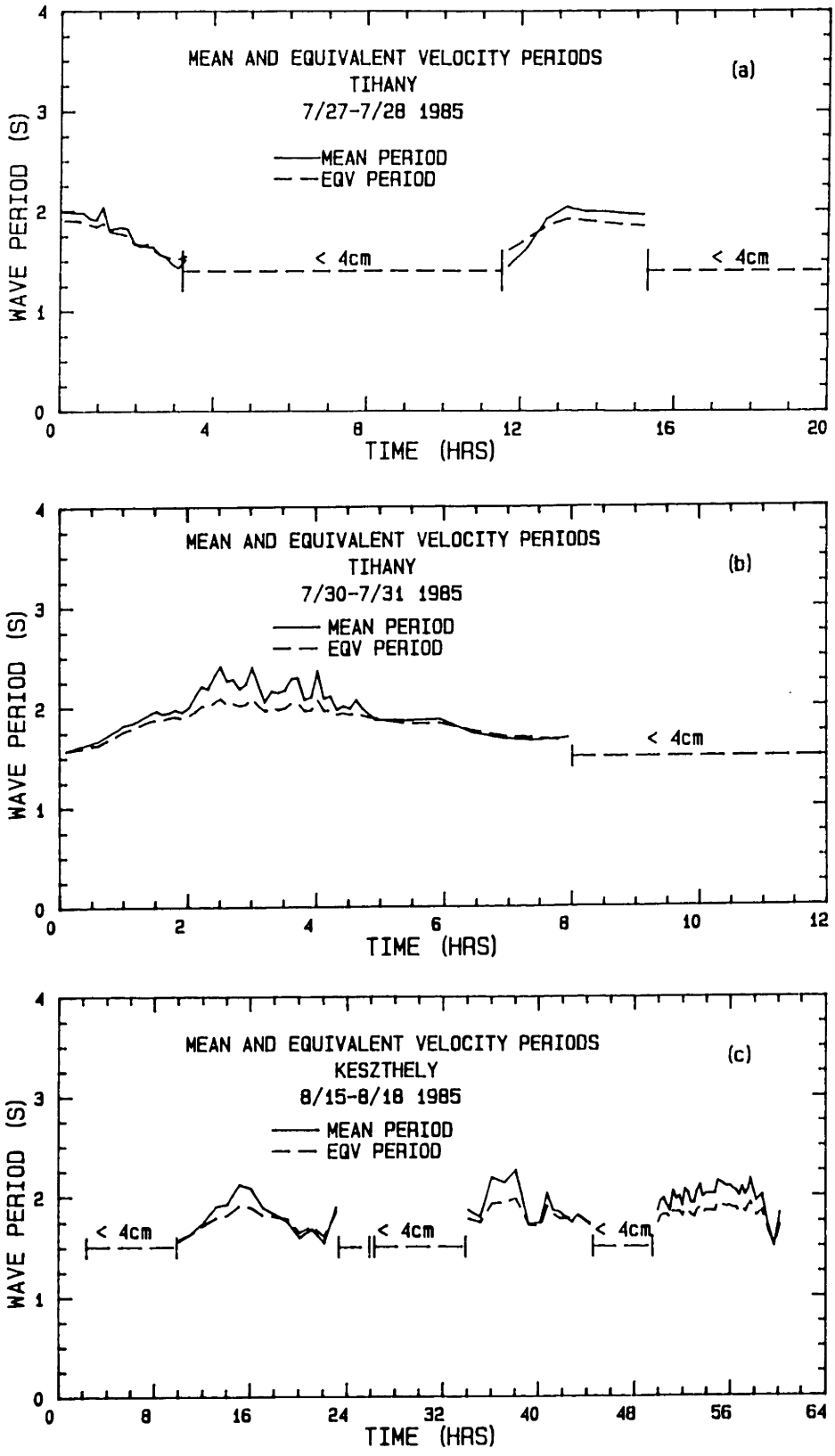

Figure 4.2 Comparison between the mean period and the equivalent velocity period for the data sets presented in Section 2.5.

(Eq. 4.10b expresses the criterion for a hydrodynamically smooth bottom.) Under typical conditions in Lake Balaton, this criterion is satisfied for a physical bottom roughness less than approximately 1 mm, (which is 10 - 100 times the sediment particle size), and therefore also is characteristic of the current boundary layer in the absence of bed forms.

Figure 4.3 shows the relative magnitudes of the computed bottom stress due to the current and due to the waves during each of the three 1985 data sets presented in Chapter 2. In each case a smooth bottom was assumed due to the lack of any evidence of bed forms. (Dives at each site during periods of substantial hydrodynamic activity failed to indicate the presence of bed forms, although irregularities on the order of 1 mm would have been difficult to observe.) The wave stress was computed using the equivalent velocity period and the significant wave height. The current stress was determined by using the mean horizontal velocity measured by the lower current meter as U(z) and the elevation above the bottom of the lower current meter as z in Eqs. (4.10a) and (4.9).

Evident from Figure 4.3 is the dominance (by at least an order of magnitude) which the wave stress has over the mean current stress. The only deviation from this occurred during the intense storm at Tihany, Figure 4.3a, when the mean velocity reached almost 30 cm/s. At this time the wind was blowing from the north causing the measurement site to be cast in the shadow of the ship station and therefore sheltered from the waves. Were this not the case, the stresses due to the current and waves would have been about equal. As discussed in Chapter 2, this event was quite unusual in terms of the intense, short duration, wind speeds observed, the

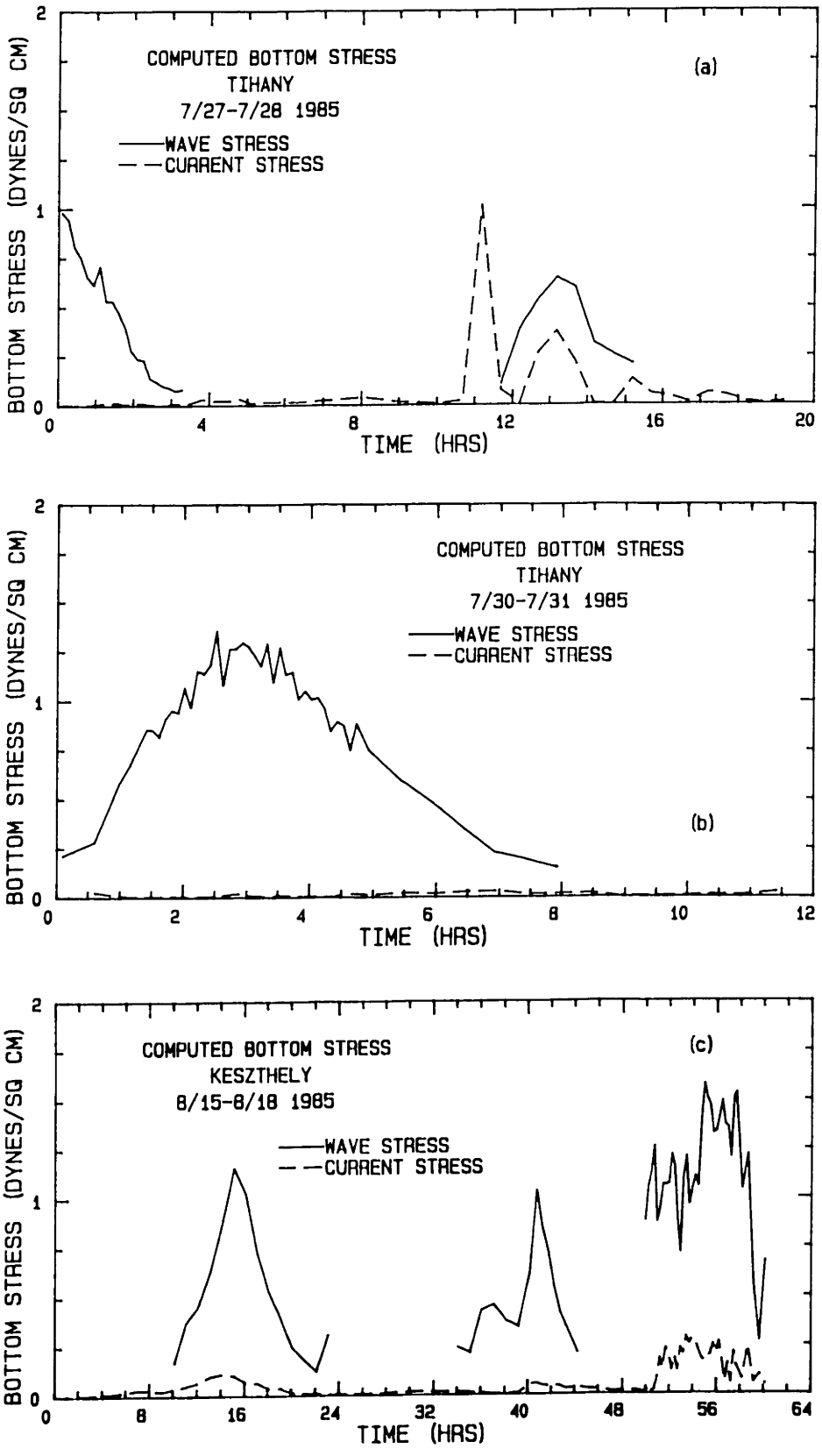

Figure 4.3 Comparison between the computed wave induced bottom stress and the computed current induced bottom stress for the data sets presented in section 2.5. Gaps in the wave stress indicate intervals of negligible waves.

rapidness with which the storm arrived and departed, and the large associated current.

Based on Figure 4.3, it is concluded that during typical storm events, the bottom stress due to the waves provides a significantly more important mechanism for resuspending bottom sediment than that due to the mean current. For this reason the bottom stress due to the mean current will largely be ignored in the remainder of this study and instead, the response of surface waves to various winds and the resulting effect on resuspension will be concentrated on. The unusual event captured in Figure 4.3a underscores the fact that in areas of particularly strong mean velocity, e.g. the Straits of Tihany, the mean current may play a more important role in the resuspension process and should not be neglected.

Before leaving the topic of the relative magnitudes of wave and current associated bottom stresses, a brief mention should be made of why the wave stress so dominates that of the current when the wave bottom orbital velocity and the near bottom mean current velocity are of similar size (as is the case in the measurements made herein). The reason is that shear stress in a neutral or stable boundary layer is proportional to the velocity gradient across the boundary layer. The thickness of a wave boundary layer can be estimated as

$$\delta_\omega \sim \sqrt{\upsilon T} \sim \sqrt{.01 \cdot 2} \sim 1.4 \text{ mm}$$

for a laminar boundary layer and somewhat larger for a turbulent boundary layer, using a characteristic 2 second period. A similar expression can be used for the current boundary layer; however, the period is associated

with changes in the mean flow which occur over much larger time scales. As a result the current boundary layer typically extends over several meters. In Lake Balaton, it is probably reasonable to assume that the current bottom boundary layer has a length scale of half the water depth (assuming the free surface boundary layer also extends over half the depth). Thus the vertical velocity gradient in the current boundary layer is much less than in the wave boundary layer, resulting in a much lower shear stress.

In Section 2.3.2, it was shown that linear wave theory did an accurate job of reproducing the variation in the wave-induced vertical velocity in the water column and can be used to describe the wave properties in general. Thus if the change in the wave height and period as a function of wind speed and direction and position on the lake can be determined, the hydrodynamics responsible for resuspension will be reasonably well quantified. To accomplish this, a wave hindcasting model was implemented in Lake Balaton. As shown in Figure 1.1 the change in water depth is quite gradual throughout most of the lake. This fact allows considerable simplification to be made in modeling the waves by assuming that they are traveling in the wind direction and that the local depth is appropriate for determining their properties. The validity of these assumptions obviously restricts the model's usefulness in areas of rapidly changing depth such as the Strait of Tihany; however, the reasonable comparisons to the available field data which result from this model seem to justify these simplifications.

4.1 WAVE MODEL

The wave hindcasting model implemented herein uses the shallow water modifications made to the SMB method as presented in CERC (1977, 1984). The model is based on successive approximations in which wave energy is added due to wind stress and subtracted due to bottom friction and percolation. The results are summarized by the following empirical equations:

$$\frac{gH_s}{W_a^2} = A \tanh \alpha \cdot \tanh \left[\frac{\gamma}{\tanh \alpha}\right] \tag{4.11}$$

$$\frac{gT}{W_a} = 2\pi B \tanh \beta \cdot \tanh \left[\frac{\delta}{\tanh \beta}\right] \tag{4.12}$$

$A = 0.283$

$B = 1.2$

$\alpha = 0.530\ (gd/W_a^2)^{0.75}$

$\beta = 0.833\ (gd/W_a^2)^{0.375}$

$\gamma = C(gF/W_a^2)^{CC}$

$\delta = E(gF/W_a^2)^{EE}$

g = acceleration of gravity (m/s^2)

d = water depth (m)

H_s = significant wave height (m)

T = wave period (s)

CERC (1977) suggests the following values be used for the remaining parameters:

$C = 0.0125$

$CC = 0.42$

$E = 0.077$

$EE = 0.25$

$W_a = W_{a10} \equiv$ wind speed 10m above the water surface (m/s)

$F \equiv$ effective fetch (m)

As discussed in Section 2.3.2, the significant wave height is the mean height of the one-third highest waves. Assuming the wave heights follow a Rayleigh probability law, the significant wave height can be statistically related to other measures of wave height, e.g.,

$$H_s \approx \sqrt{2}\, H_{rms} \tag{4.13}$$

where H_{rms} is the root mean square wave height.

The wave period computed in Eq. (4.12) is referred to as the significant wave period, although, its definition in physical terms is illusive since waves having a height of H_s may not actually exist. When determined from a wave gauge record, the significant period is often taken to be the average period of the subjectively estimated most prominant waves, or alternatively the average period of all waves having troughs below and crests above the mean water level, (zero up crossing method).

The fetch is subjectively defined as the over-water region in which the wind speed and direction are reasonably constant. In inland waters

fetches are often long in comparison to the width of the water body over their length, and the wave characteristics predicted by Eqs. (4.11) and (4.12) are often substantially greater than those observed. It is assumed that there are at least two contributing reasons for this:

(i) The wind transfers energy to the water in all directions within approximately 45^{o} either side of its principal direction. The amount of energy transferred in each direction decreases as the cosine of the angle to the central radial.

(ii) Some waves interact with the lateral shoreline and therefore this energy is lost from the wave field.

Consequently, rather than working with the absolute or straight line fetch, (defined to be the straight line distance between a wave station and the shoreline in the up-wind direction), the effective fetch is used, CERC (1977). This is computed by constructing 15 radials from the wave station to the shoreline at 6° intervals (limited by angles of 45° either side of the up-wind direction). The component of the length of each radial in a direction parallel to the wind is multiplied by the cosine of the radial's angle with the wind direction. The resulting values for each radial are summed and divided by the sum of the cosines of each radial angle.

Eqs. (4.11) and (4.12) depend only on the wind speed, water depth and fetch. Therefore they assume the wind has been blowing sufficiently for a steady state to be reached.

CERC (1984) recommends a different set of parameter values:

$C = 0.00565$

$CC = 0.5$

$E = 0.0379$

$EE = 0.333$

$W_a = 0.71\ W_{a10}^{1.23}$ (W_{a10} in m/s)

F ≡ absolute fetch (m)

In addition to changing various numerical constants, the definitions of several variables have been altered. W_a is considered to be an "adjusted wind speed," which accounts for the nonlinear relationship between wind speed and wind stress. The effective fetch was abandoned in favor of the absolute fetch since Eqs. (4.11) and (4.12) were found to underpredict wave properties when the effective fetch was used with the 1984 parameter values. Recent data have also suggested a narrower directional spread to the wave spectrum than the cosine relationship used to determine the effective fetch. Ultimately, the issue of effective fetch is unresolved as width is still expected to be important below some critical value (CERC, 1984). The meaning of the period, T, predicted by Eq. (4.12) may also be different since as the depth becomes greater, Eq. (4.12) approaches an equation predicting the period of the peak of the energy spectrum.

CERC (1984) also provides a guideline for the situation in which the waves are duration limited, (i.e., steady state has not been reached),

$$\frac{gD}{W_a} = 537\ \left(\frac{gT}{W_a}\right)^{2.33} \qquad (4.14)$$

where D is the wind duration.

This can best be used by rewriting Eq. (4.14) as

$$\frac{gT}{W_a} = \left(\frac{gD}{537\ W_a}\right)^{3/7} \tag{4.15}$$

substituting this into Eq. (4.12) and solving for the fetch.

$$F_{dur} = \frac{W_a^2}{g} \cdot \left[\frac{\tanh \beta}{E} \cdot \text{arctanh}\left[\left(\frac{gD}{537W_a}\right)^{3/7} \cdot \frac{1}{B\tanh \beta}\right]\right]^{1/EE} \tag{4.16}$$

Therefore, a wind which has been blowing for a given duration, D, will have a fetch, F_{dur}, over which steady state has been reached. The fetch to be used in Eqs. (4.11) and (4.12) is the smaller value between F_{dur} and the value determined from the lake geometry.

4.2 WIND SPEED ADJUSTMENT

Due to the planetary boundary layer, there is an increase in wind speed with distance above the earth's surface. With the assumption of a neutrally stable atmosphere close to the surface, this region can be reasonably treated as a constant stress layer and, therefore, a logarithmic velocity profile is expected to apply. This takes the form

$$W_a(z) = \frac{W_{a*}}{\kappa} \ln \frac{z}{z_o} \tag{4.17}$$

and leads to a quadratic drag law

$$\frac{\tau_a}{\rho_a} = W_{a*}^2 = C_D W_{a10}^2 \tag{4.18}$$

where $W_a(z)$ is the wind velocity a distance z above the surface, W_{a*} is the friction velocity, $\kappa = 0.4$ is the von Karman constant, z_o is the surface roughness height, τ_a is the surface shear stress, ρ_a is the density of air, C_D is a drag coefficient and $W_{a10} = W_a(z = 10m)$. All of the equations in Section 4.1. use W_{a10}, and, therefore, it is necessary to adjust a wind speed not measured at that elevation. This is easily accomplished using Eqs. (4.17) and (4.18) which together yield the relationship:

$$W_{a10} = \frac{W_a(z)}{1 + \frac{1}{\kappa}\sqrt{C_D}\,\ln(\frac{z}{10})} \tag{4.19}$$

In Eq. (4.19) C_D is a parameter which must be specified.

Numerous investigators have considered the behavior of C_D. Graf and Prost (1979) propose three general categories of the water surface state under conditions of neutral stability. They are:

(i) Light winds result in an aerodynamically smooth water surface yielding a value of C_D governed by smooth plate theory.

(ii) Medium winds result in a non-smooth surface and thus a drag which increases with roughness. C_D is expected to be a function of wind speed and fetch.

(iii) Strong winds result in a water surface state which is saturated with respect to the high frequency range of the wave spectrum. It is believed that wind interacts primarily with this part of the wave spectrum so that C_D would be independent of the wind speed.

Table 4.1 presents a sampling of the results obtained from various studies. Characteristically they are constant at very low wind speeds and have a weak linear dependence on wind speed at higher values. However, the spread in the data has often made this dependence unconvincing, e.g., Stewart (1974) and Donelan (1982). Bengtsson (1978) found no fetch effect on C_D to within 25m of shore in a small lake while Graf and Prost (1980), Donelan (1982) and Graf et al. (1984) found indirect fetch dependences through parameters expressing the wave age. Qualitatively they found that shorter fetches produced "newer" waves which have higher values of C_D. Quantitatively, this effect is not yet well described.

For the present study the relationship of Wu (1982) [See Table 4.1] was selected, as it is based on a regression of a large number of data sets in which values by less rigorous measurement techniques (e.g., the surface slope method) were discarded. Also it gives relatively "middle of the road" values of C_D. While the data used to obtain this equation are biased toward open ocean measurements, the results agree quite reasonably with the findings included in Table 4.1 in fetch limited waters. No fetch effect was explicitly included due to the quantitative uncertainty still surrounding this issue.

As a final note CERC (1984) recommends the following relationship to be used in place of Eq. (4.19)

$$W_{a10} = W_a(z)\left[\frac{10}{z}\right]^{1/7} \qquad (4.20)$$

Eq. (4.20) gives similar results to Eq. (4.19) if a value of $C_D \approx 2.7 \times 10^{-3}$ is used. This value is high compared to most of the

Table 4.1 Summary of Drag Coefficient Results

1) Van Dorn (1953) - 2m deep artificial pond

$C_D = 1.11 \times 10^{-3}$ $W_{a10} \leq 5.16$ m/s

$C_D = 1.11 \times 10^{-3} + 2.06 \times 10^{-3} \cdot (1-5.6/W_{a10})^2$ $W_{a10} \geq 5.6$ m/s

2) Fleagle, Deardorff, Badgley (1958) - Enclosed water body horizontal dimension ~ 10 km

$C_D = 1.2 \times 10^{-3}$ $W_{a10} = 3 - 9$ m/s

3) Wilson (1960) - Ocean

$C_D = 1.5 \times 10^{-3} \pm 0.8 \times 10^{-3}$ $W_{a10} < 6$ m/s

$C_D = 2.4 \times 10^{-3} \pm 0.6 \times 10^{-3}$ $W_{a10} > 10$ m/s

4. Wu (1969) - Ocean

$C_D = 1.25 \times 10^{-3} W_{a10}^{-1/3}$ $W_{a10} < 1$ m/s

$C_D = 0.5 \times 10^{-3} W_{a10}^{1/2}$ $1 < W_{a10} < 15$ m/s

$C_D = 2.6 \times 10^{-3}$ $W_{a10} > 15$ m/s

5. Brocks and Krügermeyer (1970)

$C_D = (1.3 \pm 0.18) \times 10^{-3}$ $W_{a10} = 4 - 12$ m/s

6. Ruggles (1970)

$C_D = 1.6 \times 10^{-3}$ $2 < W_{a10} < 10$ m/s

7. Huovila (1971) - Lake Pääjärvi, Horizontal dimension ~ 0.5 - 10km

$C_D = 0.9 \times 10^{-3}$

8. Bengtsson (1973) - Lake Voumb, 3 km x 5 km

$C_D = 0.9 \times 10^{-3}$ $W_{a10} < 4.5$ m/s

$C_D = 1.2 \times 10^{-3}$ $W_{a10} > 5.5$ m/s

9. Donelan, Elder and Hamblin (1974) - Lake Ontario

$C_D = 1.2 \times 10^{-3}$

10. Hicks, Drinkrow and Grauze (1974) - shallow lake with biological film

$C_D \approx 0.9 \times 10^{-3}$

11. Stewart (1974)

$C_D = 1.3 \times 10^{-3} \pm 20\%$

12. Hsu (1975)

$C_D = 0.7 \times 10^{-3}$ $W_{a10} < 5$ m/s

13. Ottsen-Hansen (1975)

$C_D = 0.8 \times 10^{-3}$ $W_{a10} < 7$ m/s

$C_D = 1.0 \times 10^{-3}$ $W_{a10} > 7$ m/s

14. Garratt (1977)

$C_D = (0.75 + 0.067 W_{a10}) \times 10^{-3}$ $4 < W_{a10} < 21$ m/s

15. Antonia et.al. (1976)

$C_D = 1.1 \times 10^{-3}$ $W_{a10} = 5 - 10$ m/s

16. Bengtsson (1976) - 11 rev of data from small lakes large lakes & sea

$C_D = 0.9 \times 10^{-3}$ $W_{a10} < 5$ m/s

$C_D = 1.1 \times 10^{-3}$ $W_{a10} < 5 - 10$ m/s

$C_D = 2.0 \times 10^{-3}$ $W_{a10} \sim 20$ m/s

17. Graf and Prost (1980) - Lake Geneva, deep water

$C_D = (0.52 + 0.064 W_{a10}) \times 10^{-3}$ $4.5 \leq W_{a10} \leq 14.5$ m/s

18. Smith (1980) Open ocean

$(C_D = 0.61 + 0.063 W_{a10}) \times 10^{-3}$ $6 \leq W_{a10} \leq 22$ m/s

19. Donelan (1982) - Lake Ontario, fetch= 12m deep water, 1.1 km to 300 km

$C_D = (0.37 + 0.137 W_{a10}) \times 10^{-3}$ $4 \leq W_{a10} \leq 17$ m/s

20. Large and Pond (1981) - Ocean deep water; fetch > 10 km

$C_D = 1.2 \times 10^{-3}$ $4 \leq W_{a10} \leq 11$ m/s

$C_D = (0.49 + 0.065 W_{a10}) \times 10^{-3}$ $11 \leq W_{a10} \leq 25$ m/s

21. Wu (1982) - Lt. Review of many data sets

$C_D = (0.8 + 0.065 W_{a10}) \times 10^{-3}$

22. Graf et. al. (1984) - Lake Geneva, near shore, 3m deep water

$C_D = (1.09 + .094 W_{a10}) \times 10^{-3}$ $7 < W_{a10} < 17.5$ m/s

results given in Table 4.1 and yields values of W_{a10} about 10 percent greater than would otherwise be calculated. While this difference is not dramatic, it underlies the caution which should be exercised in using empirical equations such as Eqs. (4.11) and (4.12), which may have relatively obscure assumptions built into them. All computations made with the 1984 model parameters use wind adjustments given by Eq. (4.20), while those using the 1977 model parameters use Eq. (4.19) and expressions for C_D from Wu, (1982).

4.3 RESULTS

The wave model described in Section 4.1 is applied below to all wind speed and wave data available for Lake Balaton. As presented in Chapter 2, this consists of historical data in the Szemes Basin from Muskalay (1973) as well as data taken at Tihany and Keszthely as a part of this study.

Szemes Historical Data

Figure 4.4 shows a comparison between the predicted and observed wave heights and periods using the historical data of Muszkalay (1973). The wind measurement elevation was approximated to be 4m based on a photograph of the field station. The model results plotted in Figures 4.4a and 4.4c are obtained using Eqs. (4.11) and (4.13) while that in Figures 4.4b and 4.4d comes directly from Eq. (4.12). Since no wind direction is given with the original data, the model was run using winds blowing along the minimum and maximum fetches existing at the field site. Also neither the original wind or wave time series data are available, so it was assumed that the waves were entirely fetch limited. Considering the overall uncertainty in the data, both the 1977 and 1984 models bracket the data quite reasonably.

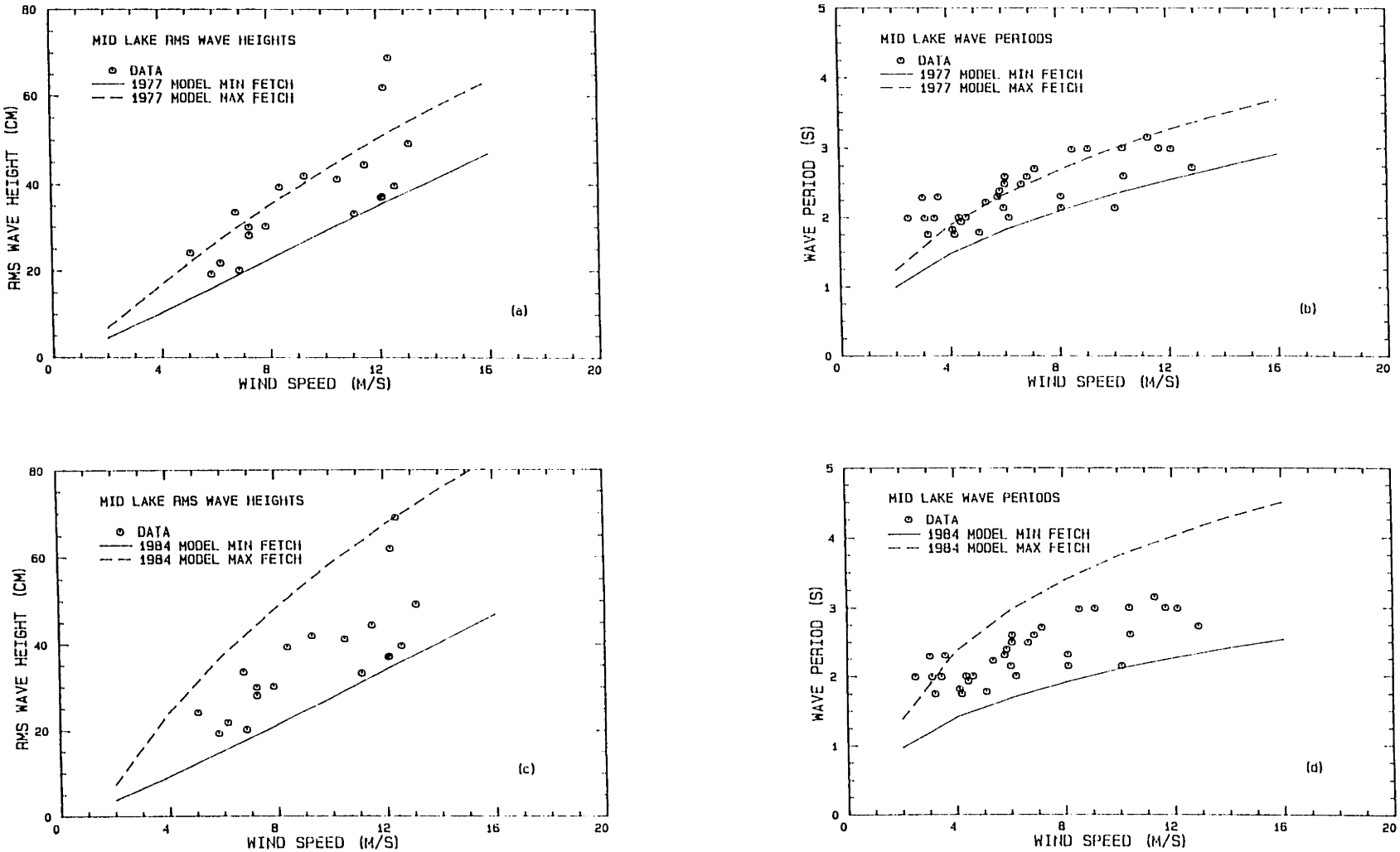

Figure 4.4 Comparison between the wave hindcasting models and historical mid-lake data of Muszkalay (1973).

The principal difference between the models is the result for maximum fetchs since the maximum absolute fetch is almost three times as long as the maximum effective fetch. Consequently, the extremes in the 1984 model enclose 94 per cent and 88 per cent of the wave height and period observations, while the 1977 model extremes enclose only 67 per cent and 45 per cent, respectively.

Figure 4.5 presents the near shore historical data of Muszkalay (1973) along with the 1977 and 1984 model predictions based on assumptions identical to those described above. In this application both models tend to underpredict the observed wave heights and periods. The reason for this appears to be the rapid change in bottom topography along the southern shore, Figure 1.1, which violates the assumption of the wind and waves being in local equilibrium. Using the criterion presented in Section 2.3.2

$$\frac{2\tilde{\epsilon}}{\tilde{\mu}^2} \cong 5.5 < 26$$

$$\left|\frac{\eta^{(2)}}{\eta^{(1)}}\right| \cong 0.23a = 0.07$$

a typical wave at the near shore site, (T = 3s, a = 0.3m, depth = 2.5m), will be described reasonably by linear wave theory. Making use of this and neglecting bottom friction, a wave normally incident on the shore would increase in amplitude less than 5 per cent and maintain an approximately constant period while shoaling from water of 4m depth to water of 2.5m depth. Thus a wave measured at the near shore station would have

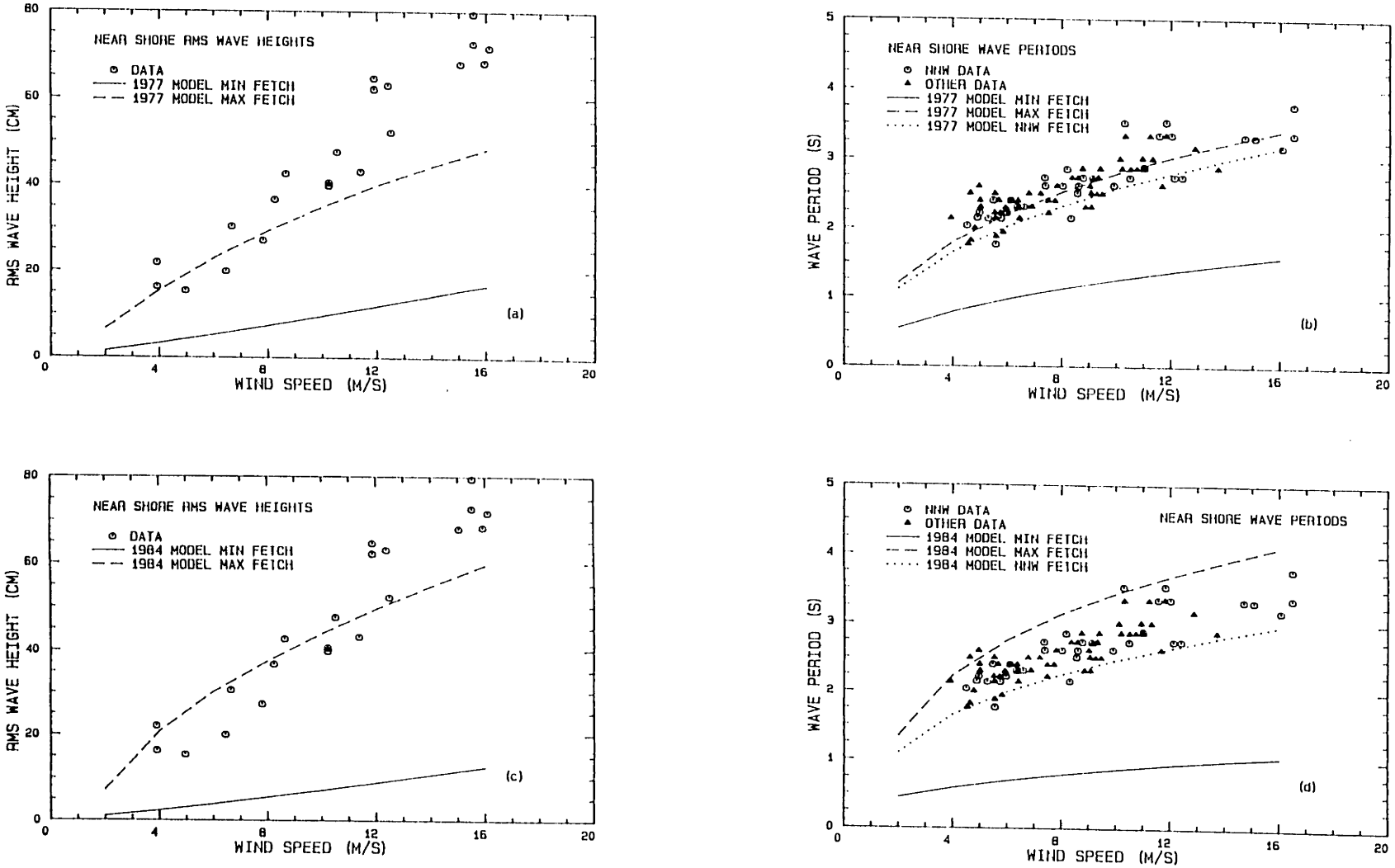

Figure 4.5 Comparison between the wave hindcasting models and historical near shore data of Muszkalay (1973).

effectively the same characteristics as when it was incident upon the southern slope. If a typical depth of 4m is used and the wave properties recomputed using the model at the near shore station, the results presented in Figure 4.6 are obtained. These show a much closer agreement with the data. Again the 1984 model brackets more of the data since it employs a longer maximum fetch.

It should be noted that the data reported by Muszkalay (1973) were determined by taking the rms wave height and period from 100 consecutive waves. It is reasonable to expect that this period would be less than the typically reported "significant wave period" described in Section 4.1 and to which the coefficients in Eqs. (4.11) and (4.12) were originally calibrated. Similarly, the periods reported by Muszkalay (1973) may have been shorter than those determined from vertical velocity measurements, as done in the present study, due to the filtering effect of the water column on the higher frequency waves.

While these comparisons are encouraging, they are not fully satisfying because of the lack of specific information about wind direction and therefore fetch length.

Tihany 1985

Comparisons of time histories of the wave model results and the measured wave properties are presented in Figures 4.7 and 4.8 for the two data sets measured at Tihany. In each case the "equivalent velocity period" was used as a measure of the wave period.

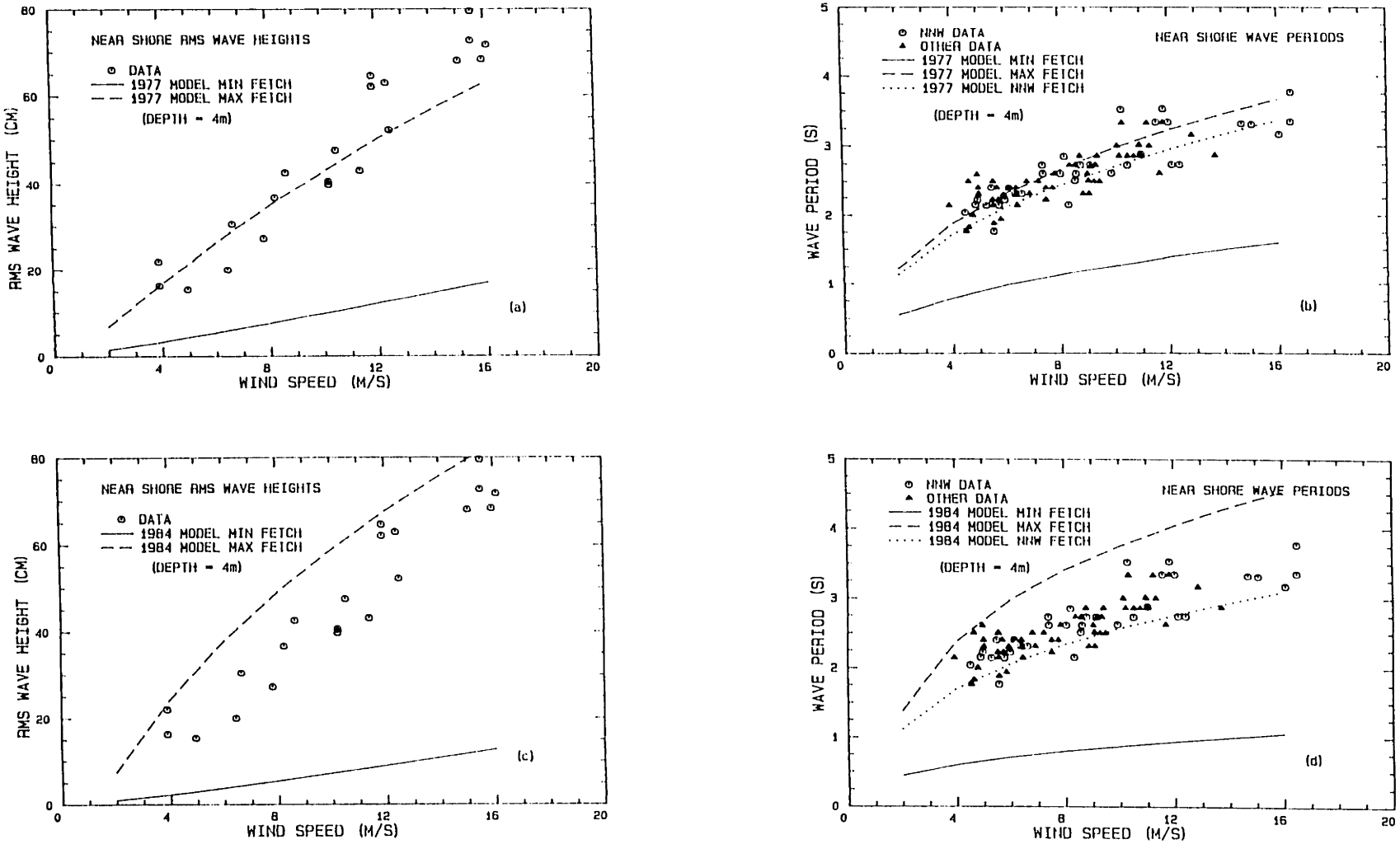

Figure 4.6 Comparison between the wave hindcasting models assumming the depth = 4 m and historical near shore data of Muzkalay (1973).

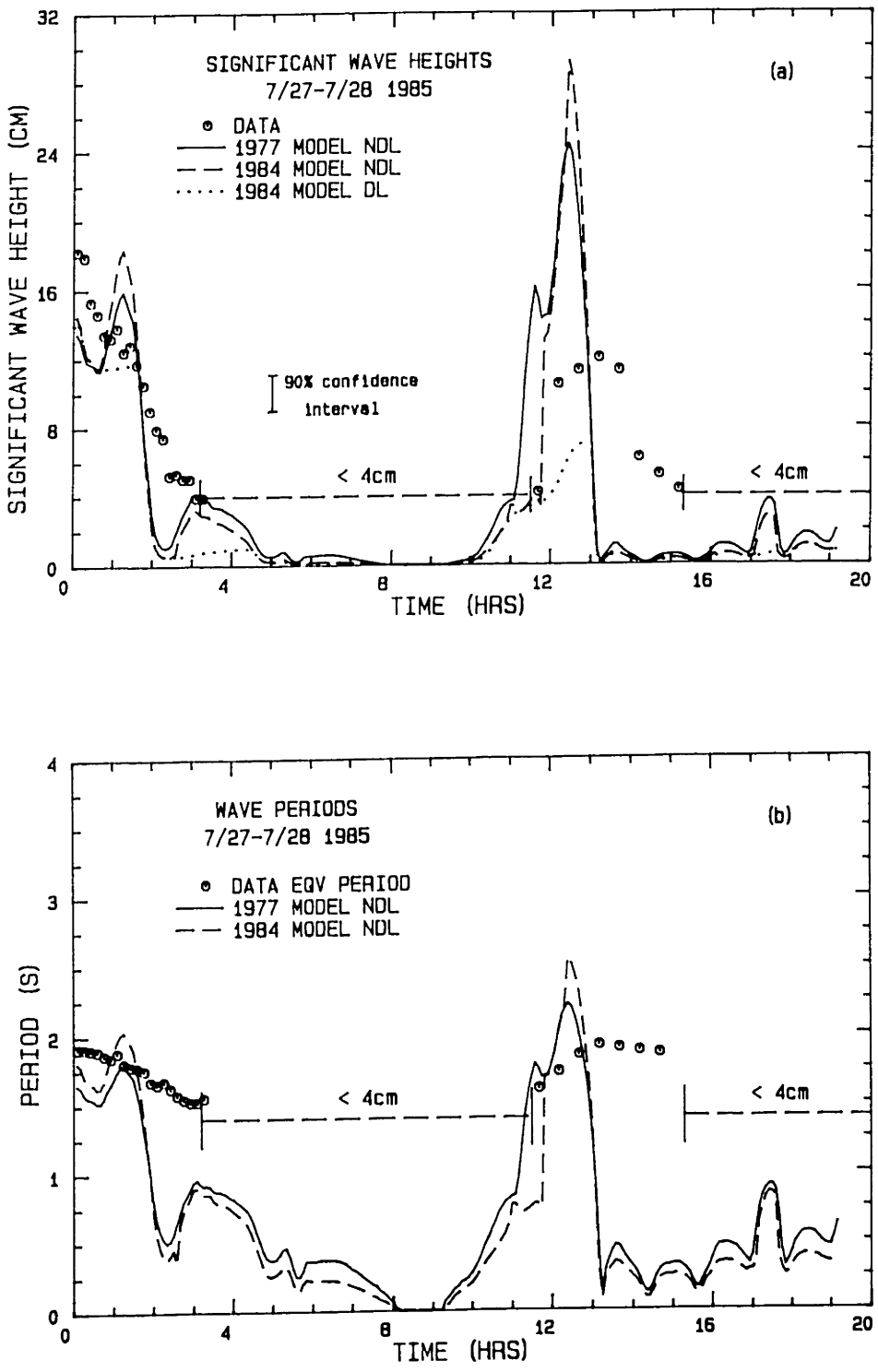

Figure 4.7 Comparison between the wave hindcasting models without duration limitation (NDL) and with duration limitation (DL) with data from the Tihany deployment, Event #1.

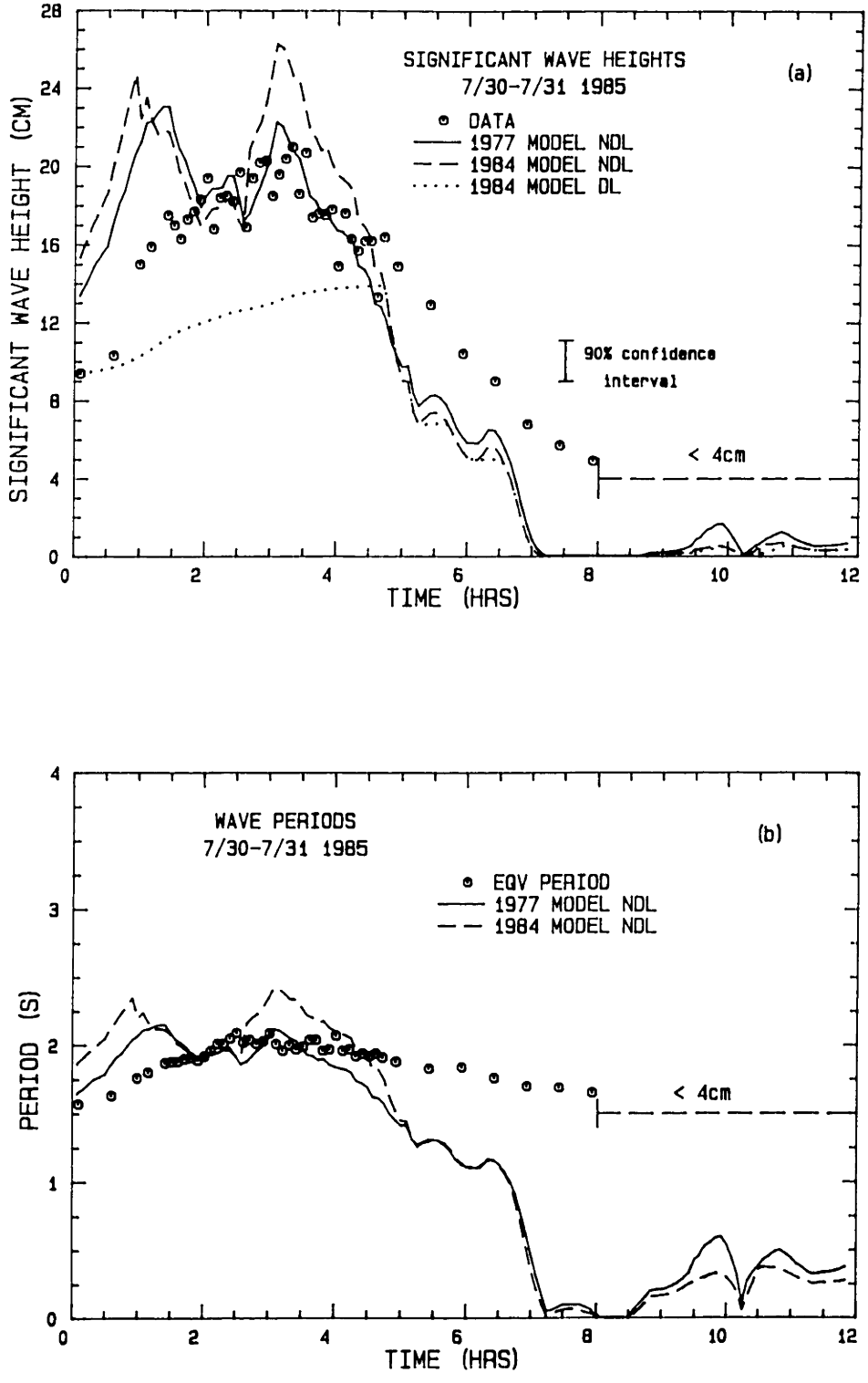

Figure 4.8 Comparison between the wave hindcasting models without duration limitation (NDL) and with duration limitation (DL) with data from the Tihany deployment, Event #2.

In each of the Figures describing wave height, three curves are shown beside the data: the 1977 model result with no duration limitation on wave growth; the 1984 model result with no duration limitation on wave growth; and the 1984 model result with duration limitation on wave growth. If the wind is constant in time, the duration limitation can be applied as suggested in Section 4.1 using Eq. (4.16) to compute the appropriate fetch. However, if the wind field changes in time, further assumptions must be made. Briefly the following procedure was adopted:

(i) the wind field was assumed to be constant over a specified time interval at the end of which it changed incrementally to its value during the next time interval.

(ii) During the first time interval following a prolonged period of zero wind, i.e., assuming an initial condition of zero wind and zero waves, Eq. (4.16) was used to compute a "duration limited fetch", F_{dur}. If the actual fetch at the observation point, F_o, was less than F_{dur}, then the waves were fetch limited and F_o was used in Eqs. (4.11) and (4.12) to compute the wave properties. However, if F_{dur} was less than F_o, the waves were duration limited and F_{dur} was used in Eqs. (4.11) and (4.12).

(iii) When the wind changed, Eq. (4.11) was inverted and solved for an equivalent fetch F_e using the wave height computed at the end of the completed interval and the wind speed of the new interval. (By doing this, the wave height, and therefore the energy, at the observation site was preserved from one interval to the next.)

(iv) Using the new time interval length and wind speed, a new value of the "duration limited fetch" was computed by adding the value obtained from Equation (4.16) to F_e. This value of F_{dur} was then compared with F_o and dealt with as described in step (ii).

Clearly this procedure is somewhat arbitrary and becomes less realistic as changes in the wind field become large or abrupt. It also does not take into consideration the propagation speed of the storm itself. In the limit, if the storm speed approaches the velocity defined by $F_{dur}/\Delta t$, (where Δt is the time interval), duration limitation would never be observed at the measurement site, (rather the waves would arrive before the wind.) No information was available on the storm propagation speed during the present study.

Thus for a number of good reasons, the poor performance of the duration limited model shown in Figures 4.7a and 4.7b is not surprising. In each case it substantially underpredicts the wave heights and, although it has not been shown, does the same for the wave periods. This performance can be improved by changing the coefficients in Eq. (4.14); however, no single set was found which was appropriate for all of the measurements. Therefore, additional efforts to directly include duration limitation on the wave growth were abandoned.

Duration may also be an issue during periods of wave decay. For example, consider the wave field generated by a uniform wind blowing over a given fetch length if the wind suddenly and completely disappeared. The waves observed at any point along the fetch would not disappear until those existing "up wind" had propagated past or been completely attenuated by

bottom friction. Attempts to include the effect of waves propagating over the fetch length at the group velocity during periods of decreasing wind were considerably complicated (i) because the wind speed rarely disappeared suddenly but rather decreased over a finite time period and (ii) because the storms were moving at an unknown velocity. As a result, no generally applicable procedure was found for including duration effects during periods of decreasing wind speed. Clearly, as the significance of transient effects increase, a more complicated wave modeling approach may become warranted. However, this would also require additional data, (e.g., the storm propagation speed), to be meaningful.

In an indirect way, the effects of duration limitation can also be included by filtering the wind speed used in the model in time so that fluctations in the wind with periods much less than the response time of the wave field are smoothed out. Strictly speaking, the filter size should in some way reflect physical properties of the waterbody and wind event, e.g. fetch length, wave propagation velocity, etc. Not surprisingly this leads back to the issues and problems raised in the direct attempts to include duration limitation. In the end, trials were made with the model using a wind field which was smoothed by a running average of various lengths backward in time. A 30 minute length seemed to give the best overall performance and, therefore, was used in all of the "no duration limitation" results where wind measurements were taken more frequently than every 30 minutes.

Returning to the comparison between the "no duration limited" models and the data collected at Tihany, (Figures 4.7 and 4.8), several features are evident. The 1984 model typically overpredicts both the observed wave

heights and the 1977 model wave heights, particularly at large fetches. At other times, the two models give quite similar results. Generally, the wave heights predicted by the 1977 model agree quite well with the data exclusive of the times that rapid changes exist in the wind conditions. Examples of periods of rapid change are the first hour of the 7/30 - 7/31 storm and particularly during the intense storm captured in the 7/27 - 7/28 data set. Typically, the models predict the waves will die more rapidly than observed because of the time required to propagate over the fetch length. Roughly quantifying this effect, a linear wave train having waves with 3 second periods in 4 m deep water travels with a group velocity of about 7.5 m/s. Thus waves require 1.5 - 2 hours to travel over a 15 km distance which is typical of the fetch at Tihany for waves coming from the east. This is in reasonable agreement with the die off period observed after 2 hours and after 12.5 hours in the 7/27 - 7/28 data set, (Figure 4.7a), and in the latter stages of the 7/30 - 7/31 event (Figure 4.8a).

The 1984 model also predicts slightly higher periods than the 1977 model. However, in this respect both models were 10 - 15 per cent below the observed periods. As a result, the leading coefficient, B, in Eq. (4.12) was increased from 1.2 to 1.4. With this adjustment, the predicted periods agree with observations during times of significant wind. However, as the wind dies, the models drastically underpredict the observations. As discussed in Section 2.5, this may be due in part to the sampling rate used to take data, i.e., no periods less than 1 sec. could be measured and periods less than about 1.5 sec. may be suspect due to the filtering effect the water column has on shorter period waves. However, another cause for the larger observed periods is the probability that as

the wind dies down, the wave field is dominated by the fossile field left over from the period of high wind rather than a continuing equilibrium condition with the dying wind.

Kesthely 1985

The results from the Keszthely data set are shown in Figure 4.9. In this case, a duration limitation on wave growth also underpredicted both the wave heights and periods, particularly during the two early events, and therefore has not been included. However, the "non duration limited" models and especially the 1977 model does an excellent job of reproducing the observed wave heights over the entire 60 hours. This is a particularly good test because the early two events had winds aligned with the lake's long axis and therefore the largest fetches, while winds in the latter event were oriented across the lake at fetches of 1 - 2 km. As was the case with the Tihany data, the 1984 model overpredicts both the wave heights and periods at longer fetches. In addition the 1984 model seems to slightly underpredict the measured values for short fetches. The 1977 model very slightly overpredicts the wave height during the rapid onset of a wind event aligned with the lake axis which is quite likely a duration limitation effect. Also during the beginning of the first event, some waves, apparently traveling in front of the storm, appear before the wind picks up. During the final event, the non-steady nature of the observed wave heights is reproduced very well by the model due to the short fetch and as a result the short time required to reach fetch limited conditions. In fact, the model's slight underprediction of the wave heights at about

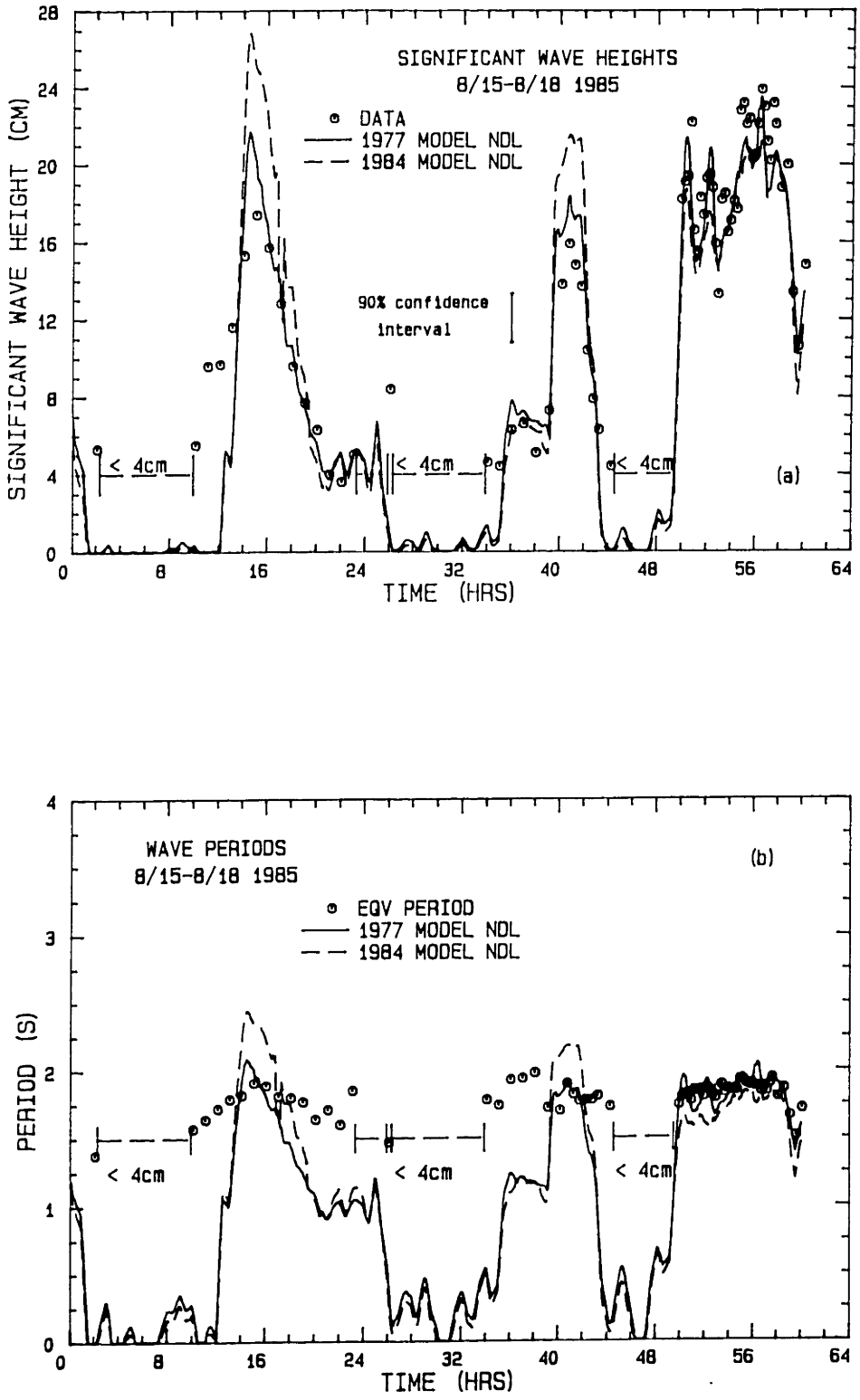

Figure 4.9 Comparison between the wave hindcasting models without duration limitation with data from the Keszthely deployment.

54-56 hours may be the result of measurement intervals which are longer than the response time over the fetch.

The wave period reached during the major part of each of the three events is very well predicted by the 1977 model using the value of 1.4 for B as found in Tihany. However, as was the case with the Tihany measurements, the observations die more slowly than the model predicts. Also during the early part of the second event, the model underpredicts the period at low wind speeds.

4.4 DISCUSSION

Considering the simplicity and empiricism contained in the wave model described by Eqs. (4.11) and (4.12) and the general lack of data avilable for its verification, the results presented in the previous section are in surprisingly good agreement with the data taken in Lake Balaton. The historical results measured at Szemes provide reasonable verification of the models for conditions characteristic of the open, deeper areas of the lake. In this application the 1984 model brackets more of the data than the 1977 model due to the use of the straight line fetch by the former. These comparisons were made using the original factor of 1.2 for the coefficient B in Eq. (4.13), although, an increase in this value to 1.4 would also represent the data quite well and actually improve the 1977 model performance. This is particularly true considering that the observed periods are probably shorter than would have been reported either from vertical velocity measurements or as "an average of the periods of the most prominant waves."

The more detailed data provided in this study show that the "no duration limited" equations using the 1977 coefficients and parameter definitions do a good job of reproducing the wave height and period during intervals of sustained winds in which the assumption of fetch limited conditions would be reasonably expected to hold. The general superiority of the 1977 model suggests that Lake Balaton may be sufficiently narrow to warrant the use of an effective fetch. Attempts to directly include duration limitation of wave growth based on Eq. (4.14) were generally not successful as Eq. (4.14) seemed to overpredict the time required to reach a fetch limited state or equivalently underpredict the "duration limited fetch." Adjustment of the coefficients in Eq. (4.14) did improve this; however, no single constant set was found to give good results for all the data. The application of Eq. (4.14) was complicated substantially by variability in the wind field and the lack of information about the storm speed. As a result the duration limitation on growth was dropped. During the stages of wave decay, the time scale for wave height attenuation was reasonably well represented by the time required for the waves to propagate over the fetch length. The wave period remained approximately constant during this interval and rarely showed any significant reduction at all. Thus a more accurate representation of the period results from assuming a constant period equal to the average value predicted by the model during the main part of the wind event. Alternatively, at least at the Tihany and Keszthely sites, a constant value of about 1.9 seconds could be used for the velocity equivalent period.

Chapter 5

Application of a Resuspension Model in Keszthely Bay

5.1 A TWO-DIMENSIONAL, DEPTH INTEGRATED TRANSPORT MODEL

In Chapter 3, the current state of the art in cohesive sediment modeling was reviewed, paying particular attention to the selection of a bottom boundary condition appropriate for use in a model to be applied to field data. It was concluded that an expression of the form:

$$\phi = - \beta\bar{c} + \beta K(\tau_b - \tau_c)^n \tag{5.1}$$

with

$$\beta \equiv w_s \frac{c_o}{\bar{c}} \tag{5.2}$$

was (1) in reasonable agreement with laboratory observations on erosion and deposition with a cohesive sediment bed, (2) simple enough with constant parameter values to be rigorously calibrated and verified given typically available field data and (3) closely tied to physically measurable quantities, i.e., settling velocity, concentration gradient and critical stress, so that intuition could be used both in calibration and in analysis of model failure.

A visual inspection of the suspended sediment time series presented in Figure 2.41 suggests that during calm periods the concentration rarely dropped below about 15 mg/ℓ. This is most likely due to the smallest inorganic particles as well as various plankton species, which were at major bloom levels during the course of this measurement period, (the water could be best described as "pea soup"). Therefore, the data suggests at

least two particle size intervals should be considered, one with a non zero settling velocity and one with a much smaller or zero settling velocity. The latter effect can be modeled by the use of a "background" concentration in Eq. (5.1) which then becomes

$$\phi = -\beta(\bar{c} - \bar{c}_{bak}) + \beta K(\tau_b - \tau_c)^n \qquad (5.3)$$

Based on Figure 2.41, this "background" concentration was taken to be constant and equal to 15 mg/ℓ.

Since it is impossible to measure ϕ directly and therefore to calibrate or verify Eq. (5.3) by itself, ϕ must be used as the bottom boundary condition for the sediment transport equation, thereby relating it to the measurable suspended sediment concentration in the water column.

The suspended sediment transport equation in depth-integrated form is:

$$\frac{\partial \bar{c}}{\partial t} = \frac{\phi}{h} - \frac{\partial}{\partial x}\left(\overline{uc} - E_x \frac{\partial \bar{c}}{\partial x}\right) - \frac{\partial}{\partial y}\left(\overline{vc} - E_y \frac{\partial \bar{c}}{\partial y}\right) \qquad (5.4)$$

which is the same as Eq. (3.6) except that the horizontal advective and diffusive/dispersive transport terms have been retained. In this equation E_x and E_y are lumped turbulent diffusion/dispersion coefficients, $\bar{u}$ and $\bar{v}$ are depth-averaged horizontal velocities, and changes in depth, h, as well as the sediment flux across the free surface have been neglected.

For general application Eq. (5.4) must be discretized and solved numerically. This is done by superimposing a grid over the waterbody in the horizontal dimension and solving Eq. (5.4) locally within each grid cell. The interactions of one cell with its neighbors are included as

lateral boundary conditions on the grid cell. The grid size is constrained so that each of the terms in Eq. (5.4) varies smoothly across a grid cell and can be approximated with a simple, prescribable form, e.g., linearly, quadratically, etc.. This implies that a characteristic value of each term can be defined for every grid cell. For example, if a grid cell is small enough that ϕ is constant across the cell, the characteristic value of ϕ, (call it $\tilde{\phi}$), would be equal to that constant value. If a larger grid size was used, ϕ might vary approximately linearly across the cell and $\tilde{\phi}$ would be the linear average value. The same is true for each of the other terms in Eq. (5.4). Variations in ϕ, as well as the other terms, occur due to changes in the sediment properties, changes in the hydrodynamic forcing and changes in the general circulation pattern. The latter two phenomenon are related to physical features of the water body such as lateral geometry and depth and to the wind field.

Eq. (5.4) can be used in several ways, depending on the known quantities. If the horizontal velocities, diffusion/dispersion coefficients and ϕ are all known as functions of time in a given grid cell and the lateral boundary conditions for that cell can be specified, Eq. (5.4) describes the time variation of the depth-averaged concentration within the cell. By coupling all the cells in a water body together and solving Eq. (5.4) simultaneously in each cell, the general sediment transport within the water body is described. Alternatively, if the horizontal velocities, diffusion/dispersion coefficients, lateral boundary conditions and the depth-averaged suspended sediment concentration are all known as functions of time in a given cell, Eq. (5.4) can be used to solve for ϕ in that cell.

Unfortunately the use of Eq. (5.4) on a single cell basis has several problems among which is the need to specify the lateral boundary conditions on a grid cell. The alternative of coupling all of the cells together is also very difficult since every cell can have a different ϕ with different coefficients in Eq. (5.3), thereby presenting an insurmountable task without measurements of $\bar{c}$ in every grid cell. Clearly, if any headway is to be made, simplifications must be introduced into Eq. (5.4).

5.2 VALIDITY OF NEGLECTING HORIZONTAL TRANSPORT

The most useful simplification which can be made to Eq. (5.4) is to neglect the horizontal transport terms entirely. Not only does this eliminate the need to specify the horizontal velocities and diffusion/dispersion coefficients, it also eliminates the need to specify lateral boundary conditions on each grid cell and, therefore, uncouples the suspended sediment concentration in each. This simplification was routinely employed in analysing data from the rotating annular laboratory flumes described in Chapter 3. It has also been applied in the field, although without much justification of its validity.

In the present study, it is necessary to know whether and under what circumstances the horizontal transport terms can be dropped. Insight can be gained by estimating the sizes of the various terms in Eq. (5.4) in a typical grid cell. To do this, it is assumed that the advective transport terms are larger than the diffusive/dispersive terms and that the x-direction is oriented in the direction of the mean flow. Using these assumptions, Eq. (5.4) can be represented as:

$$\frac{\partial \bar{c}}{\partial t} \simeq \frac{\phi}{h} - \bar{u}\frac{\partial \bar{c}}{\partial x} \tag{5.5}$$

The size of the terms in Eq. (5.5) may be estimated as follows:

$$\frac{\partial \bar{c}}{\partial t} \sim \frac{\Delta C_\ell}{T_\ell}$$

$$\bar{u} \sim U_m$$

$$\frac{\partial \bar{c}}{\partial x} \sim \frac{\Delta C_s}{L}$$

where

ΔC_ℓ = the change in time of the local concentration as measured at a single point

ΔC_s = the spatial change in concentration measured across a grid cell

U_m = the mean, horizontal, depth-averaged velocity

T_ℓ = a time scale for local changes in concentration

L = characteristic grid cell dimension

To neglect the horizontal transport term, it is necessary that the transient term in Eq. (5.5) be approximately equal to ϕ/h or equivalently that the ratio of the horizontal transport term to the transient term be much less than unity.

$$\frac{\bar{u}\dfrac{\partial \bar{c}}{\partial x}}{\dfrac{\partial \bar{c}}{\partial t}} \sim \frac{\dfrac{U_m \Delta C_s}{L}}{\dfrac{\Delta C_\ell}{T_\ell}} \ll 1 \tag{5.6}$$

or

$$T_\ell \ll T_s \tag{5.7}$$

where

$$T_s \equiv \frac{\Delta C_\ell}{\Delta C_s} \cdot \frac{L}{U_m} \tag{5.8}$$

Writing Eq. (5.6) as Eq. (5.7) shows that it is possible to recast this ratio into a comparison of time scales with the result that, if the timescale for local concentration changes, T_ℓ, is much smaller than the timescale for horizontal transport, T_s, then the horizontal transport terms are justifiably neglected from Eq. (5.4). T_s can be determined from Eq. (5.8) by estimating each of the terms on the right hand side for a given grid cell.

The data presented in Chapter 2, as well as previous numerical circulation modeling by Shanahan (1981) and physical modeling by Györke (1978), suggest a representative value of $U_m \sim 5$ cm/s in Keszthely basin.

For lack of a better assumption the representative local and spatial concentration variations will be related with an expression of the form:

$$\Delta C_\ell \sim \alpha \Delta C_s$$

where α is an unknown coefficient.

During periods of significant resuspension, α will depend on spatial changes in the sediment properties and on the hydrodynamic forcing and therefore is dependent on the selection of the grid size, L. Figure 2.3 can be used to estimate the scale of changes in the sediment properties. In the area near the Keszthely field site, the sediment varies from silt to clayey silt, with the size of these regions ranging from 1-5 km. The distinction between clayey-silt and silt is relatively arbitrary and probably involves less than a factor of 2 change in the mean particle

diameter. Thus given a uniform hydrodynamic forcing and L ~ 1 km, it can be expected that $\Delta C_\ell > \Delta C_s$ or $\alpha > 1$.

The numerical and physical circulation models which have been made of Lake Balaton, as well as satellite photographs, suggest that the mean circulation in the Keszthely Basin is dominated by a large horizontal eddy, which scales with the lateral dimensions of the basin. Therefore, this places no further constraint on the cell size in comparison to that associated with the sediment properties.

The final consideration is the scale over which the hydrodynamic forcing varies. In Chapter 4 substantial evidence was presented suggesting the predominant hydrodynamic forcing is the bottom stress associated with surface waves. At large fetches and for gradual depth changes, e.g., winds aligned with the lake axis, the scale over which the wave field varies is much greater than that over which the sediment properties vary.

However, for winds oriented across the lake, the scale over which the wave field varies is much smaller. For example, during the major storm event captured at Keszthely, (hours 48-64, Figures 2.38 - 2.41), the wind blew from approximately N30°E, yielding a fetch length at the measurement site of about 2.4 km. As a result, the wave induced bottom stress varied from zero to a maximum of about 2.0 dynes/cm^2 over this distance, while the accompanying resuspension also increased from zero over this distance. This length scale is roughly the same as that imposed by changes in the sediment properties and across this distance $\Delta C_\ell \sim \Delta C_s$ or $\alpha \sim 1$.

During periods when settling predominates α will depend principally on horizontal changes in the particle sizes in suspension. Under these conditions an idea of the magnitude of α can be obtained from a comparison of the one-dimensional settling behaviors of two sediments, (call them

sediment a and sediment b), having settling velocities w_{sa} and w_{sb}. In this case

$$\frac{d\bar{c}}{dt} = \frac{\phi}{h} = -\frac{\beta}{h}\bar{c} = -\frac{w_s c_o}{h} \tag{5.9}$$

Assuming c_o is constant and a vertically well-mixed initial condition yields

$$(\bar{c} - c_o) = -\frac{w_s c_o}{h} t \tag{5.10}$$

Therefore

$$\frac{\Delta C_\ell}{c_o} \equiv \frac{\Delta C_a}{c_o} = -\frac{w_{sa}}{h}\Delta t \tag{5.11}$$

and

$$\frac{\Delta C_s}{c_o} \equiv \frac{|\bar{c}_a - \bar{c}_b|}{c_o} = \frac{|w_{sa} - w_{sb}|\,\Delta t}{h} \tag{5.12}$$

Using the definition of α and Eqs. (5.11) and (5.12) yields

$$\alpha = \frac{\Delta C_\ell}{\Delta C_s} = \frac{w_{sa}}{|w_{sa} - w_{sb}|} \tag{5.13}$$

Eq. (5.13) recasts α in terms of the settling velocities of the two sediments. As they become equal α becomes infinite and ΔC_s approaches zero.

An idea of the expected settling velocity can be obtained from Stokes law for spherical particles of equivalent diameter:

$$w_s = \frac{gd^2}{18\upsilon}(\gamma_s - 1) \tag{5.14}$$

which is valid for

$$\frac{w_s d}{\upsilon} < 0.1$$

In this case γ_s is the specific weight (≈ 2.5), υ is the kinematic viscosity (≈ 0.01 cm^2/s) and d is the particle diameter. Using Eq. (5.14) in Eq. (5.13) yields

$$\alpha = \frac{d_a^2}{|d_a^2 - d_b^2|} \tag{5.15}$$

As noted previously near the Keszthely field site the horizontal variation in particle size over L ~ 1 km is probably less than a factor of two yielding $\alpha > 1/3$.

The only direct evidence of the size of α is from Györke (1978) who measured transects of suspended sediment concentration from shipboard during several storms in Keszthely basin. Excluding the immmediate area around the mouth of the Zala River, he typically found that less than a factor of two variation in suspended sediment concentration occurred across the bay, suggesting that $\alpha >> 1$.

To summarize, the scales which have been deduced for use in Eq. (5.8)

$U_m \sim 5$cm/s

L ~ 1 km

$\Delta C_\ell \sim \alpha \Delta C_s$

Together they yield

$$T_s = 5.6\ \alpha \text{ hours} \tag{5.16}$$

where

$\alpha \sim 1$ transverse winds

$\alpha > 1$ longitudinal winds

$\alpha > 1/3$ settling

$\alpha >> 1$ ship transects

Recalling the significance of T_s, if substantial changes in the local, depth-averaged concentration occur over times which are short compared to T_s, the horizontal transport terms can be neglected and (Eq. 5.4) can be simplified to

$$\frac{d\bar{c}}{dt} = \frac{\phi}{h} \tag{5.17}$$

Eq. (5.3) is then easily substituted into Eq. (5.17) and the following equation obtained.

$$\frac{d\bar{c}}{dt} = -\frac{\beta}{h}(\bar{c} - \bar{c}_{bak}) + \frac{\beta K}{h}(\tau_b - \tau_c)^n \tag{5.18}$$

The ultimate use of Eq. (5.18) as well as the justification of its validity depends upon measurements of the depth-averaged suspended sediment concentration which are determined by integrating vertical profiles of concentration measurements. For this purpose, a profiling instrument such as the ABSS described in Section 2.2.5 is quite useful as it represents a

single instrument capable of unobtrusively making the required measurements. Unfortunately, this instrument provided no useful data during the course of this study. Therefore, the only available concentration measurements were those made by grab samples at mid depth. Previous work by Györke (1978) in Keszthely basin and by Somlyody (1980) in the middle of the lake near Szemes and measurements made in Tihany as a part of this study (Figure 2.33) suggest that the suspended sediment concentration is reasonably uniform over the vertical. The physical reasons for this are the small particle sizes (and therefore low settling velocities) and the lake's shallowness, which allows the turbulence to be relatively uniform over the depth. Therefore, it is reasonable to expect that the mid-depth concentration measurements are representative of the depth-averaged values.

Assuming this to be true, the concentration time histories measured at the Keszthely field site and presented in Figures (2.41) and (2.42) can be used to qualify the neglect of the horizontal transport terms in Eq. (5.4) based on the criteria that

$$T_\ell \ll T_s \sim 5.6\alpha \text{ hours} \tag{5.19}$$

Considering first the large transverse storm shown toward the end of Figure 2.41, significant increases in concentration attributable to resuspension occur over time scales on the order of 0.5 hours suggesting Eq. (5.16) is satisfied. ($\alpha \sim 1$ is expected.) Similarly the initial increase in concentration associated with the other substantial transverse storm shown at the beginning of Figure 2.42 also occurred over time scales of the order of an hour or less.

The decline in concentration associated with settling in both of these events occurred much more gradually and extended over periods of 10 - 20 hours. Therefore it would appear that horizontal transport might have affected the observed sediment response during these intervals.

Two other wind events occurred during the time frame covered in Figure 2.41, both of which consisted of winds aligned with the lake axis. While the change in suspended sediment concentration produced by these winds was much smaller than the previous cases, the time scale over which this increase took place seemed to be slightly longer, i.e., in the 2-4 hour range. However, since winds aligned with the lake should give values of $\alpha > 1$, it is probably reasonable to neglect horizontal transport during these events as well.

Figures 2.42 and 2.43 show that several other wind events appear to have initiated lesser changes in the suspended sediment concentration. Unfortunately, the 2 hour sampling interval together with the difficulty in separating some of the concentration changes from random scatter in the data makes it difficult to conclude whether or not horizontal transport was important. In general, however, it appears that it should be consistent to neglect this effect in light of other simplifying assumptions which have been made, e.g., $\bar{c} \approx c_o$.

5.3 ZERO DIMENSIONAL MODEL

For constant values of β, K, n, τ_c and τ_b. Eq. (5.18) is easily solved analytically to yield

$$(\bar{c}-\bar{c}_{bak}) = (\bar{c}_i-\bar{c}_{bak})\exp\left[\frac{-\beta}{h}(t-t_i)\right] + K(\tau_b - \tau_c)^n \left[1-\exp\left[\frac{-\beta}{h}(t-t_i)\right]\right] \tag{5.20}$$

where the initial condition $\bar{c} = \bar{c}_i$ at time $t = t_i$ has been applied.

An approximate method of including the effect of a changing bottom stress, τ_b is to assume that τ_b changes in steps, i.e., it is constant for a specified interval and then changes instantaneously to another value. Eq. (5.20) can then be applied sequentially over each constant stress interval by setting $\bar{c}_i$ and t_i equal to the concentration and time at the end of the previous interval.

For reasons discussed in Chapter 4, the maximum bottom stress due to the waves will be used for τ_b. This can be computed using Eqs. (4.1) - (4.3) which are repeated below.

$$\tau_b = \frac{f_w}{2} \rho U_b^2 \tag{4.1}$$

$$RE_w = \frac{U_b A_b}{\upsilon} \tag{4.2}$$

$$A_b = U_b/\omega \tag{4.3a}$$

$$U_b = \frac{a\omega}{\sinh kh} \tag{4.3b}$$

The friction factor, f_w, is obtained either from Figure 4.1 or, for the case of a laminar wave boundary layer, which in the absence of bedforms can reasonably be expected to exist at the measurement sites, can be determined directly from the expression

$$\left(\frac{f_w}{2}\right)^2 = \frac{1}{RE_w} \tag{5.21}$$

combining these equations leads to

$$\tau_b = H_s \cdot \left[\rho \frac{\sqrt{\upsilon\omega^3}}{2 \sinh kh}\right] \tag{5.22}$$

where H_s is the significant wave height when ω and k are defined in terms of the "velocity equivalent" period as discussed in Chapter 4. The data presented in Chapter 4 showed that the velocity equivalent period was nearly constant during all of the measured wind events and was approximately equal to 1.9s. The model accurately matched this period only during intervals of substained wind. As a result, it was concluded that the model should be used to predict the period only during the major part of a storm, and this value should be adopted as constant throughout the entire storm event. On the other hand, the significant wave height varied substantially during the measurement period and was reproduced quite well by the model.

Eq. (5.22) shows that for a constant period (or frequency) and a laminar wave boundary layer the bottom stress is linearly proportional to the wave height. In this case Eqs. (5.18) and (5.20) can be written as

$$\frac{d\bar{c}}{dt} = \frac{-\beta}{h}(\bar{c} - \bar{c}_{bak}) + \frac{\beta\theta}{h}(H_s - H_c)^n \tag{5.23}$$

$$(\bar{c}-\bar{c}_{bak}) = (\bar{c}_i-\bar{c}_{bak})\exp\left[\frac{-\beta}{h}(t - t_i)\right] + \theta(H_s - H_c)^n \left[1-\exp\left(\frac{-\beta}{h}(t- t_i)\right)\right] \tag{5.24}$$

where

$$\theta = K \left(\rho \frac{\sqrt{\nu\omega^3}}{2 \sinh kh}\right)^n \qquad (5.25)$$

Therefore, under the conditions encountered at the Keszthely field site, (and at the Tihany field site), Eqs. (5.23) and (5.24) should be approximately as valid as Eqs. (5.18) and (5.20). However, it must be stressed that under more severe conditions in which the wave boundary layer turns turbulent it would be necessary to use Eq. (5.18) and (5.20).

5.4 CALIBRATION

To use either Eq. (5.20) or (5.24), five unknown parameters must be specified. It is possible to calibrate these parameters by minimizing the difference between the predicted concentrations and the observed data

It was decided that the period during which both suspended sediment and hydrodynamic measurements were made would be used for parameter calibration. An examination of Figure 2.41 indicates that during the initial two events, substantial scatter exists in the concentration measurements in relation to their absolute magnitudes. This is particularly true during the earlier event which is represented only by 2 or 3 data points. Measurements during the second event were not taken from the large research vessel which was typically anchored at the field site. Rather during this period the research boat was being used for other purposes in a different part of the lake and measurements were made from a row boat which was tied to a limnocorral that was deployed at the field site. Unfortunately, it is unknown whether these concentration measurements were influenced by the disturbed flow around the limnocorral.

Due to these data uncertainties the actual model calibration was performed using only the suspended sediment and hydrodynamic forcing data obtained during the large transverse storm.

Due to the poor dynamic performance of the wave period model the calibrations and verifications were done using Eq. (5.24), which explicitly includes only the changes in wave height. As stated above, minimal difference is expected in comparison with Eq. (5.20). If a situation arises in which substantial variations in the period can be demonstrated to occur or the wave boundary layer becomes turbulent, Eq. (5.25) can be solved for K whose value can be determined using the calibration obtained below for θ and n together with a period of about 1.9s. The suspended sediment concentration can then be modeled using Eq. (5.20).

Of the five parameters which could be calibrated, β, $\bar{c}_{bak}$, θ, H_c and n, some a priori knowledge exists for $\bar{c}_{bak}$ and β. As discussed above $\bar{c}_{bak}$ was determined from an inspection of the concentration data and held constant at 15 mg/ℓ during the calibration of the other parameters. β depends on the settling velocity and the ratio of $\bar{c}/c_o$. The former can be estimated from Eq. (5.14) knowing the particle size range. Sediment samples taken from the Keszthely field site were analysed for particle size distribution, and the results are shown in Figure 5.1. They indicate particles predominantly in the silt to clay size ranges and agree quite well with the results presented in Figure 2.3. Specifically, 61 per cent of the data falls in the range of 8 - 18 μ and yields settling velocities from 0.0052 - 0.026 cm/s. In a completely well-mixed water column, $\bar{c}/c_o$ is

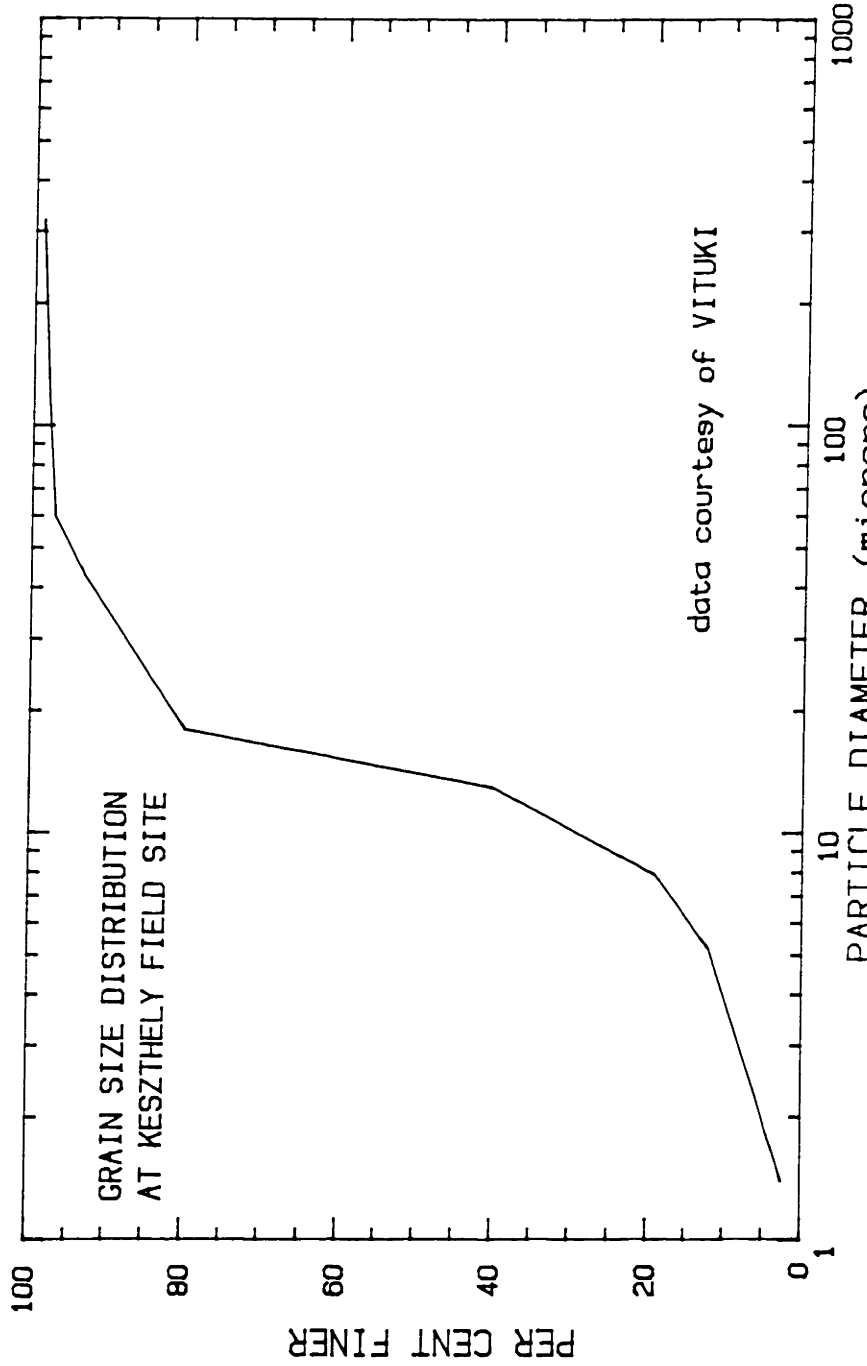

Figure 5.1 Particle size distribution of sediment from Keszthely field site.

equal to unity, although in reality, it is probably somewhat larger. Therefore a value of β near the upper end or a little above the range of settling velocities can be expected.

Calibrations for the four parameters, β, θ, H_c, and n, which were allowed to vary in Eq. (5.24) were initially attempted using a Global Optimization Procedure as applied by Somlyody (1986). However, this was found to give widly varying "optimum" parameter values depending on the initial range specified for each. Therefore this method was abandoned in favor of a systematic brute force procedure. Initially, broad ranges were specified for all of the parameters. The value of each was then varied sequentially within its range using a specified increment size. The total mean square deviation between the model and the data was recorded for each parameter set. The sets were then ranked from top to bottom in order of ascending mean square error, (MSE). While this procedure was not elegant, it was easily computerized, and the time required to make a detailed parameter search remained workable due to the reasonably small number of points comprising the calibration data set.

The result of this effort was one parameter set which gave the lowest MSE along with a large number of other sets which gave almost as low an error. This is summarized in Table 5.1 for a range of MSE up to 30 per cent above the lowest value. It might be tempting to select the parameter set giving the lowest MSE as "best"; however, to do this implies there is no error in the measured wave heights or suspended sediment concentrations and that the model is exactly correct. It is easily possible that a different paramter set, (and judging from Table 5.1, perhaps a

TABLE 5.1
Parameter Calibration Results

Mean square error	2559.2 -	3327	$(mg/\ell)^2$	* 30%*
c_{bak} =		15.0	mg/ℓ	
H_c =	0.0 -	16.75	cm	
β =	0.015 -	0.031	cm/s	
n =	0.15 -	3.95		
θ =	0.00086 -	124.6		

*Variation from lowest mean square error

Note: specific parameter combinations within in the above listed ranges yield mean square errors between 2559.2 and 3327.

significantly different set), would yield the "best" calibration if all of the measurement errors could be removed.

Assuming that $\beta \approx w_s$, the range of β values in Table 5.1 corresponds to equivalent particle diameters of 14μ to 19μ. These are in excellent agreement with the measured size distribution, thereby lending confidence, although no further definitiveness, to the calibration.

Assuming an average wave period of 1.9s and a water depth of 2m, Eq. (5.22) can be used to recast the range of critical wave heights in Table 5.1 into critical stresses of 0 - 1.4 dynes/cm^2. These values are in reasonable agreement with the critical bottom stresses observed in the steady flow laboratory experiments presented in Chapter 3. It is

unfortunate at this point that the ABSS described in Chapter 2 failed to provide useful results. Had it worked direct measurements of H_c might have been possible and a much narrower range of acceptable values for H_c could have been specified.

Figure 5.2 shows the concentration data used for the calibration along with the model output for the parameter set giving the lowest MSE and sets giving 10 and 30 per cent higher MSE. It is difficult, based on a visual inspection, to favor one parameter set over the others.

Figure 5.3 shows curves of the minimum MSE as a function of each of the parameters subject to calibration in the model. (A 45 per cent range in MSE is included in this figure.) In each curve a "flat" region exists in which a change in the parameter value produces minimal change in the MSE. For the parameters β, n, and θ the "flat" region is eventually bounded above and below by regions in which the MSE increases monotonically. H_c behaves similarly at its upper limit, although the "flat" region is physically bounded by the value of $H_c = 0$ at the lower end.

The 30 per cent range in MSE used in Table 5.1 is sufficient to completely define the "flat" regions, while the broader limits included in Figure 5.3 illustrate that the MSE grows rapidly outside of the 30 per cent range with small changes in each parameter value. Therefore this was used in the analyses described below.

The wide ranges of acceptable parameter values listed in Table 5.1 and Figure 5.3 indicate that either the model is insensitive to variations in one or more or the parameters or that too many degrees of freedom exist in the model. In the former case it may be reasonable to select an average

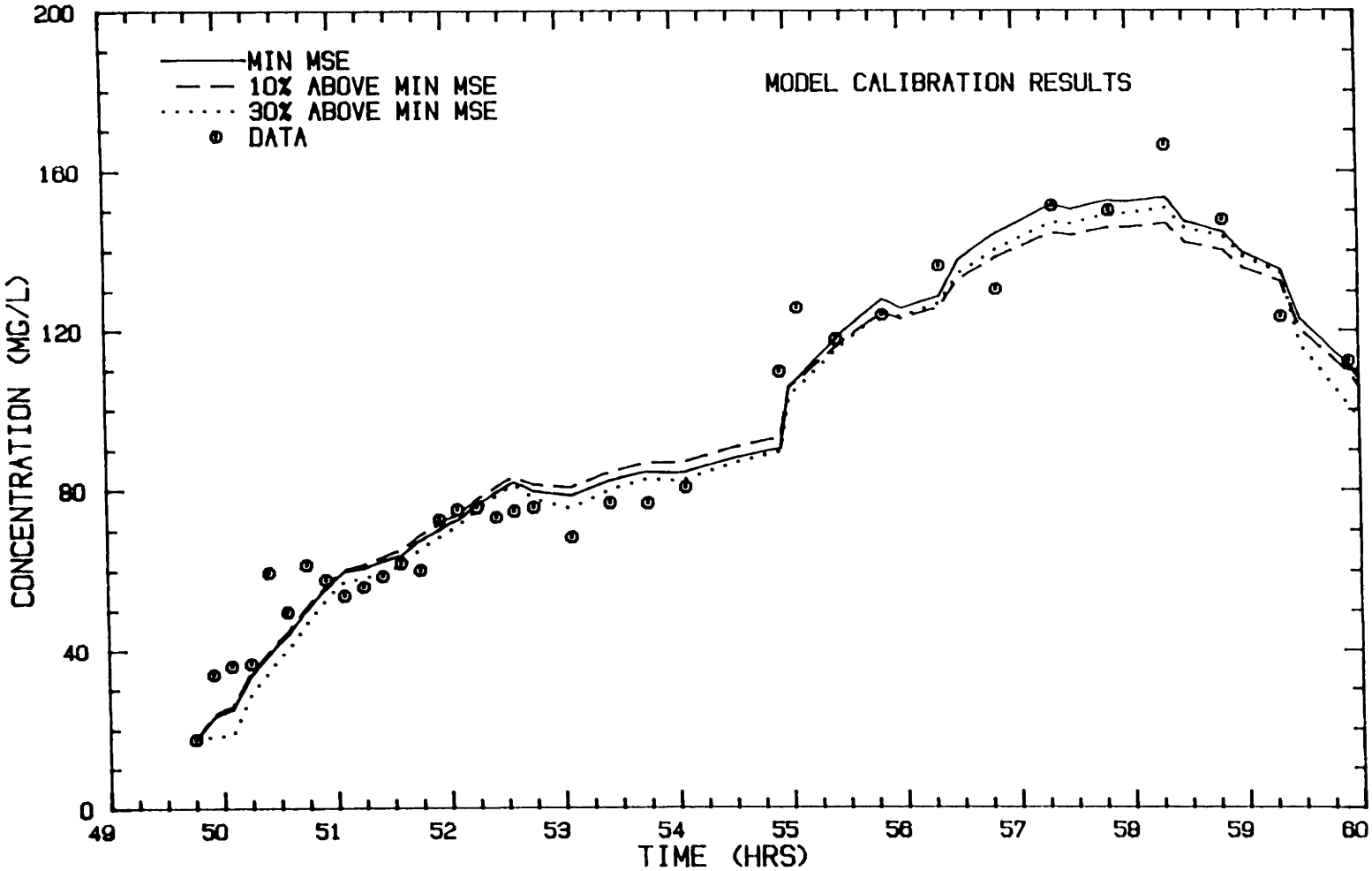

Figure 5.2 Comparison between the model calibration and field data for three parameter sets.

——— n = 3; θ = 0.0154; β = 0.022cm/s; H_c = 0 cm; MSE = 2559.2;

- - - n = 1.75; θ = 1.186; β = 0.022cm/s; H_c = 5.92 cm; MSE = 2815;

• • • n = 0.88; θ = 24.04; β = 0.022cm/s; H_c = 13.4 cm; MSE = 3327.

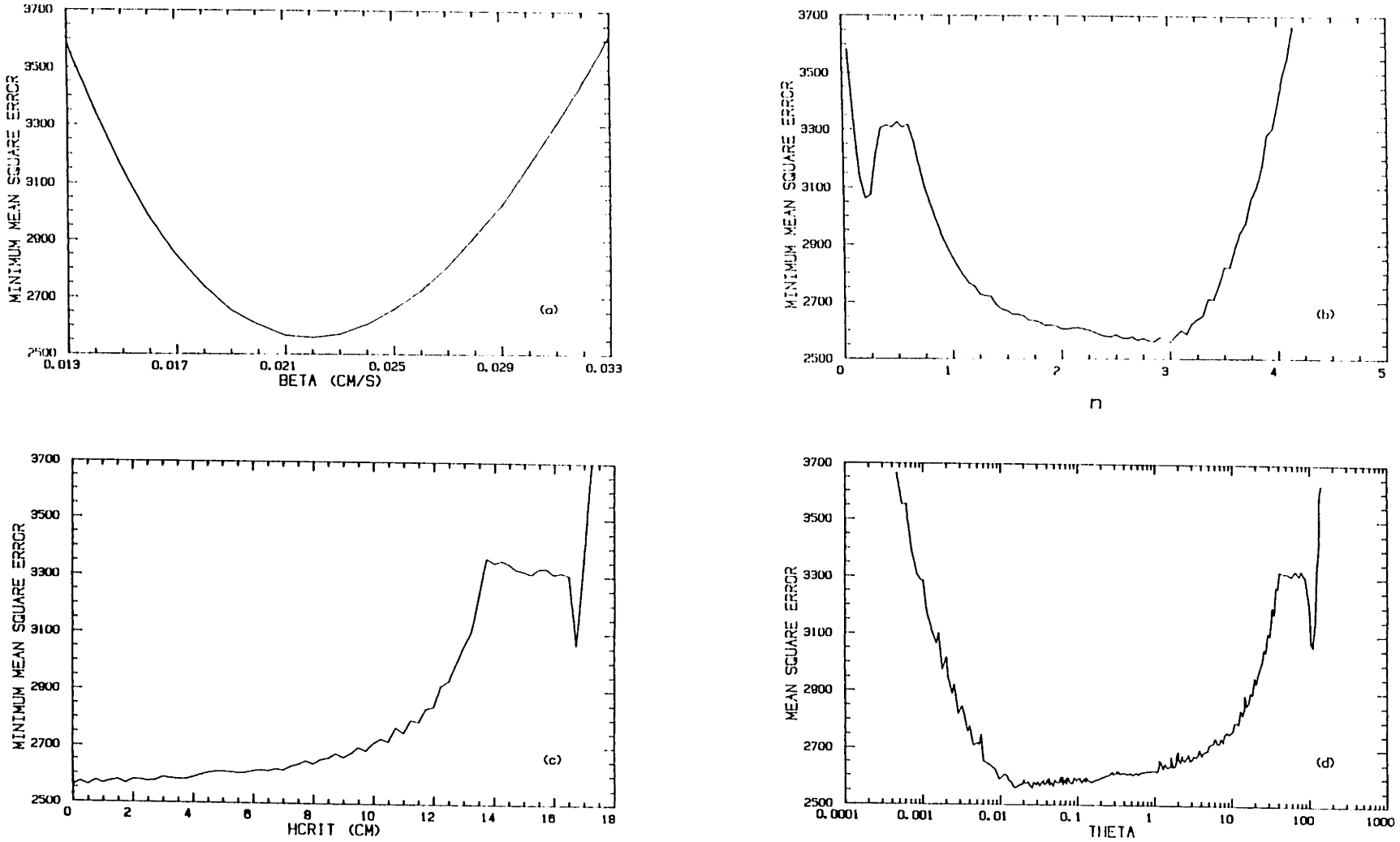

Figure 5.3 **Minimum MSE as a function of each calibrated parameter when all are allowed to vary independently.**

value from the parameter range as a reasonable calibration, particularly if it can be justified on physical grounds. In the latter case variations in two or more parameters are coupled in a way that results in an unchanged model behavior for different parameter sets. This suggests that the model should be simplified either by eliminating parameters based on physical or intuitive knowledge or by determining the coupling between parameters, thereby allowing the expression of one or more in terms of the others. To explore these possibilities, a search was made for correlations between the parameter values within each parameter set falling within the 30 per cent MSE limit presented in Table 5.1. Trials with 10 and 20 per cent MSE limits yielded nearly identical results. In this analysis each parameter set was assumed to be equally valid and therefore given an equal weighting.

Figure 5.4 illustrates the variation of β as a function of the other three calibratable parameters. It is evident that β is independent of each, and therefore that the model is relatively insensitive to β variations. As mentioned above the particle sizes corresponding to these values of β coincide very well with the measured values and actually the range is quite small considering the range in the measured size distribution. Therefore an average was taken over all of the parameter sets and used as the "calibrated value". This resulted in $\beta = 0.022$ cm/s.

Figure 5.5 indicates the relationship between the exponent, n, and the two remaining parameters. Figure 5.5a shows a striking correlation between n and θ, while Figure 5.5b shows a significant but much less defined correlation between n and H_c. The form of the correlation in Figure 5.5a can be explained by recalling the expression for E_2, i.e.,

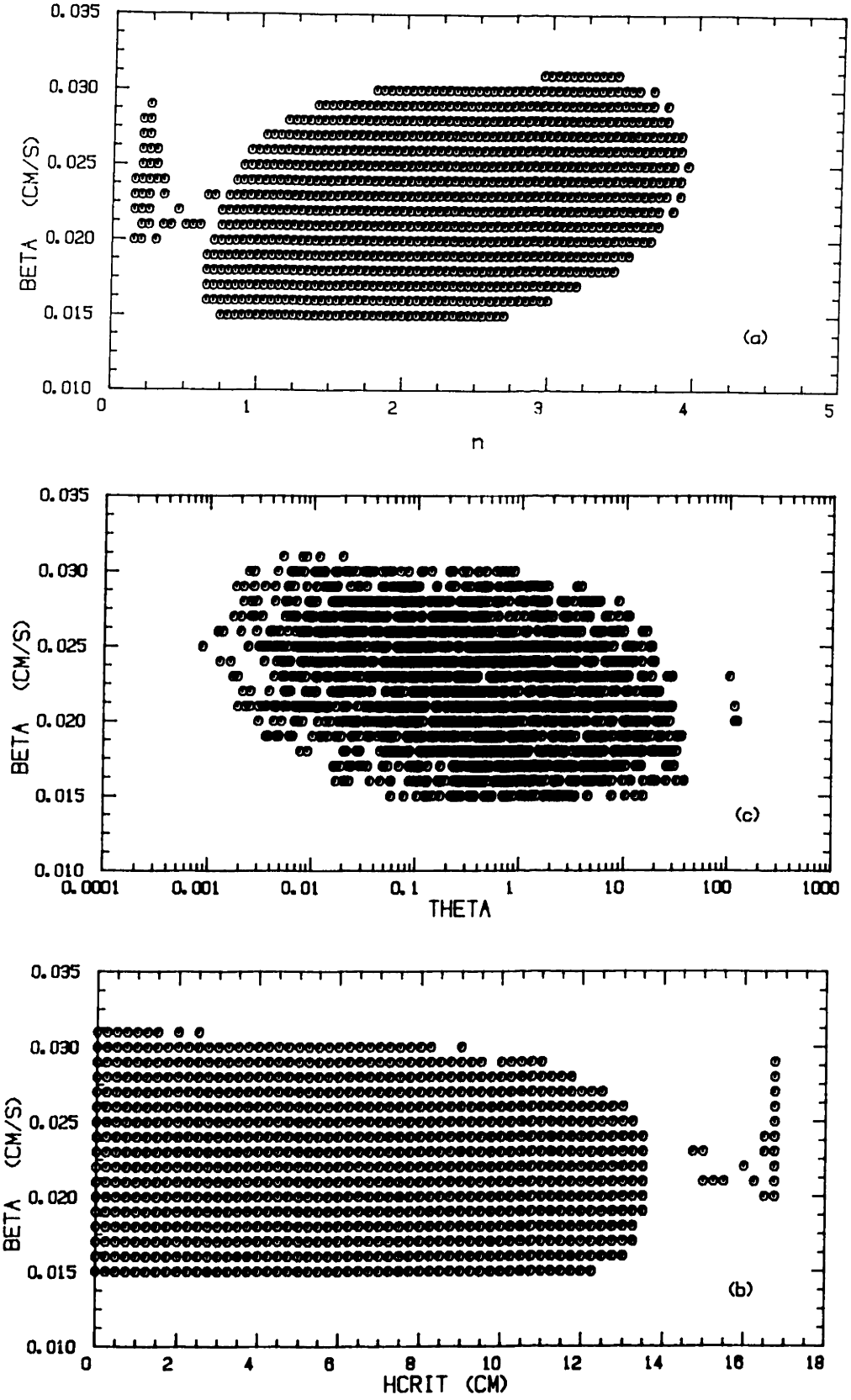

Figure 5.4 Variation of β as a function of the other three calibrated parameters for parameter sets with MSE less than 3327 when all parameters are varied independently.

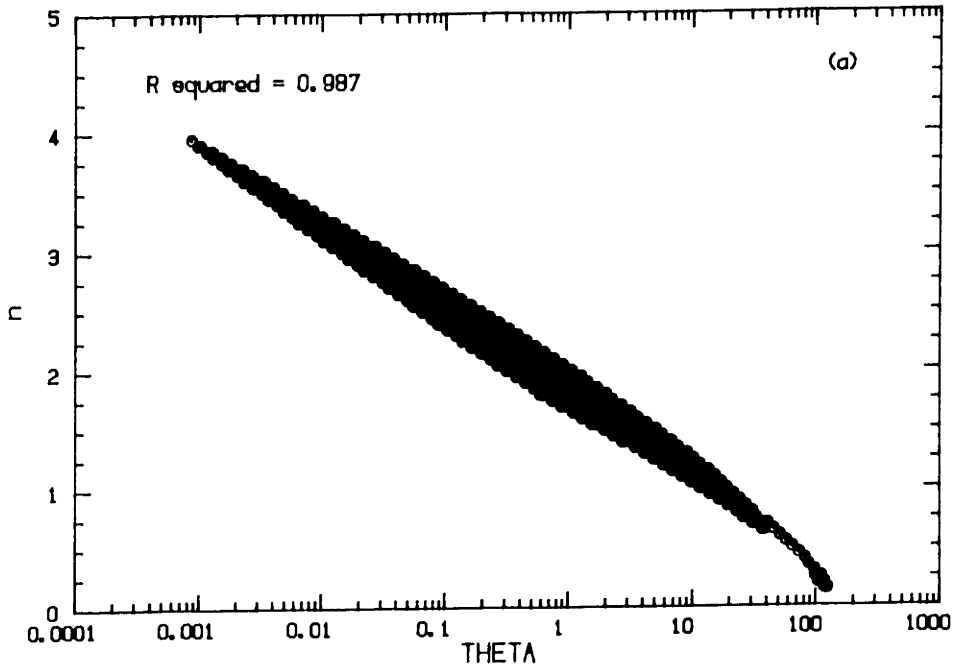

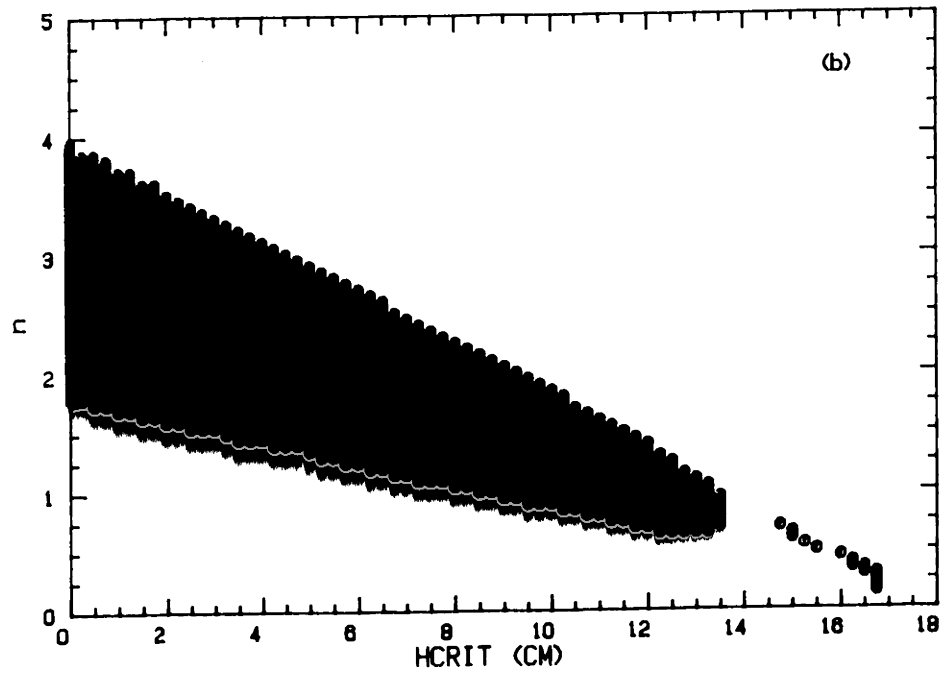

Figure 5.5 Correlation between, (a) n and θ, and (b) n and H_c, for parameter sets with MSE less than 3327 when all parameters are varied independently.

$$E_2 = \beta\, c_{ss} \tag{5.26}$$

For a constant β, E_2 is entirely dependent on C_{ss} which was expressed as

$$c_{ss} = K(\tau_b - \tau_c)^n = \theta(H_s - H_c)^n \tag{5.27}$$

Eq. (5.27) is easily rearranged to

$$n = - \frac{\log \theta}{\log(H_s - H_c)} + \frac{\log c_{ss}}{\log(H_s - H_c)} \tag{5.28}$$

Eq. (5.28) will yield a linear plot of n vs log θ for constant values of $H_s - H_c$ and c_{ss}. Figure 5.5a demonstrates that a plot of n vs log θ from the calibration parameter sets is quite linear. Using the slope and intercept of this curve gives

$$H_s - H_c = 31 \text{ cm}$$
$$c_{ss} = 500 \text{ mg}/\ell$$

Therefore, the linear correlation in Figure 5.5a indicates that a common feature of acceptable model parameter sets is that they give a value of $c_{ss} = 500$ mg/ℓ for a forcing of $H_s - H_c = 31$ cm. In actuality the scatter around the linear regression through the points in Figure 5.5a indicates that not every parameter set must give exactly these values. Rather, the model is relatively insensitive to small deviations from this common criterion. In the spirit of averaging over parameter values which do not cause appreciable changes in the model behavior, the regression relationship

$$n = -0.67 \log \theta + 1.8 \tag{5.29}$$

can be taken to represent the average coupling between n and θ.

It is not obvious what form the coupling between n and H_c has in Figure 5.5b, since the scatter due to model insensitivity obscures any functional relationship. Insertion of Eq. (5.29) into Eq. (5.27) yields

$$c_{ss} = 500 \left(\frac{H_s - H_c}{31}\right)^n \tag{5.30}$$

Therefore as long as $H_s - H_c < 31$ cm, (which is always the case in the Keszthely data), a decrease in H_c must be balanced by an increase in n to yield a constant c_{ss}. This is the trend shown in Figure 5.5b. Unfortunately the specific form of this variation is dependent on c_{ss} and H_s. In an effort to eliminate some of the scatter in Figure 5.5b the model was recalibrated using $\beta = 0.022$ cm/s and Eq. (5.29). This time a plot of values of n vs H_c from the same MSE range gave the results shown in Figure 5.6. A careful look at Figure 5.6a indicates that it coincides very closely with an average of the data in Figure 5.5b.

Figure 5.6b shows the same data but in a semi-log format which yields a highly linear regression. The resulting equation

$$\log n = -0.040 H_c + 0.48 \tag{5.31}$$

will be used to express the coupling between these parameters. As mentioned above the form of this equation has little physical significance due to its dependence on c_{ss} and H_s.

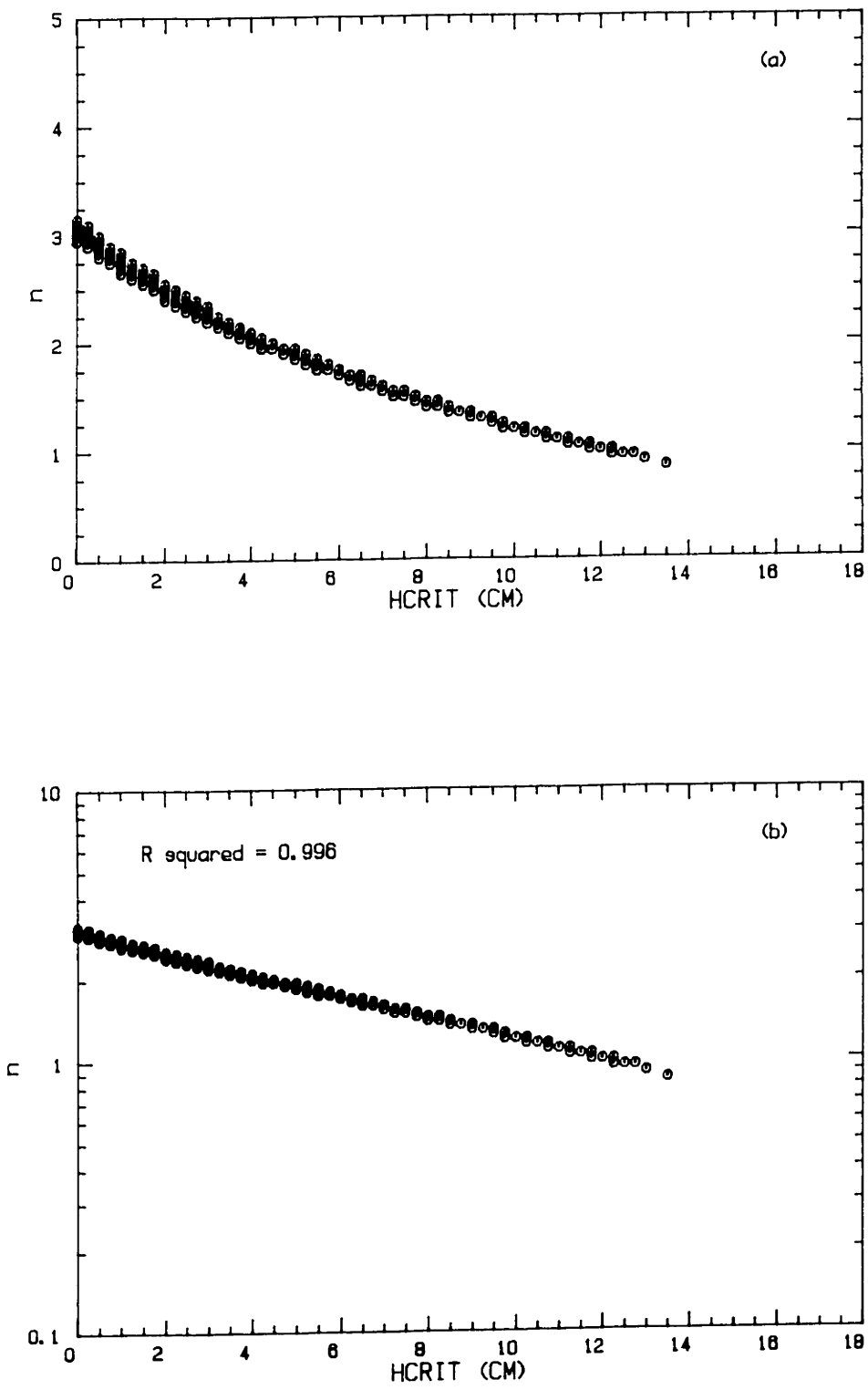

Figure 5.6 Correlation between n and H_c for parameter sets with MSE less than 3327 when β = 0.022 cm/s and n = 0.67log θ + 1.8 using an (a) arithmetic plot and (b) semilog plot.

To summarize, correlations between parameter values in each parameter set found to give a MSE within 30 per cent of the lowest MSE suggested that β was independent of other model parameters, while the parameters in the expresson for c_{ss} were closely coupled. Average values for each are β = 0.022 cm/s, n and θ Eq. (5.29), and n and H_c Eq. (5.31). Including all of these into the original model, Eq. (5.23), gives

$$\frac{d\bar{c}}{dt} = -\frac{0.022}{h}(\bar{c} - 15) + \frac{11.}{h}\left[\frac{H_s - H_c}{31.}\right]^{3x10^{-0.04H_c}} \qquad (5.32)$$

where H_c is in cm.

Eq. (5.32) indicates that only one free parameter remains, which in this case was chosen to be H_c. Unfortunately, based on the data available for calibration, it is not possible to select a single value of H_c. Rather, the model is well calibrated for a range of values as shown in Table 5.2.

5.5 VERIFICATION

In spite of the inability to determine a single calibrated value for H_c, it is useful to attempt to verify at least the model structure and the range of allowable H_c values using any additional data which is available. This was initially attempted using the entire 60 hours during which hydrodynamic and concentration data were collected. Results are shown in Figure 5.7 for three different critical wave heights. For the reasons

TABLE 5.2
Summary of Results for Varying H_c from Model Calibration Run

H_c (cm)	c_{bak} (mg/ℓ)	β (cm/s)	n, Eq. (5.31)	θ, Eq. (5.29)	MSE $(mg/\ell)^2$
0.0	15	0.022	3.02	0.01479	2650
1.0	15	0.022	2.75	0.03704	2563
2.0	15	0.022	2.51	0.08554	2621
3.0	15	0.022	2.29	0.1835	2704
4.0	15	0.022	2.09	0.3682	2767
5.0	15	0.022	1.90	0.6947	2802
6.0	15	0.022	1.74	1.240	2816
7.0	15	0.022	1.59	2.102	2823
8.0	15	0.022	1.45	3.403	2831
9.0	15	0.022	1.32	5.280	2841
10.0	15	0.022	1.20	7.881	2849
11.0	15	0.022	1.10	11.36	2851
12.0	15	0.022	1.00	15.85	2888
13.0	15	0.022	0.91	21.48	3113
14.0	15	0.022	0.83	28.34	3756*
15.0	15	0.022	0.76	36.49	4904*
16.0	15	0.022	0.69	45.95	8183*
17.0	15	0.022	0.63	56.70	18271*

*MSE error greater than 30% range in Table 5.1

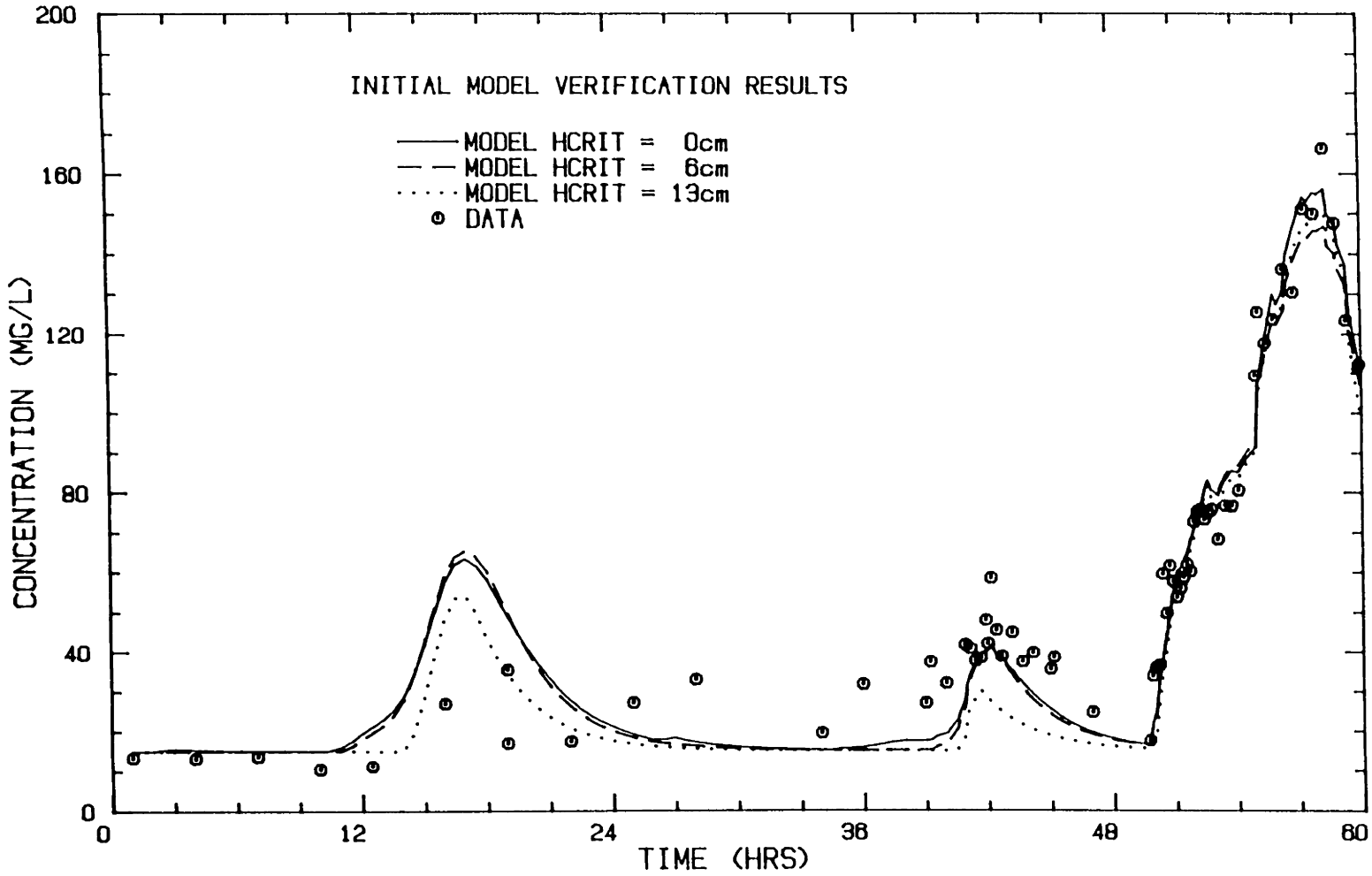

Figure 5.7 Initial verification attempt using 60 hours of measured wave heights and suspended sediment concentrations.

discussed previously it is difficult to know whether deviations between the model and the data reflect the model or poor data. In particular it appears that the peak concentration during the event at 16 hours was missed due to infrequent sampling. During the event at 40 hours the data is higher than the model predicts which is consistent with enhanced resuspension caused by flow disturbance around the limnocorral. H_c does have an effect on the model behavior during the initial two events, although it is unreasonable to fix H_c based on these results.

A larger data set available for model verification covers the entire 15 day period that concentration measurements were made in Keszthely. However, the only forcing data available are the wind measurements made at the Keszthely meteorological station. Therefore they will be used with the model developed in Chapter 4 to hindcast significant wave heights. The modeled wave heights will then be used to drive the suspended sediment model.

The wind data was recorded on a strip chart which was read and digitized by hand for use in the wave model. Differences in the measurement equipment, the type of measurement, (i.e., the meteorological station measured a scalar average windspeed while the data measured in the field study described in Chapter 2 was a vector average), the averaging period, the measurement site (particularly over land vs. over water) and the measurement elevation all tend to cause the meteorological station data to vary from that measured 2 m above the water surface as was done in the data collection portion of this study. It has been shown that the wave hindcasting model presented in Chapter 4 reproduces observed wave heights extremely well at the Keszthely field site, using the 10m windspeed as

determined from the 2m overwater values presented in Chapter 2. Therefore, it is useful to compare the 2m measurements with the data from the meteorological station during periods of overlap and correct the latter for any systematic deviations before using it with the wave model. The 60 hours of data presented in Figure 2.38 will be used for this purpose. Figure 5.8a shows a plot of the difference between the 2m windspeeds presented in Chapter 2, (hereafter called 2m windspeed) and the meteorological station windspeeds (hereafter called the MS windspeed) as a function of time. The MS data was averaged from the strip chart over 30 minute intervals while the 2m data was either interpolated or averaged to determine 30 minute average values for the corresponding times.

Between about 12 and 20 hours, the wind blows from the east, along the lake axis, and the MS windspeed is below the 2m windspeed. However, a wind of similar strength and direction was also present between hours 35 and 43 and during this period the difference between the two measurements is randomly scattered around zero. The large transverse event began at about 50 hours and during this period, the MS windspeed averaged about 0.5 m/s above the 2m windspeed. This suggests the former might be adjusted down slightly to better match the 2m windspeed.

Figure 5.8b shows the difference between the 30 minute averaged MS and 2m wind directions. As before the only systematic difference appears during the transverse event.

To account for the observed deviations during northerly winds, a "triangular shaped" adjustment was made to the MS wind data. A 40 degree clockwise shift and 0.50 m/s decrease were made to the MS wind measurements

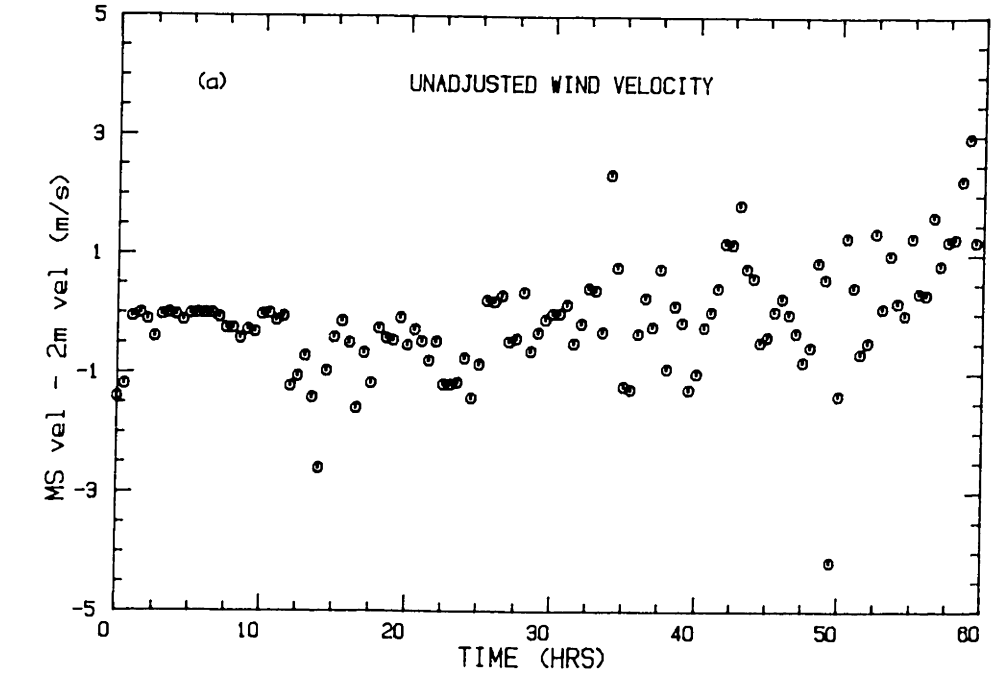

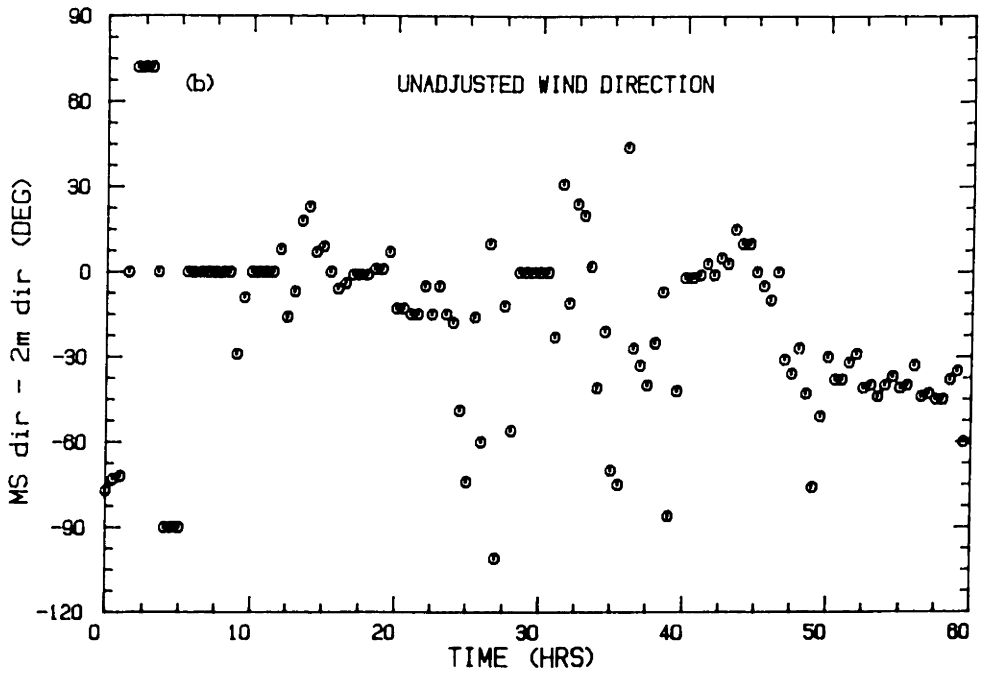

Figure 5.8 Difference between the 2m wind data and the unadjusted MS wind data. (a) wind speed (b) wind direction.

equal to N10^{o}W, while an adjustment which decreased linearly to zero over 60 degrees on either side of N10^{o}W was applied to wind measurements in this range. The results of this correction are shown in Figure 5.9 for the 60 hours of data. For both the wind speed and direction the correction yields a mean difference which is approximately zero, with random scatter on either side. Much of this scatter occurred during periods of relatively low wind speed and therefore is not particularly important. It can be attributed at least in part to an apparently higher threshold velocity of the meterological station instrument.

Figure 5.10 shows the hindcast wave heights using both the 2m wind data and the adjusted MS data. The only periods of noticeable difference are during the initial longitudinal storm and the first one-third of the large transverse event. In both cases the MS wind data underpredicts the observed wave heights and the hindcast from the 2m data. In spite of these deviations the overall agreement is quite good.

Figure 5.11 illustrates the hindcast of significant wave height and period using the adjusted MS wind data for the entire 15 data period. The two large transverse events are evident in Figure 5.11 between hours 24 - 48 and 280 - 300. Interestingly several smaller events yield wave heights only a little bit less than the transverse events, (e.g. 204 and 228 hours), even though the wind speed is significantly less (Fig. 2.43a). Figure 2.43b shows that from about 132 - 280 hours the wind was usually oriented along the lake axis from the east, thereby exposing the measurement site to the maximum fetch and resulting in larger waves.

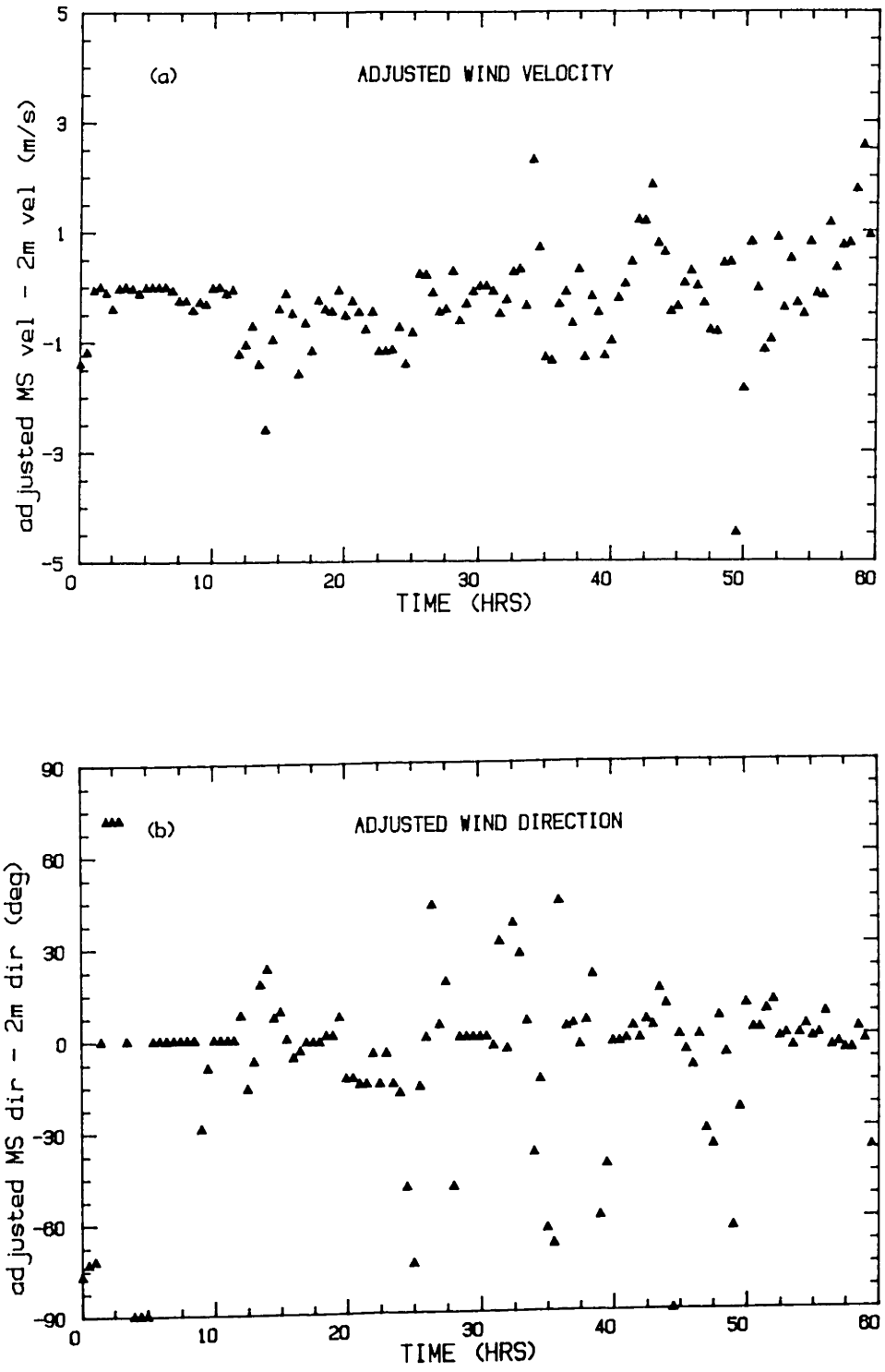

Figure 5.9 Difference between the 2m wind data and the adjusted MS wind data. (a) wind speed (b) wind direction.

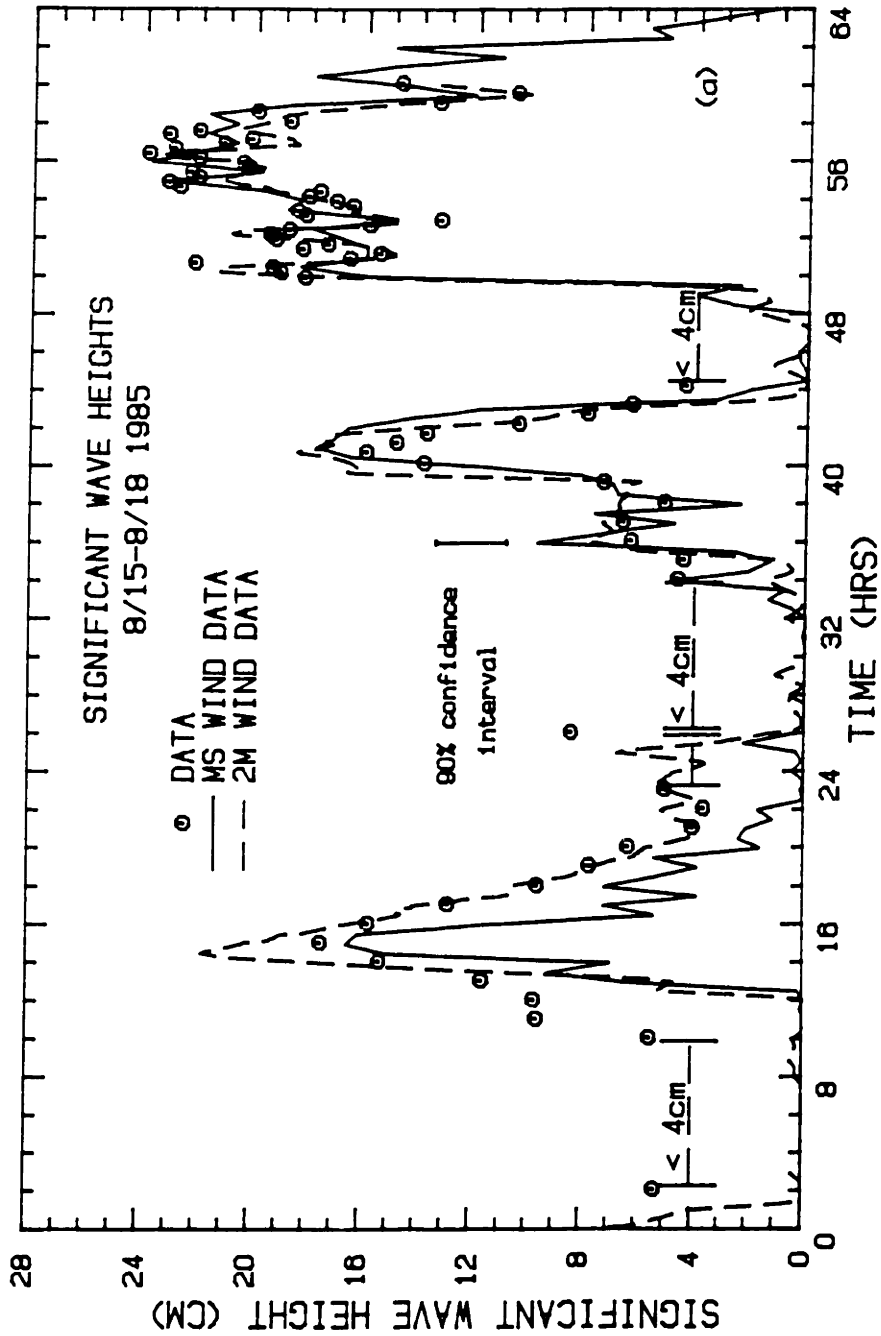

Figure 5.10 Companison between measured significant wave heights and modeled wave heights using the CERC 1977 model with 2m and adjusted MS wind data.

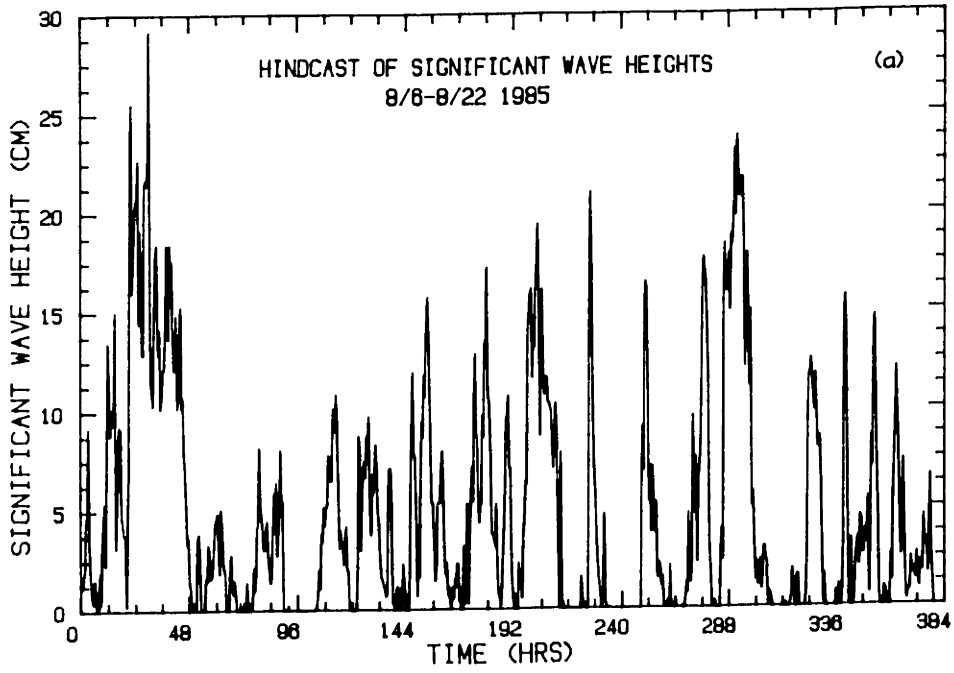

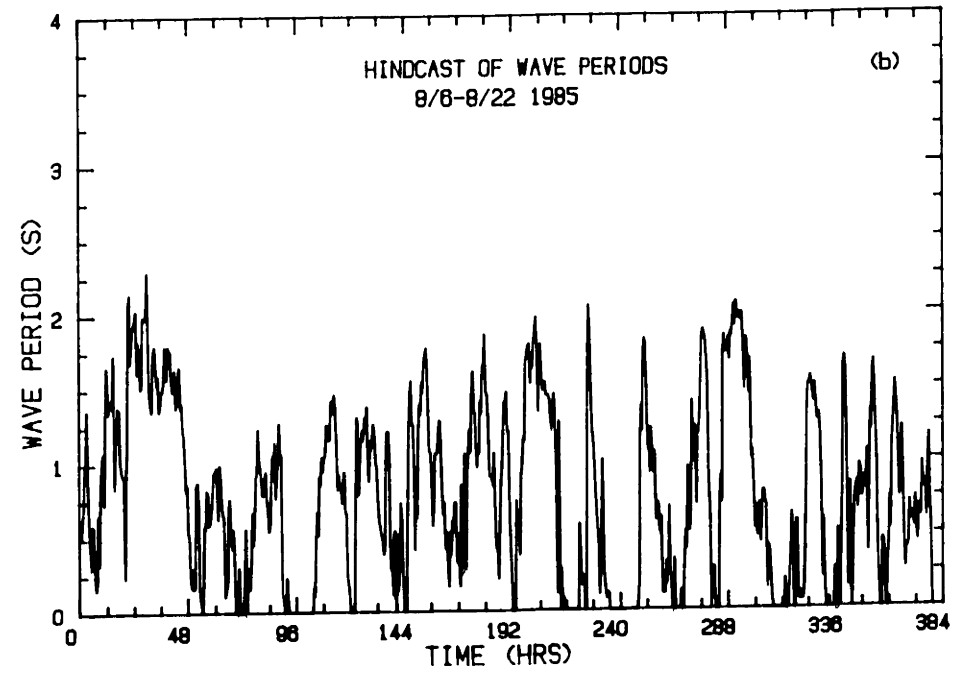

Figure 5.11 Hindcast of significant wave height and wave period for fifteen days using the adjusted MS wind data and the CERC 1977 model with B = 1.4, Eq. (4.12).

The hindcast wave periods are shown in Figure 5.11b. They indicate that 1.9s is reasonable to use as the period, particluarly during the intervals of highest significant waves, and therefore the model based on the significant wave height, as calibrated previously, can be used.

The results from the suspended sediment model for the entire 15 days are shown in Figure 5.12. Overall the correspondance between the model and the data is outstanding. The observed concentrations are well reproduced both during the initial large transverse storm and during the more prominant of the longitudinal events.

As was the case during the model calibration, the results in Figure 5.12 are quite insensitive to H_c as long as when H_c is varied θ and n are also altered according to Eqs. (5.29) and (5.31) or alternatively the model is applied as presented in Eq. (5.32). Thus the form of this model can be considered verified since no further calibration was needed for H_c, however, no conclusions can be made of the specific model parameters. Table 5.3 summarizes the model results for various values of H_c and the corresponding values of θ and n. About the only noticeable effect increasing H_c causes is the elimination of model response during small events. From this standpoint a low value of H_c is favored.

The model behavior during the initial transverse event is particularly impressive in light of results of Somlyody (1986) who attempted to calibrate a model (Table 3.7) based on wind measurements made every two hours on shipboard, at the field site, during this storm. His optimum calibration gave maximum concentrations of about 100 mg/ℓ leading him to question the validity of and to ultimately neglect the isolated peak

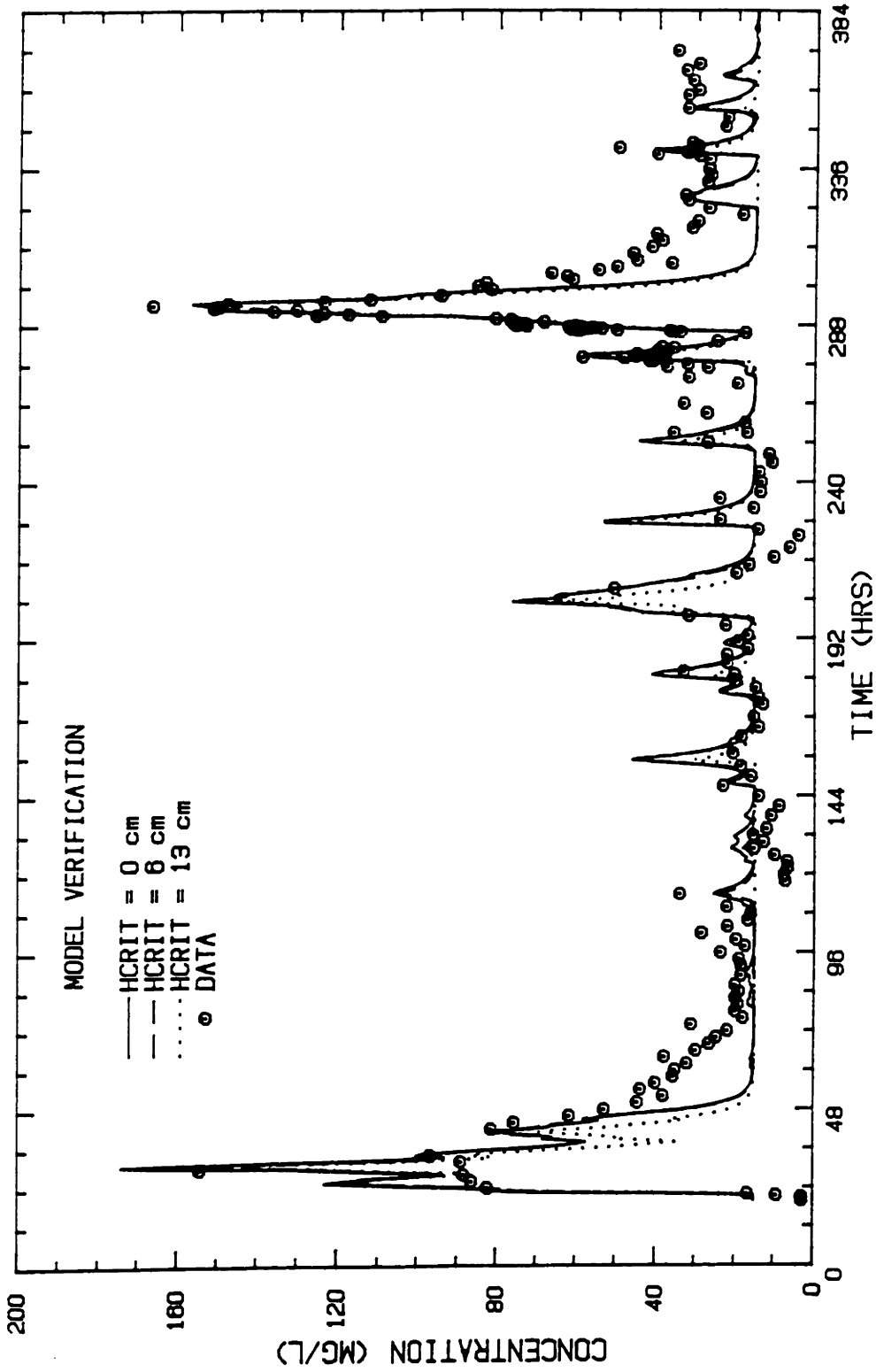

Figure 5.12 Verification of the suspended sediment concentration model with fifteen days of suspended sediment measurements.

TABLE 5.3
Summary of Results for Varying H_c from 15 Day Model Verification Run

H_c (cm)	c_{bak} (mg/ℓ)	β (cm/s)	n, Eq. (5.31)	θ, Eq. (5.29)	MSE $(mg/\ell)^2$
0.0	15	0.022	3.02	0.01479	35611
2.0	15	0.022	2.51	0.08554	35023
4.0	15	0.022	2.09	0.3682	34836
6.0	15	0.022	1.74	1.240	34778
8.0	15	0.022	1.45	3.403	35244
10.0	15	0.022	1.20	7.881	37151
12.0	15	0.022	1.00	15.85	40933
13.0	15	0.022	0.91	21.48	44458

concentration of about 150 mg/ℓ which was observed. It appears quite definite from Figure 5.12 that this peak measurement is valid.

The agreement during some of the smaller longitudinal events is impressive as well since these events test the model under significantly different conditions than those under which it was calibrated.

The largest systematic deviations occur during the deposition periods following the two major storms. In each case predicted concentrations decrease more rapidly than the observations. There are three causes which are consistent with the conceptual model developed in Chapter 3 and the discussion at the beginning of Chapter 5 which may have contributed. These are horizontal transport, bed cohesiveness, and differential settling.

Horizontal transport effects were identified earlier as potentially being most important during deposition periods. Unfortunately a definite conclusion can not be reached without concurrent data from several locations.

The laboratory evidence and the conceptual model presented in Chapter 3 show that the model which has been used in this study will not reproduce the hysteresis effect associated with repopulating the surface zone over a cohesive sediment bed. Therefore it will overpredict the rate of deposition after significant resuspension events. However, if this had an important effect on the present data, deviations between the model and observations should occur over the entire period of decreasing concentration. Figure 5.12 indicates that initially the model predicts concentration decreases relatively well. It is only as the suspended sediment level approaches the background concentration that the model deviates significantly.

On the other hand this behavior suggests differential settling is the cause of the deviation for the following reason. As sediment is eroded most of the range of particle sizes found in the sediment bed (Figure 5.1) are resuspended. The resulting suspended sediment distribution has an "average" settling velocity which is of the order of 0.022 cm/s. This is appropriate during periods of net erosion and the initial stages of net deposition. However, as deposition proceeds the large particles settle first thereby decreasing the "average" settling velocity of the distribution left in suspension. Thus the model will only behave accurately until the change in the size distribution becomes important. This is further supported by the high suspended sediment concentration

which is maintained following the second large storm. In this case the settling of the smaller particles was interrupted by several minor resuspension events and the concentration never reached the background. Alternatively no such resuspension events occurred after the first large storm and the concentration eventually returned to the background level.

5.6 DISCUSSION

Summarizing the results of this chapter, a model describing the depth-averaged suspended sediment concentration was presented which made use of the bottom boundary condition recommended in Section 3.5. An order of magnitude analysis suggested that observed increases in suspended sediment occurred over short enough intervals to minimize the importance of horizontal transport and therefore allow their neglect in the model. It was also shown that for a constant period and a laminar wave boundary layer, a model based explicitly on wave height was generally as valid as one based explicitly on the wave induced bottom stress. Due to the success obtained in Chapter 4 modeling the significant wave height and the relatively constant observed wave periods, a model based on significant wave height was used.

Calibration of the model to the storm of 8/15 - 8/16 during which both hydrodynamic data and suspended sediment concentrations were measured, yielded functional relationships between θ, n and H_c and an average value of β which corresponded quite well to independent observations of settling velocity. Making use of these, the model behavior was independent, within broad limits, of the magnitude of the one remaining free parameter which was selected to be H_c. A verification of the model using wind data from a

nearby meteorological station, the wave hindcasting model from Chapter 4 and 15 days of concentration measurements yielded excellent model results. Again the model behavior was for the most part independent of H_c, thereby precluding the specification of single values of n and θ as well. The only systematic model deviation from the observations occurred toward the end of extended periods of deposition. This behavior is likely due to differential particle settling, however, horizontal transport effects can not be definitely ruled out. It did appear that this behavior was not indicative of the hysteresis caused by the repopulating of the surface zone over a cohesive sediment bed.

Before concluding it is well to raise an issue which has been touched upon briefly at several points in this thesis; does cohesiveness significantly effect the resuspension of sediment at the Keszthely field site? The most obvious clue is the particle size distribution which, by itself, suggests cohesive bonding will be important. As a result a substantial effort was undertaken in Chapter 3 to arrive at a bottom boundary condition which was applicable to exchange with a cohesive bed and yet was simple enough to be reasonable for modeling field data. However, two characteristics associated with bed cohesiveness, the hysteresis effect due to the repopulation of a depleted surface zone and a decrease in the erosion rate in time due to bed consolidation, (which would require a variation in the erosion parameters in time to model the data), were not observed. This suggests that cohesive effects may have been unimportant either because the surface zone never became depleted or because the sediments were simply not cohesive.

A simple mass balance shows that an increase of 200 mg/ℓ in the concentration of a 2-m deep water column can be accomplished by eroding a

layer of material of 90 per cent water content which is less than 0.4mm thick. It may have been possible that bioturbation and/or residual turbulence in the water column, (perhaps associated with bottom shear from the mean flow), along with the low ionic strength of the water were sufficient to keep the upper part of the sediment bed loose and therefore minimize the importance of cohesive effects.

Some indication of a noncohesive erosion behavior may be obtained from the considerable body of knowledge associated with cohesionless sediment transport. One possibility is to check Shield's curve for an initiation of motion criterion. Using the curve presented in ASCE (1974) and a particle diameter of 15μ, a particle Reynold's number $U_* d/\upsilon = 0.2$ and a critical stress $\tau_c = 1.8$ dynes/cm^2 were found. From Eq. (5.22) this yields a critical wave height of 22 cm. However, this analysis is quite tenuous since due to the small particle diameters the point of intersection with Shield's curve is well outside the region in which it has been verified experimentally. Therefore, this result might at best suggest a value of H_c toward the upper end of the range of model values.

Alternatively, expressions relating the discharge of noncohesive sediment, q_s, to the applied forcing may provide insight into the parameters in the expresson for c_{ss}. In considering these the distinction between bed load, suspended load and total load is noted and initially only relationships developed for suspended load are considered.

Engelund (1970) found for sediment ranging from 100μ to 280μ in particle diameter in steady flow

$$\frac{q_{ss}}{q} \sim \left(\frac{u_*}{w_s}\right)^4$$

using

$$q_{ss} = c_{ss} \bar{U} h$$

$$q = \bar{U} h$$

$$\tau_b = \rho u_*^2$$

yields

$$c_{ss} \sim \frac{\tau_b^2}{w_s^4}$$

where $\bar{U}$ is the depth-average velocity, q_{ss} is the suspended sediment discharge, u_* is the friction velocity and other variables are as defined previously. A comparison with Eq. (5.25) suggests that $n \sim 2$ and $\theta \sim 1/w_s^4$. Of these relationships, the first is reasonable but the dependence of θ on w_s is contradicted by the findings shown in Figure 5.4c which shows that w_s is independent of θ.

Bagnold (1966) assumes that the potential energy associated with the sediment in suspension is a constant fraction of the "available power" in the flow. This leads to an expression of the form

$$\frac{q_{ss}}{\bar{U} h} = c_{ss} \sim \frac{\tau_b \bar{U}}{w_s} \sim \frac{\tau_b^{1.5}}{w_s}$$

This suggests $n \sim 1.5$ and $\theta \sim 1/w_s$. Again n is reasonable but θ is contrary to the modeling results.

If the distinction between suspended load, bed load and total load is relaxed numerous other relationships can be considered. Summaries of some of these are provided in Sleath (1984) and the ASCE Sedimentation Handbook, (1975). In general enough scatter exists in the expressions that they provide no assistance in determining specific values for θ or n.

Summarizing this discussion, it is not clear from the model results to what degree cohesive effects significantly influenced the observed suspended sediment concentrations at the Keszthely field site. On the contrary it seems that several characteristics of cohesive sediment behavior are noticeably absent. A brief comparision of the calibrated model parameters to expected values based on cohesionless sediment transport theory failed to provide any additional insight into this question.

Chapter 6

Summary, Contributions and Recommendations

6.1 SUMMARY OF RESULTS

Episodic resuspension and deposition of bottom sediment can have a large influence on water quality thereby making it important to be able to predict the amount of sediment which is resuspended in shallow water bodies and/or shallow regions of deeper water bodies during storm events. Unfortunately there is very little field data available in which suspended sediment concentration is measured in enough detail to develop or test models of this process. Worse yet, effectively no data exist in which the suspended sediment concentration, the hydrodynamic forcing and the wind forcing are all measured simultaneously. In response to this need, an instrument system was assembled having the capability of measuring wind speed and direction, wave characteristics, water velocities and suspended sediment concentration. The equipment could be controlled remotely by radio and could collect and store data in place. Field experiments were planned and executed in Lake Balaton, a large (700 km^2 surface area) but shallow (mean depth 3.1m) lake in Hungary, as part of a co-operative study with the Hungarian government into the causes and effects of various processes on the eutrophication of the lake. In this regard a study of sediment resuspension was particularly timely as the Hungarian government had recently implemented several measures to drastically reduce the external supply of pollutants into the lake, thereby focusing attention on the role of the sediment as an internal source for maintaining the advanced state of eutrophication in the lake.

The equipment listed above was itself quite novel as it included an ABSS ultrasonic backscattering device for determining vertical profiles of suspended sediment and two, BASS, acoustic velocity meters. Neither of these instruments had much previous usage in shallow water deployments and their application in such an environment presented new opportunities and challenges. Specifically, the shallow depths provided an opportunity to calibrate the ABSS in situ to gravitimetric determinations of suspended sediment concentration. However, an unfortunate set of circumstances combined to render the ABSS data useless. Nevertheless, this remains an interesting tool for future research from the standpoint of attempting to calibrate it to concentration measurements and because of its potential for recording critical conditions signifying the initiation of erosion.

The shallow water depths and accompanying high ratio of wave orbital velocity to mean current velocity provided a relatively untested application for BASS which has been used more commonly in conditions dominated by a mean current. It was found that the presence of a redundant measurement axis on each BASS provided the capability for a dynamic analysis of the velocity meter's performance from the same data that was used to resolve the flow components. Results from this analysis showed that a flow disturbance existed in the presence of strong surface waves which was small in comparison to the wave component but which could lead to a substantial error in other components associated with the fluctuating velocity signal, e.g. Reynold's stresses. This is particularly true for the vertical component of the fluctuating velocity at levels near the bottom.

The equipment was deployed at two locations in Lake Balaton - first about 40 m off the eastern shore of the Tihany penninsula and later about 400 m east of the western end of the lake at Keszthely.

Typical mean currents at the Tihany site were in the range of 5 cm/s and were dominated by flow through the Tihany straight, exhibiting a period characteristic of a longitudinal seiche in the lake. Also captured was one extraordinary event in which the mean velocity reached 30 cm/s. Typical storm associated winds blowing lengthwise from across the lake were capable of generating significant wave heights in excess of 20 cm and relatively constant mean periods slightly greater than 2s at the measurement site. In general resuspension appeared ineffective at this site and resulted in suspended sediment concentrations no more than about 25 mg/ℓ during a typical storm.

At the Keszthely field site the mean current was always shore parallel even in the presence of onshore winds aligned with the lake's major axis. This is consistent with previous physical and numerical modeling which has predicted the presence of a large horizontal eddy at this end of the lake. The wave characteristics at Keszthely were similar to those at Tihany and in particular a relatively constant mean wave period slightly above 2s was again observed. Sediment resuspension was much more important at this location, presumably due to the finer particle sizes, and observations during two storms showed increases from 15 mg/ℓ to 150 mg/ℓ. Wind, hydrodynamic and concentration data were recorded during the second of these storms and constitute probably the most complete field data set in existence describing resuspension in response to a storm event. Fifteen days worth of concentration data were recorded altogether at this site and

along with wind data from a nearby meteorological station provide a substantial time series for model evaluation.

Sediments in Lake Balaton are typical of those found in many lakes and estuaries since they are comprised primarily of silt and clay fractions Such sediments are expected to be cohesive in nature. A thorough review of the literature on erosion and deposition of cohesive sediment suggested two schools of thought existed on this subject, i.e., that at any time sediment exchange between the water column and the bed occurred (1) either exclusively away from the bed or exclusively toward the bed or (2) simultaneously in both directions. A simple, conceptual, double interface model (DIM) was presented which hypothesized a bidirectional exchange between the water column and a surface zone in which sediments exhibit minimal cohesive bonding and a unidirectional exchange between the surface zone and the cohesive sediment bed. This model provided a unifying mechanism for interpreting experimental results which had previously been interpreted in support of either one or the other of the two schools of thought. In particular, experiments which seemed to show a unidirectional sediment exchange were explained as a bed strength limited case of the DIM.

A consequence of the DIM was the ability to model all cohesive sediment exchange with a relationship of the form

$$\phi = E_2 - S_2 \tag{6.1}$$

in which ϕ is the net bottom sediment flux while E_2 and S_2 are the bottom fluxes entering and leaving the water column, respectively. In this context the two schools of thought reduced to two alternate approaches for

specifying ϕ, i.e.,

DIM Approach 1 (DIM A1) - specify separate relationships for ϕ_e and ϕ_d such that

$$\phi = \phi_e \quad \text{if} \quad \frac{d\bar{c}}{dt} > 0 \tag{6.2a}$$

$$\phi = \phi_d \quad \text{if} \quad \frac{d\bar{c}}{dt} < 0 \tag{6.2b}$$

DIM Approach 2 (DIM A2) - specify E_2 and S_2 individually and compute ϕ from Eq. (6.1)

A simple analytical model suggested general relationships for E_2 and S_2 of

$$S_2 = \beta \bar{c} \tag{6.3a}$$

$$E_2 = \beta c_{ss} \tag{6.3b}$$

$$\beta \equiv \frac{c_o}{\bar{c}} w_s \tag{6.3c}$$

where $\bar{c}$ is the depth-averaged suspended sediment concentration, c_o is the bottom concentration, c_{ss} is a steady-state concentration and w_s is the settling velocity. In a well-mixed water column $\beta \approx w_s$.

Verification of the conceptual model was provided by a reanalysis of erosion experiments which were known to be bed strength limited and which had previously been analysed in terms of DIM A1. The application of DIM A2 and in particular Eq. (6.3) to this data allowed values of β to be computed which were then shown to correspond quite closely to independent measurements of w_s.

Additional results from these experiments led to a proposed relationship for c_{ss} appropriate for use during bed strength limited

conditions, (i.e., when the surface zone is depopulated), of

$$c_{ss} = K(\tau_b - \tau_c)^n \tag{6.4}$$

in which K and n are coefficients which will be a function of the cohesiveness of the bed, τ_b is the applied bottom stress and τ_c is a critical stress.

Quantitative expression of ϕ_e and ϕ_d were found to be relatively complicated and require a large number of parameters to be specified, many of which had little physical significance. It seemed unrealistic that a model based on these relationships could be rigorously calibrated or verified using field data.

Alternatively a model based on DIM A2, and specifically Eqs. (6.3) and (6.4), might reasonably be implemented using constant parameter values, although in that case the model could not represent the change in strength of a consolidating bed in time, the hysteresis effect associated with the repopulation of a depleted surface zone during net deposition or the observation that steady-state concentrations reached after a period of net deposition were proportional to the initial concentration. The advantage of a DIM A2 was the fact that β has a well defined physical meaning and at least an intuitive feel for τ_c also exists on physical grounds. The resulting model has only four parameters in need of calibration, a feature which makes it much more suitable for application with field data.

In order to apply any type of resuspension model it is necessary to have a measure of the forcing which drives this process. The data collected in the field study was used to show that the bottom stress

associated with surface waves was typically much greater than that due to the mean current in Lake Balaton and therefore wave stress most likely dominates the resuspension process.

A wave hindcasting model, which was based on the shallow water modifications made to the SMB relationships as presented in CERC (1977) and CERC (1984) was implemented in the lake and compared to a statistical summary of historical data off Szemes as well as to the wind and wave data collected at Tihany and Keszthely in the field study. In this regard the wind and wave data collected as a part of this study make a valuable contribution to the otherwise small amount of data available for the verification of these wave hindcasting relationships in large shallow waterbodies.

It was found that the (1977) relationships matched the time histories of significant wave height extremely well both at Keszthely and Tihany given the implicit assumption of steady-state waves in local equilibrium with wind energy input and bottom energy loss. The (1984) model typically overpredicted the wave heights at long fetches and under predicted them at shorter fetches. This is at least in part attributable to its use of the absolute fetch rather than the effective fetch and suggests that the width to length ratio in Lake Balaton may be small enough to warrant the use of the 1977 effective fetch approach.

Observed wave periods were not as well reproduced in a dynamic sense by either version of the model although it was found that the magnitude of the "equivalent velocity period" could be matched during the major part of a wind event if the leading coefficient in the (1977) relationship for wave period was increased from 1.2 to 1.4. The "equivalent velocity period" was

defined to be the period that, when combined with the significant wave height, yields a bottom rms orbital velocity equal to the total bottom rms velocity in the surface wave band of the measured velocity spectrum. Since the bottom orbital velocity is used to compute the bottom stress it was concluded that this was the most desirable measure of the period for a predictive model.

Attempts to include duration limitation as described in CERC (1984) were thwarted by lack of information about storm propagation speeds together with the fact that changing wind speeds and directions appeared to require an extension of the model to limits it was simply not designed to treat.

Overall, considering the simplicity of this wave hindcasting model, the performance was surprisingly good.

A model describing the depth-averaged suspended sediment concentration was presented which made use of the Approach 2 bottom boundary condition. An order of magnitude analysis suggested that observed increases in suspended sediment occurred over short enough intervals to minimize the importance of horizontal transport and therefore allow their neglect in the model. It was also shown that for a constant period and conditions of a laminar wave boundary layer, a model based explicitly on wave height was generally as valid as one based explicitly on the wave induced bottom stress. Due to the success obtained in modeling the significant wave height, the relatively constant observed wave periods, and the computed presence of a laminar wave boundary layer, a model based on significant wave height was used.

Calibration of the model, Eq. 5.24, to the storm of 8/15 - 8/16, during which both hydrodynamic data and suspended sediment concentrations were measured, yielded functional relationships between θ, n and H_c, Eqs. (5.29) and (5.31), and an average value of β = 0.022 cm/s which corresponded quite well to independent observations of settling velocity. Making use of these, the model behavior was independent, within broad limits, of the magnitude of the one remaining free parameter which was selected to be H_c. A verification of the model using wind data from a nearby meteorological station, the wave hindcasting model and 15 days of concentration measurements yielded excellent results, (Figure 5.12). Again the model behavior was for the most part independent of H_c, thereby precluding the specification of single values of n and θ as well. The only systematic model deviation from the observations occurred toward the end of extended periods of deposition. This behavior is best explained by differential particle settling. It did appear that this behavior was not indicative of the hysteresis caused by the repopulation of the surface zone over a cohesive sediment bed.

It was not clear from the model results that cohesive effects significantly influenced the observed suspended sediment concentrations at the Keszthely field site. On the contrary it seems that several characteristics of cohesive sediment behavior, (e.g., changing bed strength with time since deposition and the hysteresis between erosion and deposition), were noticeably absent. A brief comparision of the calibrated model parameters to expected values based on cohesionless sediment transport theory failed to provide any additional insight into this question.

6.2 CONTRIBUTIONS

The research conducted as a part of this study has made the following contributions:

(1) A data set which includes concurrent measurements of wind forcing, hydrodynamic response/sediment forcing and sediment response to a storm event.

(2) Several data sets which provide verification for shallow water wave hindcasting relationships.

(3) Initial quantification of the performance of BASS in wave dominated flows through the exploitation of a redundant measurement axis. This allows dynamic analysis of sensor error including flow disturbance which is relatively unheard of in measurement equipment.

(4) A conceptual model for interpreting experimental results on cohesive sediment erosion and deposition. A consequence of this model was the general applicability of Eq. (6.1) as the bottom boundary condition describing cohesive sediment erosion and deposition. It is felt that this is particularly important since models based on equations similar to this have previously been used without any theoretical justification. A specific form for the terms in this model was proposed which, with constant parameter values, could reasonably be applied to field data.

(5) Calibration and verificaton of a suspended sediment concentration model, using this boundary condition, to field data.

6.3 RECOMMENDATIONS

It was somewhat unsatisfying to be unable to obtain specific values for each of the parameters in the suspended sediment model which was used herein. Arguments have been presented by Somlyody (1980) and Lavelle et al. (1984) for why the critical condition can be eliminated, or in this case suggesting $H_c = 0$. Clearly this reasoning could have been accepted in th present study and a nice, tidy, final result obtained. However, this assumption has been refuted in laboratory studies of cohesive sediment transport. Thus a major area for future research is to quantify the differences between field and laboratory settings. One way to do this is to attempt to directly observe critical conditions for erosion in the field. The ABSS may be a promising tool for this work or even more conventionally available transmissometers mounted at or very close to the bottom may be useful.

Also with regard to differentiating field and laboratory behavior, it appears that particle size alone is not enough to identify the importance of cohesive effects on resuspension, particularly in freshwater applicatons. However, at this point in time so little field data is available that this issue is very much unclear. The collection of a lot more field data will be necessary before general conclusions can be reached. It would be particularly useful if the particle size distribution of sediments in suspension could be analyzed as a part of this data collection procedure. In particular, a convenient method for determining these in situ is desperately needed so that all of the uncertainty associated with aggregation and disaggregation between the time of sampling and the time of analysis can be eliminated.

A general observation during the course of this study was that physical bottle sampling and gravitimetric analysis is very inefficient when required to be the primary source of data on suspended sediment concentration. On the other hand this is the only method which gives a direct measurement of concentration. Therefore it is recommended that the use of indirect methods, such as acoustic backscatter or light transmission, whose data can be sampled and recorded automatically be pursued as the primary data gathering mechanism. These have the advantages of not sleeping at night, etc. and to varying degrees being quite reliable. Physical sampling should be reserved for calibration and verification of the indirect measurements. This provides a much more realistic opportunity for obtaining the amount of data which will ultimately be required to gain confidence in our ability to model field situations. In particular it allows the potential for synoptic measurements in space and fine resolution in time over extended deployment periods.

Finally, it should be stressed that field programs designed to be used in erosion/deposition modeling must include measurements of the pertinent hydrodynamic forcings. There is so much which remains to be learned about the response of fine sediments to a known forcing that an unreasonably gross treatment or total neglect of the hydrodynamics may completely obscure any conclusions about the sediment behavior.

REFERENCES

Aalderink, R. H., L. Lijklema, J. Breukelman, W. Van Raaphorst, and A. G. Brinkman. 1984. Quantification of wind induced resuspension in a shallow lake, *Proc. of IAWPRC Congress*. (September) Amsterdam.

Abdel-Rahman, N. M. 1962. The effect of flowing water on cohesive beds. Ph.D. diss. Laboratory for Hydraulic Research and Soil Mechanics, Swiss Federal Institute of Technology, Zurich, Switzerland.

Anderson, F. E. .1972. Resuspension of estuarine sediments by small amplitude waves. *Journal of Sediment Petrology*, 42(3): 602-607 (September)

American Society of Civil Engineers. *1974. Sedimentation Handbook.* New York: A.S.C.E.

Antonia, R. A., A. J. Chambers, S. Rajagopalan, K. R. Sreenivasan and C. A. Friehe. 1978. Measurement of turbulent fluxes in Bass Strait," *Journal of Physical Oceanography* 8:28-37.

Ariathurai, R. and R. B. Krone. 1976. Finite Element Model for Cohesive Sediment Transport. *Journal of Hydraulics Div.* ASCE, 102(HY3): 323-338 (March)

Ariathurai, R., R. C. MacArthur and R. B. Krone. 1977. *Mathematical Model of Estuarial Sediment Transport.* Technical Report D-77-12. U. S. Army Engineers Waterways Experiement Station, Vicksburg, MS (October)

Ariathurai, R. and K. Arulanandan. 1978. Erosion rates of cohesive soils. *Journal of Hydraulics Div.*, ASCE. 104(HY2):279-283.

Bagnold, R. A. 1946. Motion of waves in shallow water-interaction between waves and sand bottom. *Proceedings, Royal Society.* London, Series A, 187:1-15.

Bagnold, R. A. 1966. An approach to the sediment transport problem from general physics. *US Geological Survey.* Prof. Paper 422-I.

Baker, E. T., G. A. Cannon and H. C. Curl Jr. 1983. Particle transport processes in a small marine bay. *Journal of Geophysical Research* 88(C14): 9661-9669 (November)

Barcia. J. 1974. Extreme fluctuations in water quality of eutrophic fish kill lakes: Effect of sediment mixing. *Water Research* 8:881-888,

Bates, M. H. and N. J. Neafus. 1980. Phosphorus release from sediments from Lake Carl Blackwell, Oklahoma. *Water Research* 14:1477-1481

Beck, M. B. 1985. Lake eutrophication: Identification of tributary nutrient loading and sediment resuspension dynamics. *Applied Mathematics and Computation* 17(4) (November)

Bendat, J. S. and A. G. Piersol. 1971. *Random Data: Analysis and Measurement Procedures*. Wiley-Interscience Publications.

Bengtsson, L. 1978. Wind induced circulation in lakes. *Nordic Hydrology* 9:75-94.

Bengtsson, L. 1973. *Wind stress on small lakes*. Bulletin Series A. No. 16. Div. Water Resources Engineering, Technical University of Lund, Sweden.

Brock, K. and L. Krugërmeyer. 1970. *The hydrodynamic roughness of the sea surface*. Report No. 14. Institute for Radiometeorologie and Meteorologie, Hamburg University.

Cacchione, D. A. and D. E. Drake. 1982. Measurements of storm-generated bottom stresses on the continental shelf. *Journal of Geophysical Research* 87(C3): 1952-1960 (March)

Cacchione, D. A. and D. E. Drake. 1979. A new instrument system to investigate sediment dynamics on continental shelves. *Marine Geology* 30:299-312.

Carlson, E. J. and P. F. Enger. 1963. *Studies of Tractive Forces of Cohesive Soils in Earth Canals*. Hydraulic Branch Report No. NYD-504. Bureau of Reclamation, Denver, CO. (October)

Carper, G. L. and R. W. Bachmann. 1984. Wind resuspension of sediments in a prairie lake. *Canadian Journal of Fisheries and Aquatic Sciences* 41(12): 1763-1767.

CERC. 1977. *Shore Protection Manual*. Vol. 1. U. S. Army Coastal Engineering Research Center, Ft. Belvoir, VA.

CERC. 1984. *Shore Protection Manual*. Vol. 1. U. S. Army Coastal Engineering Research Center, Ft. Belvoir, VA.

Christensen, R. W. and B. M. Das. 1974. Hydraulic erosion of remolded cohesive soils. *Soil Erosion: Causes and Mechanisms, Prevention and Control*. Special Report 135:8-19.

Clarke, T. L., D. J. P. Swift and R. A. Young. 1982. A numerical model of fine sediment transport on the continental shelf. *Environmental Geology* 4:117-129.

Cole, P. and G. V. Miles. 1983. Two-dimensional model of mud tranpsort. *ASCE Journal of Hydraulic Engineering* 109(1): 1-12 (January).

Davis, M. B. 1973. Redeposition of pollen grains in lake sediment. *Limnology and Oceanography* 18(1): 40-52.

Dixit, J. G. 1982. Resuspension potential of deposited kaolinite beds. Master's thesis. Department Coastal and Ocean Engineering, University of Florida.

Downing, J. P., R. W. Sternberg and C. R. B. Lister. 1981. New instrumentation for the investigation of sediment suspension processes in the shallow marine environment. *Marine Geology* 42:19-34.

Donelan, M. A. 1980. The dependence of the aerodynamic drag coefficient on wave parameters. *First International Conference on Meteorology and Air/Sea Interaction of the Coastal Zone*. The Hague, Netherlands. pp 381-387. (May).

Donelan, M. A., F. C. Elder and P. F. Hamblin. 1974. Determination of the aerodynamic drag coefficient from wind set-up (IFYGL). *Proc. Seventeenth Conference Great Lakes Res.* pp778-788.

Dunn, I. S. 1959. Tractive resistance of cohesive channels. *Journal of Soil Mechanics and Foundations Div.* ASCE. pp1-24 (June).

Einstein, H. A. and S. A. El-Sammi. 1949. Hydrodynamic forces on a rough wall. *Review of Modern Physics* 21:520-524.

Engelund, F. 1970. *A note on the mechanics of sediment suspension.* Report 21. Coastal Engineering and Hydraulics Laboratory, Technical University of Denmark.

Fisher, J. S., J. Pickral and W. E. Odum. 1979. Organic detritus particles: Initiation of motion criteria. *Limnology and Oceanography.* 24:529-532.

Fleagle, E. L., P. A. Sheppard, F. I. Badgley. 1958. Vertical distribution of wind speed, temperature and humidity above a water surface. *Journal Met. Res.* 17:141-157.

Fukuda, M. K. and W. Lick. 1980. The entrainment of cohesive sediments in freshwater. *Journal Geophysical Research* 85(C5): 2813-2824 (May).

Gabrielson, J. O. and R. J. Lukatelich. 1985. Wind-related resuspension of sediments in the Peel-Harvey Estuarine System. *Estuarine and Coastal Shelf Science* 20:135-145.

Garratt, J. R. 1977. Review of drag coefficients over oceans and continents, *Mon. Weather Rev.* 105: 915-929.

Gelencser, P., F. Szilagyi, L. Somlyody, L. Lijkelma. 1982. *A study on the influence of sediment in the phosphorus cycle in Lake Balaton.* IIASA Collaborative Paper CP-82-44. Laxenburg, Austria.

Graf, W. H. and J. -P. Prost. 1980. Aerodynamic drag and its relation to the sea state. *Arch. Met. Geoph. Biocl.*, Series A. 29:67-87.

Graf, W. H. and J. -P. Prost. 1979. The aerodynamic drag: Experiments on Lake Geneva. in *Hydrodynamics of Lakes* edited by W. H. Graf and C. H. Mortimer. Elseiver Scientific Publishing Co. pp 303-312.

Graf, W. H., N. Merzi and C. Perrinjaquet. 1984. Aerodynamic drag: measured at a nearshore platform on Lake Geneva. *Arch. Met. Geoph. Biocl.*, Series A, 33:151-173.

Grant, W. D. and O. S. Madsen. 1979. Combined wave and current interactions with a rough bottom," *Journal Geophysical Research*, 84(C4): 1797-1808.

Grant, W. D., A. J. Williams III., and S. M. Glenn. 1984. Bottom stress estimates and their prediction on the northern California Continental Shelf during CODE-1: The Importance of wave-current interaction. *Journal Physical Oceanography*, 14(3): 506-527 (March).

Grissinger, E. H. 1966. Resistance of selected clay systems to erosion by water. *Water Resources Research* 2(1):131-138.

Györke, D. "A *Lebegöanyag Koncentráció Alakulása Sekèly Tavakban, Tározókban.*" Vituki Report (in Hungarian) 7411:2-323.

Hakanson, L. and M. Janson. 1983. *Principles of lake sedimentology.* Springer Verlag. 316p.

Hakanson, L. 1977. The influence of wind, fetch, and water depth on the distribution of sediments in Lake Vänern, Sweden. *Canadian Journal Earth Science* 14:397-412.

Hayter, E. J. 1983. Prediction of cohesive sediment movement in estuarial waters. Ph.D. diss. Coastal and Oceanographic Engineering Department, University of Florida.

Hess, F. and K. W. Bedford. 1985. Acoustic backscatter system (ABSS): The instrument and some preliminary results. *Marine Geology* 66:357-380.

Hicks, B. B., R. L. Drinkrow and G. Grauze. 1974. Drag and bulk transfer coefficients associated with a shallow water surface. *Boundary Layer Meteorology* 6:287.

Holdren, G. C. and D. E. Armstrong. 1980. Factors affecting phosphorus release from intact lake sediment cores. *Env. Science and Technology* 14(1):79-87.

Hsu, S. A. 1975. Wind stress on nearshore and lagoonal waters of a tropical island. *Limnology and Oceanography* 20(1):113.

Huovila, S. 1971 Measurements of wind profile and radiation balance above the surface of Lake Pääjärvi. *Proc. Nordic IHD Field Symposium*, Vierumäki, Finland.

Jonsson, I. J. 1966. Wave boundary layers and friction factors. *Proceedings of the Tenth Conference of Coastal Engineering*, Tokyo. pp.127-148.

Kajiura, K. 1968 A model of the bottom boundary layer in waves. *Bulletin Earthquake Research Institute*, Tokyo University. 46:72-123.

Kamphius, W. J. and K. R. Hall. 1983. Cohesive Material Erosion by Unidirectional Current. *Journal Hyd. Eng.*, ASCE. 109(1): 49-61.

Kandiah. 1974. Fundamental aspects of surface erosion of cohesive soils. Ph.D. diss. University of California, Davis.

Kang, S. W., Y. P. Sheng and W. Lick. 1982. Wave action and bottom shear stresses in Lake Erie. *Journal Great Lakes Research* 8(3):482-494.

Kelly, W. E. and R. C. Gularte. 1981. Erosion resistance of cohesive soils. *Journal of Hyd. Div.*, ASCE 107(HY10):1211-1224,

Krishnamurthy, M. 1983. Incipient motion of cohesive soils. *Proceedings ASCE Hydraulics Div. Speciality Conference*, edited by H. T. Shen. pp96-101. (August).

Krone, R. B. 1983. Cohesive sediment properties and transport processes. *Proceedings ASCE Hydraulics Div. Specialty Conference*, edited by H. T. Shen. pp 66-78. (August).

Krone, R. B. 1972 *A field study of flocculation as a factor in estuarial shoaling processes*. Technical Report No. 19. Committee on Tidal Hydraulics, U. S. Army Corps ofEngineers, Vicksburg, Mississippi.

Krone, R. B. 1963. *A study of rheologic properties of estuarial sediments*. Technical Report. Hydraulic Engineering Laboratory, University of California, Berkeley.

Krone, R. B. 1962 *Flume studies of the transport of sediment in estuarial shoaling processes*. Final Report. Hydraulic Engineering Laboratory and Sanitary Engineering Research Laboratory, University of California, Berkeley. (June).

Kutas, T. and S. Herodek 1986. A complex model for simulating the Lake Balaton ecosystem," in *Modeling and Managing Shallow Lake Eutrophication with Application to Lake Balaton*, edited by L. Somlyody and G. van Straten. Ch. 12:309-322. Springer-Verlag, 1986.

Lam, D. C. L. and J. M. Jacquet. 1976. Computations of physical transport and regeneration of phosphorus in Lake Erie, fall 1970. *Journal Fish Research Board of Canada*. 33:550-563.

Large, W. G. and S. Pond. 1980. Open ocean momemtum flux measurements in moderate to strong winds," *Journal Physical Oceanography* 11:324-336.

Lavelle, J. W., H. O. Mofjeld and E. T. Baker. 1984. An in situ erosion rate for a fine-grained marine sediment. *Journal Geophysical Research* 89(C4): 6543-6552 (July).

Lavelle, J. W., R. A. Young, D. J. P. Swift and T. L. Clarke. 1978. Near-bottom sediment concentration and fluid velocity measurements on the inner continental shelf, New York. *Journal Geophysical Research* 83(c12): 6052-6062.

Lee, D., W. Lick and S. W. Kang. 1981. The entrainment and deposition of fine-grained sediments in Lake Erie. *Journal Great Lakes Research* 7(3):224-233.

Leonov, A. V. 1980. *Mathematical Modeling of Phosphorus Transformation in the Lake Balaton Ecosystem.* IIASA Working Paper WP-80-149. Laxenburg, Austria.

Lesht, B. M., T. L. Clarke, R. A. Young, D. J. P. Swift and G. L. Freeland. 1980. An empirical relationship between the concentration of resuspenced sediment and near bottom wave-orbital velocity. *Geophysical Research Letters* 7:(12)1049-1052 (December)

Lick, W. 1982. Entrainment, deposition and transport of fine-grained sediments in lakes," *Hydrobiologia* 91:31-40.

Lijklema, L. 1977. The role of iron in the exchange of phosphate between water and sediments," in *International Symposium on Interactions between Sediments and Fresh Water*, edited by H. L. Golterman. The Hague: Junk & Pudoc. pp48-56.

Madsen, O. S. and W. D. Grant. 1976. *Sediment transport in the coastal environment.* Report 209, Ralph M. Parsons Laboratory for Water Resources and Hydrodynamics, Massachusetts Institute of Technology.

Máte, F. 1985. Bottom sediment investigations in Lake Balaton. Unpublished manuscript. Balaton Limnological Research Institute. Tihany, Hungary.

Mehta, A. J. 1973. Depositional behavior of cohesive sediments. Ph.D diss. Coastal and Oceanographic Engineering Department, University of Florida.

Mehta, A. J. 1983. Characterization tests for cohesive sediments. in *Proceedings, ASCE Hydraulics Div. Specialty Conference*, edited by H. T. Shen August. pp79-84.

Mehta, A. J. and E. Partheniades. 1976. An investigation of the depositional properties of flocculated fine sediments. *Journal Hydraulic Research* 13(4):361-381.

Mehta, A. J. and E. Partheniades. 1979. Kaolinite resuspension properties. *Journal of Hyd. Div. ASCE.* 105(HY4): 411-416 (April).

Mehta, A. J., E. Partheniades, J. G. Dixit and W. H. McAnally. 1982. Properties of deposited kaolinite in a long flume. in *Proceedings ASCE Hydraulics Div. Speciality Conference* pp594-603. (August).

Migniot, P. C. 1968. Étude des propriètès physiques de différents sèdiments très fins et de leur comportement sous des actions hydrodynamiques. *La Houille Blanche* 7:591-620.

Moore, W. L. and F. D. Masch, Jr. 1962. Experiments on the scour resistance of cohesive soils" *Journal Geophysical Res.* 67(4): 1437-1449.

Muszkalay, L. 1973. Characteristics of water motions in Lake Balaton. *VITUKI* report (in Hungarian).

Ochi, M. K. 1982. Stochastic analysis and probabilistic prediction of random seas. *Advances in Hydroscience* 13:217-374.

O'Connor, B. A. and S. Zein. 1974. Numerical modelling of suspended sediment. *Proceedings, Fourteenth Coastal Engineering Conference*, ASCE 11:1109-1128.

Odd, N. V. M. and M. W. Owen. 1972. A two-layer model for mud transport in the Thames Estuary. *Proc. of the Institution of Civil Engineers, Supplement*. London. 9:175-205.

Ottsen-Hansen, N. -E. 1975. Effect of wind stress on stratified deep lake. *Journal of Hydraulics Div.*, ASCE. 101(HY8): 1037.

Ovaitt, C. A. and S. W. Nixon. 1975. Sediment resuspension and deposition in Narragansett Bay. *Estuarine and Coastal Marine Science* 3:201-217.

Parchure, T. M. 1984. Erosional behavior of deposited cohesive sediments. Ph.D thesis, Coastal and Oceanographic Engineering Department, University of Florida.

Parchure, T. M. 1980. Effect of bed shear stress on the erosional characteristics of kaolinite. Masters thesis, Coastal and Oceanographic Engineering Department, University of Florida.

Parchure, T. M. and A. J. Mehta. 1985. Erosion of soft cohesive sediment deposits. *Journal of Hydraulic Engineering*, ASCE. 111(10):1308-1326 (October)

Partheniades, E. 1977. Unified view of wash load and bed material load. *Journal of Hyd. Div.*, ASCE. 103(HY9): 1037-1057.

Partheniades, E. 1972. Results of recent investigations on erosion and deposition of cohesive sediments. in *Sedimentation*, Chapter 20, edited by H. W. Shen.

Partheniades, E. 1965. Erosion and deposition of cohesive soils. *Journal of Hydraulics Div.* ASCE. 91(HY1):105-138 (January).

Partheniades, E. 1962. A study of erosion and deposition of cohesive soils in salt water. Ph D diss., University of California, Berkeley.

Partheniades, E., R. H. Cross III and A. Ayora. 1968. Further investigations on the deposition of fine sediments in turbulent flows. *Proc. Eleventh Conference on Coastal Engineering.* London, England. 6(47): 723-742. (September).

Paul, J. F. and R. Kasprzyk and W. Lick. 1982. Turbidity in the western basin of Lake Erie. *Journal of Geophysical Research* 87(C8): 5779-5784 (July).

Pennington, W., 1974. Seston and sediment formation in Five Lake District Lakes. *Journal of Ecology* 62:215-251.

Peters, R. H. and A. Cattaneo. 1984 The effects of turbulence on phosphorus supply in a shallow Bay of Lake Memphremagog. *Verh. Internat. Verein. Limnol.* 22:185-189.

Pollman, C. D. 1983. Internal loading in shallow lakes. Ph.D. diss., Dept. Environmental Engineering Sciences, University of Florida.

Raudkivi, J. J. 1976. *Loose Boundary Hydraulics.* Pergamon Press.

Rosa, F. 1977. Sedimentation and sediment resuspension in Lake Ontario. *Journal Great Lakes Research* 11(1): 13-25.

Ruggles, K. W., 1980. The vertical mean wind profile over the ocean for light to moderate winds. *Journal Applied Meteorology* 9(3):389.

Ryding, S. O. and C. Forsberg. 1977. Sediments as a nutrient source in shallow polluted lakes. in *International Symposium on Interactions between Sediments and Fresh water*, edited by H. L. Golterman. The Hague: Junk & Pudoc. pp 227-234.

Scarlatos, P. D. 1981. On the numerical modeling of cohesive sediment transport. *Journal of Hyd. Div.*, ASCE. 19(1): 61-68.

Serruya, C. 1977. Rates of sedimentation and resuspension in Lake Kinneret. in *International Symposium on Interactions Between Sediments and Fresh Water*, edited by H. L. Golterman. The Hagues Junk & Pudoc. p48-56.

Shanahan, P. and D. R. F. Harleman. 1982. *Linked hydrodynamic and biocochemical models of water quality in shallow lakes.* Technical Report: 268. Ralph M. Parsons Laboratory for Water Resources and Environmental Engineering, Department of Civil Engineering, Cambridge, MA., Massachusetts Institute of Technology.

Sheng, Y. P. and W. Lick. 1979. The transport and resuspension of sediment in a shallow lake. *Journal of Geophysical Research* 84(C4): 1809-1826 (April).

Sleath, J. F. A. 1984. *Sea Bed Mechanics.* John Wiley & Sons.

Sly, P. G. 1977. Sedimentary environments in the Great Lakes. *International Symposium on Interactions Between Sediments and Freshwater*, edited by H. L. Golterman. The Hague, Junk & Poduc. pp76-82.

Smith, S. D. 1980. Wind stress and heat flux over the ocean in gale force winds. *Journal Physical Oceanography* 10:727-740.

Somlyody, L. 1979. *Hydrodynamical aspects of the eutrophication modeling in the case of Lake Balaton.* IIASA Collaborative Paper CP-79-1, Laxenburg, Austria.

Somlyody, L. 1980. Preliminary study on wind induced interaction between water and sediment for Lake Balaton (Szemes Basin). In *Second Proc. Joint MTA/IIASA Task Force Meeting on Lake Balaton Modeling, Veszpremi, Hungary*, edited by G. Van Straten, S. Herodek, J. Fischer, and I. Kováces. 2:26-49.

Somlyody, L. 1982. Water-quality modelling: A comparison of transport-oriented and ecology-oriented approaches. *Ecological Modelling* 17:183-207.

Somlyody, L. 1986. Wind induced sediment resuspension in shallow lake. *International Conference on Water Quality Modelling in Inland Natural Environment.* Bournemouth, England. June 1986.

Somlyody, L. and M. Virtanen. 1982. *Application of a one-dimensional hydrodynamic model to Lake Balaton.* IIASA Collaborative Paper, CP-82-47, Laxenburg, Austria.

Southard, J. B., R. A. Young and C. D. Hollister. 1971. Experimental erosion of calcerous ooze. *Journal of Geophysical Research* 76:5903-5909.

Stewart, R. W. 1974. The air-sea momentum exchange. *Boundary-Layer Meteorology* 6:151-167.

Talebbeydokhti, N. 1984. Incipient resuspension of silt-clay deposits in oscillatory and unidirectional flows. Ph.D. diss., Department Civil Engineering, Oregon State University.

Talebbeydokhti, N. and P. C. Klingeman. 1984. Incipient resuspension of silt-clay sediment. in *Proceedings ASCE Hydraulics Div. Speciality Conference*, edited by H. T. Shen. pp72-76.

Thomas, R. L., A. L. W. Kemp and C. F. M. Lewis. 1973. The surficial sediments of Lake Huron. *Canadian Journal of Earth Science* 10:226-271.

Thomas, R. L., J. M. Jaquet, A. L. W. Kemp, and C. F. M. Lewis. 1976. The surficial sediments of Lake Erie. *Journal Fish. Res. Board Canada* 33:385-403.

Van Dorn, W. G. 1953. Wind stress on an artificial pond. *Journal of Marine Research* 12(3): 249-261.

Van Straten, G. 1980. *Analysis of Model and Parameter Uncertainty in Simple Phytoplankton Models for Lake Balaton.* IIASA Working Paper, WP-80-139. Laxenburg, Austria.

Walker, T. A. and B. O'Donnell. 1981. Observations on Nitrate, phosphate and silicate in Cleveland Bay, Northern Queensland. *Australian Journal of Marine and Freshwater Research* 32:877-887.

Wells, J. T., J. M. Coleman and W. J. Wiseman Jr. 1978. Suspension and transportation of fluid mud by solitary-like waves. *Proceedings, Sixteenth Coastal Engineeering Conference*, ASCE. pp1932-1952.

Wetzel, R. G. 1975. *Limnology.* Philadelphia, PA: W. B. Saunders Company.

Williams, A. J. III. 1985. BASS, an acoustic current meter array for benthic flow-field measurements. *Marine Geology* 66:345-355.

Wilson, B. W. 1960. Note on surface wind stress over water at low and high wind speeds. *Journal Geophysical Research* 65(10): 3377.

Wu, J. 1969. Wind stress and surface roughness at air-sea interface. *Journal Geophysical Research* 74(2): 444-455.

Wu, J. 1982. Wind-stress coefficients over sea surface from breeze to hurricane. *Journal Geophysical Research* 87(C12): 9704-9706.

Yamamoto, T., T. Nagai and J. L. Figueroa. 1986. Experiments on water-soil interaction and wave-driven soil transport in clay beds. *Continental Shelf Research.* 5(4): 521-540.

Young, R. A., J. T. Merrill, T. L. Clarke, and J. R. Proni. 1982. Acoustic profiling of suspended sediments in the marine bottom boundary layer. *Geophysical Research Letters* 9(3): 175-178.

Yousef, A. Y., W. M. McLellon and H. H. Zebuth. 1980. Changes in phosphorus concentrations due to mixing by motorboats in shallow lakes. *Water Research* 14:841-852.